

THESIS / THÈSE

DOCTOR OF SCIENCES

Photochromic multicomponent crystalline materials based on N-salicylideneanilines

Carletta, Andrea

Award date:
2019

Awarding institution:
University of Namur

[Link to publication](#)

General rights

Copyright and moral rights for the publications made accessible in the public portal are retained by the authors and/or other copyright owners and it is a condition of accessing publications that users recognise and abide by the legal requirements associated with these rights.

- Users may download and print one copy of any publication from the public portal for the purpose of private study or research.
- You may not further distribute the material or use it for any profit-making activity or commercial gain
- You may freely distribute the URL identifying the publication in the public portal ?

Take down policy

If you believe that this document breaches copyright please contact us providing details, and we will remove access to the work immediately and investigate your claim.



Photochromic multicomponent crystalline materials based on *N*-salicylideneanilines

A thesis submitted by **Andrea CARLETTA**
for the fulfilment of the requirements
for the degree of Doctor in Sciences

Thesis Committee:

Prof. Johan Wouters (Université de Namur, advisor)

Dr. Laurence Leherte (Université de Namur, president of the Thesis Committee)

Prof. Benoît Champagne (Université de Namur)

Prof. Tom Leyssens (Université Catholique de Louvain-la-Neuve)

Dr. Claudio Roscini (Institut Català de Nanociència i Nanotecnologia)

April 2019

Graphisme de couverture : © Presses universitaires de Namur

© Presses universitaires de Namur & Andrea Carletta
Rempart de la Vierge, 13
B - 5000 Namur (Belgique)

Toute reproduction d'un extrait quelconque de ce livre, hors des limites restrictives prévues par la loi,
par quelque procédé que ce soit, et notamment par photocopie ou scanner, est strictement interdite

pour tous pays.

Imprimé en Belgique

ISBN : 978-2-39029-044-5

Dépôt légal: D/2019/1881/13

Université de Namur
FACULTÉ DES SCIENCES
Rue de Bruxelles 61 – 5000 Namur, Belgique

**Matériaux cristallins multi-composants photochromiques à base de dérivés
N-salicylideneanilines**

par **Andrea Carletta**

Résumé

Les dérivés *N*-salicylideneanilines sont parmi les composés synthétiques les plus étudiés du point de vue du thermo- et du photochromisme. Toutefois, à l'état solide le photochromisme est moins souvent présent dans ces systèmes, principalement dû aux conditions de volume nécessaires à la photoisomérisation *cis-trans* à la base du photoswitching (contraints stériques). Donc, tous les dérivés *N*-salicylideneaniline ne forment pas des solides photochromiques. Dans ce travail de thèse, la cocrystallisation est employée pour induire le photochromisme dans des chromophores *N*-salicylideneaniline non-photochromiques en l'état. Les systèmes multi-composants sont synthétisés suivant différentes stratégies supramoléculaires, qui se basent sur l'utilisation de ponts hydrogène(s) ou de ponts halogène(s). L'attention est portée sur la formation et la caractérisation de solides isomorphes et de solutions solides dérivées, avec comme objectif d'acquérir une meilleure compréhension fondamentale des facteurs structurels guidant l'expression du photochromisme dans les dérivés *N*-salicylideneaniline. Les dérivés *N*-salicylideneaniline et leurs cocristaux sont obtenus par synthèse méchanochimique effectuée dans un broyeur mécanique. Les caractéristiques structurales des solides cristallins sont analysées par diffraction des rayons X sur monocristaux et sur poudres (à température ambiante et basse température), spectroscopie d'émission et d'absorption à l'état solide, spectroscopie FTIR, et spectroscopie RMN ¹³C et ¹⁵N à l'état solide avec polarisation croisée à l'angle magique. La stabilité thermique est étudiée par analyse calorimétrique différentielle et analyse thermogravimétrique. Ces résultats ont révélé comment la cocrystallisation peut être employée avec succès dans le but de construire des bibliothèques de systèmes photochromiques, grâce aux changements induits à la fois au niveau du volume libre disponible dans la structure cristalline et aux nouvelles interactions moléculaires créées.

Dissertation doctorale en Sciences Chimiques

Namur, 25 Avril 2019

Université de Namur
FACULTÉ DES SCIENCES
Rue de Bruxelles 61 – 5000 Namur, Belgique

**Photochromic multicomponent crystalline materials
based on *N*-salicylideneanilines**

by **Andrea Carletta**

Abstract

N-salicylideneaniline derivatives are among the most studied man-made thermo- and photochromic systems. However, due to the volume requirements of the *cis*-*trans* photoisomerization at the basis of the photoswitching, photochromism is not easily encountered in the solid state; therefore, not every *N*-salicylideneaniline forms photochromic solids. Herein, cocrystallization is employed to induce photochromism in non-photochromic *N*-salicylideneaniline chromophores. The multicomponent systems are synthesized following various supramolecular synthetic strategies which envisage the use of hydrogen or halogen bonds. The focus is put on the formation and characterization of isomorphous solids and their solid solutions with the aim to gain insights on the structural factors controlling the expression of photochromism in *N*-salicylideneanilines.

N-salicylideneanilines and their cocrystals are obtained by mechanochemical synthesis performed in a ball mill. Structural features of the crystalline solids are analyzed by means of single-crystal (at room and low temperature) and powder X-ray diffraction (PXRD), solid-state (SS) absorption and emission spectroscopy, FTIR spectroscopy, and ¹³C and ¹⁵N crosspolarization magic angle spinning (CPMAS) SSNMR spectroscopy. Thermal stability of the solids is investigated by differential scanning calorimetry (DSC) and thermogravimetric analysis (TGA). These results reveal how cocrystallization can be successfully employed with the aim to build a library of photochromic systems thanks to the fact that it changes both the free available volume of each molecule in the crystal and the intermolecular interactions.

PhD thesis dissertation

Namur, 25 April 2019

Dedicated to Simone

*“The beautiful thing about learning is nobody
can take it away from you”*

B.B. King

Acknowledgements

Immeasurable appreciation and deepest gratitude are extended to the following persons who, in a way or another, have contributed to this thesis work.

Prof. Johan Wouters, not simply an advisor but my mentor, for his guidance, kindness and enthusiasm. Thank you for betting on me back in 2013. Thank you for believing in me throughout these four years of hard work.

Prof. Benoît Champagne (UNamur) and **Prof. Tom Leysens** (UCLouvain), members of the “*Comité d’accompagnement*”, for being always present with helpful advices and comments during my four years in the frame of the ARC ConTrast project. I will always remember and cherish the support you have given me.

Then, I would like to thank from the bottom of my heart **Xavier Buol**, **Céline Smulders** and **Margaux Simon**, for their invaluable work during their master thesis. Trying to be a good supervisor has been the most challenging yet gratifying thing of my PhD.

Bernadette Norberg and **Dr. Nikolay Tumanov** who supervised and mentored my work in crystallography, for their advices and attention in every step of my learning.

To the colleagues of the ARC ConTrast project: **Jean Quertinmont**, **Vanessa Seiler** and **Gabriel Mercier** for the time spent discussing and sharing ideas about photochromism. My thanks go to **Dr. Freddy Zutterman** and **Dr. Vincent Liegeois** for useful advices and to **Mégane Van Gysel** for fruitful collaboration.

To collaborators of UNamur: **Dr. Luca Fusaro** for guidance and support with the NMR technique. Thanks for the moments spent discussing about science (and more). **Dr. Sébastien Mouchet** for fruitful discussion and support with the microspectrophotometry. **Dr. Aurélie Plas** and **Prof. Steve Lanners** for introducing me to organic synthesis.

To **Prof. Fabrizia Grepioni**, **Dr. Simone d’Agostino**, **Dr. Floriana Spinelli** (Molecular Crystal Engineering Group University of Bologna), **Prof. Roberto Gobetto**, **Prof. Michele Chierotti** (Università degli Studi di Torino), **Dr. Barbara Ventura** (Italian National Research Council), **Prof.**

Dominik Cinčić, Prof. Vladimir Stilinović, and Dr. Marija Zbacnik (University of Zagreb) for fruitful collaboration on the topic halogen-bonded photochromic corystals. It has been an honor and a privilege working with you.

I would like to express my gratitude to **Dr. Aurora J. Cruz-Cabeza** from CCAPPE laboratory at the University of Manchester and all the members of the staff (especially **Dr. Riccardo Montis, Giulio Perini, Pietro Sacchi**) for welcoming me in their lab, for their patience and time spent together during my mancunian days.

To **Prof. Melwin Colaço** (St. Joseph's College, Bangalore) and **Luca Leoni** (Università La Sapienza, Roma) for fruitful collaboration on mechanochemical synthesis.

To all my fellow labmates in the CBS laboratory: **Anaëlle, Céline, Elise, Grégoire, Jenny, Jean, Kalina, Laurie, Marie, Mégane, Quentin, Sébastien and Thomas**. Many thanks for your presence and all the pleasant time we spent together.

I would like to thank all the PhD dissertation jury members (**Prof. Johan Wouters, Prof. Tom Leysens, Prof. Benoît Champagne, Dr. Laurence Leherter and Dr. Claudio Roscini**) for accepting to be part of the thesis committee.

I thank the **F.R.S.-FNRS** for financial support, the **PC₂** and **PTCI**.

Travel is better with friends. Big thanks to **Alvise, Arvin, Andrea, Benjamin, Carla, Fabiana, Francesco, Gauthier, Gaëlle, Giulio, Linda, Luca, Lucia, Marie, Maximilien, Pietro, Raphael, Riccardo, Rosaria, Rodolfo, Sabrina, Silvia, Sotiris, Stella, Thomas, Valerio, Xavier**.

Du fond du cœur, je remercie **Yvon, Nina and Nicolas**. Je suis profondément reconnaissant pour l'aide que vous m'avez apporté. Je ne pourrai jamais vous remercier assez.

Ringrazio la mia famiglia (**Clelia, Totino, Simone e Arcangelo**). Siete il mio orgoglio, la mia forza.

I conclude by thanking my awesome girlfriend, **Anaëlle**. From introducing me to solid state chemistry, to reading early drafts of my papers... to simply being my source of inspiration every day.

Table of Contents

Preface	1
Chapter 1. Introduction and aim of the work	11
<i>N</i> -salicylideneanilines: photochromism, bulky substitution, dihedral angle rule	11
<i>N</i> -salicylideneanilines vs <i>N</i> -salicylideneaminopyridines in the construction of multicomponent materials	16
Aim of the work	19
References	20
Chapter 2. Cocrystallization of <i>N</i>-salicylidene-3-aminopyridines with dicarboxylic acids: isostructurality, polymorphism and effects on photochromism	23
Introduction	24
Methods	26
Results and discussion	28
Solid-state synthesis and cocrystallization	28
Structural analysis	29
Solid-state photo- and thermochromism	34
Optical-structural property relationships	37
Conclusions	40
References	41
Chapter 3. <i>N</i>-salicylideneaminopyridinium salts and the strategy of the bulky anions: anion induced isostructurality, solid solubility and photochromism induced through tetra-aryl boxes	45
Introduction	46
Experimental methods	49
Results and discussion	53
Structural characterization	53
Photochromism and thermochromism	60
Dichroism of 1	63
Conclusions	65
References	66

Chapter 4. Designing photochromic materials through halogen bond: Bromo- vs Iodo-substitution	71
Introduction	72
Results and discussion	75
Structural characterization	75
Solid-state NMR	81
Thermochromic and photochromic behavior	85
Conclusions	95
Experimental Section	96
References	102
Chapter 5. Playing with structural isomers and stoichiometry	107
Introduction	108
Experimental Section	111
Results and Discussion	116
Structural Characterization	116
Solid-state photochromism	120
In-depth structural comparison: Predictability of photochromism based on Φ and V_{free}	122
Conclusions	128
References	130
Conclusion	137
Annex A to chapter 2	143
Annex B to chapter 3	161
Annex C to chapter 4	177
Annex D to chapter 5	207

Preface

Preface

Over the past decade, we have witnessed a growing interest in the development of cocrystallization procedures to address poor solubility issues of non-ionizable pharmaceutical molecules, or to improve other physicochemical properties such as melting point or hygroscopicity.¹⁻³ Cocrystallization (intended in the broadest sense of the word, *i.e.* combination of two entities in the same crystal lattice (**Figure 1**)) has also been employed as a resolution tool to resolve a racemic mixture of drug substances and, more recently, attention has been prompted to drug-drug formulations.^{4,5} Recent advances of cocrystallization lie in its use as a design element in the creation of **multipurpose materials**⁶ (see section 1.2). Luminescent⁷⁻⁹ or smart materials which respond to various external stimuli such as light¹⁰⁻¹² or heat,^{13,14} or even mechano-,¹⁵ solvato-,¹⁶ and vapo-responsive¹⁷ solids are few examples of multicomponent materials designed by cocrystallization.

In this renewed framework, this thesis deals with the advantages of **cocrystallization to develop organic photochromic crystalline materials**.^{10,18-20} Photochromism is a color change phenomenon occurring in materials due to reversible transformation of chemical species/molecules/substances following the absorption of electromagnetic radiation.²¹ Photochromic materials can lead to a broad range of applications, *e.g.* in information storage and electronic display systems, in optical switching devices like ophthalmic glasses, or in photomechanical materials.²¹ Understanding the relationship between the nature of the two components (the cofomer and the active molecule/chromophore), the crystal structure and the optical properties is at the heart of this work, because it will lead to a better understanding of the structure-optical relationships of solid materials and help for designing materials with improved photochromism.

One main advantage of cocrystallization is that one can potentially build an infinite number of crystal forms for the same molecule of interest (by varying the cocrystal former) without changing the chemical nature of the molecule itself.

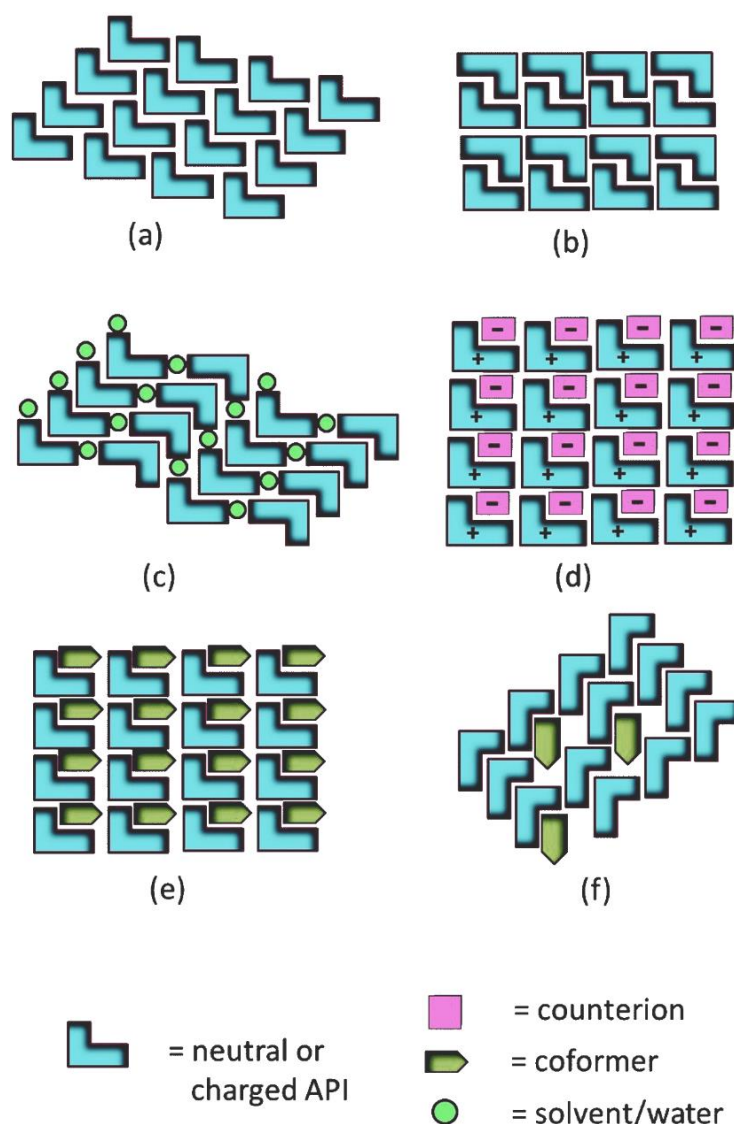


Figure 1. Polymorphs (a, b) and multicomponent solid forms (c-f): solvates (c), salts (d), cocrystals (e) and solid solutions (f).

The extensive work on cocrystallization has demonstrated how versatile this approach is for the creation of libraries of crystalline solids with newly-designed properties. Thanks to the last 30 years work in solid state chemistry, we are nowadays able to seek if two molecules are likely to combine to form cocrystals by simply applying the concept of “*supramolecular synthon*” (*i.e* spatial arrangements of intermolecular non-covalent interactions that frequently occur in supramolecular structures) introduced by Desiraju in its seminal work published in 1989.²² However, despite the huge progresses in the field of Crystal Packing Prediction (CSP), we are

not able yet to confidently predict how and in which ratio these molecules will assemble in the solid state.²³ Moreover, the ultimate goal of crystal engineering lies in the design of solids with desired physical and chemical properties through the study of intermolecular interactions and crystal packing.²⁴ But **are we there yet?** Are we really able to “*design*” solids with “*desired*” physical properties? These points were raised by Aakeröy in his opinion article called “*is there any point in making cocrystals?*” published in 2015:²⁵

“is there any point in making cocrystals?

*...what kind of fundamental new insight and understanding has this burst of activity generated? What we are learning from fundamental studies on the synthesis and characterization of cocrystals is already positively affecting the design of new functional solids, but equally important is the task of seeking a better understanding of how fundamental laws of physics manifest themselves in ordered crystalline materials.”*²⁵

The biggest concern of Aakeröy is that despite all the efforts made by the crystal engineering community, we are not able to translate these efforts into real fundamental knowledge yet. In other words, we are not able to link crystal structure to bulk properties. Why?

*“... it seems that the cocrystal community is occasionally a victim of its own success. ...One should not shy away from the fact that a large number of publications truly are ‘routine’ and merely offer a crystal-structure report, maybe accompanied by measurements of some rather random physical properties, without any design strategy in place or without discussing the new structural data in a larger relevant context.”*²⁵

As a matter of fact, despite the huge number of cocrystals that can be synthesized for one molecule, comparison of crystal structures is not always straightforward.

In which cases can cocrystals *differing in composition or structure* be compared? How can they be defined as similar or dissimilar? Which one of these dissimilarities will mostly affect their physicochemical properties?

One way of simplifying the problem is to favor the comparison of solids obtained by **keeping composition or crystal structure constant**.

Polymorphs are solids with *same composition but different crystalline structure* (**Figure 1**). An example of two polymorphic forms is graphite and diamond: they are made of the same atoms, but behave (and look) very different. Polymorphism is extensively studied for the dramatic effects molecular arrangement can have in dissolution/solubility/stability of pharmaceutical solids, therefore affecting the quality, safety and efficacy of the drug product.

In contrast, much less attention has been given to the study of isostructurality (**Figure 2**). The IUCr (International Union of Crystallography) defines isostructurality as: “Crystalline solids that have the *same structure, but not necessarily the same cell dimensions nor the same chemical composition*, and with a 'comparable' variability in the atomic coordinates to that of the cell dimensions and chemical composition”.²⁶ The lack of attention to this phenomenon is in part due to its rare occurrence.²⁷ In this context, another intriguing aspect of cocrystallization is its use for the construction of isostructural solid forms via **cocrystallization-induced isostructurality**.²⁷⁻³⁰ The solid-state structure of a compound is a function of the position and nature of the functional groups and the intermolecular forces. Consequently, molecules bearing different chemical functions tend to crystallize following distinct packing modes. The cocrystallization-induced isostructurality describes the use of cocrystallization as a tool to force two chemically different molecules, which possess distinct packing preferences, to form isostructural cocrystals. In other words, cocrystallization overcomes the functional group dissimilarities that determine the selection of the space group.²⁷⁻³⁰ Within the frame of designing isostructural photochromic materials, **two strategies** can be defined depending on which one of the two cocrystal partners (chromophore or coformer) is changed. Both these two approaches will be developed in this thesis work.^{10,14,31}

On the one hand, the strategy “**same chromophore/different coformer**”, permits to evaluate the supramolecular effects of the surroundings on a given chromophore embedded in several highly similar architectures (isostructural) which differ by subtle, systematic and predictable modifications (“single-point” modifications).

“Cocrystals represent new classes of compounds where bulk physical properties may be amenable to finetuning by making modular and controllable alterations to the crystalline lattice that ‘houses’ an active molecular species.”²⁵

On the other hand, the complementary production and evaluation of isostructural cocrystals obtained through the strategy “**different chromophore/same coformer**” would allow for corroboration of the hypotheses formulated in the first place.

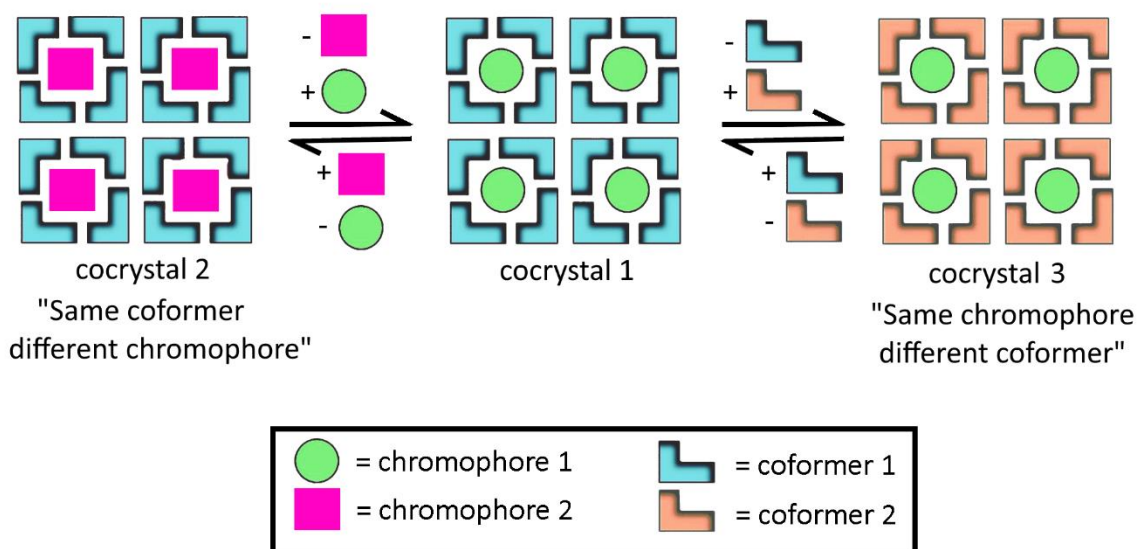


Figure 2. Isostructural cocrystals obtained from “cocrystal 1” by changing the active molecule (cocrystal 2) or the coformer (cocrystal 3)

Another topic that will be dealt with in this thesis is **substitutional solid solutions**.^{32–35} These compounds are multicomponent solids which do not obey Dalton’s law of multiple proportion. Their stoichiometry is not limited to integral values but can be varied in continuum (in a limited range of concentrations).^{32–35} Crystallographically

speaking, the components of a solid solution are not characterized by specific crystallographic positions, therefore, their structure is disordered. The two (or more) constituents of a solid solution may be soluble over a broad range of relative concentrations producing a crystalline solid with physical properties varying continuously over this concentration range or which shows characteristics of the combined substances.^{32–35} Solid solutions have been applied to various fields of crystal engineering to study optical, electrical, and photochemical properties of molecular and ionic crystals.^{36–39} Herein, solid solutions will be studied for *N*-salicylideneanilines (*chapter 2*) and *N*-salicylideneaminopyridinium salts (*chapter 3*).

From a technical point of view, both synthesis of chromophores and cocrystallization were performed in the solid state by ball milling. Output of the mechanosynthesis was studied by powder X-ray diffraction (PXRD) and structures of the cocrystals approached experimentally using single-crystal X-ray diffraction (SCXRD). Optical analysis of all obtained crystals and cocrystals was performed by considering their solid UV-Vis Diffuse Reflectance spectra taken before and after irradiation (in *chapter 4*, emission spectroscopy and SSNMR are also included in the study). Thermal stability of the solids was investigated by differential scanning calorimetry (DSC).

This work will be articulated as a publication thesis. Each chapter is composed of scientific papers containing the results obtained during four years of PhD studentship.

Chapter 1 is an introduction on photochromism and *N*-salicylideneanilines as model compounds for the study of photochromism in the solid state. Attention is given on the use of *N*-salicylideneaminopyridines as building blocks for cocrystal studies in place of *N*-salicylideneanilines (this part is adapted from a work we published in *CrystEngComm* in 2018). *Chapter 1* ends with the description of the objectives of this thesis work.

Chapter 2 contains the first work we authored on the topic “alteration of the photochromic properties by cocrystallization”. An *N*-salicylideneaminopyridine

crystallizing in a non-photochromic crystal was selected for cocrystallization studies with dicarboxylic acids. Cocrystallization affected both the starting color of the powders (which turned from orange to pale yellow) and their photoresponsiveness. We demonstrated how cocrystallization can be used to “turn photochromism on” in a non-photochromic chromophore and how this property lies on the crystal structure and not on the chromophore itself.

In *Chapter 3* the *N*-salicylideneaminopyridine, presented in *Chapter 2*, is alkylated to form alkylpyridinium derivatives. We reported the use of bulky counterions (tetraphenylborate salts) as the strategy to obtain photochromic solids.

In *Chapter 4* and *Chapter 5* is reported the application of the halogen bond in the construction/design of photochromic systems.

Chapter 6 contains the general conclusions on the whole set of results and perspectives of this thesis work.

Annexes A-D, containing supporting information to *Chapters 2-5*, conclude the thesis.

I conclude this preface by expressing my gratitude to all the co-authors of the publications included in this work.

Enjoy the reading.

- 1) Tilborg, A.; Norberg, B.; Wouters, J. *Eur. J. Med. Chem.* **2014**, *74*, 411–426.
- 2) Bolla, G.; Nangia, A.; Nangia, A.; Franco-Perez, J.; Jung-Cook, H.; Tanida, S.; Terada, K.; Quéré, L.; Raggueneau, V.; Maneglier, B.; Castaigne, S.; Chomienne, C.; Chrétien, S.; Rousselot, P.; Leboulch, P. *Chem. Commun.* **2016**, *52* (54), 8342–8360.
- 3) Duggirala, N. K.; Perry, M. L.; Almarsson, Ö.; Zaworotko, M. J. *Chem. Commun.* **2016**, *52* (4), 640–655.
- 4) Springuel, G.; Leyssens, T. *Cryst. Growth Des.* **2012**, *12* (7), 3374–3378.
- 5) Harmsen, B.; Leyssens, T. *Cryst. Growth Des.* **2018**, *18* (6), 3654–3660.
- 6) Christopherson, J.-C.; Topić, F.; Barrett, C. J.; Friščić, T. *Cryst. Growth Des.* **2018**, acs.cgd.7b01445.
- 7) Grepioni, F.; d’Agostino, S.; Braga, D.; Bertocco, A.; Catalano, L.; Ventura, B. *J. Mater. Chem. C* **2015**, *3* (36), 9425–9434.
- 8) d’Agostino, S.; Grepioni, F.; Braga, D.; Ventura, B. *Cryst. Growth Des.* **2015**, *15* (4), 2039–2045.
- 9) Yan, D.; Delori, A.; Lloyd, G. O.; Friščić, T.; Day, G. M.; Jones, W.; Lu, J.; Wei, M.; Evans, D. G.; Duan, X. *Angew. Chemie Int. Ed.* **2011**, *50* (52), 12483–12486.
- 10) Carletta, A.; Buol, X.; Leyssens, T.; Champagne, B.; Wouters, J. *J. Phys. Chem. C* **2016**, *120* (18), 10001–10008.
- 11) Mercier, G. M.; Robeyns, K.; Leyssens, T. *Cryst. Growth Des.* **2016**, *16* (6), 3198–3205.
- 12) Schmidt, G. M. J. *Pure Appl. Chem.* **1971**, *27* (4), 647–678.
- 13) Rawat, H.; Samanta, R.; Bhattacharya, B.; Deolka, S.; Dutta, A.; Dey, S.; Raju, K. B.; Reddy, C. M. *Cryst. Growth Des.* **2018**, *18* (5), 2918–2923.

- 14) Carletta, A.; Spinelli, F.; d'Agostino, S.; Ventura, B.; Chierotti, M. R.; Gobetto, R.; Wouters, J.; Grepioni, F. *Chem. - A Eur. J.* **2017**, *23* (22), 5317–5329.
- 15) Liu, G.; Liu, J.; Ye, X.; Nie, L.; Gu, P.; Tao, X.; Zhang, Q. *Angew. Chemie* **2017**, *129* (1), 204–208.
- 16) Sun, Y.; Lei, Y.; Dong, H.; Zhen, Y.; Hu, W. *J. Am. Chem. Soc.* **2018**, *140* (20), 6186–6189.
- 17) Adak, A.; Panda, T.; Raveendran, A.; Bejoymohandas, K. S.; Asha, K. S.; Prakasham, A. P.; Mukhopadhyay, B.; Panda, M. K. *ACS Omega* **2018**, *3* (5), 5291–5300.
- 18) Staehle, I. O.; Rodríguez-Molina, B.; Khan, S. I.; Garcia-Garibay, M. A. *Cryst. Growth Des.* **2014**, *14* (7), 3667–3673.
- 19) Sliwa, M.; Létard, S.; Malfant, I.; Nierlich, M.; Lacroix, P. G.; Asahi, T.; Masuhara, H.; Yu, P.; Nakatani, K. *Chem. Mater.* **2005**, *17* (18), 4727–4735.
- 20) Sliwa, M.; Mouton, N.; Ruckebusch, C.; Aloïse, S.; Poizat, O.; Buntinx, G.; Métivier, R.; Nakatani, K.; Masuhara, H.; Asahi, T. *J. Phys. Chem. C* **2009**, *113* (27), 11959–11968.
- 21) Zhang, J.; Zou, Q.; Tian, H. *Adv. Mater.* **2013**, *25* (3), 378–399.
- 22) Desiraju, G. R. (Gautam R. . *Crystal engineering : the design of organic solids*; Elsevier, 1989.
- 23) Cruz-Cabeza, A. J. *Sci. Comment. Acta Cryst* **2016**, *72*, 437–438.
- 24) Desiraju, G. R. *J. Am. Chem. Soc.* **2013**, *135* (27), 9952–9967.
- 25) Aakeröy, C. *Acta Crystallogr. Sect. B Struct. Sci. Cryst. Eng. Mater.* **2015**, *71* (4), 387–391.
- 26) Isomorphous crystals - Online Dictionary of Crystallography

- http://reference.iucr.org/dictionary/Isomorphous_crystals (accessed Feb 13, 2019).
- 27) Cinčić, D.; Friščić, T.; Jones, W. *New J. Chem.* **2008**, *32* (10), 1776–1781.
 - 28) Cinčić, D.; Friščić, T.; Jones, W. *Chem. Mater.* **2008**, *20* (21), 6623–6626.
 - 29) Cinčić, D.; Friščić, T.; Jones, W. *Chem. - A Eur. J.* **2008**, *14* (2), 747–753.
 - 30) Cinčić, D.; Friščić, T.; Jones, W. *Chem. Mater.* **2008**, *20* (21), 6623–6626.
 - 31) Carletta, A.; Colaço, M.; Mouchet, S. R.; Plas, A.; Tumanov, N.; Fusaro, L.; Champagne, B.; Lanners, S.; Wouters, J. *J. Phys Chem C.* **2018**, *122* (20), 10999–11007.
 - 32) Cruz-Cabeza, A. J.; Lestari, M.; Lusi, M. *Cryst. Growth Des.* **2018**, *18* (2), 855–863.
 - 33) Schur, E.; Nauha, E.; Lusi, M.; Bernstein, J. *Chem. - A Eur. J.* **2015**, *21* (4), 1735–1742.
 - 34) Lusi, M. *Cryst. Growth Des.* **2018**, *18* (6), 3704–3712.
 - 35) Lusi, M.; Vitorica-Yrezabal, I. J.; Zaworotko, M. J. *Cryst. Growth Des.* **2015**, *15* (8), 4098–4103.
 - 36) Weerasekara, R. K.; Uekusa, H.; Hettiarachchi, C. V. *Cryst. Growth Des.* **2017**, *17* (6), 3040–3047.
 - 37) d’Agostino, S.; Fornasari, L.; Grepioni, F.; Braga, D.; Rossi, F.; Chierotti, M. R.; Gobetto, R. *Chem. - A Eur. J.* **2018**, *24* (56), 15059–15066.
 - 38) Belitzky, A.; Weissbuch, I.; Posner-Diskin, Y.; Lahav, M.; Lubomirsky, I. *Cryst. Growth Des.* **2015**, *15* (5), 2445–2451.
 - 39) Theocharis, C. R.; Desiraju, G. R.; Jones, W. *J. Am. Chem. Soc.* **1984**, *106* (12), 3606–3609.

Chapter 1

Introduction and aim of the work

1.1 *N*-salicylideneanilines: photochromism, bulky substitution, dihedral angle rule

Photochromism is a chemical process, occurring under the influence of electromagnetic radiation, in which a compound undergoes a reversible change between two states having different absorption properties, *i.e.* different colors. The reversibility of the process is the reason for the many uses of photochromism. The back reaction can be induced photochemically (by light), by thermal means or simply by removing the light source (thermal decay).¹

Azo-benzenes, stilbenes, spiropyrans, diarylethenes, fulgides, or *N*-salicylideneanilines are among the most common photoswitchable molecules.² Photochromic materials can lead to a broad range of applications, *i.e.* in information storage and electronic display systems, in optical switching devices like ophthalmic glasses and sensors.¹ For practical use photochromic materials must develop a strong color rapidly upon irradiation, the return to the initial state must be controllable and the response must be constant through many coloration cycles.² Therefore, the understanding of the physics and chemistry of the color change and its utilization in technology has become a topic of extensive research. Photochromic materials have been produced by encapsulation of the chromophores in self-assembled molecular host-capsules³ or polymeric core-shell capsules,⁴ by dispersion in a polymeric matrix,⁵ or confinement in zeolites⁶ and in cyclodextrines.⁷ Development of crystalline photochromic materials has also been at the center of much of the research efforts in this field.² Crystalline forms of the original organic materials might be more stable and resistant to fatigue and they often show longer-lived meta-stable species.⁸ However, the reduced number of chromic systems responding at the crystal state, the limited understanding of the photochemical processes in these conditions and the fact that the response is often limited to the surface, represent the limitations in the use of crystalline materials.⁸

This thesis deals with the use of crystallization-based methods for development of materials with improved photochromic properties.^{9–11} *N*-salicylideneanilines (imines

of salicylaldehyde) are the systems we have chosen to study. These systems have received particular attention, due to the ease of preparation and their dual behavior, photochromic and thermochromic, in the solid state. The switching mechanism is based on three interconvertible species: a colorless enol form, a yellow *cis*-keto form and a red *trans*-keto form.¹²⁻¹⁵ The accepted mechanism for thermochromism is a temperature dependent ground-state keto-enol tautomerization via intramolecular proton transfer between the enol form and the *cis*-keto form. If these two forms are properly irradiated (~ 365 nm for the enol form and ~ 450 nm for the *cis*-keto form), they undergo a *cis-trans* photo-isomerization toward the *trans*-keto form (~ 560 nm), through the formation of an excited *cis*-keto intermediate, originating from an excited state intramolecular proton transfer (ESIPT) process in case of excitation of the enol tautomer.¹²⁻¹⁵ The process can be reversed either photochemically or by thermal means (**Figure 1**).¹

While thermochromism is a general property of *N*-salicylideneanilines, photochromism is encountered in a minor number of cases in the solid state. It has been suggested that the most important condition for the manifestation of photochromism of *N*-salicylideneanilines is a secure reaction volume sufficient for the photoinduced isomerization in the constrained solid media.

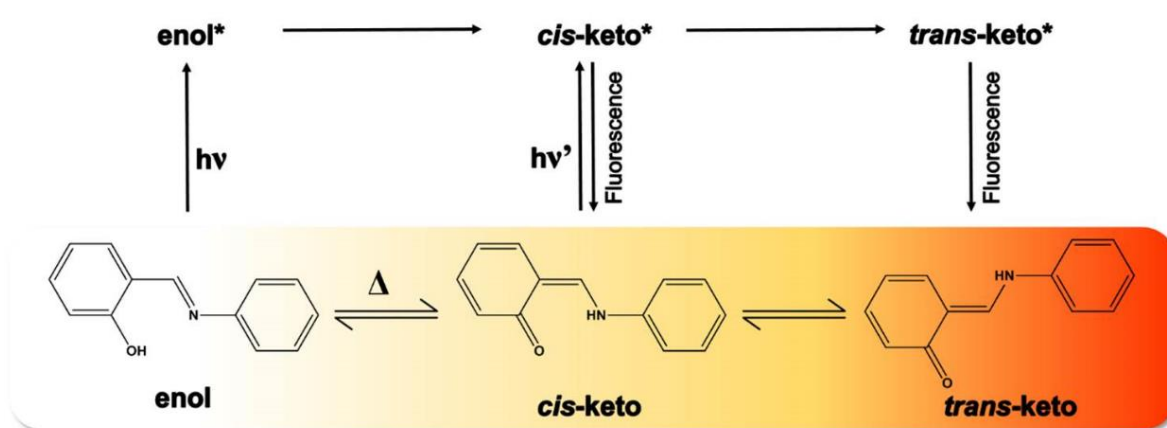


Figure 1. General pathway of ground and excited state thermo- and photochromic processes in *N*-salicylideneanilines.

Several works define the concept of open- versus closed-packed structures. Open structures are characterized by molecules in a twisted conformation (with dihedral angle between aryl rings, Φ , $> 30^\circ$). In contrast, closed-packed arrangements are characterized by near-planar molecules ($\Phi < 20^\circ$) stacked with short interplanar distances from 3.3 Å to 3.5 Å.¹⁶ These same parameters, along with the “free available volume (V_{free}), have also been proposed like descriptors of the likelihood of photochromism.^{12,17–19}

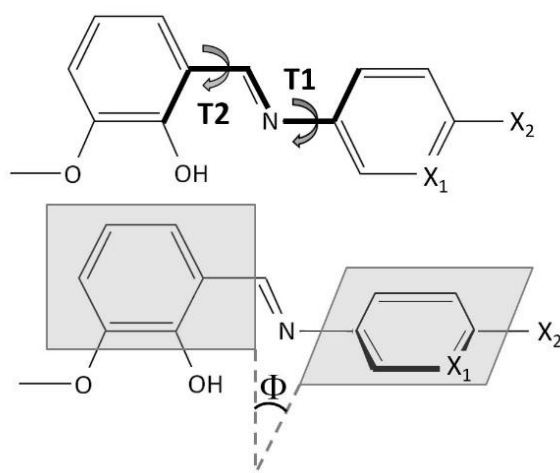


Figure 2. Definition of the **T1** and **T2** torsion angles and Φ in anil derivatives.

According to this concept, various synthetic methods for the selective preparation of photochromic *N*-salicylideneaniline crystals have been reported so far. Most of these methods consist in the introduction of bulky substituents which are meant to act as space openers to, eventually, generate photochromic solids.⁸ An example is represented by the introduction of *tert*-butyl groups at the 3,5-positions of the salicylidene moiety. Most of the crystals obtained with this approach show photochromic behavior (**Figure 3**, top). A second example has been provided by Garcia-Garibay and coworkers who reported an engineered *N*-salicylideneaniline derivative, acting also as molecular rotor, in which the *para*-positions are occupied by bulky trityl group (**Figure 3**, bottom).²⁰

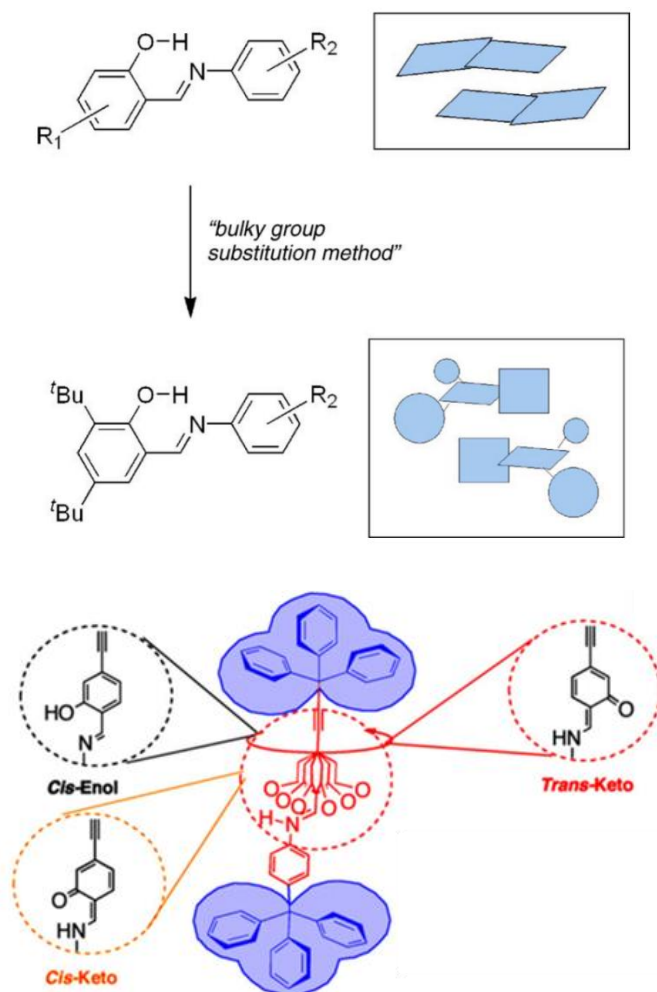


Figure 3. Bulky group substitution method.^{8,20}

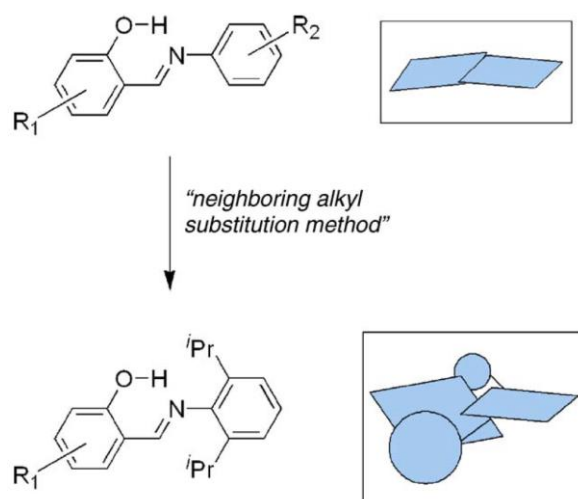


Figure 4. Chemical modification methods for engineering photochromism.^{8,20}

A second method for the preparation of photochromic crystals, the “*neighboring alkyl substitution method*” (**Figure 4**), is based on the introduction of alkyl groups at proper positions to avoid the non-photochromic planar conformation. The introduction of two alkyl groups at the 2,6-positions of aniline moiety has been shown to be the most effective substitution for this purpose.⁸

Besides being synthetically challenging, these approaches lead to new compounds that do not always present the required photochromic properties. Indeed, this approach has shown its limitations since changes in photochromic properties are induced by both the molecular environment and by the new chemical nature of the compound.²⁰ This aspect might be considered as one of the main reasons for which structural factors involved in the expression of photochromism in *N*-salicylideneanilines are not yet understood.²¹

In this context, we propose our cocrystallization approach as an alternative/complementary method to the chemical modification-based methods. The introduction of a cofomer in the crystalline system is expected to modify the interactions as well as the available volume providing the necessary degrees of freedom for the photoisomerization to occur. Changing the physical properties of the final assembly without altering the chemical nature of the main (chromophore) component represents an added value of this approach, that will be used to discover new features linking crystal structure to photochromism.

1.2 *N*-salicylideneanilines vs *N*-salicylideneaminopyridines in the construction of multicomponent materials[†]

N-salicylideneaminopyridines offer important advantages for what concerns the construction of multicomponent crystal forms with respect to the classical *N*-salicylideneaniline derivatives. In particular the N-atom of the pyridine moiety can act as a strong H- (see Chapter 2) or X-bond acceptor making the formation of cocrystals easier through these interactions.^{10,16,22} Alternatively, the N-atom can be easily alkylated to form various pyridinium salts (see Chapter 3).²³

Recently, we have reported a study conducted on an *N*-salicylideneaniline and an *N*-salicylideneaminopyridine to evaluate their ability to form cocrystals with a series of halogen bond donors.⁹ Over the past three decades halogen bonding²⁴ has been a growing area of research covering the fields of crystal engineering,²⁵ solution chemistry,²⁶ material chemistry.^{9,27–29} Compared to hydrogen bonding, halogen bonds tend to be much more directional with the typical R-X...Y bond angle being closer to 180°, and their strength can be easily tuned by the choice of the halogen atom (I or Br).³⁰ In spite of the continuously expanding research on halogen bonds, the data available in the Cambridge Structural Database (CSD)³¹ are limited compared to hydrogen bonds. The study of halogen-bonded cocrystals, *i.e.* multicomponent solids, has become one of the most attractive areas of research in the solid-state chemistry of halogen-bonded materials.²⁵ One of the main reasons for this interest lies in the continuous effort of supramolecular chemists to obtain sufficient data for establishing a complete insight into the flexibility and predictability of halogen bond synthons,³² as well as how these interactions may compete with each other and with hydrogen bonds.³³

[†]Adapted from: Carletta, Andrea, et al. "Halogen-bonded cocrystals of *N*-salicylidene Schiff bases and iodoperfluorinated benzenes: hydroxyl oxygen as a halogen bond acceptor." *CrystEngComm* 20 (2018): 5332-5339.

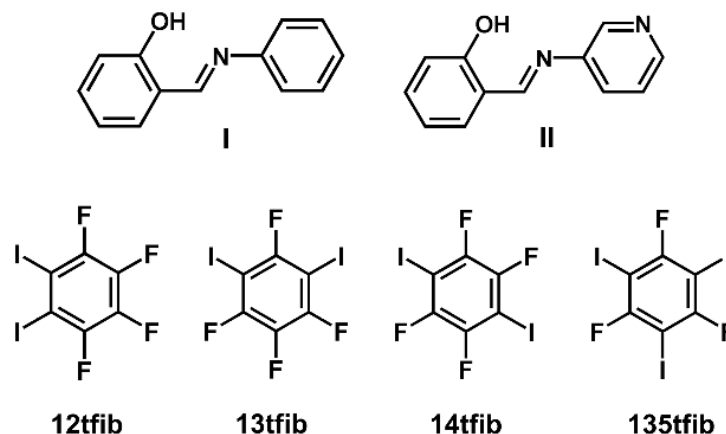


Figure 5. Halogen bond acceptors (first row) and donors (second row).

To explore the halogen bonding preference of the *o*-hydroxyimine hydroxyl group, we have prepared two imines as halogen bond acceptors: salicylideneaniline (**I**) and a 3-pyridyl analogue (**II**) derived by condensation of salicylaldehyde and 3-aminopyridine. These two Schiff bases were selected as two simplest representatives of *o*-hydroxyimines, where one (**II**) possesses a potentially competing halogen bond acceptor (pyridine nitrogen), and the other (**I**) does not (**Figure 5**). For cocrystal screening, as halogen bond donors we used perfluorinated iodobenzenes: 1,2-, 1,3-, 1,4-diiidotetrafluoro-benzene (**12tfib**, **13tfib**, **14tfib**) and 1,3,5-triiodotrifluoro-benzene (**135tfib**).

Our attempts to prepare cocrystals of **I** were generally unsuccessful and the only cocrystal of **I** obtained does not exhibit a halogen bond involving the hydroxyl oxygen (as one would expect) but exhibits an interaction of type C-I \cdots π (**Figure 6**). Similar interaction patterns have been reported by d'Agostino *et al* in the synthesis of cocrystals between *trans*-stilbene and **14tfib**.²⁸ Our results highlight that the O-atom of *N*-salicylideneaniline on its own does not provide sufficient bonding to allow formation of cocrystals through halogen bond.

The tendency toward cocrystal formation with halogen donors was found to be higher for derivative **II**. Cocrystals were obtained with three out of four of the selected donors: **II**·**14tfib**, **II**·**13tfib**, **II**·**135tfib**, **II**₂·**135tfib** (**Figure 7**). In all cases, the pyridine nitrogen is used in halogen bonding as expected. The hydroxyl group was found to act as a halogen bond acceptor in three out of four crystal structures

determined in this study: **II·13tfib**, **II·135tfib** and **II₂·135tfib**. This interaction acts as an important structural feature which, together with the I···N interaction, determines the overall crystal structure generating assemblies differing in type (chains, helices, tetramers) and composition (1:1 or 2:1 stoichiometry). As such, it represents a significant intermolecular interaction for crystal engineering using *o*-hydroxy Schiff bases.

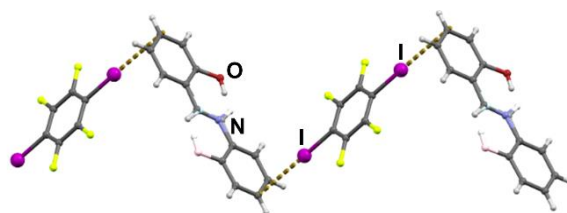


Figure 6. Halogen-bonded chain in the crystal structure of **I·14tfib**. Atoms of one component of the disordered molecule of **I** are shown a lighter colour.

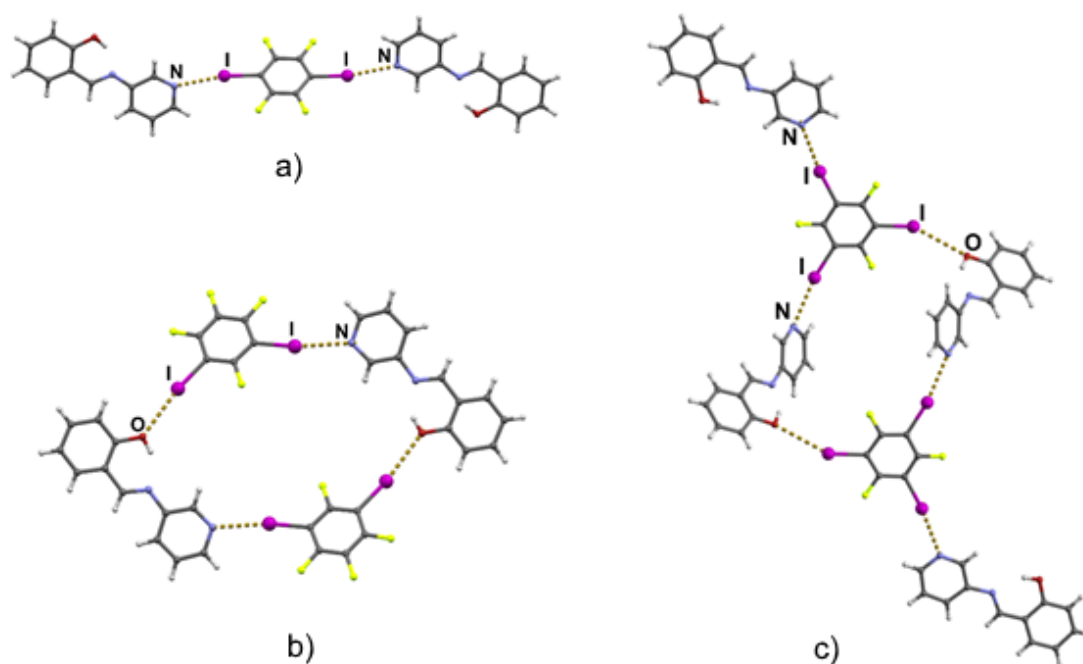


Figure 7. Halogen-bonded patterns of compound **II** with **14tfib** (a), **13tfib** (b) and **135tfib** (c).

1.3 Aim of the work

The two main objectives of this thesis are:

- **To verify if cocrystallization affects solid state photochromism.** To fulfill this task, a selection of chromophores is cocrystallized through various synthetic strategies: Hydrogen-bonded (*chapter 2*) and halogen-bonded cocrystals (*chapters 4 and 5*) or salts (*chapter 3*) are obtained.
- **To gain insight on the features responsible for photochromism in the solid state through the study of isostructural (co)crystals and solid solutions.** The currently adopted descriptors for prediction of photochromism in the solid state (Φ and V_{free}) are tested on isostructural solids and their solid solutions. If the two prediction rules are satisfied, no differences in the photochromic behavior should be observed within an isostructural series of solids. In *chapter 5*, these descriptors are also tested in cocrystals made of isomeric molecules. The advantage of working with isomers is that they have a similar (if not equal) molecular volume. This aspect allows a better comparison of the free available spaces between cocrystals.

1.4 References

- 1) Bamfield, P. *Chromic Phenomena*; Royal Society of Chemistry: Cambridge, **2010**.
- 2) Zhang, J.; Zou, Q.; Tian, H. *Adv. Mater.* **2013**, 25 (3), 378–399.
- 3) Sliwa, M.; Létard, S.; Malfant, I.; Nierlich, M.; Lacroix, P. G.; Asahi, T.; Masuhara, H.; Yu, P.; Nakatani, K. *Chem. Mater.* **2005**, 17 (18), 4727–4735.
- 4) Julià-López, A.; Hernando, J.; Ruiz-Molina, D.; González-Monje, P.; Sedó, J.; Roscini, C. *Angew. Chemie Int. Ed.* **2016**, 55 (48), 15044–15048.
- 5) Jochum, F. D.; Theato, P. *Macromolecules* **2009**, 42 (16), 5941–5945.
- 6) Casades, I.; Álvaro, M.; García, H.; Pillai, M. N. *European J. Org. Chem.* **2002**, 2002 (13), 2074.
- 7) Hadjoudis, E.; Yannakopoulou, K.; Chatziefthimiou, S. D.; Paulidou, A.; Mavridis, I. M. *J. Photochem. Photobiol. A Chem.* **2011**, 217 (2–3), 293–298.
- 8) Amimoto, K.; Kawato, T. *J. Photochem. Photobiol. C Photochem. Rev.* **2005**, 6 (4), 207–226.
- 9) Carletta, A.; Zbačnik, M.; Vitković, M.; Tumanov, N.; Stilinovic, V.; Wouters, J.; Cinčić, D. *CrystEngComm* **2018**, 20, 5332–5339
- 10) Carletta, A.; Spinelli, F.; d’Agostino, S.; Ventura, B.; Chierotti, M. R.; Gobetto, R.; Wouters, J.; Grepioni, F. *Chem. - A Eur. J.* **2017**, 23 (22), 5317–5329.
- 11) Weerasekara, R. K.; Uekusa, H.; Hettiarachchi, C. V. *Cryst. Growth Des.* **2017**, 17 (6), 3040–3047.
- 12) Hadjoudis, E.; Mavridis, I. M. *Chem. Soc. Rev.* **2004**, 33 (9), 579–588.
- 13) Harada, J.; Fujiwara, T.; Ogawa, K. *J. Am. Chem. Soc.* **2007**, 129 (51), 16216–16221.

- 14) Harada, J.; Uekusa, H.; Ohashi, Y. *J. Am. Chem. Soc.* **1999**, 121 (24), 5809–5810.
- 15) Ogawa, K.; Kasahara, Y.; Ohtani, Y.; Harada, J. *J. Am. Chem. Soc.* **1998**, 120 (28), 7107–7108.
- 16) Sugiyama, H.; Uekusa, H. *CrystEngComm* **2018**, 20 (15), 2144–2151.
- 17) Hutchins, K. M.; Dutta, S.; Loren, B. P.; MacGillivray, L. R. *Chem. Mater.* **2014**, 26 (10), 3042–3044.
- 18) Johmoto, K.; Sekine, A.; Uekusa, H. *Cryst. Growth Des.* **2012**, 12 (10), 4779–4786.
- 19) Robert, F.; Naik, A. D.; Tinant, B.; Robiette, R.; Garcia, Y. *Chem. - A Eur. J.* **2009**, 15 (17), 4327–4342.
- 20) Staehle, I. O.; Rodríguez-Molina, B.; Khan, S. I.; Garcia-Garibay, M. A. *Cryst. Growth Des.* **2014**, 14 (7), 3667–3673.
- 21) Houjou, H.; Kato, T.; Huang, H.; Suzuki, Y.; Yoshikawa, I.; Mutai, T. *Cryst. Growth Des.* **2019**, 19 (2), 1384–1390.
- 22) Zbačnik, M.; Vitković, M.; Vulić, V.; Nogalo, I.; Cinčić, D. *Cryst. Growth Des.* **2016**, 16 (11), 6381–6389.
- 23) Carletta, A.; Colaço, M.; Mouchet, S. R.; Plas, A.; Tumanov, N.; Fusaro, L.; Champagne, B.; Lanners, S.; Wouters, J. *J Phys Chem C* **2018**, 122, 20, 10999-11007
- 24) Cavallo, G.; Metrangolo, P.; Milani, R.; Pilati, T.; Priimägi, A.; Resnati, G.; Terraneo, G. *Chem. Rev.* **2016**, 116 (4), 2478–2601.
- 25) Raatikainen, K.; Rissanen, K. *CrystEngComm* **2011**, 13 (23), 6972.
- 26) Beale, T. M.; Chudzinski, M. G.; Sarwar, M. G.; Taylor, M. S. *Chem. Soc. Rev.* **2013**, 42 (4), 1667–1680.

- 27) Priimagi, A.; Cavallo, G.; Metrangolo, P.; Resnati, G. *Acc. Chem. Res.* **2013**, 46 (11), 2686–2695.
- 28) d’Agostino, S.; Grepioni, F.; Braga, D.; Ventura, B. *Cryst. Growth Des.* **2015**, 15 (4), 2039–2045.
- 29) Christopherson, J.-C.; Topić, F.; Barrett, C. J.; Friščić, T. *Cryst. Growth Des.* **2018**, 18 (2), 1245–1259.
- 30) Metrangolo, P.; Neukirch, H.; Pilati, T.; and Resnati, G. *Acc. Chem. Res.* **2005**, 38(5), 386-395.
- 31) Groom, C. R.; Bruno, I. J.; Lightfoot, M. P.; Ward, S. C.; IUCr. *Acta Crystallogr. Sect. B Struct. Sci. Cryst. Eng. Mater.* **2016**, 72 (2), 171–179.
- 32) Fourmigué, M. *Curr. Opin. Solid State Mater. Sci.* **2009**, 13 (3–4), 36–45.
- 33) Aakeröy, C. B.; Wijethunga, T. K.; Haj, M. A.; Desper, J.; Moore, C. *CrystEngComm* **2014**, 16 (31), 7218.

Chapter 2

Cocrystallization of N-salicylidene-3-aminopyridines with dicarboxylic acids: isostructurality, polymorphism and effects on photochromism.[†]

[†]Carletta, Andrea, et al. "Polymorphic and isomorphous cocrystals of a *N*-salicylidene-3-aminopyridine with dicarboxylic acids: tuning of solid-state photo-and thermochromism." *The Journal of Physical Chemistry C* 120 (2016): 10001-10008.

Polymorphic and Isomorphic Cocrystals of a *N*-salicylidene-3-aminopyridine with Dicarboxylic Acids: Tuning of Solid-state Photo- and Thermo-chromism

Andrea Carletta,¹ Xavier Buol,¹ Tom Leyssens,² Benoît Champagne,¹ and Johan Wouters*¹

¹ Unité de Chimie Physique, Théorique et Structurale, Chemistry Department, University of Namur, 61 rue de Bruxelles, B-5000 Namur, Belgium

² Institute of Condensed Matter and Nanosciences, Université Catholique de Louvain, Louvain-La-Neuve, Belgium

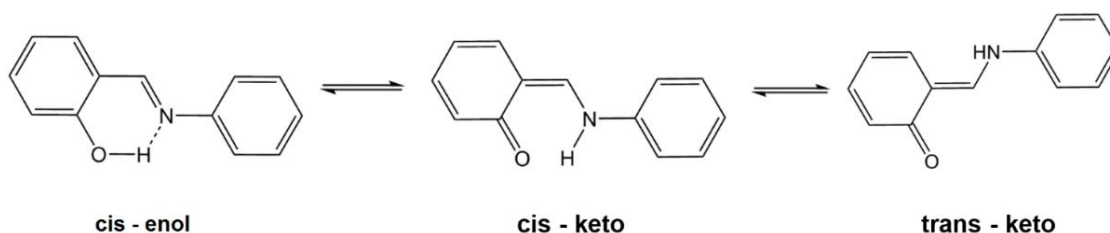
Abstract. The crystal structures and optical properties of (*E*)-2-methoxy-6-(pyridin-3-yliminomethyl)phenol (**1**), a *N*-salicylidene-3-aminopyridine, and its 2:1 dimorphic cocrystals with fumaric acid (**2** and **3**) and succinic acid (**4** and **5**) were studied at solid state in order to understand the effects of cocrystallization and molecular packing on their photo- and thermo-chromic behavior. New criteria for prediction of the chromic properties, based on the rationalization of the intermolecular interaction in the crystal, are also proposed. These results confirm once more the influence of the molecular packing on the chromic properties of solids and extend it, to polymorphic and isomorphic cocrystals.

2.1. Introduction

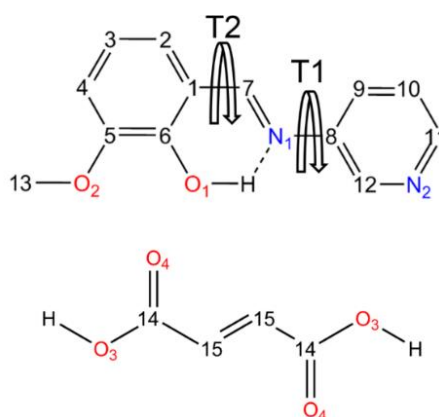
Dynamic materials are characterized by their potential to adjust their structure and properties in response to environmental stimuli. Such dynamic materials offer advantages as selected properties can reversibly be turned ‘on’ and ‘off’. Thermo- and photochromic systems, can change their color in response to temperature variation and light irradiation, respectively. Those materials can lead to a broad range of applications, *e.g.* in information storage and electronic display systems, in optical switching devices like ophthalmic glasses and in non-linear optics.¹⁻⁴

N-Salicylideneanilines (anils) are among the most common photo- and thermo-switchable molecules. They are documented to exhibit both thermo- and photochromism at the solid state.⁵⁻⁶ The accepted mechanism for thermochromism is a temperature dependent keto-enol tautomerization between an uncolored enol form and a yellow *cis*-keto form.⁷ When properly irradiated, the enol form and the *cis*-keto form produce a red *trans*-keto form, the photoproduct, by *cis-trans* isomerization (**Scheme 1**).⁸

While thermochromism is a general property of anils in the solid state, photochromism is not easily encountered in crystalline state.⁵ It has been stated that both properties are dependent on geometric considerations (in particular **T1** and **T2** torsion angles, **Scheme 2**) and steric requirements. According to these empirical rules, near-planar anils (**T1**, should be less than 20°) in closed packed environment are more likely to exhibit thermochromic properties. In contrast, non-planar conformations (**T1** > 30°) and open crystal structures promote a photochromic character (**Scheme 2**).⁹⁻¹⁰ To remediate these issues, efforts have focused on changing the nature of the molecule, by chemical modification, by introduction of bulky groups, to open the crystal packing and facilitate the molecular motions.¹¹⁻¹³ Another promising alternative consists in modifying the crystal structure by a crystal engineering approach. Confining the molecules in metal organic frameworks (MOFs),¹⁴⁻¹⁵ encapsulating them in cyclodextrines,¹⁶ or dispersing them in a polymeric matrix can induce photochromism in a *N*-salicylideneaniline derivative.



Scheme 1. General pathway of thermo- and photochromism in the case of *N*-salicylideneanilines



Scheme 2. Crystallographic numbering scheme for chromophore (*E*)-2-methoxy-6-(pyridin-3-yliminomethyl)phenol (**1**) and for fumaric acid (**FA**). **T1** refers to C7-N1-C8-C9 torsion angle and **T2** to the C6-C1-C7-N1 angle. Numbering scheme for succinic acid (**SA**) is the same as for **FA** (half molecule is generated by an inversion point center in the middle of the C15–C15 double bond)

Cocrystallization, *i.e.* the combination of two neutral molecules in the same crystal lattice, has also been recently employed for this purpose.^{9,17} The introduction of a cofomer in the crystalline system modifies the intermolecular interactions as well as the available volume and, therefore, could provide extra degrees of freedom. The physical properties of the final assembly can, therefore, be tuned without altering the chemical nature of the main (chromophore) component. In this study, we present the crystal structures of (*E*)-2-methoxy-6-(pyridin-3-yliminomethyl)phenol (**1**, **Scheme 2**), a *N*-salicylidene-3-aminopyridine, and its 2:1 dimorphic cocrystals with fumaric acid (**2** and **3**) and succinic acid (**4** and **5**).

Mechanochemical synthesis is used to prepare the solids of interest. Optical solid-state properties are also studied, by means of UV-Vis diffuse reflectance spectroscopy in order to understand the effects of cocrystallization and molecular packing on their photo- and thermochromic behavior.

2.2. Methods

Materials. *Ortho*-Vanillin and 3-aminopyridine were sourced from Sigma-Aldrich (Steinheim, Germany) and used as received. Solvents used for crystallization are commercially available (Acros Organic, Geel, Belgium) and were used without further purification.

Grinding experiments. Dry grinding was performed with a Retsch MM 400 Mixer Mill, equipped with two grinding jars in which five 2-mL Eppendorf tubes can be installed and eight to ten stainless steel grinding balls (1 mm diameter) in a sample.

Single-Crystal X-Ray Diffraction (SCXRD). SCXRD experiments were performed on a Gemini Ultra R system (4-circle kappa platform, Ruby CCD detector) using Mo K α ($\lambda = 0.71073 \text{ \AA}$) (for 1 and 5) and Cu K α ($\lambda = 1.54184 \text{ \AA}$) (for 2-4) radiations. Selected crystals were mounted on the tip of a quartz pin using cyanoacrylate (Commercial glue). Full data sets were collected at room temperature after cell parameters were estimated from a pre-experiment run. Structures were solved by direct methods using WinGX suite of programs with Sir-2014 and then refined using SHELXL-2014. Non-hydrogen atoms were anisotropically refined and the hydrogen atoms (not implicated in H-bonds) in the riding mode with isotropic temperature factors fixed at 1.2 times $U(\text{eq})$ of the parent atoms. Hydrogen atoms implicated in hydrogen bonds were localized by Fourier difference maps. CCDC 1456341, 1060634, 1060636, 1400289 and 1456340 entries contain the supplementary crystallographic data for this paper and can be obtained free of charge via www.ccdc.cam.ac.uk/data_request/cif.

Powder X-Ray Diffraction (PXRD) Diffraction data have been collected on a PANalytical Bragg–Brentano diffractometer, using Ni-filtered Cu K α radiation ($\lambda=1.54179$ Å) at 40 kV and 40 mA with a X'Celerator detector. Each sample was analyzed between 4 and 50° in 2 θ with a step size of ca. 0.0167° and a total scan time of 3 min 48 s.

Structure visualization and exploration of the crystal packing. Images from structural data were drawn with Mercury v. 3.1¹⁸ software. Hirshfeld surfaces mapped with D_{norm} function and 2D molecular fingerprint plots were used in order to rationalize intermolecular interactions. The calculated surfaces are mapped using the Auto function of color scaling of Crystal Explorer v.3.¹⁹ In total, 52 structures were retrieved and fully analyzed with Mercury v. 3.1 and Crystal Explorer v.3 software along with 1-4 of this work.

Search in the Cambridge Structural Database (CSD). A statistical study in CSD²⁰ (updated January 2016) for the two tautomeric forms was performed using the ConQuest program to search and retrieve information, with a two-dimensional representation of the compound as search group. Only structures with an R-factor < 5 and with no disorder were used for the calculation of the average bond lengths in the enol (415 structures found) and *cis*-keto tautomer (31 structures found).

Diffuse reflectance spectroscopy. Spectra were recorded on a Varian 5E spectrophotometer. Pure powdered solids have been used for measurement to avoid matrix effects. Thermal fading rate was determined at 555 nm.

Differential Scanning Calorimetry (DSC). DSC analysis was performed from 80°C to 200°C at a scanning rate of 5°C/min on a Perkin Elmer DSC 7.0, equipped with the data analyzer and data treatment program PYRIS 1997-1998. Solid samples (mass of ca. 3 mg) were placed in aluminum sample pans with pierced sealed lids and helium was used as purge gas with a flow rate of 40 mL/min.

2.3. Results and discussion

2.3.1. Solid-state synthesis and cocrystallization

Compound **1** ((*E*)-2-methoxy-6-(pyridin-3-yliminomethyl)phenol) was synthesized by dry grinding (in a ball mill) of equimolar amounts of 3-aminopyridine and *ortho*-vanillin.²¹⁻²² The orange powder product obtained, was analyzed by powder X-ray diffraction (PXRD) analysis. Presence of new peaks due to the formation of the Schiff base are detected. Residual peaks of 3-aminopyridine (*i.e.* around 20.4°, 23.4° and 28.8°) are still observed while contribution from *ortho*-vanillin is not detected anymore confirming a near-total conversion of the reactants (**Figure S1**).

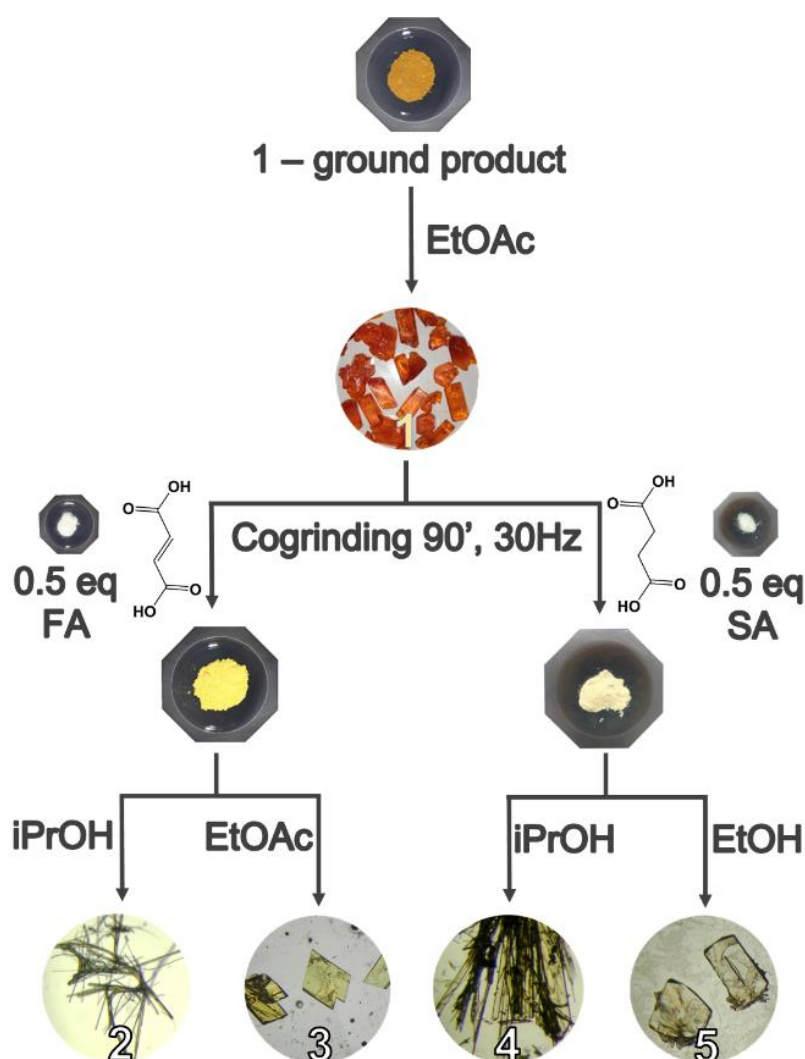


Figure 1. Synthetic route to cocrystals with FA (**2** and **3**) and with SA (**4** and **5**)

Orange prism-like single crystals of compound **1**, suitable for X-ray analysis, were obtained by slow evaporation from a saturated solution in ethyl acetate after 3 days. Dimorphic cocrystals of type $(\mathbf{1})_2 \cdot \mathbf{FA}$ (labelled **2** and **3**) and of type $(\mathbf{1})_2 \cdot \mathbf{SA}$ (labelled **4** and **5**) were synthesized in the solid state according to the scheme presented in **Figure 1**. Cogrounding of **1** with **FA** in a 2:1 molar ratio, (for 90' at 30 Hz) resulted in a yellow crystalline powder. PXRD analysis of the ground product reveals partial but selective formation of **3**. Recrystallization in several solvents was performed in order to obtain single-crystals suitable for X-ray diffraction. Yellow needle crystals of **2** were obtained by slow evaporation from a saturated solution in 2-propanol. Yellow plate crystals of **3** were obtained by recrystallization in ethyl acetate. Cogrounding of crystals of **1** with **SA** in a 2:1 molar ratio, (for 90' at 30 Hz) yielded a white crystalline powder. PXRD diffractogram of this product shows peaks characteristic of **5**. Recrystallization in 2-propanol yielded yellow needles (cocrystal **4**) after 4 days. Colorless blocks of **5** were instead obtained from a saturated ethanol solution (**Figure S2** and **S3**).

2.3.2. Structural analysis

Single crystals of all obtained material were structurally investigated by single crystal X-ray diffraction (SCXRD) at room temperature. Structure of **1** has already been reported (CSD refcode EDEQAG²³).

Crystal 1. The orange prisms of **1** belong to the orthorhombic crystal system, with $P2_12_12_1$ as space group. Compound **1** molecules adopt a twisted conformation ($\mathbf{T1} = -32.2(3)^\circ$) with a near-planar $\mathbf{T2}$ torsion angle ($\mathbf{T2} = 2.0(3)^\circ$) constrained at this value by the presence of an intramolecular H-bond forming a 6-membered pseudo-ring ($\text{O1} \cdots \text{H1O} \cdots \text{N1}$, $S_1^1(6)$). Selected bond lengths are given in **Table 1**.

Cocrystal 2. The obtained yellow needle-like crystals belong to the monoclinic crystal system, space group $P2_1/n$. The asymmetric unit contains one molecule of **1** and a half molecule of **FA**.

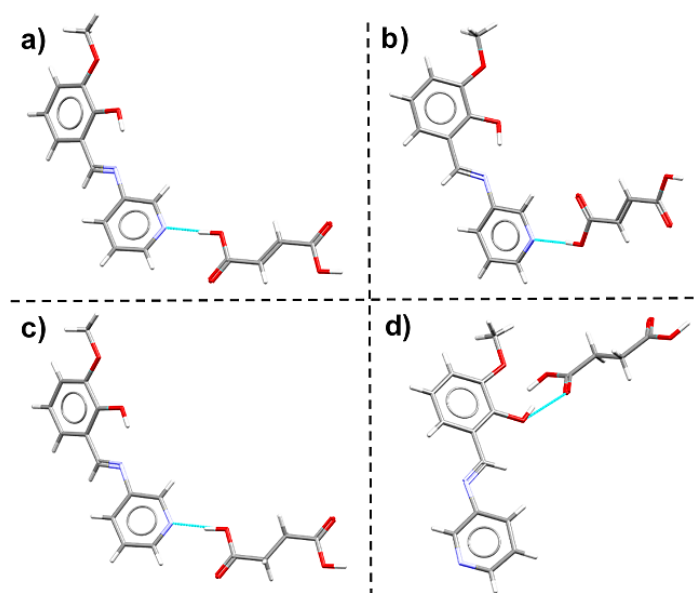


Figure 2. Supramolecular synthons in cocrystal **2** (a), **3** (b), **4** (c) and **5** (d).

The structure corresponds to a cocrystal and not a salt, as clearly indicated by C=O and C–O double and single bond lengths for the carboxylic acids of **FA**. The protons remain on the carboxylic group of the coformer. In the crystal network, cocrystal former and chromophore are noncovalently bonded by a $\text{OH}\cdots\text{N}_{(\text{pyridine})}$ H-bond ($\text{O3}-\text{H2O}\cdots\text{N2}$, $D_2^2(10)$). The carbonyl group of **FA** works as acceptor towards several C–H groups of three distinct compound **1** molecules giving rise to the $\text{C11}-\text{H11}\cdots\text{O4}$ (with the same molecule, **Figure 2**), $\text{C10}-\text{H10}\cdots\text{O4}$ and $\text{C13}-\text{H13}\cdots\text{O4}$ short contacts (**Figure 3**). Compound **1** molecules adopt a $\mathbf{T1} = -31.3(4)^\circ$ tilted conformation with a near-planar $\mathbf{T2}$ torsion angle ($\mathbf{T2} = 1.0(4)^\circ$). The major tautomeric form observed at room temperature is the enol form, as deduced from bond lengths (**Table 1**, **Figure S7** and **S8**).

Cocrystal 3. The obtained yellow plates belong to the same crystal system and group like **2** ($P2_1/n$). Here also a molecule of **FA** binds two molecules of **1** by H-bonding the *N*-atom in the pyridine moiety to form a cocrystal, not a salt. The formed supramolecular synthon is different from **2** being the $\text{C12}-\text{H12}$ bond involved in a short contact with the O4 atom of **FA** ($\text{C12}-\text{H12}\cdots\text{O4}$, **Figure 2**).

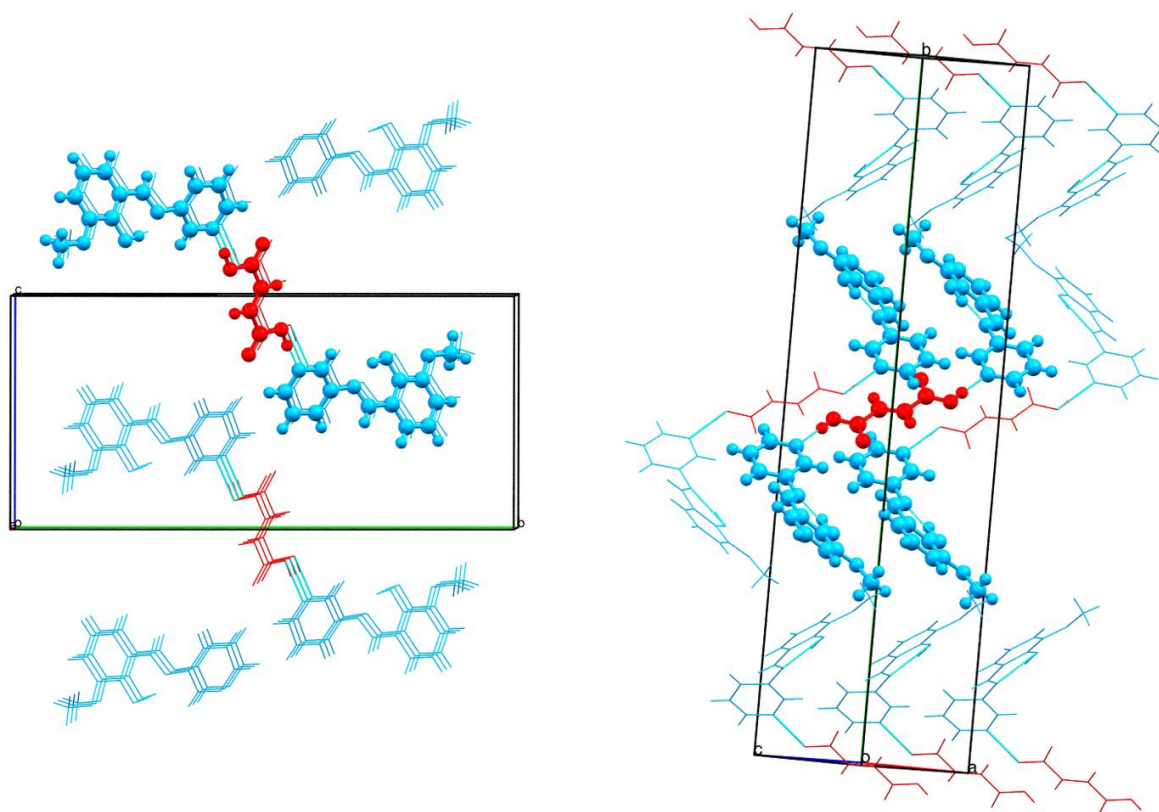


Figure 3. Crystal packing of cocrystal **2** (left) and **3** (right). **FA** is represented in red, the chromophore in blue.

Another relevant difference in the packing concerns the disposition of the **FA** in the crystal structure. In **3**, a molecule of **FA** is sandwiched between two pyridine moieties of two anil molecules. The conformation adopted by the chromophore is characterized by a dihedral angle between ring planes, Φ , of about 41.0° (**T1** = $40.6(3)^\circ$, **T2** = $1.4(3)^\circ$). The major tautomeric form observed at room temperature is the enol form, as deduced from bond lengths (**Table 1**).

Cocrystal 4. The obtained yellow needle-like crystals belong to the monoclinic space group $P2_1/n$. The asymmetric unit contains one molecule of **1** and a half molecule of **SA**. X-ray diffraction data revealed the isostructurality between **4** and **2**. Torsion angle values are $-31.6(2)^\circ$ and $0.7(2)^\circ$ for **T1** and **T2**, respectively. The major tautomeric form observed at room temperature is mainly the enol form.

Cocrystal 5. The colorless block obtained belong to the monoclinic crystal system, space group $I2/a$. The found crystal structure is a 2:1 cocrystal of **1** and **SA**. The structure is a polymorph of cocrystal **4** (**Figure 4**). Interestingly, insertion of a molecule of **SA** in the crystal network causes disruption of the intramolecular $O1-H1O\cdots N1$ H-bond needed for the tautomerization and the cis/trans isomerization processes. Therefore, molecules are under the *trans*-enol form. Torsion angle values are $15.0(2)^\circ$ and $-174.90(14)^\circ$ for **T1** and **T2**, respectively.

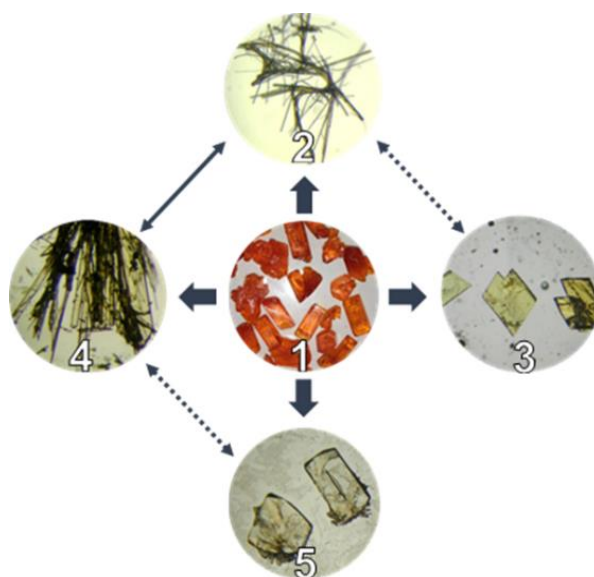


Figure 4. Structural relationship between cocrystals. Dashed double arrows indicates crystals related by polymorphism (**2 vs 3**, and **4 vs 5**). A solid double arrow indicates isomorphism (**2 vs 4**).

Structure information can be retrieved from comparison of bond lengths of the six-membered pseudo-cycle $N1-C7-Cl-C6-O1-H1O$ of **1-4** with those of **5** (**Table 1**). Remarkably, bond lengths of **5** pseudo-cycle differ from those of other crystal structures, due to the presence of Resonance-Assisted Hydrogen Bonding (RAHB) in **1-4**.²⁴ A survey on the CSD (last update January 2016) has also been performed for *cis*-enol and *cis*-keto anil structures in order to find the average bond length values for the two tautomers (**Table 1**).

Table 1. Bond lengths of the six-membered pseudo-ring of the five crystallographic structures, and average values retrieved from the CSD survey.

Bond	1-RT (Å)	2-RT (Å)	3-RT (Å)	4-RT (Å)	5-RT (Å)
N1–C7	1.281(3)	1.284(3)	1.281(3)	1.281(2)	1.266(2)
C7–C1	1.448(3)	1.444(3)	1.446(3)	1.446(2)	1.459(2)
C1–C6	1.403(3)	1.400(3)	1.403(3)	1.402(2)	1.398(2)
C6–O1	1.353(3)	1.350(3)	1.350(2)	1.346(2)	1.357(2)
O1–H10	0.95(3)	0.90(4)	0.96(3)	0.86(2)	0.89(2)
	Average <i>cis-enol</i> structure (Å)	Average <i>cis-keto</i> structure (Å)			
N1–C7	1.282	1.303			
C7–C1	1.446	1.411			
C1–C6	1.406	1.432			
C6–O1	1.347	1.294			
O1–H10	0.892	/			
N1–H10	/	0.929			

We found a number of 415 structures under the *cis-enol* form and 31 structures under the *cis-keto* form. Comparison of **1-4** bond length with the average bond lengths of *cis-enol* and *cis-keto* forms allow to attribute unambiguously **1-4** to the *cis-enol* form (**Table 1**). Indeed, attempts to observe the keto form by using the crystal data collected at room temperature have been unsuccessful. Fourier difference maps do not show in any case a significant residual electronic density peak located near the N1 nitrogen atom, compatible with a keto character for the room temperature structures. This aspect is in agreement with the fact that the keto form is detectable by room temperature SCXRD only if the O-atom is acceptor of an intermolecular H-bond that stabilizes this form.⁷ **Figure 4** summarizes structural relationships between crystal structures of **1-5**.

In all cases, PXRD patterns simulated on the basis of the single crystal structure coordinates match the experimental PXRD data collected on the bulk powdered crystals, confirming that the structures reported for each new cocrystal correspond to

the whole batch that will be further characterized by UV-Vis solid-state spectroscopy.

2.3.3. Solid-state photo- and thermochromism

In order to determine the solid-state thermochromic behavior of crystals of **1** and of its cocrystals, a visual evaluation of the color before and after immersion in liquid nitrogen (77 K) was first performed. Crystals of **1** were found to be strongly thermochromic with a color change from orange-red to the pale yellow (**Figure 5** and **S9**). On the contrary, only a weak color change from the yellow to the pale yellow was found for **2**, **3** and **4** when the temperature lowered. No color change was found for **5**, in accordance with the fact that tautomerization cannot take place in absence of the intramolecular H-bond.

Solid-state photochromism of the samples was also investigated. After 60' irradiation at 365 nm, crystalline powders of **1** and **5** did not change their color whereas a strong photochromism from the yellow to the orange-red was found for **2-4** (**Figure 5**).

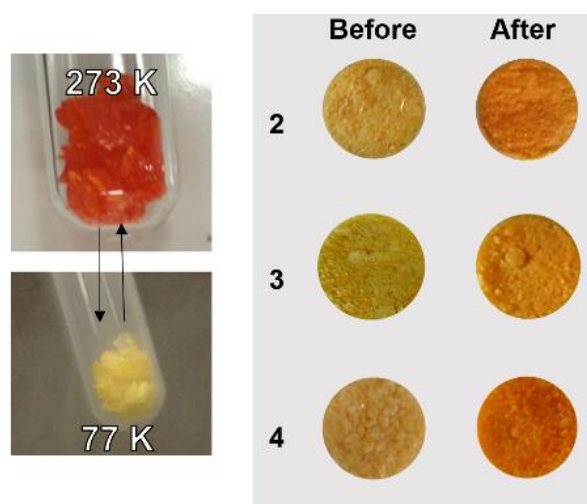


Figure 5. Thermochromism in crystals of **1** (left). Color of microcrystalline powder of **2**, **3** and **4** before and after UV irradiation (365 nm, right).

In order to determine the relative contributions of the *cis*-enol and the keto forms UV-diffuse reflectance measurements before and after UV irradiation²⁵ were carried

out for pure powders of **1-5** (**Figure 5**). No photochromic response (*i.e* no difference between the spectra taken before and after irradiation) was observed for **1** and **5** (**Figure S10**). The spectrum of **1** is characterized by a large absorption band below 450 nm, which is assigned to the *cis*-enol form, and by a second band that extends from 450 nm to 550 nm which is assigned to the *cis*-keto form. The spectrum of **5**, is characterized by a unique absorption band (λ_{max} at 375 nm) extending up to 420 nm, assigned to the *trans*-enol form. Spectra of **2-4** are very similar, also being characterized by an absorption band under 450 nm and a weak shoulder that extends up to 550 nm. This latter can be assigned to the small equilibrium concentration of *cis*-keto form which explains the yellow coloration of these cocrystals. A dramatic change in the spectra of **2-4** is detected after UV irradiation (at 365 nm). Three different bands are detected corresponding to the enol form and keto forms of (*E*)-2-methoxy-6-(pyridin-3-yliminomethyl)phenol. The band below 450 nm corresponds to the enol form whereas a contribution of the *cis*-keto form is observed between 450 and 550 nm. Above 550 nm, a third band appears which is attributed to the *trans*-keto form (**Figure 6**)²⁶. Enhancement of the keto absorption was similar for the isostructural cocrystals **2** and **4** which present an increasing factor¹¹ of about 3.39 and 3.52, respectively. The increasing factor in keto form for **3** is instead of about 2.53. Kinetic analysis of the thermal fading reaction of the photoinduced species were performed on **2** and **3** by using the following equation:⁹

$$\ln \left(\frac{A_0 - A_\infty}{A_t - A_\infty} \right) = kt$$

where A_0 , A_t and A_∞ are the absorbance values at 0 at a time t , and at the time when the recovery of the initial state is complete, respectively; k represents the rate constant (s^{-1}) and t is the time (s).

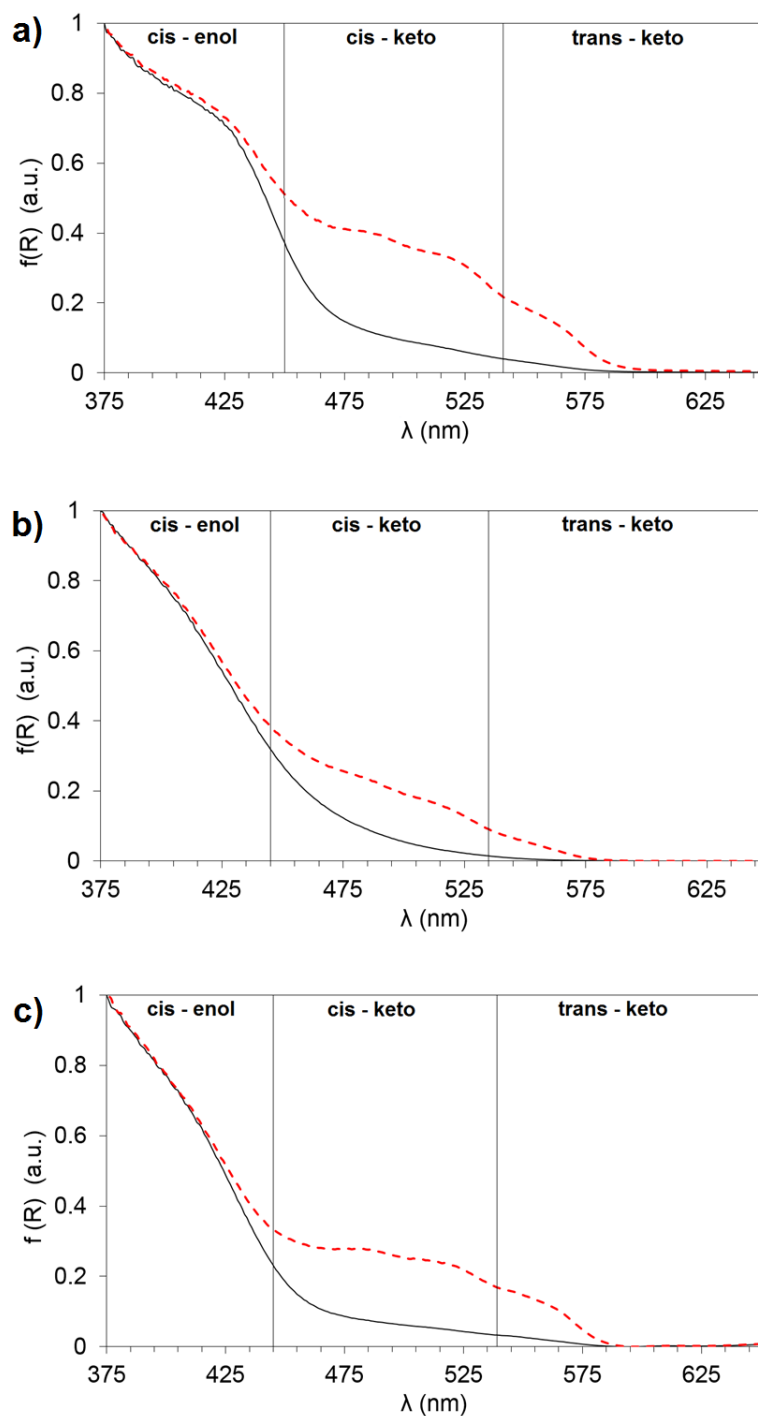


Figure 6. Kubelka Munk spectra of **2** (a), **3** (b) and **4** (c) before (solid black line) and after (dotted red line) UV irradiation (365 nm).

Despite their identical molecular composition, **2** and **3** polymorphic cocrystals show different relaxation rates of the photoproduct. This confirms the role of molecular packing in the determination of final photophysical properties. The relaxation process consists, in both cases, in a two-stage decay.¹⁴ The values of the

rate constants are: $k_1 = 1.22 \times 10^{-5} \text{ s}^{-1}$ and $k_2 = 8.06 \times 10^{-6} \text{ s}^{-1}$, for **2**, and $k_1 = 6.07 \times 10^{-5} \text{ s}^{-1}$ and $k_2 = 3.35 \times 10^{-5} \text{ s}^{-1}$ for **3**, respectively, which can be considered as moderately slow first order processes (**Figure 7**). To the best of our knowledge, **2** represents, up to now, the slowest relaxing anil cocrystal in the literature. The slowest relaxation kinetics for a single component crystal were found for *N*-(3,5-di-*tert*-butylsalicylidene)-4-aminopyridine ($k = 1.8 \times 10^{-8} \text{ s}^{-1}$).²⁷

Another interesting example has recently been reported by Garcia and coworkers regarding the *N*-salicylidene-*p*-aminobenzenesulfonate diallylhexylammonium salt ($k = 2.4 \times 10^{-7} \text{ s}^{-1}$).²⁸

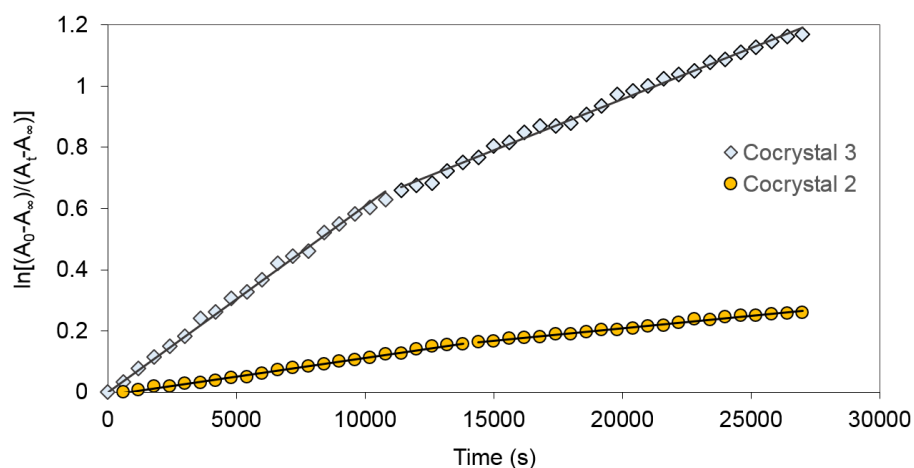


Figure 7. Thermal fading rate of the *trans*-keto band in **2** and **3**.

2.3.4. Optical-structural property relationships

It has been stated that photo- and thermochromism of *N*-salicylideneanilines depend on geometric considerations and steric requirements. Near-planar anils (with **T1** < 20°) in closed packed environment (with average centroid distance of 3.3-3.5 Å) are more likely to only exhibit thermochromic properties. In contrast, non-planar conformations (**T1** > 30°) should promote a photochromic character.⁹⁻¹⁰

Table 2. Torsion angles (**T1**), dihedral angles (Φ) and mpd in **1-4** structures. (Mpd is the mean planar distance between a centroid and a molecule that lies in a parallel plane. Cg1 is calculated at the salicylidene moiety whereas Cg3 is calculated at the C15=C15 bond).

	1	Cocrystal 2	Cocrystal 3	Cocrystal 4
T1 (°)	- 32.2	- 31.4	40.6	- 31.6
Φ (°)	31.75	31.21	40.92	32.25
Mpd (Cg1 ... Cg1) (Å)	3.434	3.514	3.713	3.526
Mpd (Cg1 ... Cg3) (Å)	/	/	3.403	/

Cocrystals **2-4** are photochromic and present a **T1** angle greater than 30° in accordance with this empiric rule. Nevertheless, crystal **1** does not obey the rule, being non-photochromic with **T1** = -32.2° (**Table 2**).

Several studies have, however, shown the limit of such predictions in single component crystals (SCC)²⁹ and, recently, in multicomponent crystals (MCC).^{17,28}

In this context, we selected the most recent structures of photochromic and thermochromic crystalline solids. The selected structures were plotted, along with the new structures presented in this work, on the basis of their **T1** value. As shown in **Figure 8a**, several structures do not obey the rule of the **T1** value and furthermore, the predictability of the photo- and thermochromic character based on **T1** considerations is even lower in MCC. When in a SCC, a planar conformation is a sufficient condition to allow *N*-salicylideneaniline molecules to stack together giving rise to a photo-inactive closed structure, in MCCs this consideration is no longer relevant, because of the structural mismatch produced by the insertion of a cofomer in the crystal structure. Moreover, as recently reported by Hutchins *et al.*, planar anils in cocrystals could exhibit a structure without stacking presence and show photochromic properties anyway.¹⁷

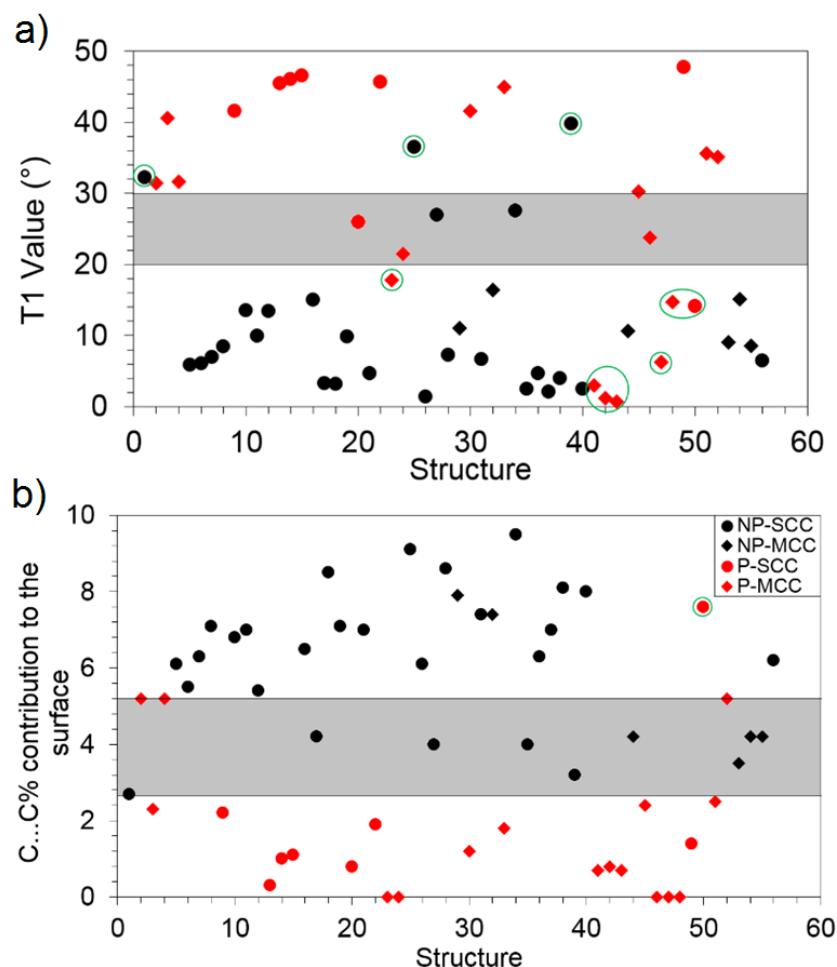


Figure 8. Influence of **T1** (a) and **C...C%** (b) in explanation of the photochromic behavior in single component crystals (SCCs) and multicomponent crystals (MCCs). (NP = non photochromic; P = photochromic). Structures representing an exception to the prediction model are inscribed in a green circle.

Therefore, we propose here a new criterion to try to predict the optical properties, based on the rationalization of the intermolecular interaction in a crystal. In particular, we quantified the π - π stacking interactions in a crystal structure by means of Hirshfeld surfaces. These surfaces represent an interesting way to explore the crystal packing and to quantify the contribution of each interaction-type in a structure.³⁰ Quantification of the π - π stacking interactions can be performed by calculation of the C...C percent contribution to the Hirshfeld surface (C...C%).³⁰

The bigger the C···C% value, the bigger the contribution of the π - π stacking interactions to the structure, and consequently the more closed the structure.

We found a strong correlation (**Figure 8b**) between C···C contacts and the chromic behavior of the selected structures. No correlation was found using other intermolecular interaction types. Calculated values of C···C% extend from 0.0% to 9.5%. A first region comprised between 0.0% and 2.6% includes all structures with a photochromic character. A second region comprised between 5.2% and 9.5% includes non-photochromic structures. If the C···C% value falls between 2.6% and 5.2% (grey highlighted area), the crystal can be either photochromic or non-photochromic. Interestingly, this method is valuable for both SCC and MCC structures with planar or twisted conformation and, therefore, overcomes the limitation of the method based on the torsion angle value.

2.4. Conclusions

The crystal structures and optical properties of (*E*)-2-methoxy-6-(pyridin-3-yliminomethyl)phenol (**1**), a *N*-salicylidene-3-aminopyridine, and its 2:1 cocrystals with fumaric acid (**2** and **3**) and succinic acid (**4** and **5**) were studied at solid state in order to study the effects of cocrystallization and molecular packing on solid-state photo- and thermochromic behavior. To the best of our knowledge this is the first case of polymorphic (**2** with respect to **3**, and **4** with respect to **5**) and isomorphous (**2** with respect to **4**) anil cocrystals in literature. Orange crystals of **1** are exclusively thermochromic and become paler after exposure to liquid nitrogen temperature (77 K). Yellow cocrystals of **2**, **3**, and **4** are slightly thermochromic but strongly photochromic and turn red after UV irradiation. Colorless cocrystals of **5** do not show any photo- and or thermochromic property. Despite their identical molecular composition, **2** and **3** polymorphic cocrystals show different relaxation rates of the photoproduct form. On the contrary isomorphous cocrystals **2** and **4** exhibit similar

increasing factor of the keto absorption band and, therefore, similar photochromic behavior. These results underline the determinant role of molecular packing on the final solid-state thermo- and photochromic properties and extend it, for the first time, to polymorphic and isomorphous cocrystals of pyridin-anils. They also highlight the possibility to reconsider thermochromic molecules for realization of new photochromic systems by cocrystallization. Interestingly, a new criterion based on quantification of π - π stacking interactions, based on the C \cdots C% contribution parameter provided by calculation of Hirshfeld surfaces, improves the prediction method based on the torsion angle value.

2.5. References

- 1) Zhang, J.; Zou, Q.; Tian, H. *Adv. Mater.* **2013**, *25*, 378-399.
- 2) Ségerie, A.; Castet, F.; Kanoun, M. B.; Plaquet, A.; Liégeois, V.; Champagne, B. *Chem. Mater.* **2011**, *23*, 3993-4001.
- 3) Cusido, J.; Deniz, E.; Raymo, F. M. *Eur. J. Org. Chem.* **2009**, *13*, 2031-2045.
- 4) Kawata, S.; Kawata, Y. *Chemical Reviews* **2000**, *100*, 1777-1788.
- 5) Hadjoudis, E.; Mavridis, I. M. *Chem. Soc. Rev.* **2004**, *33*, 579-588.
- 6) Safin, D. A.; Garcia, Y. *RSC Adv.* **2013**, *3*, 6466-6471.
- 7) Ogawa, K.; Kasahara, Y.; Ohtani, Y.; Harada, J. *J. Am. Chem. Soc.* **1998**, *120*, 7107-7108.
- 8) Harada, J.; Uekusa, H.; Ohashi, Y. *J. Am. Chem. Soc.* **1999**, *121*, 5809-5810.
- 9) Johmoto, K.; Sekine, A.; Uekusa, H. *Cryst. Growth Des.* **2012**, *12*, 4779-4786.
- 10) Johmoto, K.; Ishida, T.; Sekine, A.; Uekusa, H.; Ohashi, Y. *Acta Crystallogr. Sect. B-Struct. Sci.* **2012**, *68*, 297-304.
- 11) Staehle, I. O.; Rodríguez-Molina, B.; Khan, S. I.; Garcia-Garibay, M. A. *Cryst. Growth Des.* **2014**, *14*, 3667-3673.
- 12) Sliwa, M.; Létard, S.; Malfant, I.; Nierlich, M.; Lacroix, P. G.; Asahi, T.; Masuhara, H.; Yu. P.; Nakatani, K. *Chem. Mater.* **2005**, *17*, 4727-4735.
- 13) Kawato, T.; Koyama, H.; Kanatomi, H.; Tagawa, H.; Iga, K. *J. Photochem. Photobiol. A.* **1994**, *78*, 71-77.
- 14) Amimoto, K.; Kawato, T. *J. Photochem. Photobiol. C* **2005**, *6*, 207-226.
- 15) Haneda, T.; Kawano, M.; Kojima, T.; Fujita, M. *Angew. Chem. Int. Ed.* **2007**, *46*, 6643-6645.
- 16) Hadjoudis, E.; Yannakopoulou, K.; Chatziefthimiou, S. D.; Paulidou, A.; Mavridis, I. M. *J. Photochem. Photobiol. A* **2011**, *217*, 293-298.
- 17) Hutchins, K. M.; Dutta, S.; Loren, B. P.; MacGillivray, L. R. *Chem. Mater.* **2014**, *26*, 3042-3044.
- 18) Macrae, C. F.; Bruno, I. J.; Chisholm, J. A.; Edgington, P. R.; McCabe, P.; Pidcock, E.; Rodriguez-Monge, L.; Taylor, R.; van de Streek J.; Wood, P. A. *J. Appl. Cryst.* **2008**, *41*, 466-470.

- 19) Wolff, S. K.; Grimwood, D. J.; McKinnon, J. J.; Turner, M. J.; Jayatilaka, D.; Spackman, M. A. **2012**. CrystalExplorer (Version 3.0). University of Western Australia.
- 20) Allen, F. H. *Acta Crystallogr. Sect. B-Struct. Sci.* **2002**, *58*, 380-388.
- 21) Carletta, A.; Dubois, J.; Tilborg, A.; Wouters, J. *CrystEngComm.* **2015**, *17*, 3509-3518.
- 22) Zbačnik, M.; Nogalo, I.; Cinčić, D.; Kaitner, B. *CrystEngComm.* **2015**, *17*, 7870-7877.
- 23) Jing, Z. L.; Li, R. N.; Yang, N. *Acta Crystallogr. Sect. E.-Struct Rep. Online* **2007**, *63*, o3001.
- 24) Sanz, P.; Mo, O.; Yanez, M.; Elguero, J. *J. Phys. Chem. A.* **2007**, *111*, 3585-3591.
- 25) Fujiwara, T.; Harada, J.; Ogawa, K. *J. Phys. Chem. B.* **2004**, *108*, 4035-4038
- 26) Jacquemin, P. L.; Robeyns, K.; Devillers, M.; Garcia, Y. *Chem. Eur. J.* **2015**, *21*, 6832-6845.
- 27) Nakatani, K.; Delaire, J. A. *Chem. Mater.* **1997**, *9*, 2682-2684.
- 28) Jacquemin, P. L.; Robeyns, K.; Devillers, M.; Garcia, Y. *Chem. Commun.* **2014**, *50*, 649-651.
- 29) Robert, F.; Naik, A. D.; Tinant, B.; Robiette, R.; Garcia, Y. *Chem. Eur. J.* **2009**, *15*, 4327-4342.
- 30) McKinnon, J. J.; Spackman, M. A.; Mitchell, A. S. Novel Tools for Visualizing and Exploring Intermolecular Interactions in Molecular Crystals. *Acta Crystallogr. Sect. B-Struct. Sci.* **2004**, *60*, 627-668.

Chapter 3

N-salicylideneaminopyridinium salts and the strategy of the bulky anions: anion induced isostructurality, solid solubility and photochromism induced through tetra-aryl boxes[†]

[†]Carletta, Andrea, et al. "Tetraphenylborate Anion Induces Photochromism in *N*-Salicylideneamino-1-alkylpyridinium Derivatives Through Formation of Tetra-Aryl Boxes." *The Journal of Physical Chemistry C* 122, (2018): 10999-11007.

Tetraphenylborate Anion Induces Photochromism in *N*-salicylideneamino-1-Alkylpyridinium Derivatives through Formation of Tetra-Aryl Boxes

Andrea Carletta,^{1,2} Melwin Colaço,³ Sébastien R. Mouchet,^{1,4,5} Aurélie Plas,² Nikolay Tumanov,^{1,2} Luca Fusaro,¹ Benoît Champagne,¹ Steve Lanners,² and Johan Wouters^{1,2*}

¹ Namur Institute of Structured Matter (NISM), University of Namur, 61 rue de Bruxelles, B-5000 Namur, Belgium.

² Namur Research Institute for Life Sciences (NARILIS), University of Namur, 61 rue de Bruxelles, B-5000 Namur, Belgium.

³ Department of Chemistry, St Joseph's College, P O Box 27094, Bangalore 560 027, India

⁴ School of Physics, University of Exeter, Stocker Road, Exeter EX4 4QL, United Kingdom

⁵ Department of Physics, University of Namur, Rue de Bruxelles 61, B-5000 Namur, Belgium

Abstract. *N*-Salicylideneanilines are interesting model compounds for understanding solid-state photochromism. The introduction of bulky substituents (trityl or tert-butyl groups) by chemical modification of the *N*-salicylideneaniline derivative is an effective method to build up photochromic solids. Alternatively, we propose, herein, a supramolecular approach to design photochromic materials which

involves the introduction of a bulky anion in the structure. In this context, this is the first report on *N*-salicylideneamino-1-alkylpyridinium salts (iodide and tetraphenylboride salts). Iodide salts were obtained by alkylation of the parent *N*-salicylideneaminopyridine with the appropriate iodoalkane (iodomethane or iodoethane) in acetone. The iodide salts were used as starting material for the production of tetraphenylborate salts by anion-exchange in methanol. All solids were characterized by means of X-ray diffraction and absorption spectroscopy. The effect of different counterions as well as of the crystal structure on the solid-state photochromism is investigated.

3.1. Introduction

Photochromism is a color change phenomenon occurring in materials due to reversible transformation of chemical species/molecules/substances following the absorption of electromagnetic radiation.¹⁻³ Photochromic materials are potential candidates in information storage, optical switching devices and nonlinear optics to name a few.¹⁻³

N-salicylideneaniline derivatives are among the most studied thermo- and photo-switchable systems.⁴ They can switch between three different colored forms: a colorless enol form, a yellow *cis*-keto form and red *trans*-keto form (**Figure 1**). This color scheme can be affected by both chemical substitution to the chromophore and by the crystal packing. Thermochromism arises from a ground state tautomerization in which the enol form and the *cis*-keto form are involved. Irradiation of the crystalline solid with UV light results in an excited state intramolecular proton transfer (ESIPT) followed by a *cis-trans* photoisomerization with final formation of a red-colored *trans*-keto isomer.^{5,6} The color transition from pale yellow to red is characteristic of all photochromic *N*-salicylideneanilines. Due to steric requirements of the *cis-trans* isomerization, photochromism is rarely encountered in the solid state.^{4,7} Several works define the concept of open- versus closed-packed structures. Open structures are characterized by molecules in a twisted conformation (with

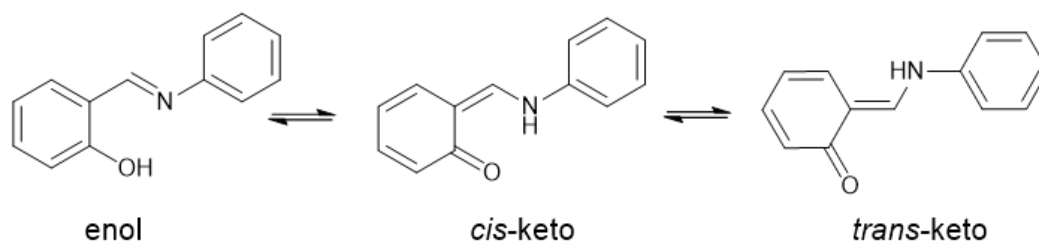


Figure 1. Chemical species involved in photo- and thermochromism of *N*-salicylideneanilines.

dihedral angle between phenyl rings $> 30^\circ$) and dominated by edge-to-face interactions. In contrast, closed-packed arrangements are characterized by near-planar molecules stacked with short interplanar distances from 3.3 Å to 3.5 Å.^{8,9}

It has been suggested that only open-packed arrangements are optimal for photoisomerization to occur (photochromic solids). It has also been shown that the introduction of bulky substituents (trityl or *tert*-butyl groups) by chemical modification^{7,10} or introduction of a coformer^{11–15} in the crystal structure (salification,^{13,16} complexation^{17,18} or cocrystallization by hydrogen^{9,11} or halogen bonds¹⁴) are effective methods to build photochromic solids. However, structural factors involved in the expression of photochromism in *N*-salicylideneanilines are not yet understood.^{14,19,20}

The use of supramolecular approaches in the design of optical materials²¹ is a rapidly growing domain of research.^{21–25} By cocrystallization, multiple crystal forms can be built for the same *N*-salicylideneaniline molecule without any need to chemically introduce substituents which could affect the electronic state of the chromophore.¹¹ Another aspect of this approach is the possibility to obtain isostructural solid forms via the so-called coformer-induced isostructurality.^{26–28} Actually, cocrystallization can overcome the functional group dissimilarities that control the crystal packing. Therefore, it can be considered as an efficient tool for the construction of materials having the same architecture (isostructural) but with systematically tunable properties (punctual modifications).^{29–31} Studying the photochromic behavior of

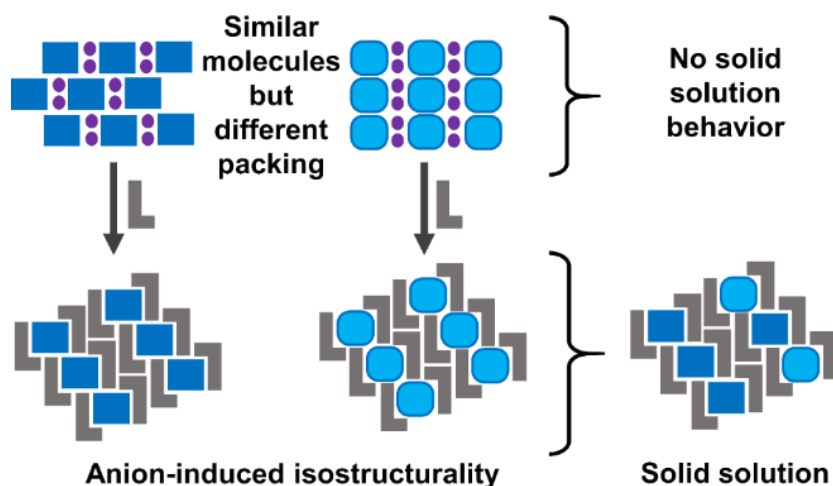


Figure 2. Anion-induced isostructurality and solid solution behavior triggered in the newly obtained isostructural multicomponent systems (purple circle = small anion, L-shaped grey object = bulky anion, blue rectangle = cation **1**, light blue rounded rectangle = cation **2**).

molecules embedded in highly similar environments, as it happens in isostructural cocrystals, could provide insights on factors that determine photochromism.¹⁴

A last advantage of cocrystallization, which is a direct consequence of the induced isostructurality, is the possibility to prepare solid solutions³² of the chromophores (**Figure 2**). The substances may be soluble over a broad range of relative concentrations,^{33,34} producing a crystalline solid with properties varying continuously over this concentration range^{33,34} or which shows characteristics of the two (or more) combined substances.³⁵

In this context, we study the effects of crystal structure and counteranion size on the solid-state photochromism in some example of *N*-salicylideneamino-1-alkylpyridinium salts (iodide and tetraphenylboride salts). Iodide salts were obtained by alkylation of the parent *N*-salicylideneaminopyridine using the appropriate iodoalkane (iodomethane for **1**, and iodoethane for **2**) in acetone. The iodide salts, **1** and **2**, were used as starting material to prepare the bulky tetraphenylborate salts **3**

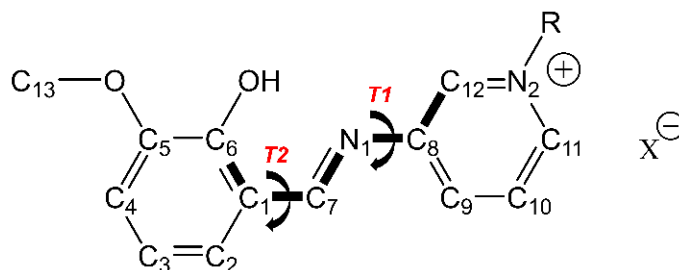


Figure 3. Chemical diagram and numbering scheme of salts under study (**1**: R = Me, X= I. **2**: R = Et, X= I. **3**: R = Me, X= BPh₄. **4**: R = Et, X= BPh₄). Torsion angles, discussed in the text, are **T1**: C₆–C₁–C₇–N₁ and **T2**: C₇–N₁–C₈–C₁₂. Dihedral angle between the two aromatic rings is labelled as Φ (not shown in the figure).

(from **1**) and **4** (from **2**) by anion-exchange in methanol (**Figure 3****Figure**). Salts **3** and **4** were mixed in a solid solution of **3**_{0.62}**4**_{0.38} type isostructural to the starting salts **3** and **4**.

3.2. Experimental methods

Materials. *ortho*-Vanillin (2-hydroxy-3-methoxybenzaldehyde), 3-aminopyridine, iodomethane and iodoethane were purchased from Sigma-Aldrich and used as received. Solvents used for synthesis and crystallization (MeOH, acetone and acetonitrile from Acros Organic Geel, Belgium) are commercially available and were used without further purification.

Synthesis of the compounds

(E)-2-Methoxy-6-(pyridin-3-yliminomethyl)phenol was synthesized by mechanochemical synthesis^{11,36} following a procedure reported earlier.^{37,38} Dry grinding was performed in a 2 mL Eppendorf tube using a Retsch MM 400 Mixer Mill.

Synthesis of 1. 3-{(E)-[(2-Hydroxy-3-methoxyphenyl)methylidene]amino}-1-methylpyridin-1-ium iodide. (E)-2-Methoxy-6-(pyridin-3-yliminomethyl)phenol ($C_{13}H_{12}N_2O_2$, 0.8 g) was dissolved in acetone (16 mL) under stirring. Subsequently, iodomethane (261 μ L) was added dropwise to the solution and the reaction mixture was stirred overnight at room temperature. A yellowish-orange solid was obtained, recovered by filtration and washed with acetone. Yield: 86 %. The recovered solid was analyzed by powder X-ray diffraction. Its powder pattern matched with the one calculated from the single-crystal structure of **1** (**Figure S1**). Prisms of compound **1**, suitable for single-crystal X-ray diffraction, were obtained by slow evaporation from a saturated solution in acetonitrile after 4 days. Crystals were found to be dichroic, *i.e.* they exhibit two different colors (yellow and red in this particular case) when observed at different angles (especially with polarized light).

Synthesis of 2. 1-Ethyl-3-{(E)-[(2-hydroxy-3-methoxyphenyl)methylidene]amino}pyridin-1-ium iodide. (E)-2-Methoxy-6-(pyridin-3-yliminomethyl)phenol ($C_{13}H_{12}N_2O_2$, 0.8 g) was dissolved in acetone (16 mL) under stirring. Iodoethane (336 μ L) was then added dropwise to the solution and the reaction mixture was stirred overnight at room temperature. A yellowish-orange solid was recovered by filtration and washed with acetone. Yield: 75 %. The recovered solid was analyzed by powder X-ray diffraction. Its powder pattern matched with the one simulated from the single-crystal structure (**Figure S1**) of **2**. Orange needles of compound **2**, suitable for single-crystal X-ray diffraction, were obtained by slow evaporation from a saturated solution in ethyl acetate after 3 days.

Synthesis of 3. 3-[(E)-[(2-Hydroxy-3-methoxyphenyl)methylidene]amino]-1-methylpyridin-1-ium tetraphenylborate. A stoichiometric amount of $NaBPh_4$ was added to a solution of 50 mg of **1** in 4 mL of methanol. The solution was warmed until complete dissolution was achieved and then kept at room temperature to form a yellow precipitate of **3**. This yellow product was filtered, washed in MeOH and dried under vacuum.

Comparison of the diffractogram of the ground powder, taken directly after synthesis, with the one calculated from single-crystal data for **3**, confirms selective formation of solid **3** (**Figure S1**). Single crystals suitable for X-ray analysis were obtained by slow evaporation of saturated solutions in MeOH after 4 days.

Synthesis of 4. 1-Ethyl-3-[(E)-[(2-hydroxy-3-methoxyphenyl)methylidene]amino]pyridin-1-ium tetraphenylborate. A stoichiometric amount of NaBPh₄ was added to a solution of 50 mg of **2** in 4 mL of MeOH. The solution was warmed until complete dissolution was achieved. This solution was kept at room temperature to form a precipitate of **4**. This yellow product obtained was filtered, washed in MeOH and dried under vacuum.

Comparison of the powder pattern, of the as-synthesized product, with the calculated diffractogram from single-crystal data of **4** (see the structural characterization section), reveals selective formation of solid **4** (**Figure S1**).

Synthesis of 3_{0.62}-4_{0.38} solid solutions. Equimolar quantities of **3** and **4** were dissolved in ethyl acetate. Crystals of **3_{0.62}-4_{0.38}** suitable for X-ray analysis were obtained by slow evaporation of solvent at room temperature after 2 days.

Characterization

Single-Crystal X-ray Diffraction. Single-crystal diffraction data for **1-4** and **3_{0.62}-4_{0.38}** were collected at 20 °C on an Oxford Diffraction Gemini Ultra R system (4-circle kappa platform, Ruby CCD detector) using Mo K α ($\lambda = 0.71073$ Å) radiation for **1-3** and Cu K α ($\lambda = 1.54184$ Å) for **4** and **3_{0.62}-4_{0.38}**. The structures were solved by SHELXT³⁹ and then refined by full-matrix least square refinement of $|F|^2$ using SHELXL-2016.⁴⁰ Non-hydrogen atoms were refined anisotropically; hydrogen atoms (except those bounded to disordered atoms) were located from difference Fourier map. Hydrogen atoms non-involved in hydrogen bonding were refined in the riding mode with isotropic temperature factors fixed at $1.2U_{eq}$ of the parent atoms

($1.5U_{\text{eq}}$ for methyl group). Coordinates of the hydrogen atoms implicated in hydrogen bonds were refined. Static positional disorder in the pyridine moiety of crystalline **3** (due to simultaneous presence of two near-equally plausible conformations, **Figure S2**) was refined with 0.78 : 0.22 occupancies ratio. Similar disorder was detected for **4** and **3_{0.62}-4_{0.38}**, but only for one chromophore ion in the asymmetric unit and occupancy of the minor component was ~6%. However, inclusion of this disorder in the refinement does not improve significantly the refinement while requiring many parameters, so we decide not to include it in the final refinement. Substitutional disorder (methyl/ethyl group) was refined in the **3_{0.62}-4_{0.38}**. The initially occupancies ratio obtained from the refinement was close to the one from NMR data, but refinement was not stable, so occupancies ratio was fixed to 0.62 : 0.38. The program Mercury⁴¹ was used for molecular graphics.

Powder X-ray Diffraction Measurements. X-ray powder patterns (Cu $K\alpha$ radiation, step size 0.017° ; 45 mA, 30 kV) were collected in the 2θ range $5-40^\circ$ using a Panalytical X'Pert PRO diffractometer (Bragg-Brentano geometry, X'Celerator detector). The program Mercury was used for calculation of X-ray powder patterns from single crystal data.

UV-Vis diffuse reflectance. Measurements were performed on pure powder samples. Reflectance spectra of solid samples were acquired with a Varian 5E spectrophotometer equipped with a “praying mantis” diffuse reflection accessory and was converted to absorption spectra using the Kubelka–Munk function.⁴² Photochromism investigations were performed by irradiating powder samples by using a MAX-303 lamp (Xenon light source 300W) at 360 nm (by use of 20 nm bandpass filters). Thermal fading was analyzed by monitoring the evolution of absorption at 500 nm (Spectra measured each 10 min over 1200 min, in a dark environment).

NMR spectroscopy. The proton NMR spectra were collected on a Varian VNMRS 400 MHz NMR spectrometer operating at 25°C . Quantitative ^1H NMR spectra were

recorded using an excitation pulse of 90° and a recycle delay equal to 10.0 s (maximum longitudinal relaxation time = 2.0 s). The ^1H chemical shifts were calibrated using the residual signal of DMSO (2.50 ppm). After the single crystal X-ray diffraction experiment, a single crystal of the solid solution $\mathbf{3}_x\mathbf{4}_{(1-x)}$ was transferred in a coaxial NMR tube and dissolved in deuterated DMSO. The composition of crystals of $\mathbf{3}_x\mathbf{4}_{(1-x)}$ was therefore determined by NMR spectroscopy. The NMR spectrum shows only peaks that are characteristic of ions **3** and **4** (and of the tetraphenylborate anion). By integrating the area underneath those peaks, the relative ratio of **3** and **4** in $\mathbf{3}_x\mathbf{4}_{(1-x)}$ was determined quantitatively. Solid solution composition is of type $\mathbf{3}_{0.62}\text{-}\mathbf{4}_{0.38}$. The same composition was found for polycrystalline powders used for UV-Vis diffuse reflectance.

When DMSO is used, the enol tautomeric form is the one detected.

Micro-spectrophotometry. The UV-Vis transmission spectra of a single crystal of **1** were acquired using a conventional optical microscope (OLYMPUS BX61) in transmission mode equipped with an optical fiber connected to a spectrophotometer (Ocean Optics USB4000). A polarized white light source was used for each measurement and the analyzer was removed. A total of 13 spectra were acquired on single crystals of **1**, to study its dichroic behavior, by moving the polarizer from 0° to 180° by 15° steps (integration time of 500 ms averaged over 5 scans).

3.3. Results and discussion

3.3.1. Structural characterization

The aim of this structural characterization section is to find common structure features and to correlate them with the expression of photochromism in the systems under study. The crystal packing features of **1-4** are discussed below (see **Table S1** and **S2** for crystallographic parameters). This is accompanied by an analysis of the **T1** and **T2** torsion angles and of the Φ angle defined in **Figure 3**. The **T2** angle is close to 0° in all derivatives due to the intramolecular hydrogen bond involving the

–OH group and the imino group. $\mathbf{T1}$ and Φ have been indicated as descriptors of the likelihood of solid-state photochromism in previous works. Specifically, it was stated that photochromism is preferentially encountered for $\mathbf{T1} > 25^\circ$ and/or $\Phi > 30^\circ$. The twisted conformation resulting from $\mathbf{T1}$ values greater than 25° (or $\Phi > 30^\circ$) should account for an open crystal packing which should be required for photochromism.^{4,7,43} However, several workers have shown the limits of this prediction rule both in single-component and multi-component crystal systems (cocrystals, salts, solvates).^{4,9,11,14,18,44} Nevertheless, for the sake of completeness, values of Φ are provided in the structure analysis (values of $\mathbf{T2}$ and $\mathbf{T1}$ are provided in **Table S3**).

Compound 1. Compound **1** crystallizes in the $P2_1/c$ space group. The tautomeric form observed under the experimental conditions is the enol form, as deduced from selected bond lengths (**Table S4**) and hydrogen position. Ions of **1** present a near-flat conformation with calculated value of Φ of about $1.9(2)^\circ$. Piles of stacked centrosymmetric dimers (head-to-tail stacking) propagate along the b -axis. Adjacent piles are symmetrically related by 2-fold screw axes running parallel to the piles. The resulting crystal packing assumes a *herringbone* feature⁴⁵ when viewed along the c -axis (**Figure 4**).

Compound 2. Compound **2** crystallizes in the $P2_1/c$ space group. The only tautomeric form detected under the experimental conditions is the enol form. $\mathbf{T2}$ torsion angle is constrained by an intramolecular H-bond to a near-planar value. The overall conformation of the chromophore is planar and described by $\Phi = 2.1(2)^\circ$. A head-to-tail stacking between chromophore ions is present as for **1**. The stacked centrosymmetric dimers propagate along the a -axis. However, the resulting crystal packing shows a *layered* aspect when viewed along the crystallographic b - and c -axis (**Figure 4**).

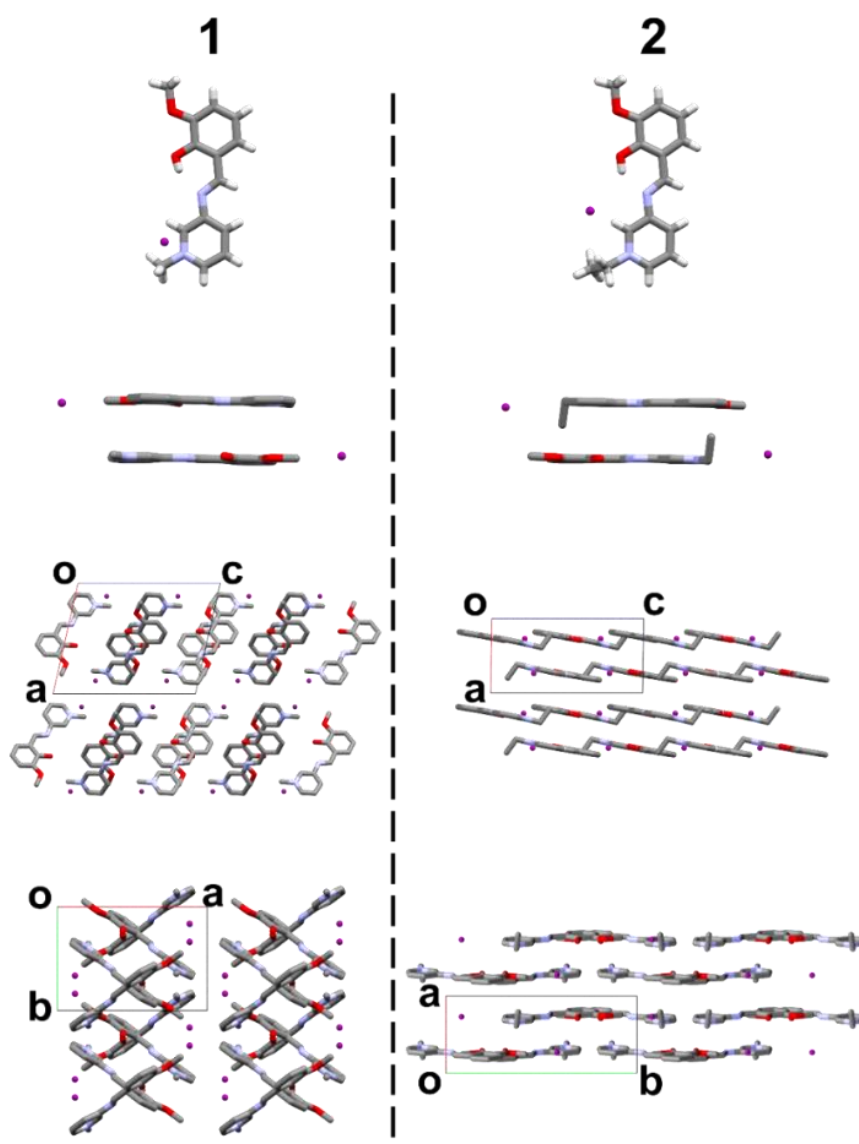


Figure 4. Asymmetric unit of **1** (left) and **2** (right) along with the head-to tail dimers and view along the *b*- and *c*-axis (from top to bottom).

Compound 3. Compound **3** crystallizes in the $P2_1/n$ space group with one chromophore and one tetraphenylborate in the asymmetric unit. The only tautomeric form detected under the experimental conditions is the enol form.

The methylpyridinium moiety, of the *N*-salicylideneamino-1-alkylpyridinium derivative in crystalline **3**, is affected by a static positional disorder due to simultaneous presence of two near-equally plausible conformations. The two

conformers present a non-planar conformation tilted by a Φ angle of about $42.5(3)^\circ$ and $44.3(3)^\circ$ in the disordered moiety (**Figure S2**). Introduction of bulky anions in the structure disrupts the head-to-tail stacking observed in **1** and **2**. Two tetraphenylborate anions interact, through their phenyl groups, with the methylpyridinium moiety of the chromophore resulting in a cage-like assembly (tetra-aryl box) held by $\pi \cdots \pi$ stacking and electrostatic interactions. The vanillidene moiety is outside of the cage but partially hindered by the tetraphenylborate anions for interactions with other chromophore ions. The only detected interactions directed to the vanillidene moiety are weak orthogonal C—H \cdots O contacts (see **Figure 5**). In principle, one half of the chromophore is strongly bound whereas a second half is only weakly bound.

Compound 4. Compound **4** crystallizes in the triclinic $P\bar{1}$ space group with two ions of chromophore and two of tetraphenylborate in the asymmetric unit. Despite belonging to a different space group, solids **3** and **4** are isostructural (see **Figure 5** for structure overlap, and **Figure S1**).⁴⁶ The ethyl group acts by slightly deforming the structure, a factor which leads to decrease of symmetry (see **Table 1**). The only tautomeric form detected under the experimental conditions is the enol form. The two crystallographically independent chromophore ions show Φ of $37.6(2)^\circ$ and $48.6(3)^\circ$, respectively (see **Table S1**).

Solid solution 3_{0.62}-4_{0.38}. Solid **3_{0.62}-4_{0.38}** crystallizes in the triclinic $P\bar{1}$ space group with two ions of chromophore and two of tetraphenylborate in the asymmetric unit (**Figure S3**). Dihedral Φ angle for the two crystallographically independent chromophores is $39.2(3)^\circ$ and $44.6(3)^\circ$ (see **Table S2**). This solid solution is isostructural to the starting solids **3** and **4** as confirmed by analysis of unit cell parameters (see **Table 1**). One should take into account that β angle of **3** is supplementary to the one of **4** and **3_{0.62}-4_{0.38}**, so they are different only due to unit cell choice conventions for triclinic and monoclinic systems (see **Table 1**).

Table 1. Cell parameters of **3**, **4** and **3_{0.62}-4_{0.38}**

	3	3_{0.62}-4_{0.38}	4
Space group	$P2_1/n$	$P\bar{1}$	$P\bar{1}$
a (Å)	11.2697(2)	11.2975(2)	11.3269(3)
b (Å)	16.2411(2)	16.5277(2)	16.7355(5)
c (Å)	17.4036(3)	17.3521(3)	17.4740(5)
α (°)	90	89.2858(12)	89.396(2)
β (°)	104.2390(18)	75.1350(15)	74.793(3)
γ (°)	90	88.9588(13)	88.828(2)
V (Å ³)	3087.56(9)	3130.96(9)	3195.71(17)

The **3_{0.62}-4_{0.38}** solid solution obeys Vegard's law: a linear relation exists between the unit cell volume of the solid solution and the concentrations of the constituent elements, *i.e.* **3** and **4**.⁴⁷ Calculated composition from Vegard's law is of 0.60 : 0.40, which is very close to values obtained by NMR experiment.

Attempts to obtain a solid solution of $\mathbf{1}_x\mathbf{2}_{(x-1)}$ type have so far been unsuccessful. In fact, it has been shown how an ethyl (solid **2**) in place of a methyl (solid **1**) substitution dramatically changes the structure from a *herringbone* arrangement to a *layered* one in solids **1** and **2**. The lack of isostructurality suggests that the protruding ethyl group (of **2**) cannot be fitted in the compact structure of **1**. This is the main reason for which a $\mathbf{1}_x\mathbf{2}_{(x-1)}$ solid solution could not be obtained. Instead, in structures **3** and **4**, the tetra-aryl box⁴⁸ (**Figure 5**) formed by two bulky anions represents a loose region of the crystal packing where the protruding ethyl group can be accommodated without significant steric strain. In other words, the tetra-aryl box "hides" the protruding alkyl group (methyl or ethyl) and the resulting networks are, therefore, isostructural (**Figure 5**).

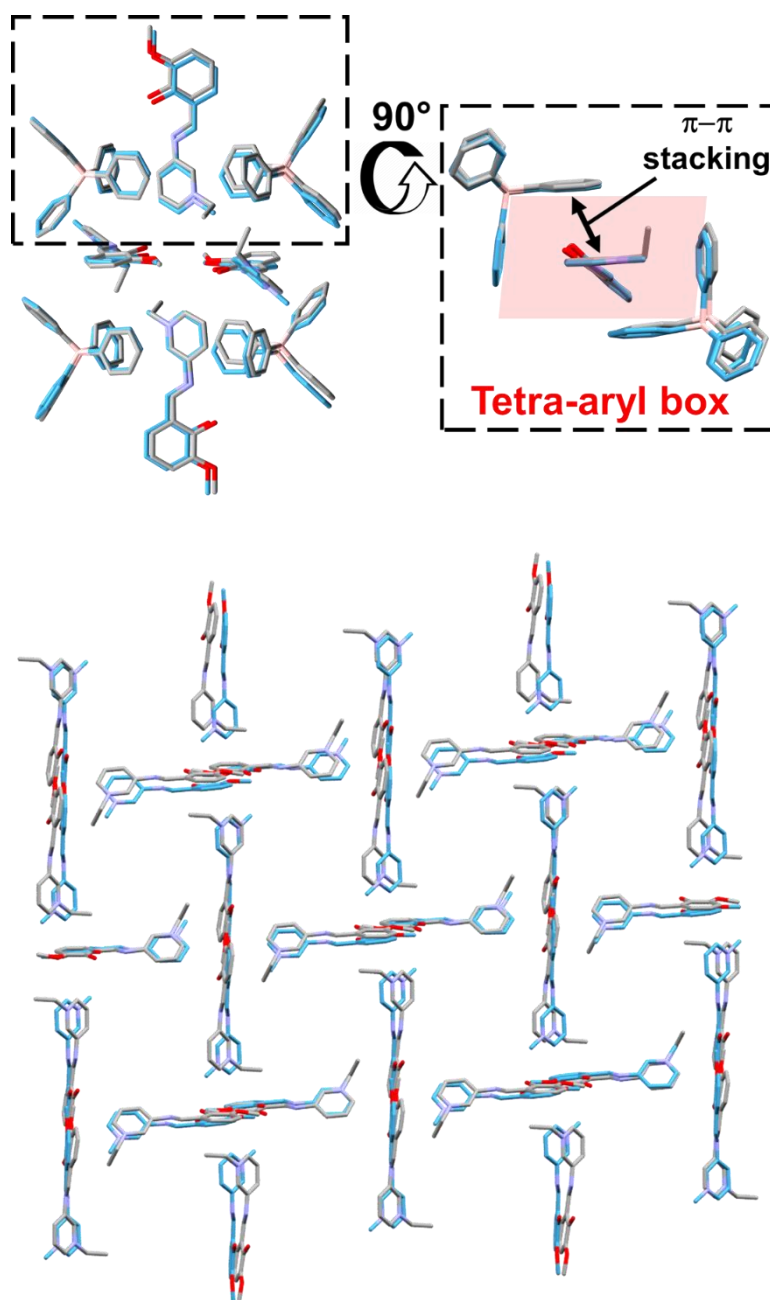


Figure 5. Superimposed crystal structures of **3** (blue) and **4** (grey). An 8-membered supramolecular assembly (top left). View of a tetra-aryl box highlighted by a red area (top right). Overview of chromophores orthogonal arrangement in **3** and **4** by omitting the tetraphenylborate anions. Hydrogen atoms and disorder (in **3**) have been omitted for clarity.

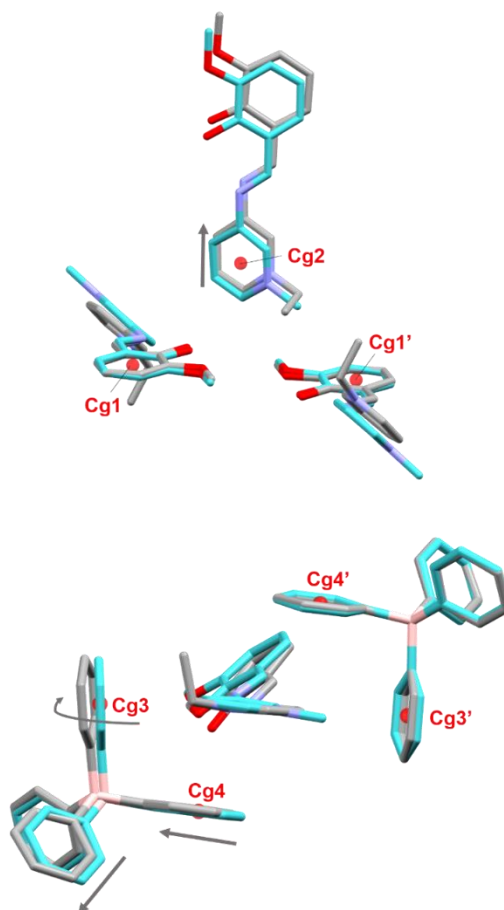


Figure 6. Centroids labelling (Selected distances are reported in **Table 2**) adopted in description of **3** (blue sticks), **4** (grey sticks) and their solid solution **3_{0.62}4_{0.38}** (not shown). Arrows show the shift in the structure from **3** to **4**.

This case of coformer-induced (or anion-induced) isostructurality suggests that **3** and **4** can generate a solid solution (**Figure 2**).³² However, it must be pointed out that isostructurality is not a necessary requirement for two molecules to be mixed as long as the flexibility of the crystal packing can compensate steric hindrance and variation of lattice energy.^{33,34,49}

Selected distances listed in **Table 2** (centroid labelling in **Figure 6**) confirm this structural flexibility showing that the ethyl group acts by slightly opening the tetra-aryl boxes and by slightly increasing the distance between chromophore ions. This aspect is corroborated by analysis of the structural parameters of the **3_{0.62}4_{0.38}** which show values intermediate between those of **3** and **4**.

Table 1. Selected distances in structures **3**, **4**, and their solid solution **3_{0.62}4_{0.38}** (centroids labelling is provided in **Figure 6**).

Distance (Å)	3	3_{0.62}4_{0.38}	4
Cg1 ⋯ Cg1'	8.500(4)	8.497(4)	8.560(3)
Cg1 ⋯ Cg2	5.790(4)	5.797(3)	5.838(3)
Cg3 ⋯ Cg3'	9.971(3)	9.994(3)	10.157(3)
Cg4 ⋯ Cg4'	7.845(3)	7.792(3)	7.929(3)
B1 ⋯ B1'	11.498(3)	11.404(3)	11.694(3)

3.3.2. Photochromism and thermochromism

The photochromic behavior of powder samples of compounds **1-4** was investigated by irradiating the samples at 365 nm. While irradiation of compounds **1** and **2** did not produce appreciable changes in their Kubelka-Munk (absorption) spectra (**Figure S4** and **S5**), the same experiment for **3** and **4** resulted in significant increase in the 500–600 nm spectral region. The observed variation can be ascribed to the appearance of the absorption contribution of the *trans*-keto tautomer in the 500–600 nm region of the spectrum consistent with a yellow-to-red color change (**Figure S4** and **S5**). Therefore, only **3** and **4** present a photochromic behavior. From a structural point of view, the non-photochromic character of solids **1** and **2** can be safely ascribed to their closed packing with chromophores arranged in head-to-tail stacked dimers (**Figure 4**) with short interplanar distances (3.278(3) Å for **1** and 3.360(3) Å for **2**). Conversely, mismatching of the structure, due to the tetraphenylborate anions in **3** and **4**, induces disruption of the head-to-tail stacking observed in **1** and **2**, thus facilitating the pedal motion mechanism^{6,50} needed for the photoisomerization. Color change can be appreciated by naked eye as shown in **Figure 7**.

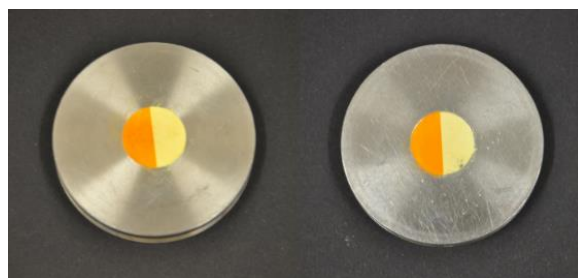


Figure 7. Photochromic color change in powdered form of **3** (left) and **4** (right). Half of the powder was covered by an aluminum foil to avoid exposition to the 365 nm irradiation. The irradiated part, on the left, is orange.

By leaving **3** and **4** in the dark at RT (**Figure 8**) the red coloration fades over the time as a result of the thermal decay of the *trans*-keto form. This thermal fading process is well described by a bi-exponential decay as has been previously reported (**Figure 8** and **Figure S6-S8**).^{7,10,51} Small differences are found in the kinetics of thermal fading processes which reveal that **3** undergoes the slowest process ($t_1 = 78.5 \pm 1.9$ min, $t_2 = 470.4 \pm 6.9$ min) while **4** is of about 1.6 times faster ($t_1 = 45.3 \pm 0.6$ min, $t_2 = 476.4 \pm 3.2$ min). Remarkably, the **3**_{0.62}**4**_{0.38} solid solution is also photochromic and shows a conversion time ($t_1 = 55.0 \pm 1.7$ min, $t_2 = 471.2 \pm 7.8$ min) which is in between that of **3** and **4**. These values corroborate observations based on the crystal structures and show how the ethyl substituent is not directly involved in intermolecular interactions but acts by slightly opening the tetra-aryl boxes of the structure and by slightly increasing distance between chromophore ions which are both favorable factors for the photoisomerization to occur. It is noteworthy that the thermal decay, and so the photochromic behavior, of the solid solution **3**_{0.62}**4**_{0.38} is closer to the one of **4** although this latter is the minor component of the solid solution. As a matter of fact, although **4** is the minor constituent of the solid solution, 38% of substitution is already enough to decrease symmetry. Therefore, the solid solution crystallizes in the $P\bar{1}$ space group, like solid **4**, rather than in the $P2_1/n$ group, observed for solid **3**.

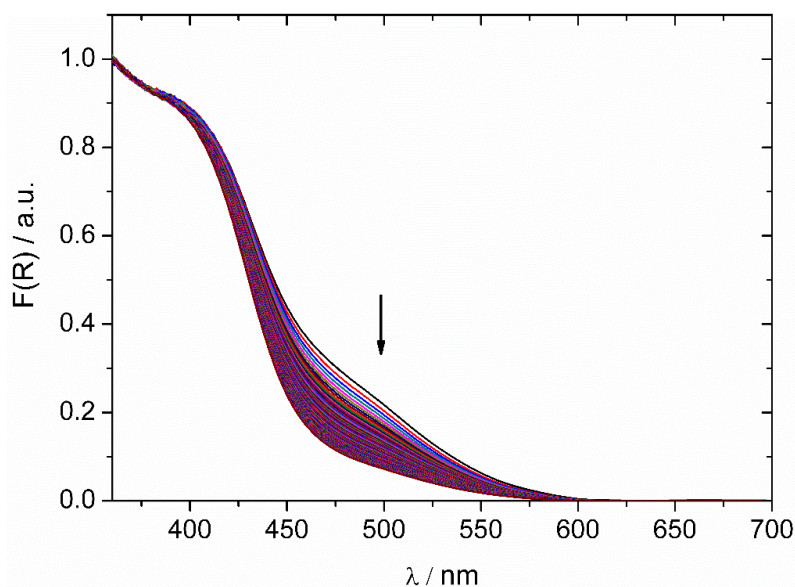


Figure 8. Kubelka-Munk spectra of solid **4** showing the two-steps thermal decay of the *trans*-keto form.

Root mean square deviation (RMSD) was calculated on superimpositions of clusters of 6 tetraphenylborate ions (number of atoms = 150) in structures **3**, **4**, and solid solution **3**_{0.62}-**4**_{0.38}, in order to investigate to which of the two starting solids (**3** and **4**) the solid solution is structurally closer. Value of RMSD is of 0.294 Å for solid solution **3**_{0.62}-**4**_{0.38} related to solid **3** and of 0.166 Å for solid solution **3**_{0.62}-**4**_{0.38} related to solid **4** (**Figure S9**). Even if the three structures can be considered as isostructural, the RMSD values obtained highlight that the solid solution is structurally closer to solid **4** than to solid **3**. This result suggests that it is not the major component that determines the thermal fading behavior but the combined effect that both components together have on the crystal structure. Microcrystalline powders show moderate (**1** and **2**) and low (**3** and **4**) thermochromism (**Figure S10**).

3.3.3. Dichroism of **1**

Dichroic materials are characterized by a change in their color when observed at different angles, especially under polarized light. This phenomenon of color change corresponds to a change in their absorption spectra related to their orientation relative to a source of linearly-polarized light. The absorption of light depends on the relative orientation between molecular transition dipole moment and the direction of polarization of the linearly-polarized light. Light is expected to be most strongly absorbed by the chromophore if these two directions coincide (0° orientation).⁵² Dichroic materials can have applications as polarizers, beam splitters or optical filters.²⁵ The control of dichroism by a crystal engineering^{53,54} approach is a new domain of research. A pioneering work on this topic is authored by Bushuyev and coworkers who reported modulation of dichroism by halogen bond cocrystallization of 4,4'-dihaloctafluoroazobenzenes.²⁵ They concluded that the control over dichroic properties of a material is based on avoiding the formation of *herringbone* structural motifs. Conversely, parallel alignments, like supramolecular chains, lead to highly dichroic materials. Another relevant consequence of a linear (chain) arrangement is that, in principle, dichroism should be observed regardless of the crystal face being chosen.²⁵ In this context, we studied dichroism in **1-4** (see experimental section for more details). To the best of our knowledge this is the first entry in the literature for *N*-salicylideneamino-1-alkylpyridinium salts derivatives. From a structural point of view, none of the reported solids presents a purely linear arrangement (chains). Solid **1**, which present a *herringbone* arrangement by looking toward the *c*-axis, showed a strong face-dependent dichroism (**Figure S11-S13**). In particular, $(0\bar{1}1)$ showed a weak color transition from red (darker coloration at 0°) to orange upon 90° rotation of the polarizer (**Figure 9** and **Figure S14**). On the contrary, the color of the $(\bar{1}00)$ crystal face dramatically changes from orange-red to greenish-yellow (**Figure 9** and **Figure S15**).

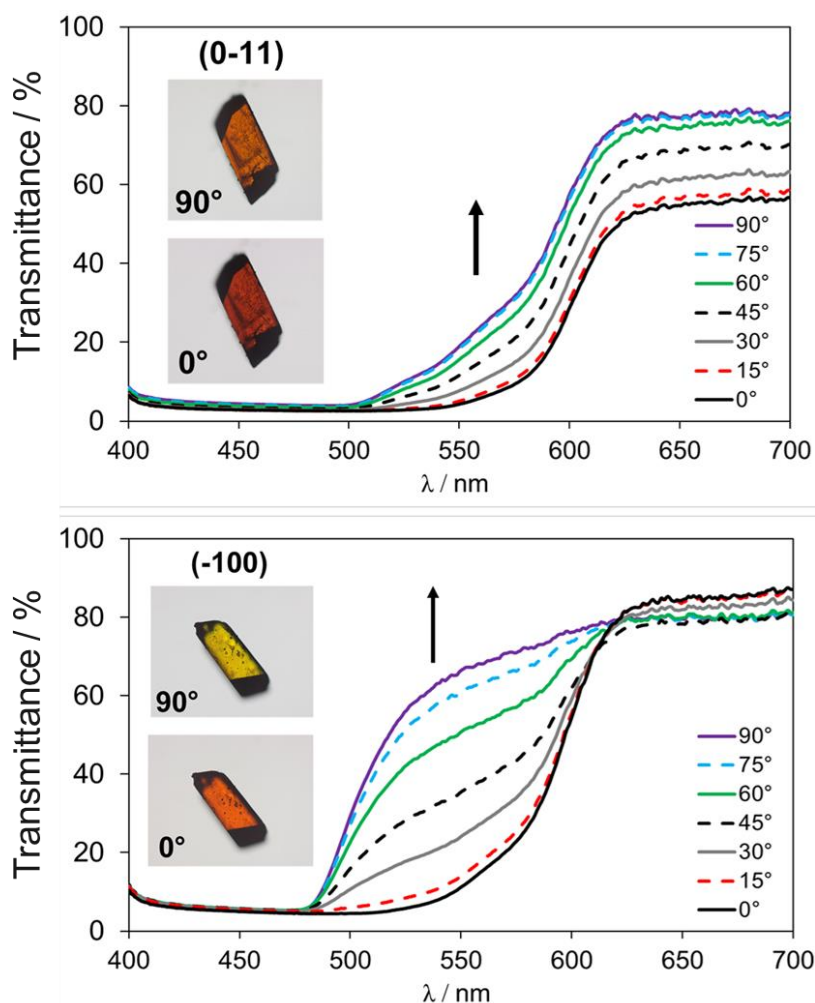


Figure 9. Face-dependent dichroic behavior of **1** observed on the $(0\bar{1}1)$ crystal face (top) and on the $(\bar{1}00)$ crystal face (bottom).

Transmittance spectra quantify the color transition showing a high increase in the 500-600 nm range on changing the linearly-polarized light angle (**Figure 9**). Isostructural, solids **3** and **4** were both found to be non-dichroic, regardless the face being observed. Solid **2** was found to be weakly dichroic (**Figure S16**). These results are in agreement with reports from literature and show how the *herringbone* packing can lead to nearly perfect isotropic optical properties at certain crystal faces.^{53,54}

3.4. Conclusions

We have reported here the use of a crystal engineering approach for the construction of photochromic solids based on the use of bulky anions. To the best of our knowledge, this is the first entry in the literature for the *N*-salicylideneamino-1-alkylpyridinium salts (iodide salts, **1** and **2**, and tetraphenylboride salts, **3** and **4**).

We have shown how the small iodine anions (in **1** and **2**) determine formation of highly compact crystal structures. Although, the overall crystal packing of **1** and **2** is different (with the first showing a *herringbone* structure, the latter showing a layered one), both solids are non-photochromic due to the dense packing and to the presence of head-to-tail dimers with short interplanar distances. The replacement of iodide, in **1** and **2**, by the bulky tetraphenylborate anion (solids **3** and **4**) leads to a multiplicity of effects.

First, the resulting solids **3** and **4** are both photochromic due to disruption of head-to-tail stacking structural motifs in non-photochromic compounds **1** and **2**.

Secondly, tetraphenylborate salts, **3** and **4**, are isostructural. This effect, the anion-induced isostructurality, is due to formation of tetra-aryl boxes which permit the accommodation of the alkyl group (methyl for **3** and ethyl for **4**) bound to the pyrimidine moiety of the chromophores, overcoming the molecular differences.

Thirdly, the achieved isostructurality allows **3** and **4** to be mixed in a **3**_{0.62}-**4**_{0.38} solid solution isostructural to the starting salts **3** and **4**. All three isostructural solids (**3**, **4** and **3**_{0.62}-**4**_{0.38}) are photochromic confirming the role of crystal structure in determination of photochromism. The study of kinetics of thermal fading reveals that **3** undergoes the slowest process ($t_1 = 78.5 \pm 1.9$ min, $t_2 = 470.4 \pm 6.9$ min) while **4** is of about 1.6 times faster ($t_1 = 45.3 \pm 0.6$ min, $t_2 = 476.4 \pm 3.2$ min). Remarkably, the **3**_{0.62}-**4**_{0.38} solid solution is also photochromic and shows a conversion time ($t_1 = 55.0 \pm 1.7$ min, $t_2 = 471.2 \pm 7.8$ min) which is intermediate between the one of **3** and **4**. This trend is consistent with structure data and shows that the ethyl group acts by slightly opening the tetra-aryl boxes of the structure and by slightly increasing distances between chromophore ions, two favorable factors for photoisomerization.

It is noteworthy that the thermal decay, and so the photochromic behavior, of the solid solution $3_{0.62}4_{0.38}$ is closer to the one of **4** although this latter is the minor component of the solid solution. The calculation of RMSD reveals that the solid solution is structurally closer to **4** than **3** even though the former is the minor constituent (38 %). This result suggests that it is not the major component that determines the thermal fading behavior but the combined effect that both components have on the crystal structure.

Microcrystalline powders show moderate (**1** and **2**) and low (**3** and **4**) thermochromism.

Dichroism results are in agreement with reports from literature and show how the *herringbone* packing leads to nearly perfect isotropic optical properties at certain crystal faces (face-depended dichroism).

3.5. References

- 1) Zhang, J.; Zou, Q.; Tian, H. *Adv. Mater.* **2013**, 25 (3), 378–399.
- 2) Kawata, S.; Kawata, Y. *Chem. Rev.* **2000**, 100 (5), 1777–1788.
- 3) Cusido, J.; Deniz, E.; Raymo, F. M. *European J. Org. Chem.* **2009**, 2009 (13), 2031–2045.
- 4) Hadjoudis, E.; Mavridis, I. M. *Chem. Soc. Rev.* **2004**, 33 (9), 579–588.
- 5) Ogawa, K.; Kasahara, Y.; Ohtani, Y.; Harada, J. *J. Am. Chem. Soc.* **1998**, 120 (28), 7107–7108.
- 6) Harada, J.; Uekusa, H.; Ohashi, Y. *J. Am. Chem. Soc.* **1999**, 121 (24), 5809–5810.
- 7) Amimoto, K.; Kawato, T. *J. Photochem. Photobiol. C Photochem. Rev.* **2005**, 6 (4), 207–226.
- 8) Fukuda, H.; Amimoto, K.; Koyama, H.; Kawato, T. *Org. Biomol. Chem.* **2003**, 1 (9), 1578–1583.
- 9) Hutchins, K. M.; Dutta, S.; Loren, B. P.; MacGillivray, L. R. *Chem. Mater.* **2014**, 26 (10), 3042–3044.
- 10) Staehle, I. O.; Rodríguez-Molina, B.; Khan, S. I.; Garcia-Garibay, M. A. *Cryst. Growth Des.* **2014**, 14 (7), 3667–3673.
- 11) Carletta, A.; Buol, X.; Leyssens, T.; Champagne, B.; Wouters, J. *J. Phys. Chem. C* **2016**, 120 (18), 10001–10008.
- 12) Mercier, G. M.; Robeyns, K.; Leyssens, T. *Cryst. Growth Des.* **2016**, 16 (6), 3198–3205.
- 13) Jacquemin, P.-L.; Robeyns, K.; Devillers, M.; Garcia, Y. *Chem. - A Eur. J.* **2015**, 21 (18), 6832–6845.
- 14) Carletta, A.; Spinelli, F.; d'Agostino, S.; Ventura, B.; Chierotti, M. R.; Gobetto, R.; Wouters, J.; Grepioni, F. *Chem. - A Eur. J.* **2017**, 23 (22), 5317–5329.
- 15) Sliwa, M.; Naumov, P.; Choi, H.-J.; Nguyen, Q.-T.; Debus, B.; Delbaere, S.; Ruckebusch, C. *ChemPhysChem* **2011**, 12 (9), 1669–1672.

- 16) Jacquemin, P.-L.; Robeyns, K.; Devillers, M.; Garcia, Y. *Chem. Commun.* **2014**, 50 (6), 649–651.
- 17) Yamazaki, Y.; Sekine, A.; Uekusa, H. *Cryst. Growth Des.* **2017**, 17 (1), 19–27.
- 18) Robert, F.; Naik, A. D.; Tinant, B.; Robiette, R.; Garcia, Y. *Chem. - A Eur. J.* **2009**, 15 (17), 4327–4342.
- 19) Houjou, H.; Ikedo, H.; Yoshikawa, I. *Chem. Commun.* **2017**, 53 (79), 10898–10901.
- 20) Quertinmont, J.; Carletta, A.; Tumanov, N. A.; Leysens, T.; Wouters, J.; Champagne, B. *J. Phys. Chem. C* **2017**, 121 (12), 6898–6908.
- 21) Christopherson, J.-C.; Topić, F.; Barrett, C. J.; Friščić, T. *Cryst. Growth Des.* **2018**, 18 (2), 1245–1259.
- 22) d’Agostino, S.; Grepioni, F.; Braga, D.; Ventura, B. *Cryst. Growth Des.* **2015**, 15 (4), 2039–2045.
- 23) Wang, H.; Hu, R. X.; Pang, X.; Gao, H. Y.; Jin, W. J. *CrystEngComm* **2014**, 16 (34), 7942–7948.
- 24) Xu, J.; Liu, X.; Ng, J. K.-P.; Lin, T.; He, C. *J. Mater. Chem.* **2006**, 16 (35), 3540–3545.
- 25) Bushuyev, O. S.; Friščić, T.; Barrett, C. J. *Cryst. Growth Des.* **2016**, 16 (2), 541–545.
- 26) Cinčić, D.; Friščić, T.; Jones, W. *Chem. - A Eur. J.* **2008**, 14 (2), 747–753.
- 27) Cinčić, D.; Friščić, T.; Jones, W. *New J. Chem.* **2008**, 32 (10), 1776–1781.
- 28) Cinčić, D.; Friščić, T.; Jones, W. *Chem. Mater.* **2008**, 20 (21), 6623–6626.
- 29) Marabello, D.; Antoniotti, P.; Benzi, P.; Canepa, C.; Mortati, L.; Sassi, M. P.; *Acta Crystallogr. Sect. B Struct. Sci. Cryst. Eng. Mater.* **2017**, 73 (4), 737–743.
- (30) Zhang, W.-L.; He, Z.-Z.; Xia, T.-L.; Luo, Z.-Z.; Zhang, H.; Lin, C.-S.; Cheng, W.-D. *Inorg. Chem.* **2012**, 51 (16), 8842–8847.

- 31) Hutchins, K. M.; Unruh, D. K.; Verdu, F. A.; Groeneman, R. H. *Cryst. Growth Des.* **2018**, 18 (2), 566–570.
- 32) Kitaigorodskii, A. I. *Mixed Crystals*; Springer-Verlag: Berlin, 1984.
- 33) Cruz-Cabeza, A. J.; Lestari, M.; Lusi, M. *Cryst. Growth Des.* **2018**, 18 (2), 855–863.
- 34) Lusi, M.; Vitorica-Yrezabal, I. J.; Zaworotko, M. J. *Cryst. Growth Des.* **2015**, 15 (8), 4098–4103.
- 35) Weerasekara, R. K.; Uekusa, H.; Hettiarachchi, C. V. *Cryst. Growth Des.* **2017**, 17 (6), 3040–3047.
- 36) James, S. L.; Adams, C. J.; Bolm, C.; Braga, D.; Collier, P.; Frišćić, T.; Grepioni, F.; Harris, K. D. M.; Hyett, G.; Jones, W.; et al. *Chem. Soc. Rev.* **2012**, 41 (1), 413–447.
- 37) Zbačnik, M.; Kaitner, B. *CrystEngComm* **2014**, 16 (20), 4162.
- 38) Carletta, A.; Dubois, J.; Tilborg, A.; Wouters, J. *CrystEngComm* **2015**, 17 (18), 3509–3518.
- 39) Sheldrick, G. M. *Acta Crystallogr. Sect. A Found. Adv.* **2015**, 71 (1), 3–8.
- 40) Sheldrick, G. M. Crystal Structure Refinement with SHELXL. *Acta Crystallogr. Sect. C, Struct. Chem.* **2015**, 71, 3.
- 41) Macrae, C. F.; Edgington, P. R.; McCabe, P.; Pidcock, E.; Shields, G. P.; Taylor, R.; Towler, M.; van de Streek, J. *J. Appl. Crystallogr.* **2006**, 39 (3), 453–457.
- 42) Gates, B. C.; Knözinger, H.; Jentoft, F. C. *Advances in Catalysis Vol. 52*; Academic Press, 2009.
- 43) Johmoto, K.; Sekine, A.; Uekusa, H. *Cryst. Growth Des.* **2012**, 12 (10), 4779–4786.
- 44) Avadanei, M.; Cozan, V.; Shova, S.; Paixao, J. A. *Chem. Phys.* **2014**, 444, 43–51.
- 45) Minemawari, H.; Tanaka, M.; Tsuzuki, S.; Inoue, S.; Yamada, T.; Kumai, R.; Shimoi, Y.; Hasegawa, T. *Chem. Mater.* **2017**, 29 (3), 1245–1254.

- 46) Childs, S. L.; Wood, P. A.; Rodríguez-Hornedo, N.; Reddy, L. S.; Hardcastle, K. I. *Cryst. Growth Des.* **2009**, 9 (4), 1869–1888.
- 47) Denton, A. R.; Ashcroft, N. W. *Phys. Rev. A* **1991**, 43 (6), 3161–3164.
- 48) Dean, P. A. W.; Jennings, M.; Rajalingam, U.; Craig, D. C.; Scudder, M. L.; Dance, I. G. *CrystEngComm* **2002**, 4 (9), 46–50.
- 49) Schur, E.; Nauha, E.; Lusi, M.; Bernstein, J. *Chem. - A Eur. J.* **2015**, 21 (4), 1735–1742.
- 50) Harada, J.; Ogawa, K. *Chem. Soc. Rev.* **2009**, 38 (8), 2244.
- 51) Sliwa, M.; Létard, S.; Malfant, I.; Nierlich, M.; Lacroix, P. G.; Asahi, T.; Masuhara, H.; Yu, P.; Nakatani, K. *Design, Chem. Mater.* **2005**, 17, 4727–4735.
- 52) Christopherson, J.-C.; Potts, K. P.; Bushuyev, O. S.; Topić, F.; Huskić, I.; Rissanen, K.; Barrett, C. J.; Friščić, T. *Faraday Discuss.* **2017**, 203, 441–457.
- 53) Braga, D. *Chem. Commun.* **2003**, 108 (22), 2751–2754.
- 54) Desiraju, G. R. *Angew. Chemie Int. Ed.* **2007**, 46 (44), 8342–8356.

Chapter 4

Designing photochromic materials through halogen bond: Bromo- vs Iodo-substitution.[†]

[†]Carletta, Andrea, et al. "Halogen-Bond Effects on the Thermo-and Photochromic Behaviour of Anil-Based Molecular Co-crystals." *Chemistry–A European Journal* 23, (2017): 5317-5329.

Halogen Bond Effects on the Thermo- and Photochromic Behaviour of Anil-Based Molecular Co-crystals

Andrea Carletta,^{†1} Floriana Spinelli,^{‡2} Simone d'Agostino,² Barbara Ventura,^{*3}
Michele R. Chierotti,⁴ Roberto Gobetto⁴, Johan Wouters,^{*1} Fabrizia Grepioni^{*2}

¹ Department of Chemistry, University of Namur (UNamur), Rue de Bruxelles 61, Namur, 5000 (Belgium)

² Università di Bologna, Dipartimento di Chimica G. Ciamician, Via Selmi 2, 40126 Bologna, Italy

³ Istituto per la Sintesi Organica e la Fotoreattività (ISOF) – CNR, Via P. Gobetti 101, 40129 Bologna, Italy.

⁴ Dipartimento di Chimica and NIS Centre, Università di Torino, via Giuria 7, 10125 Torino, Italy.

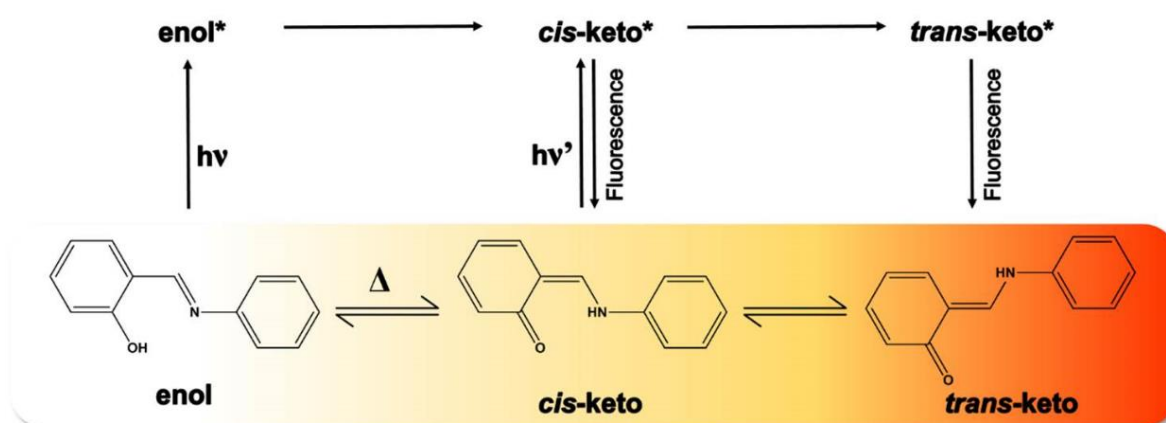
† Both authors contributed equally to this work

Abstract. *N*-salicylideneanilines are among the most studied thermochromic and photochromic systems in the solid state. Although thermochromism is a general property of crystalline *N*-salicylideneanilines, photochromism is known in a limited number of cases. We report here, as a method for the construction of thermo- and photo-responsive molecular architectures, the cocrystallization of 1,2,4,5-tetrafluoro-3,6-diiodobenzene (**I2F4**) with three selected imines of *o*-vanillin, named **1**, **2** and **3**, obtained via condensation reaction with 3-aminopyridine, 4-bromoaniline and 4-iodoaniline, respectively. All crystals and cocrystals have been characterized by means of solid-state complementary techniques (crystallography, solid state

NMR, absorption and emission spectroscopy). The role of halogen bonding and crystal packing in the optical and chromic properties of all solid materials is discussed. All solids exhibit thermochromic behavior, and three of them (**2**, **2**·**I2F4** and **3**·**I2F4**) are found to be also photochromic. Imine derivative **3** crystallizes in two different polymorphic forms (**3A** and **3B**) and a solvate (**3_{solv}**). The bromo- and iodo-derivatives **2** and **3B** are isomorphous and form isomorphous cocrystals with **I2F4**, but behave differently when exposed to UV light, as only crystalline **2** is photochromic. Interestingly, replacement of bromine with iodine seems to turn off the photochromism, as also crystalline **3A** and **3_{solv}**, and even the **2_{0.7}3_{0.3}** solid solution, do not manifest photochromic behavior.

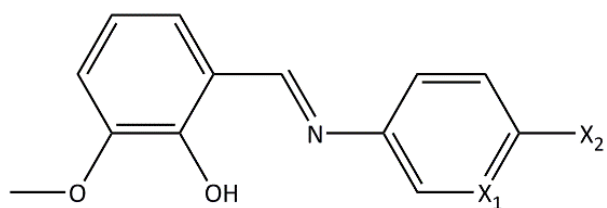
4.1. Introduction

Thermo- and photochromism are color change phenomena induced by variation of temperature and by absorption of electromagnetic radiation, respectively.¹ Photo- and thermochromic materials have been attracting increasing interest due to their broad range of applications *e.g.* in information storage, electronic display systems, optical switching devices and sensors.^{2,3} Among thermo- and photochromic compounds, *N*-salicylideneanilines and their derivatives have received particular attention, due to ease of preparation and their ability to switch between three different forms: a colorless enol form, a yellow *cis*-keto form and a red *trans*-keto form.⁴ The accepted mechanism for thermochromism is a temperature dependent ground-state keto-enol tautomerization via intramolecular proton transfer between the enol form and the *cis*-keto form.⁵ If these two forms are properly irradiated, they undergo a *cis-trans* photo-isomerization toward the *trans*-keto form, through the formation of an excited *cis*-keto intermediate, originating from an excited state intramolecular proton transfer (ESIPT) process in case of excitation of the enol tautomer (**Scheme 1**).⁶ Most *N*-salicylideneanilines exhibit thermochromic behavior in their solids, whereas photochromism is rarely observed. According to the proposed “pedal-motion” mechanism of *cis-trans* photoisomerization, photochromism should be observed



Scheme 1. General pathway of ground and excited state thermo- and photochromic processes in *N*-salicylideneanilines.

only if the molecule possesses the necessary reaction volume for the isomerization to occur within the crystal.⁷ It has been stated that only non-planar anils characterized by dihedral angles $\Phi > 30^\circ$ between the aromatic ring planes should exhibit photochromic properties. In contrast, near-planar conformations ($\Phi < 20^\circ$) should promote a close-packed molecular arrangement that would hinder rotational motion in the crystal, resulting in non-photochromic behavior.^{4,8} However, a number of studies has shown the limit of such empirical rule.^{9–11} A first method adopted for the design of solid photochromic forms is the introduction of bulky substituents, like *tert*-butyl or trityl groups, that can act as space-openers.^{12,13} A promising alternative to the chemical modification approach is represented by *crystal engineering*.^{14–19} Cocrystallization and salification have shown to be two effective methods to induce photochromic properties in anil-based systems.^{9,11,20} We report cocrystallization of *N*-salicylidene-aniline/aminopyridine derivatives with a halogenated cofomer, 1,2,4,5-tetrafluoro-3,6-diiodobenzene (**I2F4**).²¹ The specific advantages derived from the use of the halogen bond²² in the construction of supramolecular architectures are nowadays demonstrated in materials science (*e.g.* supramolecular liquid crystals,²³ supramolecular gelators,²⁴ fluorescence-enhancement²⁵ and phosphorescent materials^{26,27}) and in drug development.²⁸



Scheme 2. Molecular diagram for the 2-hydroxy-3-methoxybenzaldehyde derivatives **1** ($X_1 = \text{N}$, $X_2 = \text{H}$), **2** ($X_1 = \text{C}$, $X_2 = \text{Br}$) and **3** ($X_1 = \text{C}$, $X_2 = \text{I}$).

In this light, we have selected three different imines (labeled here **1**,²⁹ **2**³⁰ and **3**, see **Scheme 2**) of 2-hydroxy-3-methoxybenzaldehyde (*i.e.* *ortho*-vanillin) as model compounds for cocrystallization, to assess the role of both crystal packing and halogen bonding in tuning the photo- and thermochromic properties of *N*-salicylideneanilines.

Compound **1** belongs to the family of *N*-salicylide-3-aminopyridines, whereas compounds **2** and **3** are *p*-halo monosubstituted *N*-salicylideneanilines. Specifically, in the first case we expect the N-atom of the pyridine moiety of **1** to act as a halogen-bond acceptor for **I2F4** by formation of an $\text{N}_{\text{pyridine}} \cdots \text{I}$ synthon in a **1** \cdot **I2F4** cocrystal). In the other two cases (**2** \cdot **I2F4** and **3** \cdot **I2F4** cocrystals), due to the absence of the strong $\text{N}_{\text{(pyridine)}}$ -atom acceptor, the halogen-bond interaction with the cofomer is expected to be directed toward the hydroxyl moiety of the chromophore (the tautomerization center), by a $\text{O}_{\text{(hydroxyl)}} \cdots \text{I}$ synthon. Presence of the para-halogen atom in **2** and **3** potentially allows for halogen \cdots halogen interactions (unsymmetrical $\text{I} \cdots \text{Br}$ and symmetrical $\text{I} \cdots \text{I}$ type, for **2** and **3**, respectively).³¹ Mechanochemical synthesis is used to prepare the solids of interest.^{32,33} All crystalline solids obtained are investigated by means of X-ray single crystal (at room and low temperature) and powder diffraction, solid-state absorption and emission spectroscopy, Fourier-transformed IR spectroscopy and ¹³C and ¹⁵N CPMAS solid-state NMR.

4.2. Results and discussion

4.2.1. Structural characterization

The crystal packing features of parent compounds **1**, **2** and **3** and of the cocrystalline materials obtained by reaction with **I2F4** will be discussed in the following. This is accompanied by an analysis of the **T1** and **T2** torsion angles. The **T2** angle in the enol tautomer is usually close to 0° , because the intramolecular hydrogen bond involving the $-OH$ group and the imine nitrogen forces the fragment to be planar. The value of the Φ angle between the ring planes will also be considered, and its value related to the solid-state photochromic or non-photochromic behavior of all the compounds presented in this work.

The starting compounds: **1**, **2** and **3**



Figure 1 . Single crystals of compounds **1** (left), **2** (middle) and **3_{solv}**, (right) obtained by recrystallization from solution of the mechanosynthesis products.

Compound 1. Compound **1** crystallizes in the orthorhombic $P2_12_12_1$ space group. The tautomeric form observed at both room temperature^[22] and 108 K is the enol form, as deduced from selected bond lengths (**Table 1**). The crystal cohesion is mainly due to dispersion forces, as the only strong hydrogen bond is of the intramolecular type ($S_1^1(6)$): it involves the hydroxyl group and the iminic nitrogen, and constraints the **T2** torsion angle to the near-planar value of $2.0(3)^\circ$ (see **Table 1**). The **T1** torsion angle exhibits a value of about -32° in both the RT and the LT

determinations. Calculated value of Φ (dihedral angle between aromatic rings) is 31.4° in the RT structure and 31.7° at low temperature. Despite having $\Phi > 30^\circ$, **1** has been reported to present only thermochromic behavior.⁹

Compound 2. Compound **2** crystallizes in the orthorhombic $P2_12_12_1$ space group. As in the case of **1**, the only tautomeric form detected at the experimental conditions (both RT and 147 K) is the enol form. The hydroxyl group on one side, and the iminic nitrogen on the other side, force the **T2** torsion angle to a near-planar value, whereas **T1** and Φ are 12.9° and 10.5° , respectively (see **Table 1**). No important variations on bond length and torsion angles are found by comparison between LT and RT crystallographic determinations. The crystal packing is dominated by π -stacking, with piles of molecules arranged in a zig-zag fashion, as shown in **Figure 2**. Compound **2** is reported to present only solid-state thermochromism.³⁴

Compound 3. The substitution of bromine for iodine results in a tendency to form multiple crystal forms (see **Figure 3**). Firstly, orange-red blocks ($P2_1/c$) were obtained by slow evaporation from a saturated solution in EtOH (form **3A**). Molecules of **3** in structure **3A** are affected by positional disorder around a *pseudo* mirror plane perpendicular to the molecular plane (see Experimental). Near-planar molecules (**T1** ca. 2 deg.) are stacked along the *c*-axis and then arranged in a zig-zag fashion by a synergy of C–I \cdots I (halogen \cdots halogen interactions of type II) and C–H \cdots π contacts (see **Figure 3**). Secondly, recrystallization in toluene yielded orange-red prisms. This second crystal form, labeled **3B** ($P2_12_12_1$ space group), is isomorphous with **2** (see **Figure 3**). Lastly, large orange-red prisms were formed via slow evaporation of an EtOAc solution (form **3_{solv}**). These latter belong to the triclinic $P\bar{1}$ space group, with two molecules in the asymmetric unit.

Table 1. Selected geometries: bond distances, torsion angles **T1** and dihedral angles Φ between the benzene rings

	N1–C7 (Å)	C6–O1 (Å)	T1 (deg)	T2 (deg)	Φ (deg)
1 (RT)	1.281(3)	1.353(3)	-32.2(3)	1.4(3)	31.4
1 (LT)	1.289(3)	1.357(3)	-32.1(3)	2.0(3)	31.7
2 (RT)	1.281(7)	1.350(6)	12.9(4)	2.8(8)	10.5
2 (LT)	1.291(4)	1.356(3)	12.9(5)	2.4(6)	10.5
3_{solv} (RT)	1.281(7)	1.352(7)	1.1(7)	1.0(8)	2.4
	1.269(6)	1.345(6)	18.1(8)	1.1(8)	20.0
3_{solv} (LT)	1.293(5)	1.359(5)	5.2(5)	1.2(6)	7.8
	1.298(4)	1.364(4)	20.8(5)	0.6(5)	20.4
3A	1.301(11)	1.323(7)	18(1)	2(1)	15.8
3B	1.263(12)	1.352(10)	16(1)	4(2)	14.3
2_{0.7}3_{0.3}	1.310(13)	1.358(11)	18(2)	3(2)	13.4
1₂·I2F4 (RT)	1.282(6)	1.342(4)	153.6(4)	0.8(6)	34.3
1₂·I2F4 (LT)	1.297(9)	1.357(9)	153.6(7)	0(1)	34.8
2₂·I2F4 (RT)	1.268(6)	1.362(6)	36.1(7)	1.9(7)	34.4
2₂·I2F4 (LT)	1.290(5)	1.363(4)	35.4(5)	2.0(5)	33.0
3₂·I2F4 (RT)	1.272(6)	1.358(5)	34.2(6)	2.6(7)	31.3
3₂·I2F4 (RT)	1.291(4)	1.357(4)	31.3(4)	2.0(4)	29.3

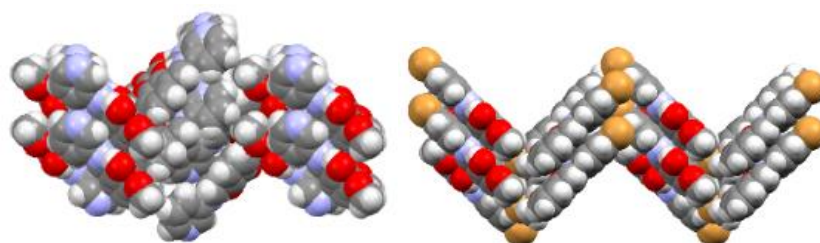


Figure 2. Crystal packing in solid **1** (left) and **2** (right).

Within the $\mathbf{3}_{\text{solv}}$ structure, pairs of molecules interact by π - π stacking in a head-to-tail fashion. Pairs are arranged over a layer in a herringbone pattern, in which molecules are held together by C-I $\cdots\pi$ contacts. Crystalline $\mathbf{3}_{\text{solv}}$ is, however, characterized by the presence of large voids in its structure (see **Figure 3**), which could provide the necessary degree of freedom for the *cis/trans* photoisomerization. TGA measurements on $\mathbf{3}_{\text{solv}}$ show a weight loss (ca. 4%) at ca. 50-60 °C and a corresponding endothermic event in the DSC at 62°C, indicating the presence of crystallization solvent; the solid is stable up to melting ($T_{\text{DSC}} = 131$ °C), which means that molecules of **3** are arranged in a robust framework. The solvent molecules must be distributed in the large cavities within the structure, but the amount of solvent is probably non-stoichiometric and with a high percentage of empty pores that could vary from crystal to crystal; collecting data at low temperature did not help in the detection of solvent in the structure.

Molecules of **3** are found in their enol form in all the forms characterized here (**3A**, **3B** and $\mathbf{3}_{\text{solv}}$), as deduced from selected bond lengths (**Table 1**); no relevant variations of bond length and torsion angles are found by comparison between LT and RT crystallographic determinations.

Solid solution of 2 and 3. Solids **2** and **3B** are isomorphous, *i.e.* they crystallize in the same space group with similar cell parameters, and differ only for the type of halogen atom; isomorphous compounds are usually able to form solid solution, in various ranges of composition. In order to explore the relative influence of bromine and iodine on the photochromic behavior of **2** (see the photochromism section) we tried to prepare a 1:1 solid solution. Single crystals of the resulting product turned out to contain a larger amount of the bromine derivative, corresponding to the formula $\mathbf{2}_{0.7}\mathbf{3}_{0.3}$. The solid solution is isomorphous with the pure bromine and iodine parent compounds (see **Table 1**); the bromine and iodine atoms are disordered over the entire structure.

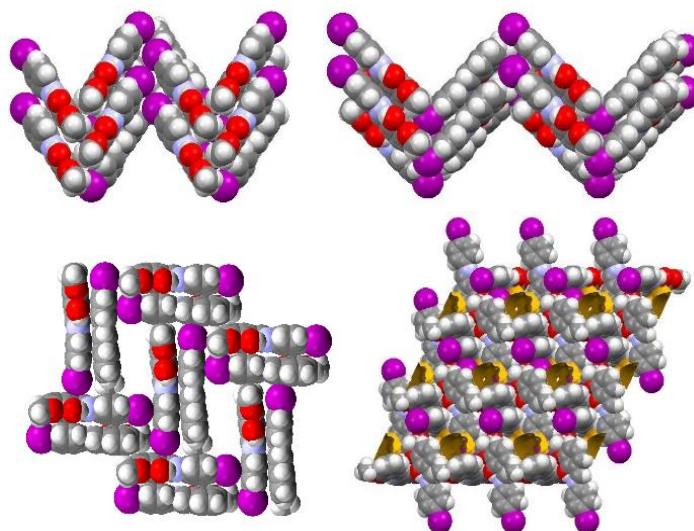


Figure 3. Herring-bone motifs and π -stacking in crystalline **3A** (top left; only the main image of disorder is shown), **3B** (top right, isomorphous with **2**) and **3_{solv}** (bottom left and bottom right); the yellow contour surfaces represent the large pores probably occupied by solvent in non-stoichiometric amount.

Cocrystals of 1, 2 and 3 with I2F4



Figure 4. Single crystals of compounds **1₂·2F4** (left), **2₂·I2F4** (middle) and **3₂·I2F4** (right), obtained by recrystallization from solution of the mechanosynthesis products (see Experimental).

Cocrystal 1₂·I2F4. Yellow-orange needles have been obtained upon recrystallization of the as synthesized ground powder product from EtOAc/cyclohexane. They belong to the monoclinic crystal system, $P2_1/n$ space group (**Table S3**), with one molecule of **1** and half a molecule of **I2F4** in the

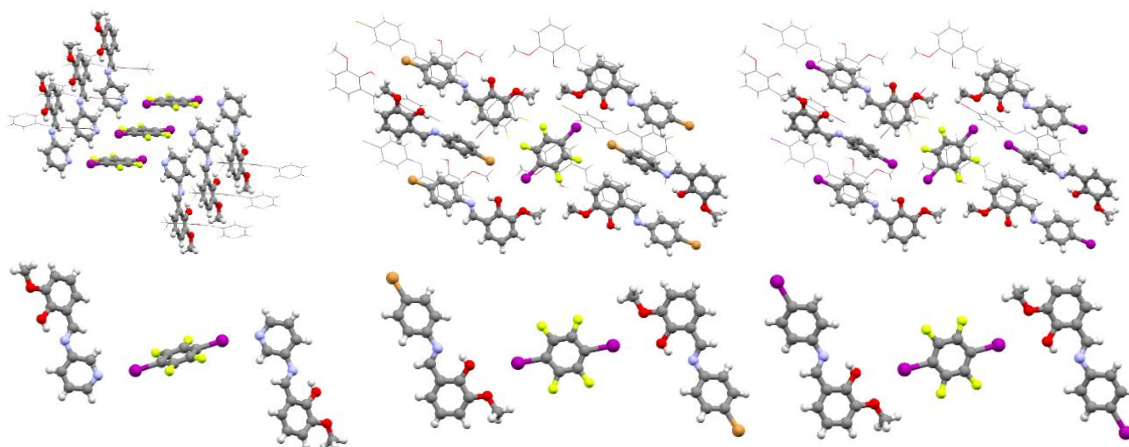


Figure 5. Molecular relative arrangements in crystalline **1·I₂F₄** (left), **2·I₂F₄** (middle) and **3·I₂F₄** (right, isomorphous with **2·I₂F₄**) and relevant interactions involving halogen atoms in the three cocrystals (bottom).

asymmetric unit. The only observed tautomeric form, both at room and low temperature, is the enol one, as deduced from bond lengths (**Table 1**). Molecules are twisted with $\Phi = 34.3^\circ$ (**T1** = $32.8(6)^\circ$). By comparing torsion angles **T1** and **T2** in crystalline **1** and in the cocrystal **1·I₂F₄**, no relevant change in the overall shape of compound **1** molecules is detected. In the crystal structure one molecule of **I₂F₄** binds two molecules of **1** via halogen bonds of the $I \cdots N_{(\text{pyridine})}$ type. Piles of molecules of **1** are stacked in a *segregated* fashion along the *a*-axis (see **Figure 5**, left).

Cocrystal 2·I₂F₄. Orange prisms have been obtained after recrystallization of the as-synthesized ground powder product from EtOAc/cyclohexane. They belong to the monoclinic crystal system, with $P2_1/n$ as space group. The observed tautomeric form (both at room and low temperature) is the enol form, as deduced from bond distances. As seen for the previously presented structures, the **T2** torsion angle is near-planar and the **T1** torsion angle exhibits a value of about $36.1(7)^\circ$ at RT and of $35.4(5)^\circ$ at LT. Measured value of Φ is of about 34.4° (RT) and 33.0° (LT). The crystal structure is characterized by a layered network in which molecules within the same layer interact edge-to-face, and interlayer forces are mainly due to edge-to-face stacking

between molecules of **2** and to a *mixed-stacking* involving **I2F4** and the salicylidene moiety of **2** (**Figure 5**, middle). Directional interactions of the $I \cdots O_{(\text{hydroxyl})}$ type are also present (structure parameters are provided in **Table S4**).

Cocrystal 3₂·I2F4. Orange prisms suitable for X-ray diffraction have been obtained after recrystallization of the as synthesized powder product from EtOAc/cyclohexane. They are isostructural with **2₂·I2F4** (**Figure 5**, right). The observed tautomeric form (both at room and low temperature) is the enol form, as deduced from bond distances (see **Table 1**).

4.2.2. Solid-state NMR

The tautomerism and the halogen bond (XB) occurrence were investigated by ^{13}C and ^{15}N CPMAS solid-state NMR experiments.

The SSNMR technique is known for providing clear evidence of the tautomeric state of a molecule thanks to its multinuclear approach based on the analysis of the ^1H , ^{13}C and ^{15}N nuclei. Indeed, their chemical shift strongly depends on the position of both double bonds and protons. Several examples of solid-state NMR and diffraction investigations of tautomeric and desmotrophic systems such as pyrazoles and pyrazolinones^{35–38} are reported in the literature.³⁹ Recently, the tautomeric state of Pigment Yellow 138 has been investigated by solid-state 1D and 2D multinuclear NMR experiments and direct evidence of the presence of the NH-tautomer was provided by ^1H - ^{14}N HMQC solid-state NMR at very fast MAS. 2-thiobarbituric acid is a representative case because both polymorphism and tautomeric polymorphism have been found and studied by X-ray crystallography as well as by ^1H , ^{13}C and ^{15}N CPMAS NMR.⁴⁰ This method was also successfully applied to determine the tautomeric state of the poorly crystalline phases III (HT-form)⁴¹ and IV⁴² of barbituric acid. In a similar approach also the XB occurrence can be easily probed by SSNMR by looking at the shifts of the nuclei involved in the interaction such as halogen atoms, ^{13}C and ^{15}N .^{28,43,44}

The ^{13}C (with relevant assignments) and ^{15}N CPMAS spectra are reported in **Figure 6** and **Figure 7**, respectively. The ^{15}N chemical shifts with assignments are listed in **Table 2**. Concerning the starting compounds (**1**, **2** and **3_{solv}**) and the cocrystals (**1₂·I2F4**, **2₂·I2F4** and **3₂·I2F4**), the ^{13}C chemical shifts of the C-OH and of the N=CH atoms as well as the ^{15}N chemical shift of the N=C atom are consistent with the enol form. At room temperature, all structures are characterized by the N \cdots H-O interaction as confirmed by the ^{15}N chemical shift of the N=CH atom around 285 ppm. The shifts observed upon cocrystal formation can be mainly related to packing effects rather than N \cdots O distances variations (see X-ray data). In the ^{13}C CPMAS spectra, the number of signals is consistent with one independent molecule ($Z'=1$) for all samples but for **3**, which is characterized by two sets (or much broader peaks) of resonances in agreement with two independent molecules in the unit cell ($Z'=2$) as found by X-ray diffraction.

In **1₂·I2F4**, the occurrence of a XB involving the pyridine nitrogen (N_{py}) atom has been easily verified by the ^{15}N CPMAS spectrum (**Figure 7**). Indeed, the N_{py} signal undergoes a low frequency shift, from 318.4 to 304.6 ppm upon cocrystallization of **1** with **I2F4** clearly indicating the XB formation (**Figure 7**). Similar shifts have been already reported not only for HB and XB formation but also upon metal coordination in agreement with the minor contribution of the lone pair to $\sigma_{\text{loc}}^{\text{p}}$ since removed by quaternization.⁴⁴⁻⁴⁸ The formation of the XB interaction is also confirmed in the ^{13}C CPMAS spectrum by the high-frequency shift of the C-I resonance from 77.0 ppm (pure **I2F4**) to 79.3 ppm (**1₂·I2F4**). This is in agreement with the lengthening of the C-I bond (from 2.075 to 2.095 Å) and it is consistent with previously reported shifts. Interestingly, the shift of the C-I peak observed for **2₂·I2F4** and **3₂·I2F4** is in the opposite direction, toward lower frequencies (from 77.0 ppm for pure **I2F4** to 74.4 and 74.5 ppm, respectively).

This is an indication that the XB interaction is very weak as confirmed also by the long I \cdots O distances (I \cdots O_{CH3}= 3.264 and 3.243 Å for **2₂·I2F4** and **3₂·I2F4**, respectively compared to **1₂·I2F4**, I \cdots N_{py}= 2.878 Å) and the poor directionality (C-

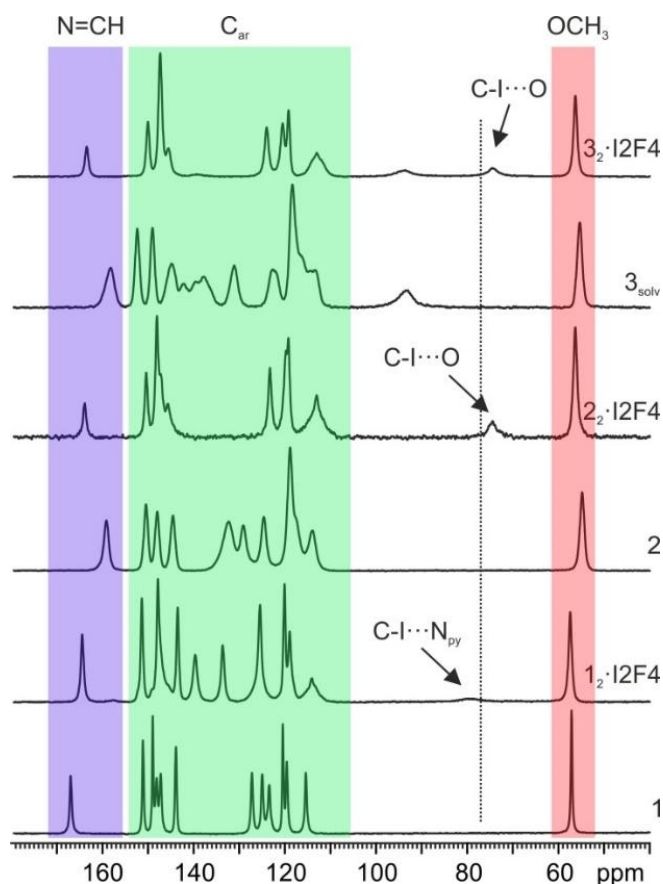


Figure 6. Room temperature ^{13}C (150.91 MHz) CPMAS spectra with relevant assignments of compounds **1**, **2** and **3_{solv}** and their cocrystals **1₂·I2F4**, **2₂·I2F4** and **3₂·I2F4**, recorded at 20 kHz. The dotted line represents the position of the C-I signal of pure **I2F4**.

$\text{I}\cdots\text{O}_{\text{CH}_3} = 140.7$ and 145.1° for **2₂·I2F4** and **3₂·I2F4**, respectively compare to **1₂·I2F4**, $\text{C-I}\cdots\text{N}_{\text{py}}=168.9^\circ$). Thus, the ^{13}C chemical shift is more influenced by packing effects than by the polarization induced by the XB. In other words, it seems that the driving force for the cocrystal formation for **2₂·I2F4** and **3₂·I2F4** is the packing efficiency rather than the XB interaction formation.

Table 2. Room temperature ^{15}N chemical shifts with assignments for compounds **1**, **2** and **3_{solv}** and their cocrystals **1₂·I2F4**, **2₂·I2F4** and **3₂·I2F4**

Sample	$\delta^{15}\text{N}$	Note
1	318.4	N_{py}
	282.4	$\text{C}=\text{N}\cdots\text{H}-\text{O}$
1₂·I2F4	304.6	$\text{N}_{\text{py}}\cdots\text{I}$
	279.2	$\text{C}=\text{N}\cdots\text{H}-\text{O}$
2	277.0	$\text{C}=\text{N}\cdots\text{H}-\text{O}$
2₂·I2F4	290.3	$\text{C}=\text{N}\cdots\text{H}-\text{O}$
3_{solv}	286.9	$\text{C}=\text{N}\cdots\text{H}-\text{O}$
3₂·I2F4	288.9	$\text{C}=\text{N}\cdots\text{H}-\text{O}$

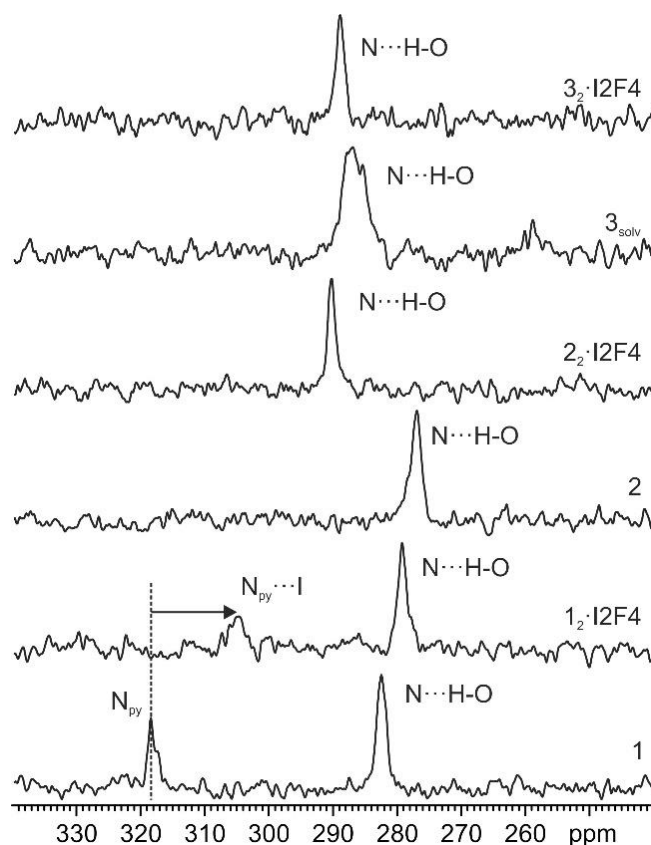


Figure 7. Room temperature ^{15}N (60.81 MHz) CPMAS spectra of compounds **1**, **2** and **3_{solv}** and their cocrystals **1₂·I2F4**, **2₂·I2F4** and **3₂·I2F4**, recorded at 12 kHz.

4.2.3. Thermochromic and photochromic behavior

The crystals of *N*-salicylideneanilines have been historically divided into two groups: thermo- and photochromic ones. Thermochromic crystals were defined as deeply colored at room temperature and pale yellow as the temperature is lowered. Whereas, photochromic crystals are pale yellow and they turn red, when irradiated with UV light.⁴⁹ Generally, a compact crystal packing determines purely thermochromic solids whereas photochromism is observed for open crystal packings. However, recent works on *N*-salicylideneanilines and on *N*-salicylideneaminopyridines (as single component systems, and as cocrystals or salts) revealed that a dense crystal packing could, sometimes, lead to photochromism as well.^{9,10} Moreover, it is also true that photochromism and thermochromism are not mutually exclusive as thought before.^{9,11,20} Besides this, Harada *et al.* reported that the temperature induced shift of the tautomeric equilibrium (thermochromism) could not be the unique cause of the color change as it also depends on an increase of fluorescence intensity, dominating the resulting visual color at low temperature in some cases.⁴⁹

Absorption and emission properties of solid compounds **1**, **2**, **3_{solv}** and cocrystals **1₂·I2F4**, **2₂·I2F4** and **3₂·I2F4**, both as crystals and as powders (ground crystals), have been determined at room temperature and upon cooling at 77K, in order to assess their thermochromic behavior, which could be qualitatively observed comparing vials of all crystalline materials before and after plunging them in liquid nitrogen (see **Figure 8**). Photochromism was instead investigated by absorption and emission spectroscopy or by FTIR spectroscopy upon irradiation at 365 nm. For solids which showed photochromism, both kinetics of the photochemical back reaction (upon excitation of the samples at 546 nm) and thermal fading (by leaving the samples in the dark at room temperature) were investigated. Absorption spectra of powder samples of compounds **1**, **2**, **3_{solv}** and relevant cocrystals are shown in **Figure 9** (the same comparison is reported in **Figure S4** for crystal samples).

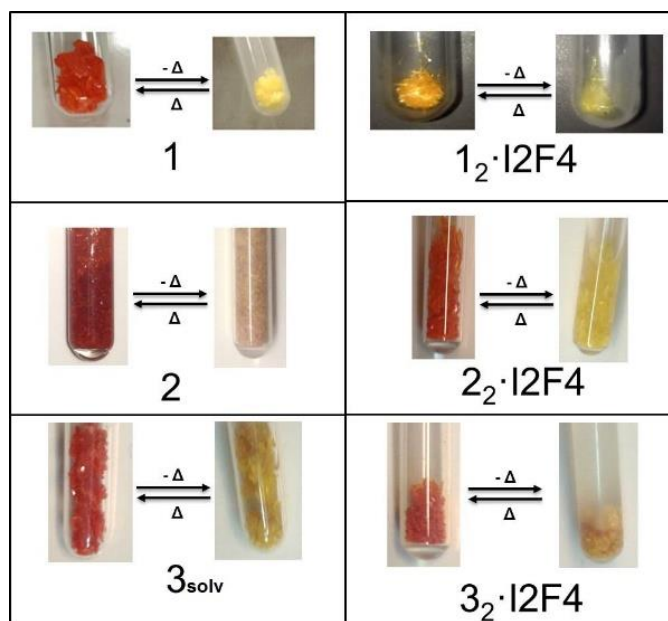


Figure 8. The qualitative, visual comparison of color change for crystals and cocrystals of **1**, **2** and **3_{solv}**, before (left) and after (right) immersion in liquid nitrogen.

The spectra of **1**, **2**, and **3_{solv}** show two distinct broad absorption bands, one extending below 430 nm and the other in the 430-550 nm region. The two bands can be ascribed to π - π^* absorption of the enol form and of the thermally populated *cis*-keto form of the compounds, respectively, in analogy with literature reports.^{8,10,49-51} The presence of the band around 470 nm testifies the existence of the *cis*-keto tautomer at room temperature even if this was not identified by other characterization techniques (X-ray diffraction and NMR measurements in the solid state).⁵ A similar discrepancy has been reported in some cases^{52,53} and can be attributed to a high absorption coefficient of the *cis*-keto form.⁵⁴ The spectra of the cocrystals show similar features, with a reduction of the contribution of the band at 470 nm in particular for **1₂·I2F4** and **2₂·I2F4**. The absorption spectra of the samples in their crystal form (**Figure S4**) show a different intensity distribution of the bands, with an apparent amplification of the absorption in the 430-550 nm range. The latter can derive from a flattening of the spectrum in the region of high absorption ($\lambda < 430$ nm) and intensification in the

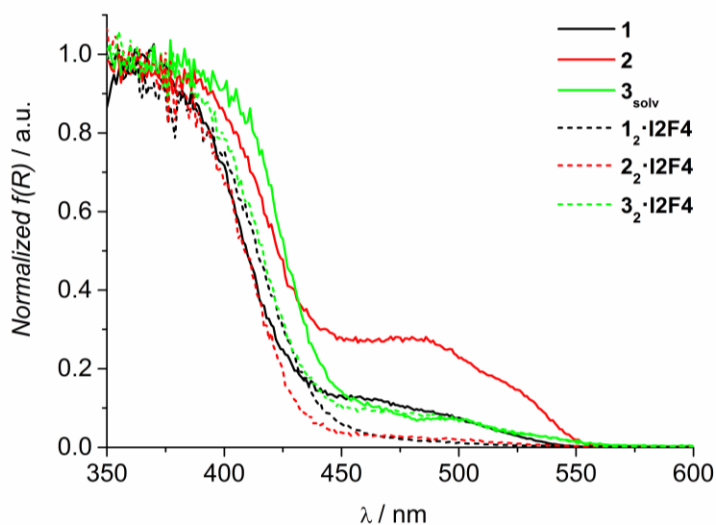


Figure 9. Normalized absorption spectra of powder samples of compounds **1**, **2**, **3_{solv}** and respective cocrystals.

long wavelength range where the absorption is weaker due to optical effects, related to scattering and reflection, occurring in the large size (mm regime) crystals.⁵⁵ Room temperature emission spectra of compounds **1**, **2**, **3_{solv}** and respective cocrystals are reported in **Figure 10** for powder samples and in **Figure S5** for crystal samples. Identical emission spectral features were obtained upon excitation both in the 350-430 nm and in the 430-550 nm regions. Excitation spectra collected at 650/660 nm (reported in **Figure S6** and **S7** for powders and crystals, respectively) overlap both absorption bands with similar relative intensity. The observed emission can therefore be ascribed to fluorescence of the *cis*-keto tautomer, obtained either *via* direct excitation of the thermally equilibrated *cis*-keto form or by excitation of the enol tautomer, followed by an excited state intramolecular proton transfer (ESIPT) process.⁴ We had no evidence of enol emission below 500 nm, as generally observed for salicylideneaniline derivatives, due to the fast kinetics of the ESIPT process, occurring in the sub-ps/few ps time regime in the solid state.^{56,57}

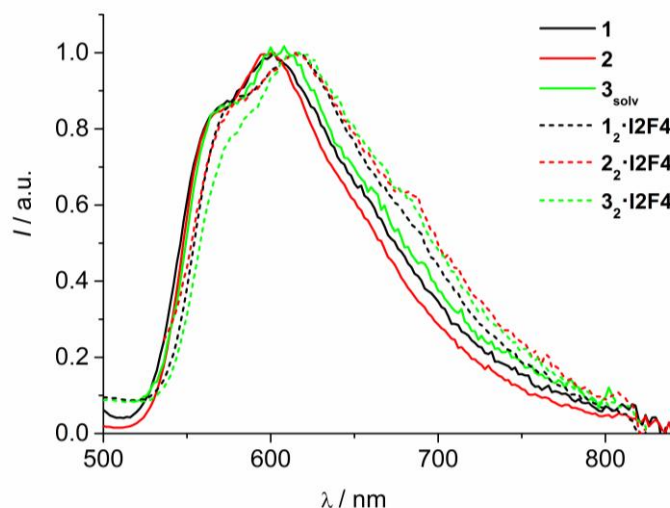


Figure 10. Normalized room temperature emission spectra of powder samples of compounds **1**, **2**, **3_{solv}** and respective cocrystals. $\lambda_{\text{exc}} = 480$ nm.

A comparison of the emission features of compounds **1**, **2**, **3_{solv}** and their cocrystals reveal similar spectra within the two series. Simple compounds **1**, **2** and **3_{solv}** show maxima at ca. 600 nm while cocrystals fluorescence is red-shifted by 10-20 nm (**Figure 10** and **S5** and **Table 3**), indicating a general excited state stabilization effect due to cocrystallization. Absolute emission quantum yields were found to be below the limit of detection of our system (2%) and single exponential decays with lifetimes of few hundreds of ps were measured for all compounds (**Table 3**). The latter data confirm the nature of the emission as resulting from the low-lying singlet excited state of the *cis*-keto tautomer.^{56,57} A general trend in lifetime decrease is observed when moving from simple compounds to cocrystals (**Table 3**), likely due to an external heavy atom effect induced by the halogenated cofomer.²⁶

Emission properties of compounds **1**, **2**, **3_{solv}** and respective cocrystals were further investigated at 77 K in both powder and crystal samples. The emission spectra (**Figure 11** and **S8** for powders and crystals, respectively) show features similar to those observed at room temperature, with a higher spectral resolution. In particular, in the 540-590 nm region, a clear band appears in place of the weak shoulder detected

Table 3. Fluorescence data at room temperature and 77 K for powder samples (in square brackets values for single crystal samples).

	298 K		77K	
	$\lambda_{\max} / \text{nm}^a$	τ / ps^b	$\lambda_{\max} / \text{nm}^a$	τ / ps^b
1	568 sh, 600	344	558, 598, 646 sh	185 (15%), 693 (85%)
	[574 sh, 602]	[344]	[558, 600, 642 sh]	[273 (30%), 858 (70%)]
2	568 sh, 598	508	556, 594, 644 sh	164 (5%), 1328 (95%)
	[572 sh, 598]	[511]	[558, 594, 642 sh]	[158 (5%), 1358 (95%)]
3_{solv}	570 sh, 606	175	558, 602, 650 sh	205 (30%), 674 (70%)
	[578 sh, 610]	[180]	[560, 604, 652 sh]	[314 (55%), 896 (45%)]
1₂·I2F4	580 sh, 616	191	570, 610, 664 sh	204 (60%), 436 (40%)
	[584 sh, 616]	[210]	[570, 610, 662 sh]	[262 (70%), 713 (30%)]
2₂·I2F4	580 sh, 614	133	574, 612, 662 sh	176 (50%), 401 (50%)
	[580 sh, 616]	[113]	[572, 608, 656 sh]	[240 (50%), 456 (50%)]
3₂·I2F4	584 sh, 614	97	576, 616, 668 sh	180 (30%), 334 (70%)
	[580 sh, 618]	[98]	[578, 618, 670]	[212 (70%), 454 (30%)]

^a From corrected emission spectra. ^b Fluorescence lifetimes, excitation at 407 nm.

at room temperature and blue-shifted by ca. 10 nm with respect to it (**Table 3**). The appearance of a blue shifted emission peak at low temperature, observed in similar systems, has been interpreted in terms of an emissive *cis*-keto excited state characterized by a distorted and less stable conformation. This conformation is quenched at room temperature due to a fast relaxation to the more stable planar excited state responsible for emission in the longer wavelength region.^{4,49,58} The bi-exponential behavior of the emission decay observed on the whole spectral region for all the examined compounds (**Table 3**) corroborates the existence of a conformational change in the excited states of the *cis*-keto form in the present case.

The emission spectra of the cocrystals are bathochromically shifted by 10-20 nm compared to those of the parent compounds, similarly to the room temperature behavior. Low temperature excitation spectra collected at 600-620 nm show a pronounced depression of the 430-550 nm absorption region with respect to the same spectra collected at room temperature (see **Figure S9** and **S10** and, as one representative comparison, **Figure S11**). This behavior, responsible of the yellowing of the color of the samples at low temperature observable with the naked eye, is due to the decrease of the population of the *cis*-keto tautomer in the ground state. The low temperature, indeed, inhibits the thermal enol-keto tautomerism and suppresses the formation of the *cis*-keto form, absorbing in the 430-550 nm region. The observed emission, ascribed to the excited *cis*-keto tautomer, is a result of the fast ESIPT process that follows excitation of the enol tautomer, which is operative also at low temperature (a barrierless or proton tunnelling process has been suggested).^{52,56} By comparison of room temperature and 77 K excitation spectra we can conclude that all the examined compounds and cocrystals exhibit thermochromism. The photochromic behavior of powder samples of compounds **1**, **2**, **3_{solv}** and of the corresponding cocrystals has been investigated by irradiating the samples at 365 nm (see the Experimental Section for details). While irradiation of compounds **1**, **1₂·I2F4** and **3_{solv}** did not produce appreciable changes in their absorption spectra (see **Figure S13**), the same experiment for **2**, **2₂·I2F4** and **3₂·I2F4** brought significant variations in the absorption spectral features. For these compounds the emission behavior upon excitation at 400 nm has been analyzed as a function of the irradiation time. **Figure 12** shows the absorption and emission spectral changes observed for cocrystal **3₂·I2F4** upon irradiation at 365 nm (the results of analogous experiments for **2** and **2₂·I2F4** are reported in **Figure S14** and **S15**). Irradiation causes an increase of absorption in the 450-600 nm region, reaching a photostationary state after 40 minutes of exposure (**Figure 12a**, **S14a** and **S15a**). The observed variation can be ascribed to the appearance of the absorption contribution of the *trans*-keto tautomer,

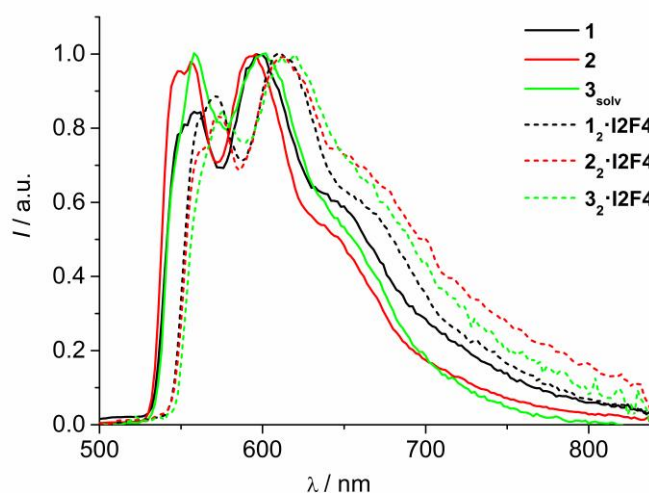


Figure 11. Normalized emission spectra at 77 K of powder samples of compounds **1**, **2**, **3_{solv}** and respective cocrystals. $\lambda_{\text{exc}} = 450$ nm.

formed as a result of an enol \rightarrow *trans*-keto photoreaction, in the longer wavelength range of the spectrum (500-600 nm).^{9,12,13,59}

The emission spectrum evolves with a change in the relative intensity of the bands, i.e. an increase in the 600-800 nm region at the expense of the shoulder at 560-570 nm (**Figure 12b**, **S14b** and **S15b**; the spectra have been arbitrarily scaled to better visualize changes in the intensity ratio). Excitation spectra collected at 575 nm and 650 nm in the photostationary state (**Figure S16**) evidence that absorption in the 450-600 nm contributes to a larger extent to emission at 650 nm. The emission emerging in the 600-800 nm region can therefore be safely ascribed to the *trans*-keto form of the investigated *N*-salicylidene anilines. Emission lifetimes measured for $\lambda > 650$ nm in the photostationary state (449 ps, 126 ps and 97 ps for **2**, **2₂·I2F4** and **3₂·I2F4**, respectively) were found to be very similar to those obtained before irradiation (see reference with values reported in **Table 3**). Among the three photochromic compounds, cocrystal **3₂·I2F4** is the one showing the largest spectral changes due to photoisomerization.

As a mechanism of the photochromic reaction it has been suggested that, upon excitation of the enol form and proton transfer, the excited distorted keto intermediate can deactivate either to the lower lying *cis*-keto and to the *trans*-keto excited states, being precursor of both.^{52,58} Emission from the photogenerated *trans*-keto tautomer has been anyway rarely reported.^{10,53,60,61}

The initial absorption spectra of **2**, **2₂·I2F4** and **3₂·I2F4** are completely recovered either photochemically, upon excitation of the samples at 546 nm or thermally, by leaving the samples in the dark at room temperature. **Figure S17-S19** show spectral and kinetic features of the recovery processes. While photochemical back reactions are characterized by a bi-exponential behavior, the thermal fading processes are well described by first order reactions. A two-stage thermal decay of the *trans*-keto form of anils in the solid state has been previously reported.^{9,12,13,62} It can be noticed that the two cocrystals show much faster back reactions compared to simple compound **2**: the photoconversion kinetics of the *trans*-keto tautomer are of the order of tens of seconds for **2₂·I2F4** and **3₂·I2F4** and tens of minutes for **2** (**Figure S17-S19**). Concerning the thermal fading, conversion times of 604 min, 65 min and 186 min have been measured for the *trans*-keto form of **2**, **2₂·I2F4** and **3₂·I2F4** respectively, confirming that **2** undergoes the slowest process.

FTIR spectroscopy measurements are in agreement with the photochromic behavior observed in absorption and emission spectroscopy, but they also add new information concerning the polymorphic modifications of compound **3_{solv}** (**3A** and **3B**) and the **2_{0.7}3_{0.3}** solid solution. Of all crystalline materials under study only compound **2** and the cocrystals **2₂·I2F4** and **3₂·I2F4** clearly display a photochromic behavior. It is worth noting that **2** represents a positive violation of the dihedral angle Φ rule, while crystalline **1** and its cocrystal **1₂·I2F4** represent a negative one since they are non photochromic despite suitable values of Φ . For those compounds which showed photochromism the general behavior is as follows: FTIR spectra collected before and after 20 min irradiation at 365 nm present some variations which are in agreement with the formation of the *trans*-keto form.^{11,63}

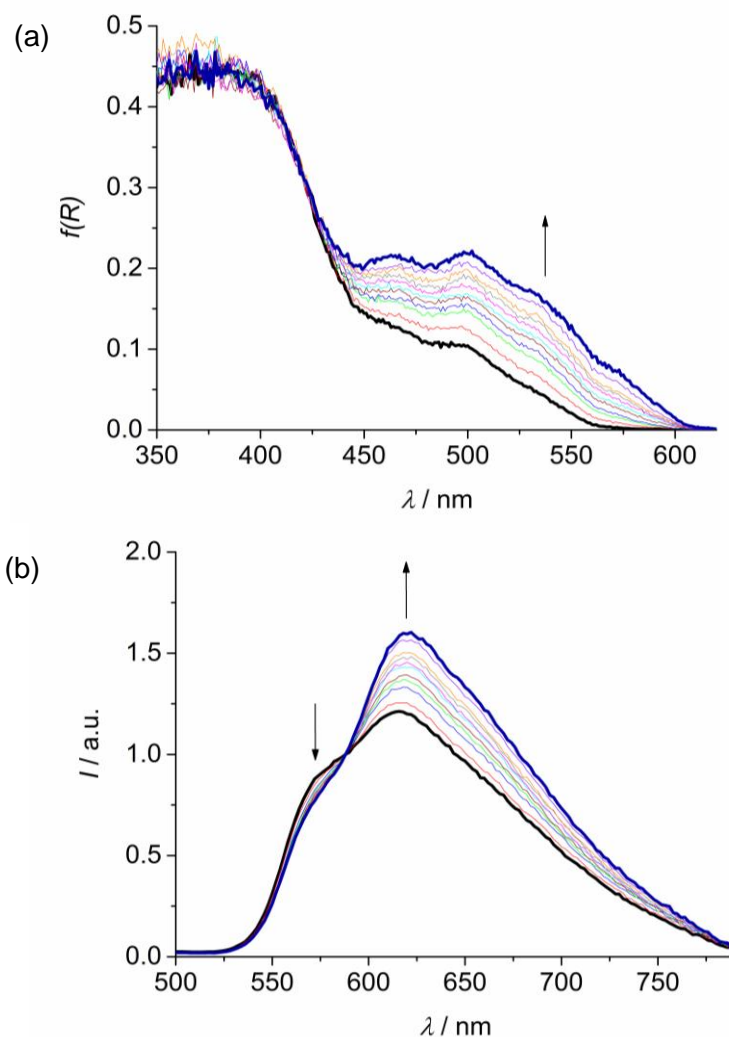


Figure 12. Absorption (a) and emission (b) spectra of **3₂-I2F4** before (black thick) and after (blue thick) irradiation at 365 nm for 40 min (20 min LP and 20 min HP, see Experimental Section for details). Thin lines represent spectra at intermediate times. In (b) the spectra are arbitrarily normalized at 588 nm; $\lambda_{\text{exc}} = 400 \text{ nm}$.

The band around 1612 cm^{-1} (ascribed to the C=N stretching of the *enol* form) decreases, and the small band around 1642 cm^{-1} (due to the C=O stretching of the *trans-keto* tautomer) appears.

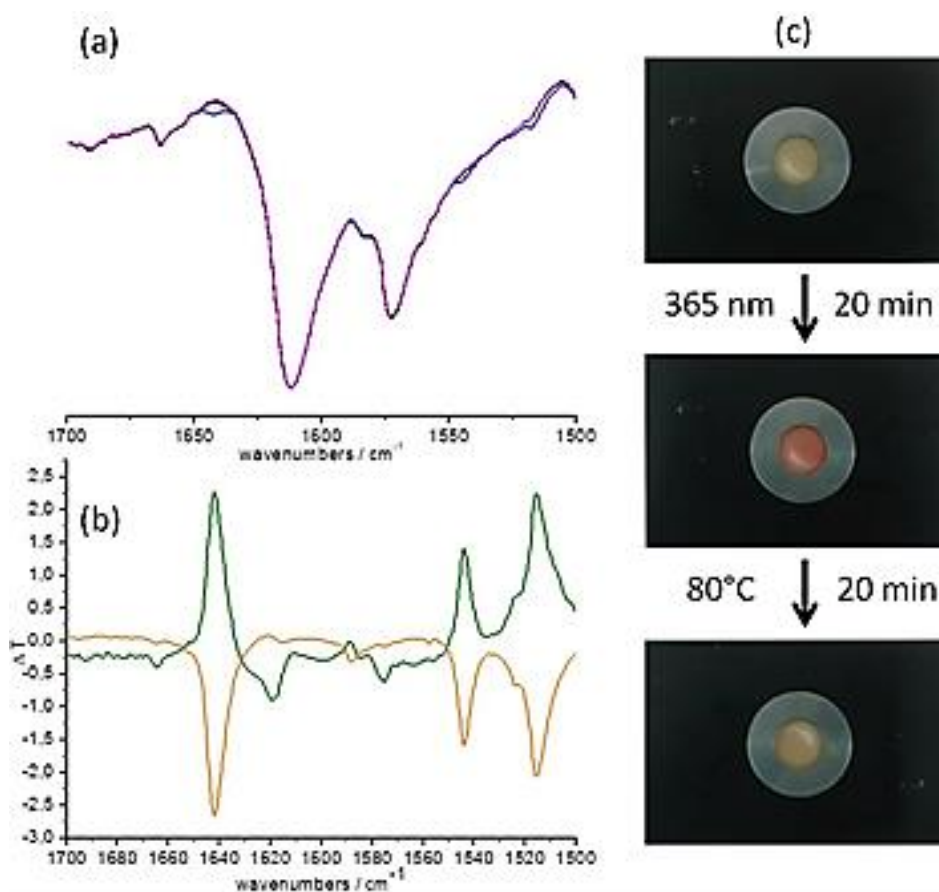


Figure 13. FTIR spectroscopy for $2 \cdot \text{I}_2\text{F}_4$ dispersed in KBr pellets: (a) IR spectra of the untreated sample (black), after 20 min irradiation at 365 nm (blue) and after thermal recovery (magenta). (b) Difference spectra between the untreated and the irradiated sample (green) and between the irradiated and the thermal recovered one (orange). (c) Pictures taken on the KBr pellets used for the FTIR measurements.

After thermal treatment (80°C, 20 min) the original spectrum is recovered, indicating the reversibility of the process. The two processes are mirrored in the color change from yellow to orange upon irradiation, and to yellow again after thermal treatment (80°C, 20 min). This behavior is shown in **Figure 13** for the cocrystal $2 \cdot \text{I}_2\text{F}_4$; **Figure S23-S24** in the ESI file show the behavior of all the other compounds discussed in the present work.

4.3. Conclusions

In conclusion, we have used a cocrystal strategy to modulate thermochromism and photochromism in a series of selected *N*-salicylideneanilines and *N*-salicylideneaminopyridines.

Mechanosynthesis allowed formation of the desired products with high yield and no need to use further solvent-based methods. In the case of compound **3**, the solid **3A** is selectively obtained. Recrystallization of powder of **3A** (as synthesized product) yielded two new crystal forms: **3B** (toluene, isostructural to **2**) and **3_{solv}** (EtOAc solvate). Such a tendency toward the formation of multiple crystal forms has not been observed for **2**.

Halogen bonding interactions of various strength are found within the presented crystal structures: particular attention has been given to the role of the C—I \cdots O_(hydroxyl) interaction in affecting the enol/*cis*-keto tautomerism. Contrary to what has been proven for the intermolecular C—OH \cdots O_(hydroxyl) hydrogen bond, the C—I \cdots O_(hydroxyl) halogen bond does not displace the ground state enol/*cis*-keto balance toward the *cis*-keto form, neither at room nor at low temperature. This can be seen as a clear advantage in the construction of thermochromic solids given that supramolecular effect of formation of an intermolecular H-bond could reduce the color variation of anil-based systems.⁶⁴

All crystal forms present a strong thermochromic behavior (from yellow-orange to pale yellow by lowering the temperature) and, in addition, some of them (crystalline **2**, **2₂·I2F4** and **3₂·I2F4**) are also photochromic, although several studies in the field report that these properties are mutually exclusive. In all systems, photochemical back reaction and thermal fading process are well described as a bi-exponential and as a first order reaction, respectively.

Both negative (crystalline **1**, **1₂·I2F4**) and positive (crystalline **2**) violations of the dihedral angle-based rule have been found. It is also noteworthy that crystals, **2** and **3B**, despite their isostructurality, do not show the same chromic behavior although they were expected to behave similarly. In fact, **2** is photochromic whereas **3B** does

not show such a behavior. What is even more remarkable is that the combination of compound **2** and **3** in a $2_{0.7}3_{0.3}$ solid solution (isostructural to solids **2** and **3B**) leads to a non-photochromic solid. We speculate that this effect can in part be due to the hindering effect of the large iodine atom on the free pedal motion in the tight $P2_12_12_1$ packing. A similar trend is observed for **2**·**I2F4** and **3**·**I2F4** cocrystals. In this case the *p*-iodine substituent is not big enough to turn photochromism off but it is enough to slow down, of about three times, the thermal fading process. For **2**·**I2F4** and **3**·**I2F4** cocrystals, the ability to undergo photoisomerization is increased with respect to **2** as confirmed by the fact that their photochemical back reaction (tens of minutes for **2** and tens of seconds for **2**·**I2F4** and **3**·**I2F4** respectively) and thermal fading process (of about 604 min, 65 min and 186 min for **2**, **2**·**I2F4** and **3**·**I2F4** respectively) are much faster. This is consistent with a structure opening effect made by the insertion of the cocrystal former (**I2F4**) in the structure.

These results reveal how subtle structure changes can dramatically affect the solid-state photochromic behavior and highlight how empirical rules, based only on structural considerations, are not suitable for the rationalization/prediction of photochromism.

4.4. Experimental Section

Materials. *ortho*-Vanillin (*2-Hydroxy-3-methoxybenzaldehyde*), 3-aminopyridine, 4-bromoaniline and 4-iodoaniline were sourced from Sigma-Aldrich (Steinheim, Germany) (>99% chemical purity) and used as received. Solvents used for crystallization (EtOH, EtOAc, cyclohexane and toluene from Acros Organic, Geel, Belgium) are commercially available and were used without further purification.

Synthesis of the compounds

All *N*-salicylideneanilines, *N*-salicylideneaminopyridines and their cocrystals were synthesized by mechanosynthesis.^{9,65,66} Dry grinding was performed with a Retsch MM 400 Mixer Mill, equipped with two grinding jars in which five 2 mL Eppendorf tubes can be installed with 8–10 stainless steel grinding balls (1 mm diameter) in a sample.

Synthesis of 1. (E)-2-methoxy-6-(pyridin-3-yliminomethyl)phenol. The title compound was synthesized by dry grinding of equimolar amounts of 3-aminopyridine and *ortho*-vanillin. Powder X-ray diffraction (PXRD) analysis highlights the presence of new peaks due to the formation of the Schiff base product. Residual peaks of both reactants are not observed in the ground product confirming a near-total conversion (**Figure S25a**). Orange prisms of compound **1**, suitable for X-ray analysis, have been obtained by slow evaporation from a saturated solution in ethyl acetate after 4 days.

Synthesis of 2. 2-[(1E)-[(4-bromophenyl)imino]methyl]-6-methoxyphenol. The title compound was synthesized by dry grinding of equimolar amounts of 4-bromoaniline and *ortho*-vanillin. Powder X-ray diffraction (PXRD) analysis also highlights the presence of new peaks due to the Schiff base product formation. Residual peaks of both reactants are not observed in the ground product confirming a near-total conversion. Orange needles of compound **2**, suitable for X-ray analysis, have been obtained by slow evaporation from a saturated solution in ethyl acetate after 3 days.

Synthesis of 3A, 3B, 3_{solv}. 2-[(1E)-[(4-iodophenyl)imino]methyl]-6-methoxyphenol. The title compound was synthesized by dry grinding of equimolar amounts of 4-iodoaniline and *ortho*-vanillin. Powder X-ray diffraction (PXRD) highlights new peaks coming from the crystalline Schiff base product formed during grinding. Residual peaks of both reactants are not observed in the ground product confirming a near-total conversion. Recrystallization in several solvents was performed in order to obtain single crystals suitable for X-ray diffraction. Moreover, two polymorphs and a solvate form of **3** were obtained, depending on the crystallization conditions.

Orange-red blocks of form **3A** were obtained by slow evaporation of a saturated solution in EtOH. Orange-red crystals of form **3B** were obtained by seeding with **2** a saturated solution in toluene, and leaving it to slowly evaporate, while orange-red prisms of form **3_{solv}** were obtained by recrystallization from ethyl acetate.

Comparison of the PXRD diffractogram of the ground powder, taken directly after synthesis, with PXRD diffractograms calculated on the basis of single crystal data for **3A**, **3B** and **3_{solv}**, reveals selective formation of form **3A** (**Figure S25a**).

Synthesis of the 2_{0.7}-3_{0.3} solid solution. Equimolar quantities of **2** and **3_{solv}** were dissolved in ethyl acetate; after 2 days crystals of suitable dimensions for X-ray diffraction were obtained by slow evaporation of solvent at room temperature.

Synthesis of 1₂·I2F4. Cocrystallization was achieved by grinding (120' at 30 Hz) of compound **1** and **I2F4** at a 2:1 molar ratio. Comparison of the PXRD diffractogram of the ground powder, taken directly after synthesis, with PXRD diffractogram calculated from the single crystal structure of **1₂·I2F4**, reveals selective formation of **1₂·I2F4** cocrystal (**Figure S25b**). Single-crystals suitable for X-ray diffraction were obtained by slow evaporation of saturated solutions in ethanol/cyclohexane. Orange-yellow needles have been obtained after 5 days.

Synthesis of 2₂·I2F4. Cocrystallization was performed by dry grinding (120' at 30 Hz) of compound **2** and **I2F4** in a 2:1 molar ratio. Comparison of the PXRD diffractogram of the ground powder, with PXRD diffractogram calculated from the single crystal structure of **2₂·I2F4**, highlights selective formation of 2:1 **2₂·I2F4** cocrystal. After recrystallization in ethanol/cyclohexane, orange prisms have been obtained.

Synthesis of 3₂·I2F4. Cocrystallization was performed by dry grinding (120' at 30 Hz) of compound **3** and **I2F4** in a 2:1 molar ratio. Comparison of the PXRD diffractogram of the ground powder, with the calculated PXRD diffractogram of **3₂·I2F4**, shows selective formation of 2:1 **3₂·I2F4** cocrystal. After recrystallization in ethanol/cyclohexane, orange prisms have been obtained after 4 days.

Characterization

FTIR spectroscopy. FTIR spectra were collected using a Bruker Alpha FTIR spectrometer. FTIR spectra in the range 1700-1500 cm^{-1} were run on KBr pellets (sample amount: 1-2 mg, KBr amount: 200 mg), resolution was set to 2 cm^{-1} , and 128 cycles for both background and measurement were collected. Spectra were run twice, before and after 20 min of UV irradiation (365 nm) on the same pellet sample, when a change in the color or in the spectrum was noticed, a further spectrum was measured after thermal treatment (pellet kept in the oven at 80°C for 20 minutes). Pellets were irradiated directly in the sample holder using 2 UV-LED (LED ENGINE LZ1-10UV00-0000, $\lambda = 365$ nm) placed at a distance of 1 cm each.

Crushed pellets were subjected to powder X-Ray diffraction analysis to exclude any solid state reaction triggered by pressure during pellet formation. As evidenced by powder patterns all crystalline materials resulted stable and did not react with KBr during pellet preparation (see ESI).

Solid-state NMR. Solid-state NMR experiments were acquired on a Jeol ECZR 600 instrument operating at 600.17, 150.91 and 60.81 MHz for ^1H , ^{13}C and ^{15}N nuclei, respectively. The samples were packed in a 3.2 mm rotor (volume = 50 μL) and spun at 20 and 12 kHz for ^{13}C and ^{15}N nuclei, respectively. All data were collected at ambient probe temperatures. All ^{13}C and ^{15}N experiments employed the RAMP-CP pulse sequence (^1H 90° pulse=2.189 μs , contact time = 9 and 4 ms, respectively) with the TPPM ^1H decoupling with an rf field of 75 kHz during the acquisition period. Detailed acquisition parameters may be found in the Supporting Information (**Table S5**). ^{13}C and ^{15}N chemical shift scales were referenced with the resonance of hexamethylbenzene (^{13}C methyl signal at 17.4 ppm), and glycine (^{15}N signal at 33.4 ppm with respect to NH_3), respectively as external standards.

Absorption and emission spectroscopy, photochemistry. Measurements were performed both on crystals as such and on gently crushed powder samples placed inside two quartz slides. Reflectance spectra of solid samples were acquired with a PerkinElmer Lambda 9 UV/Vis/NIR spectrophotometer equipped with a 60 mm

integrating sphere and converted in absorption spectra using the Kubelka–Munk function.⁶⁷ Emission spectra were collected in front-face mode with an Edinburgh FLS920 fluorimeter equipped with a Peltiercooled Hamamatsu R928 PMT (200–850 nm), and corrected for the wavelength dependent phototube response. Absolute emission quantum yields were determined according to the method reported by Ishida et al.,⁶⁸ by using the same fluorimeter equipped with a 4 inch Labsphere integrating sphere. The limit of detection of the system is 0.020. Measurements at 77K made use of quartz capillary tubes immersed in liquid nitrogen contained in a home-made quartz Dewar. Band maxima and luminescence intensities are obtained with uncertainties of 2 nm and 10%, respectively. Fluorescence lifetimes were determined with an IBH 5000F time-correlated single-photon counting apparatus equipped with a TBX Picosecond Photon Detection Module by using a pulsed 407 nm laser diode (59 ps pulse width) powered by a Hamamatsu C4725 light pulser as excitation source. Analysis of the fluorescence decay profiles against time was accomplished with the Decay Analysis Software DAS6 provided by the manufacturer. The estimated error on lifetime determinations is 10%.

Photochromic investigations have been performed by irradiating a thin layer of the powder sample, placed inside two quartz slides, by using a collimated 100 W Hg arc lamp and selecting the desired spectral lines (365 or 546 nm) by means of bandpass interference filters. Forward reactions ($\lambda_{\text{irr}} = 365$ nm) made use of two different light powers: 2 mW cm⁻² (low power: LP) and 20 mW cm⁻² (high power: HP), the former obtained by using a neutral density filter. For back reactions ($\lambda_{\text{irr}} = 546$ nm) the light intensity was 5 mW cm⁻¹. Thermal fading was analyzed by a reflectance (%) time scan at a single wavelength (500 nm) performed with the spectrophotometer described above; the experimental conditions allowed for a close to dark environment.

Crystal Structure determination. Single-crystal diffraction data for **1**, **2**, **3_{solv}**, **1₂·I2F4**, **2₂·I2F4** and **3₂·I2F4** were collected at RT and LT on a Gemini Ultra R system (4-circle kappa platform, Ruby CCD detector) using Mo K α ($\lambda = 0.71073\text{\AA}$)

radiations. Single-crystal diffraction data for **3A**, **3B** and **2_{0.7}-3_{0.3}** were collected at RT on an Oxford X'Calibur S CCD diffractometer equipped with a graphite monochromator (Mo K α radiation, $\lambda = 0.71073\text{\AA}$). Selected crystals were mounted on the tip of a quartz pin using cyanoacrylate (commercial glue). Structures were solved by direct methods using the WinGX suite of programs⁶⁹ with Sir-2014⁷⁰ and then refined using either SHELX-97 or SHELXL-2014.⁷¹ Non-hydrogen atoms were anisotropically refined and the hydrogen atoms (not implicated in H-bonds) in the riding mode with isotropic temperature factors fixed at 1.2 times U(eq) of the parent atoms. Hydrogen atoms implicated in hydrogen bonds were localized by Fourier difference maps. The solvent of crystallization in the structure of **3_{solv}** could not be unambiguously determined, therefore, the contribution of the solvent to the calculated structure factors was taken into account by using the SQUEEZE procedure of PLATON.⁷² Positional disorder (70:30) in crystalline **3A** was treated by first refining the occupancy parameter of iodine, then fixing the occupancy factor and freely refining the thermal parameter. The whole minor image of disorder was located experimentally, but only the iodine atom was refined anisotropically. Disorder in the bromine/iodine position was treated analogously in the solid solution **2_{0.7}3_{0.3}**. The program Mercury⁷³ was used for molecular graphics. Structures have been submitted to the Cambridge Structure Database⁷⁴ (CSD refcodes: 1407547, 1407548, 1456341, 1483225-1483232, 1523380-1523382)

Powder Diffraction Measurements. X-ray powder diffractograms in the 2θ range 5-40° (step size 0.02°; time/step, 20s; 40mA x 40kV) were collected on a Panalytical X'Pert PRO automated diffractometer equipped with a X'Celerator detector and in Bragg-Brentano geometry using Cu K α radiation. The program Mercury⁷³ has been used for simulation of X-ray powder patterns from single crystal data.

Thermogravimetric Analyses (TGA). TGA measurements were performed with a Perkin-Elmer TGA7 in the temperature range 40 – 350 °C under N₂ gas flow at a heating rate of 5.00 °C min⁻¹.

Differential Scanning Calorimetry (DSC). DSC measurements were performed with a Perkin-Elmer PyrisDiamond DSC. Samples (3 – 5 mg) were placed in aluminum open pans. Heating was carried out at 5.00 °C min⁻¹ for all samples, in the temperature range 40 – 140 °C.

4.5. References

- 1) J. Zhang, Q. Zou, H. Tian, *Adv. Mater.* **2013**, *25*, 378–399.
- 2) S. Kawata, Y. Kawata, *Chem. Rev.* **2000**, *100*, 1777–1788.
- 3) J. Cusido, E. Deniz, F. M. Raymo, *European J. Org. Chem.* **2009**, *2009*, 2031–2045.
- 4) E. Hadjoudis, I. M. Mavridis, *Chem. Soc. Rev.* **2004**, *33*, 579–588.
- 5) K. Ogawa, Y. Kasahara, Y. Ohtani, J. Harada, *J. Am. Chem. Soc.* **1998**, *120*, 7107–7108.
- 6) J. Harada, H. Uekusa, Y. Ohashi, *J. Am. Chem. Soc.* **1999**, *121*, 5809–5810.
- 7) J. Harada, K. Ogawa, *Chem. Soc. Rev.* **2009**, *38*, 2244–2252.
- 8) K. Johmoto, T. Ishida, A. Sekine, H. Uekusa, Y. Ohashi, *Acta Crystallogr. Sect. B Struct. Sci.* **2012**, *68*, 297–304.
- 9) A. Carletta, X. Buol, T. Leyssens, B. Champagne, J. Wouters, *J. Phys. Chem. C* **2016**, *120*, 10001–10008.
- 10) F. Robert, A. D. Naik, B. Tinant, R. Robiette, Y. Garcia, *Chem. - A Eur. J.* **2009**, *15*, 4327–4342.
- 11) K. M. Hutchins, S. Dutta, B. P. Loren, L. R. MacGillivray, *Chem. Mater.* **2014**, *26*, 3042–3044.
- 12) I. O. Staehle, B. Rodríguez-Molina, S. I. Khan, M. A. Garcia-Garibay, *Cryst. Growth Des.* **2014**, *14*, 3667–3673.
- 13) M. Sliwa, S. Létard, I. Malfant, M. Nierlich, P. G. Lacroix, T. Asahi, H. Masuhara, P. Yu, K. Nakatani, *Chem. Mater.* **2005**, *17*, 4727–4735.
- 14) G. R. Desiraju, *Angew. Chemie Int. Ed.* **2007**, *46*, 8342–8356.
- 15) G. R. Desiraju, *Angew. Chemie Int. Ed. English* **1995**, *34*, 2311–2327.

- 16) D. Braga, F. Grepioni, *Making Crystals by Design : Methods, Techniques and Applications*, Wiley-VCH, **2007**.
- 17) K. Biradha, R. Santra, *Chem. Soc. Rev.* **2013**, *42*, 950–67.
- 18) D. Braga, L. Brammer, N. R. Champness, *CrystEngComm* **2005**, *7*, 1–19.
- 19) C. B. Aakeröy, N. R. Champness, C. Janiak, *CrystEngComm* **2010**, *12*, 22–43.
- 20) P.-L. Jacquemin, K. Robeyns, M. Devillers, Y. Garcia, *Chem. - A Eur. J.* **2015**, *21*, 6832–6845.
- 21) M. Zbačnik, M. Vitković, V. Vulić, I. Nogalo, D. Cinčić, *Cryst. Growth Des.* **2016**, *16*, 6381–6389.
- 22) G. Cavallo, P. Metrangolo, R. Milani, T. Pilati, A. Priimägi, G. Resnati, G. Terraneo, *Chem. Rev.* **2016**, *116*, 2478–2601.
- 23) J. Xu, X. Liu, J. K.-P. Ng, T. Lin, C. He, *J. Mater. Chem.* **2006**, *16*, 3540–3545.
- 24) L. Meazza, J. A. Foster, K. Fucke, P. Metrangolo, G. Resnati, J. W. Steed, *Nat. Chem.* **2012**, *5*, 42–47.
- 25) F. Grepioni, S. d’Agostino, D. Braga, A. Bertocco, L. Catalano, B. Ventura, *J. Mater. Chem. C* **2015**, *3*, 9425–9434.
- 26) S. d’Agostino, F. Grepioni, D. Braga, B. Ventura, *Cryst. Growth Des.* **2015**, *15*, 2039–2045.
- 27) H. Wang, R. X. Hu, X. Pang, H. Y. Gao, W. J. Jin, *CrystEngComm* **2014**, *16*, 7942–7948.
- 28) M. Baldrigli, G. Cavallo, M. R. Chierotti, R. Gobetto, P. Metrangolo, T. Pilati, G. Resnati, G. Terraneo, *Mol. Pharm.* **2013**, *10*, 1760–1772.
- 29) Z.-L. Jing, R.-N. Li, N. Yang, *Acta Crystallogr. Sect. E Struct. Reports Online* **2007**, *63*, o3001–o3001.
- 30) C.-S. Zheng, N. Yang, M. Li, Z.-L. Jing, *Acta Crystallogr. Sect. E Struct. Reports Online* **2005**, *61*, o3613–o3614.
- 31) P. Metrangolo, G. Resnati, *Chem. - A Eur. J.* **2001**, *7*, 2511–2519.

- 32) D. Braga, L. Maini, F. Grepioni, *Chem. Soc. Rev.* **2013**, *42*, 7638.
- 33) S. L. James, C. J. Adams, C. Bolm, D. Braga, P. Collier, T. Friščić, F. Grepioni, K. D. M. Harris, G. Hyett, W. Jones, A. Krebs, J. Mack, L. Maini, A. G. Orpen, I. P. Parkin, W. C. Shearouse, J. W. Steed, D. C. Waddell, *Chem. Soc. Rev.* **2012**, *41*, 413–447.
- 34) E. Hadjoudis, M. Vittorakis, I. Moustakali-Mavridis, *Tetrahedron* **1987**, *43*, 1345–1360.
- 35) M. Angeles García, C. López, R. M. Claramunt, A. Kenz, M. Pierrot, J. Elguero, *Helv. Chim. Acta* **2002**, *85*, 2763–2776.
- 36) W. Holzer, R. M. Claramunt, C. López, I. Alkorta, J. Elguero, *Solid State Nucl. Magn. Reson.* **2008**, *34*, 68–76.
- 37) J. Elguero, F. H. Cano, C. Foces-Foces, A. L. Llamas-Saiz, H. Limbach, F. Aguilar-Parrilla, R. M. Claramunt, C. López, *J. Heterocycl. Chem.* **1994**, *31*, 695–700.
- 38) C. Foces-Foces, A. L. Llamas-Saiz, R. M. Claramunt, C. López, J. Elguero, *J. Chem. Soc. Chem. Commun.* **1994**, *118*, 49–1145.
- 39) J. Elguero, *Cryst. Growth Des.* **2011**, 4731–4738.
- 40) M. R. Chierotti, L. Ferrero, N. Garino, R. Gobetto, L. Pellegrino, D. Braga, F. Grepioni, L. Maini, *Chem. - A Eur. J.* **2010**, *16*, 4347–4358.
- 41) D. M. Többens, J. Glinneman, M. R. Chierotti, J. van de Streek, D. Sheptyakov, *CrystEngComm* **2012**, *14*, 199–236.
- 42) M. U. Schmidt, J. Brüning, J. Glinnemann, M. W. Hützler, P. Mörschel, S. N. Ivashevskaya, J. van de Streek, D. Braga, L. Maini, M. R. Chierotti, R. Gobetto, *Angew. Chemie Int. Ed.* **2011**, *50*, 7924–7926.
- 43) C. M. Widdifield, G. Cavallo, G. A. Facey, T. Pilati, J. Lin, P. Metrangolo, G. Resnati, D. L. Bryce, *Chem. - A Eur. J.* **2013**, *19*, 11949–11962.
- 44) M. Baldrighi, D. Bartesaghi, G. Cavallo, M. R. Chierotti, R. Gobetto, P. Metrangolo, T. Pilati, G. Resnati, G. Terraneo, *CrystEngComm* **2014**, *16*, 875–5904.

- 45) R. Pettinari, F. Marchetti, C. Pettinari, F. Condello, B. W. Skelton, A. H. White, M. R. Chierotti, R. Gobetto, *Dalt. Trans.* **2016**, 45, 5404–5404.
- 46) M. R. Chierotti, R. Gobetto, *Chem. Commun.* **2008**, 1621-1634.
- 47) I. Yavari, J. D. Roberts, *Magn. Reson. Chem.* **1979**, 12, 87–91.
- 48) P. Cerreia Vioglio, M. R. Chierotti, R. Gobetto, *CrystEngComm* **2016**, 18, 9173–9184.
- 49) J. Harada, T. Fujiwara, K. Ogawa, *J. Am. Chem. Soc.* **2007**, 129, 16216–16221.
- 50) T. Fujiwara, J. Harada, K. Ogawa, *J. Phys. Chem. B* **2004**, 108, 4035–4038.
- 51) G. M. Mercier, K. Robeyns, T. Leyssens, *Cryst. Growth Des.* **2016**, 16, 3198–3205.
- 52) E. Hadjoudis, A. Rontoyianni, K. Ambroziak, T. Dziembowska, I. M. Mavridis, *J. Photochem. Photobiol. A Chem.* **2004**, 162, 521–530.
- 53) M. Avadanei, V. Cozan, S. Shova, J. A. Paixão, *Chem. Phys.* **2014**, 444, 43–51.
- 54) J. W. Ledbetter, *J. Phys. Chem.* **1966**, 70, 2245–2249.
- 55) a) G. Kortüm, W. Braun, G. Herzog, *Angew. Chemie Int. Ed.* 1963, 2, 333–341. b) G. Kortüm, "Reflectance spectroscopy - Principles, Methods Applications" Springer-Verlag, Berlin - Heidelberg - New York, 1969.
- 56) S. Taro, T. Kobayashi, T. Inabe, *J. Phys. Chem. A* **1997**, 101, 644–649.
- 57) M. Sliwa, N. Mouton, C. Ruckebusch, S. Aloïse, O. Poizat, G. Buntinx, R. Métivier, K. Nakatani, H. Masuhara, T. Asahi, *J. Phys. Chem. C* **2009**, 113, 11959–11968.
- 58) D. Higelin, H. Sixl, *Chem. Phys.* **1983**, 77, 391–400.
- 59) D. A. Safin, K. Robeyns, M. G. Babashkina, Y. Filinchuk, A. Rotaru, C. Jureschi, M. P. Mitoraj, J. Hooper, M. Brela, Y. Garcia, *CrystEngComm* **2016**, 12, 106.
- 60) D. A. Safin, M. G. Babashkina, K. Robeyns, Y. Garcia, *RSC Adv.* **2016**, 6, 53669–53678.

- 61) F. Robert, P.-L. Jacquemin, B. Tinant, Y. Garcia, *CrystEngComm* **2012**, *14*, 4396.
- 62) K. Johmoto, A. Sekine, H. Uekusa, *Cryst. Growth Des.* **2012**, *12*, 4779–4786.
- 63) T. Haneda, M. Kawano, T. Kojima, M. Fujita, *Angew. Chemie Int. Ed.* **2007**, *46*, 6643–6645.
- 64) M. Zbačnik, B. Kaitner, *Croat. Chem. Acta* **2016**, *89*, 125–132.
- 65) A. Carletta, J. Dubois, A. Tilborg, J. Wouters, *CrystEngComm* **2015**, *17*, 3509–3518.
- 66) M. Zbačnik, B. Kaitner, *CrystEngComm* **2014**, *16*, 4162.
- 67) B. C. Gates, H. Knözinger, F. C. Jentoft, *Advances in Catalysis Vol. 52*, Academic Press, **2009**.
- 68) H. Ishida, S. Tobita, Y. Hasegawa, R. Katoh, K. Nozaki, *Coord. Chem. Rev.* **2010**, *254*, 2449–2458.
- 69) L. J. Farrugia, *J. Appl. Cryst.* **2012**, *45*, 849–854.
- 70) M. C. Burla, R. Caliandro, B. Carrozzini, G. L. Casciarano, C. Cuocci, C. Giacovazzo, M. Mallamo, A. Mazzone, G. Polidori, *J. Appl. Cryst.* **2015**, *48*, 306–309.
- 71) G. M. Sheldrick, *Acta Crystallogr. Sect. C, Struct. Chem.* **2015**, *71*, 3.
- 72) A. L. Spek, *J. Appl. Cryst.* **2003**, *36*, 7–13.
- 73) C. F. Macrae, P. R. Edgington, P. McCabe, E. Pidcock, G. P. Shields, R. Taylor, M. Towler, J. van de Streek, *J. Appl. Cryst* **2006**, *39*, 453–457.
- 74) F. H. Allen, *Acta Crystallogr. Sect. B-Struct. Sci.* **2002**, *58*, 380–388.

Chapter 5

Playing with structural isomers and stoichiometry.[†]

[†]Carletta, Andrea, et al. "Playing with Isomerism: Cocrystallization of Isomeric *N*-Salicylideneaminopyridines with Perfluorinated Compounds as Halogen Bond Donors and Its Impact on Photochromism." *Crystal Growth & Design* 18 (2018): 6833-6842

Playing with Isomerism: Cocrystallization of Isomeric *N*-Salicylideneaminopyridines with Perfluorinated Compounds as Halogen Bond Donors and Its Impact on Photochromism

Andrea Carletta¹, Marija Zbačnik², Mégane Van Gysel¹, Matea Vitković², Nikolay Tumanov,¹ Vladimir Stilinović², Johan Wouters^{*,1}, and Dominik Cinčić^{*,2}

¹Department of Chemistry, Namur Institute of Structured Matter (NISM), University of Namur, 61 rue de Bruxelles, B-5000 Namur, Belgium

²Department of Chemistry, Faculty of Science, University of Zagreb, Horvatovac 102a, HR-10000 Zagreb, Croatia.

Abstract. In *N*-salicylideneaniline derivatives, photochromism occurs by a two-step isomerization mechanism. Photochromism has been reported to be closely related to the molecular conformation of the *N*-salicylideneanilines (described by the dihedral angle Φ) and to the free available space (V_{free}) in the crystal. In this contribution, we focus on cocrystals of isomeric *N*-salicylideneaminopyridines with perfluorinated halogen bond donors as co-formers. The advantage of working with isomers is that they have a similar (if not equal) molecular volume. This aspect means that the evaluation and comparison of the free available spaces between cocrystals is not affected by the differences in the molecular volumes of their constituents. Cocrystals were synthesized by a one-pot procedure which allowed concomitant formation of covalent (imine) and non-covalent (halogen) bonds. Each cocrystal was characterized by X-ray diffraction and its photochromism was assessed by UV-Vis

diffuse reflectance. Our results suggest that the Φ/V_{free} model, grossly oversimplifies the complexity of the dynamic phenomenon behind the photoisomerization of *N*-salicylideneanilines. For the above-mentioned reasons, careful examination of intermolecular interactions and crystals packing (localization of voids, evaluation of intermolecular interactions and stacking modes) should be taken into account and used to supplement the current proposed model based on Φ and V_{free} .

5.1. Introduction

Since its first introduction by G. Schmidt in 1971, the term ‘crystal engineering’ has broadened considerably, encompassing various aspects of supramolecular chemistry.¹ The ultimate goal of crystal engineering lies in the design of solids with desired physical and chemical properties through the study of intermolecular interactions and crystal packing.²⁻⁵ Nowadays, cocrystallization (the phenomenon of aggregation of two or more chemical entities in the same crystal lattice) has become a popular tool for the improvement of physical and chemical properties of pharmaceuticals.⁶⁻⁸ However, applications of cocrystals go beyond pharmaceuticals. In fact, over the past few years, we have witnessed a growing interest in the development of cocrystallization procedures to generate luminescent⁹⁻¹¹ or smart photo-,¹²⁻¹⁷ thermo-,¹⁶⁻²² mechano-,^{19,23} solvato-,²⁴ and vapo-responsive^{19,25} solids but also dichroic²⁶⁻²⁸ and energetic materials.²⁹⁻³¹

In this work, we will be focused on the crystal engineering of solid-state photochromism through cocrystallization with classical perfluorinated halogen bond (XB) donors.³² Over the past several decades halogen bonds³³ have been well recognized in crystal engineering^{18,34,35} and are among the most interesting non-covalent interactions³⁶, of the family of σ -hole interactions.^{37,38} They have been used for constructing supramolecular assemblies such as cocrystals,³⁹⁻⁴¹ and functional materials.⁴²⁻⁴⁴ Photochromism is a light induced reversible change of color due to the transformation of a chemical species into another having different absorption

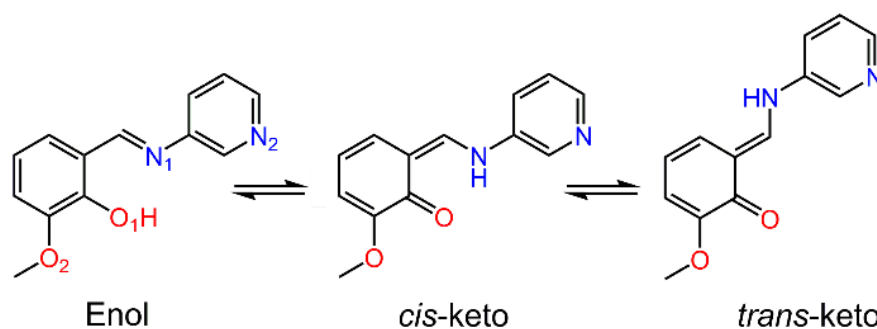


Figure 1. Tautomers of *N*-salicylideneaminopyridine derivatives (labeling scheme of the heteroatoms is reported for the enol form).

spectrum.⁴⁵ We will investigate the effects of cocrystallization on selected cocrystals of *N*-salicylideneaminopyridine derivatives. These derivatives belong to a class of compounds, the imines of salicylaldehyde (*N*-salicylideneanilines), which can manifest photochromism in the solid state.^{46,47} The proposed two-step mechanism (**Figure 1**) consists of an excited-state proton transfer (enol to *cis*-keto) and a subsequent *cis-trans* photoisomerization (*cis*-keto to *trans*-keto).

Despite this well-known mechanism,^{45,48-50} much remains to be learned about factors that control the expression of photochromism in the solid state. The first proposed factor for the prediction of photochromism was identified in the molecular conformation of the *N*-salicylideneaniline and interplanar separation between these molecules in the crystal packing.⁵⁰ Jomoto *et al.* supported this hypothesis by a systematic investigation on salts and cocrystals of two *N*-salicylideneanilines.¹⁷ They concluded that when the conformation is “non-planar” – that means that the dihedral angle between the two aromatic rings is more than 30° - the *N*-salicylideneaniline will likely be photochromic. Instead, when the dihedral angle (Φ) is less than 20° the solid will be non-photochromic. However, several exceptions to this rule were later reported.^{16,51-54} Another descriptor of photochromism was proposed by Garcia *et al.*⁵¹: the “free available space” (V_{free}). The idea behind these two models is that the less compact the crystal packing, the more likely the solid will be photochromic. These models were recently reviewed by Sugiyama and Uekusa in a new series of cocrystals of *N*-salicylideneaminopyridine derivatives.⁵⁵

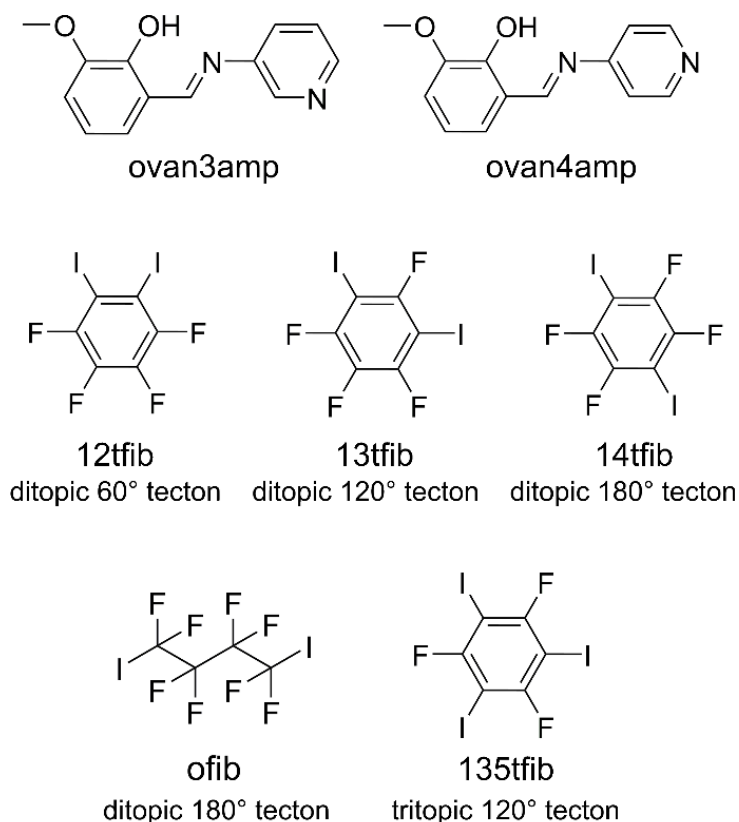


Figure 2. Chromophores (**ovan3amp** and **ovan4amp**) and co-formers used in the present work

In this study, they suggest that the combined evaluation of V_{free} and of Φ improves the description and the prediction of photochromism. To go deeply in this investigation, we decided to work on two isomeric *N*-salicylideneanilines which were cocrystallized with a series of halogen donors (three of which themselves are isomeric diiodoperfluorobenzenes). One of the advantages of working with isomers is that they can have similar (if not equal) volume requirements. This aspect means that the free available space will strictly be a function of the molecular packing and not of the differences in the molecular volumes of the constituents of the cocrystal. The two selected isomeric *N*-salicylideneaminopyridines, namely **ovan3amp** and **ovan4amp** (**Figure 2**), are obtained from condensation reaction between *o*-vanillin and 3- or 4-aminopyridine, respectively. Cocrystal formers employed (**Figure 2**) are halogen bond donors 1,4-diiidotetrafluorobenzene (**14tfib**) and its *meta*- and *ortho*-

isomers (1,3-diiodotetrafluorobenzene, **13tfib**, and 1,2-diiodotetrafluorobenzene, **12tfib**). We have also included in this study the tritopic co-former 1,3,5-triiodo-2,4,6-trifluorobenzene (**135tfib**), and 1,4-diiodooctafluorobutane (**ofib**). The latter is a 180° ditopic XB donor, like **14tfib**, giving the possibility to obtain two isomorphous cocrystals. We will provide a systematic structural investigation with a thorough characterization of photochromism by UV-Vis diffuse reflectance spectroscopy. Parameters currently proposed for the rationalization of photochromism (Φ and V_{free}) were determined for each cocrystal.

5.2. Experimental Section

As the mechanochemical synthesis of imines⁵⁶⁻⁵⁸ and their halogen-bonded cocrystals^{15,59,60} has been previously described as an efficient synthetic approach, we performed cocrystal screening by grinding.^{61,62} *N*-salicylideneaminopyridine-based cocrystals were synthesized by mechanochemistry in a one-pot single-step procedure. All three reactants (*o*-vanilline, an aminopyridine and a halogenated co-former) were milled in a ball mill jar. The as-synthesized powders were characterized by means of powder X-ray diffraction. The experimental patterns obtained were compared with the ones calculated from the single-crystal structures to identify the output of the synthesis. Besides the low-waste characteristics of the mechanochemical approach, the application of this one-pot single-step synthesis has two important advantages: its timesaving properties and the easiness to deal with sticky paste products. The classical synthesis of *N*-salicylideneanilines (condensation reaction between an aldehyde and an aniline) is usually performed on a Dean–Stark apparatus. This procedure requires relatively long reaction times (typically 8-24 hours) and proceeds at reflux temperature. The product is typically recovered by crystallization/precipitation to afford 60-85% yields.^{52,54} These condensation reactions require less than 60 minutes when performed by mechanochemistry (at 30 Hz) in stainless-steel grinding jars and the chemical conversion is near-total (**Figure**

S1-S2). One issue of the ball milling is that sticky products can arise during the milling procedure. The products may stick to the balls or the sides of the milling jar, reducing the energy transfer and thus leading to inefficient mixing or milling and therefore lower conversion/reaction yields. For instance, compound **ovan4amp** (synthesized from *o*-vanillin and 4-aminopyridine) appears as a viscous red oil in which the miller balls are trapped. Adding the halogenated cocystal former to the pre-synthesized **ovan4amp** results in a sticky paste showing traces of a viscous red oil. Instead, we noticed that simultaneous addition and milling of *o*-vanillin, 4-aminopyridine and the halogenated co-former led to high conversion of cocystal (**Figure S1**). In all cases, free-flowing powders were obtained. Detailed synthetic procedures are reported below. Powder diffractograms are reported in **Figure S1-S2**.

Mechanosynthesis of ovan3amp·12tfib. *o*-Vanillin (182.0 mg, 1.20 mmol), 3-aminopyridine (112.1 mg, 1.20 mmol) and **12tfib** (481.2 mg, 1.20 mmol) were placed in stainless steel grinding jars (25 mL). Mechanochemistry was performed during 60 minutes at 30 Hz. A yellow-orange powder product was obtained. Its powder pattern matched the one simulated from single-crystal X-ray data (**Figure S2**). Yellow-orange plates suitable for structure determination were obtained in a 50:50 mixture of EtOAc/cyclohexane.

Mechanosynthesis of ovan3amp·13tfib. *o*-Vanillin (364.0 mg, 2.40 mmol), 3-aminopyridine (224.2 mg, 2.40 mmol) and **13tfib** (380 μ l, 2.40 mmol) were placed in stainless steel grinding jars (25 mL). Mechanochemistry was performed during 60 minutes at 30 Hz. An orange-red powder product was obtained. Its powder pattern matched the one simulated from single-crystal X-ray data (**Figure S2**). Orange-red platy crystals suitable for structure determination were obtained in a 50:50 mixture of EtOAc/cyclohexane.

Mechanosynthesis of (ovan3amp)₂·14tfib. *o*-Vanillin (370.6 mg, 2.42 mmol), 3-aminopyridine (227.7 mg, 2.42 mmol) and **14tfib** (486.3 mg, 1.21 mmol) were placed in stainless steel grinding jars (25 mL). Mechanochemistry was performed during 60 minutes at 30 Hz. An orange-red powder product was obtained. Its powder

pattern matched the one simulated from single-crystal X-ray data (**Figure S2**). Yellow-orange needle-shaped crystals were obtained in a 50:50 mixture of EtOAc/cyclohexane. Crystal structure of **(ovan3amp)₂·14tfib** is retrieved from the literature (CSD refcode: SEDFIT01¹⁵)

Mechanosynthesis of (ovan3amp)₂·ofib. *o*-Vanillin (364.0 mg, 2.40 mmol), 3-aminopyridine (224.2 mg, 2.40 mmol) and **ofib** (219 μ l, 1.20 mmol). Mechanosynthesis was performed during 60 minutes at 30 Hz. An orange-red powder product was obtained. Its powder pattern matched the one simulated from single-crystal X-ray data (**Figure S2**). Yellow-orange needle-shaped crystals were obtained from chloroform.

Mechanosynthesis of (ovan3amp)₂·135tfib. *o*-Vanillin (175.7 mg, 1.15 mmol), 3-aminopyridine (108.2 mg, 1.15 mmol) and **135tfib** (293.1 mg, 0.58 mmol) were placed in stainless steel grinding jars (25 mL). Mechanosynthesis was performed during 60 minutes at 30 Hz. A yellow-orange powder product was obtained. Its powder pattern matched the one simulated from single-crystal X-ray data (**Figure S2**). Yellow-orange needle-shaped crystals suitable for structure determination were obtained in a 50:50 mixture of EtOAc/cyclohexane.

Mechanosynthesis of (ovan4amp)₂·12tfib. *o*-Vanillin (419.6 mg, 2.74 mmol), 4-aminopyridine (257.9 mg, 2.74 mmol) and **12tfib** (551.4 mg, 1.37 mmol) were placed in stainless steel grinding jars (25 mL). Mechanosynthesis was performed during 60 minutes at 30 Hz. An orange powder product was obtained. Its powder pattern matched the one simulated from single-crystal X-ray data (**Figure S1**). Orange prism-shaped crystals suitable for structure determination were obtained by slow evaporation from a saturated EtOAc solution.

Mechanosynthesis of (ovan4amp)₂·14tfib. *o*-Vanillin (457.7 mg, 2.99 mmol), 4-aminopyridine (281.3 mg, 2.99 mmol) and **14tfib** (600.9 mg, 1.50 mmol) were placed in stainless steel grinding jars (25 mL). Mechanosynthesis was performed during 60 minutes at 30 Hz. An orange powder product was obtained. Its powder pattern matched the one simulated from single-crystal X-ray data (**Figure S1**).

Orange prism-shaped crystals suitable for structure determination were obtained by slow evaporation from a saturated EtOAc solution.

Mechanosynthesis of *ovan4amp*·*135tfib*. *o*-Vanillin (195.6 mg, 1.28 mmol), 4-aminopyridine (120.6 mg, 1.28 mmol) and **135tfib** (651.1 mg, 1.28 mmol) were placed in stainless steel grinding jars (25 mL). Mechanochemistry was performed during 60 minutes at 30 Hz. An orange powder product was obtained. Its powder pattern matched the one simulated from single-crystal X-ray data (**Figure S1**). Orange prism-shaped crystals suitable for structure determination were obtained by slow evaporation from a saturated EtOAc solution.

Single-crystal X-ray diffraction. Single-crystal diffraction data for **ovan3amp**·**12tfib** (293 K), (**ovan3amp**)₂·**135tfib** (293 K) and (**ovan3amp**)₂·**ofib** (100 K) were collected on an Oxford Diffraction Gemini Ultra R system (4-circle kappa platform, Ruby CCD detector) using Mo K_α ($\lambda = 0.71073 \text{ \AA}$) radiation. Diffraction measurements for **ovan3amp**·**13tfib** (298 K), **ovan4amp**·**12tfib** (293 K), (**ovan4amp**)₂·**14tfib** (150 K) and **ovan4amp**·**135tfib** (298 K) were performed on an Oxford Diffraction Xcalibur Kappa CCD X-ray diffractometer using Mo K_α radiation. The structures were solved by SHELXT⁶³ and then refined by full-matrix least square refinement of $|F|^2$ using SHELXL-2016.⁶⁴ Non-hydrogen atoms were refined anisotropically; hydrogen atoms were located from difference Fourier map. Hydrogen atoms non-involved in hydrogen bonding were refined in the riding mode with isotropic temperature factors fixed at $1.2U_{eq}$ of the parent atoms ($1.5U_{eq}$ for methyl group). Coordinates of the hydrogen atoms implicated in hydrogen bonds were refined. The program Mercury⁶⁵ was used for molecular graphics. Structure (**ovan3amp**)₂·**14tfib** (115 K) was retrieved from the CCDC database (SEDFIT01¹⁵). CSD refcodes: 1547940, 1548140, 1548172, 1552262, 1582770, 1850125, 1850126.

Powder X-ray Diffraction Measurements. X-ray powder patterns (Cu K_α radiation, step size 0.017°; 45 mA, 30 kV) were collected in the 2θ range 5-40° using a Panalytical X'Pert PRO diffractometer (Bragg-Brentano geometry, X'Celerator

detector). The program Mercury was used for calculation of X-ray powder patterns from single crystal structure data.

Full interaction maps. Full Interaction Maps⁶⁶ (FIMs) were used to explore the hydrogen bond and halogen bond donor/acceptor areas in molecules **ovan3amp** and **ovan4amp**. Chromophore molecules used for calculation of FIMs were taken from the structures (**ovan3amp**)₂·**135tfib** and **ovan4amp**·**135tfib**, respectively. FIMs are density maps indicating donor/acceptor interaction propensities of functional groups onto whole molecules taking into account steric factors. FIMs are generated from 3D Isostar scatterplots of individual pairs of functional groups. Carbonyl probe (used to find H-bond donor hotspot onto the molecule), uncharged NH probe (used to find H-bond acceptor hotspot onto the molecule), C-F probe (used to find hotspots for the interaction with fluorine atoms of the co-former) and C-I probe (used to find halogen bond acceptor hotspot onto the molecule) were used to generate the FIMs.

Calculation of V_{free} and molecular volume. Molecular volumes (needed for the calculation of V_{free}) were calculated from the Molinspiration free toolkit (www.molinspiration.com).⁶⁷ These molecular volumes have been obtained by fitting sum of fragment contributions to 3D volume (fully optimized by the semiempirical AM1 method) for a training set of about twelve thousand molecules.⁶⁷ V_{free} was therefore calculated as reported by Garcia and co-workers.⁵¹ In cases where compared cocrystals presented the same molecular formula, the density (ρ) obtained from the single-crystal X-ray diffraction experiments is also provided.

UV-Vis diffuse reflectance. Measurements were performed on pure microcrystalline powder samples on a Varian 5E spectrophotometer equipped with a “praying mantis” diffuse reflection accessory. Measured reflectance spectra of solid samples were converted to absorption spectra using the Kubelka–Munk function.⁶⁸ Photochromism investigations were performed by irradiating powder samples by using a MAX-303 lamp (Xenon light source 300W) at 360 nm (by use of 20 nm bandpass filters) during 15 minutes. Thermal fading was analyzed by monitoring the

evolution of absorption at 500 nm in a dark environment. Spectra were measured each 4 min over 180 min, in a dark environment for **(ovan3amp)₂·135tfib**. For the slowest thermal decaying solid, **ovan3amp·12tfib**, spectra were taken each 20 min for 2160 min (36 h). Spectra of **(ovan3amp)₂·ofib** were measured each 20 min over 800 min.

5.3. Results and Discussion

5.3.1. Structural Characterization

The chromophores we have selected belong to the family of the *N*-salicylideneaminopyridines. These compounds offer important advantages for what concerns the construction of multicomponent crystal forms with respect to the classical *N*-salicylideneaniline derivatives. In particular the N-atom of the pyridine moiety can act as a strong H- or X-bond acceptor making the formation of cocrystals easier through these interactions.^{15,16,55,59} Alternatively, the N-atom can be easily alkylated to form various pyridinium salts.⁶⁹ The vanillidene moiety has also been shown to be involved in halogen and hydrogen bonds in which both the two O-atoms may be involved.^{15,16,57} In particular, the presence of the methoxy group has been shown to increase the tendency toward cocrystal formation given that it can act as an “ancillary” acceptor to generate slightly bifurcated halogen bond geometries or a symmetrical bifurcated halogen bond.⁶⁰ In some derivatives this acceptor area interacts with the H–C(sp²) iminic hydrogen of a second *N*-salicylideneaminopyridine molecule. Full interaction maps calculated for carbonyl (red), uncharged NH (blue), C-F (green) and C-I (purple) probes on **ovan3amp** (**Figure 3a**) and **ovan4amp** (**Figure 3b**) provide a 3D visualization of the interaction preferences for these two molecules. Combination of these donor and acceptor properties contributes to a variety of supramolecular assemblies differing in type (chains, rings or discrete 2- or 3-component assemblies) and composition (*N*-salicylideneaminopyridine and the co-formers are usually assembled in a 1:1 or 2:1

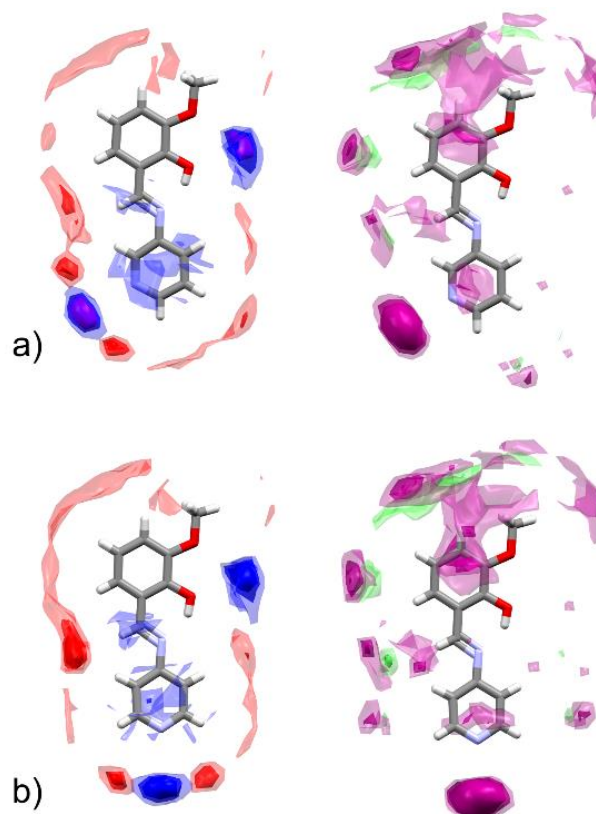


Figure 3. Full interaction maps calculated on (a) **ovan3amp** and (b) **ovan4amp** derivatives. Interaction maps are calculated for carbonyl (red), uncharged NH (blue), C-I (purple) and C-F (green) probes.

stoichiometry) in which the *N*-salicylideneaminopyridine derivative is involved. For these reasons, *N*-salicylideneaminopyridines are versatile systems for the construction of an extensive library of multicomponent systems.

Compound **ovan3amp** formed cocrystals with each of the five selected co-formers. For all of them structure determination by single-crystal X-ray diffraction was possible. Cocrystals exhibit a 1:1 or 2:1 stoichiometry: **ovan3amp**·**12tfib**, **ovan3amp**·**13tfib**, (**ovan3amp**)₂·**14tfib**,¹⁵ (**ovan3amp**)₂·**ofib** and (**ovan3amp**)₂·**135tfib**. When the stoichiometry is 2:1, the supramolecular synthon found is the I···N halogen bond directed toward the pyridine moiety of the chromophore.

Table 1. Geometry of halogen bonds in the prepared cocrystal structures
(numbering scheme is reported in **Figure 1**).

Compound Name	Contact type A...I	d(A...I) / Å	A...I-C angle / °
ovan3amp·12tfib	N2...I	3.014(5)	163.2(2)
	O1...I	3.473(4)	152.8(1)
	O2...I	3.315(4)	156.1(1)
ovan3amp·13tfib	N2...I	2.861(4)	173.2(1)
	O1...I	3.066(3)	175.2(1)
	O2...I	3.457(3)	135.8(1)
(ovan3amp)₂·14tfib	N2...I	2.855(6)	168.5(2)
(ovan3amp)₂·ofib	N2...I	2.772(2)	176.7(1)
(ovan3amp)₂·135tfib	N2...I	2.902(4)	178.3(2)
	O1...I	3.284(4)	151.9(2)
	O2...I	3.154(4)	157.3(2)
(ovan4amp)₂·12tfib	N2...I ^a	2.889(5)	175.1(2)
	N2...I	2.838(6)	172.3(2)
	N2...I ^a	2.962(5)	161.5(2)
(ovan4amp)₂·14tfib	N2...I	2.812(2)	170.3(1)
ovan4amp·135tfib	N2...I	2.829(4)	172.1(1)

^a Two crystallographically independent molecules in the cocrystal

This condition generates discrete 3-membered assemblies constituted by two molecules of chromophore bridged by a co-former molecule (**Figure 4c-d**). When, instead, the stoichiometry is 1:1 the vanillidene moiety is also involved in the interaction with the co-former (I...O synthon). In this case, the supramolecular assemblies are rather chains or 4-membered rings (**Figure 4a-b**). Compound **ovan4amp** formed cocrystals with 3 of the 5 selected co-formers. These cocrystals are: **(ovan4amp)₂·12tfib**, **(ovan4amp)₂·14tfib**, **ovan4amp·135tfib** (**Figure 4f-h**). Crystallographic parameters of structure determination and refinement are provided in **Table S1**. Halogen bond geometries are provided in **Table 1**.

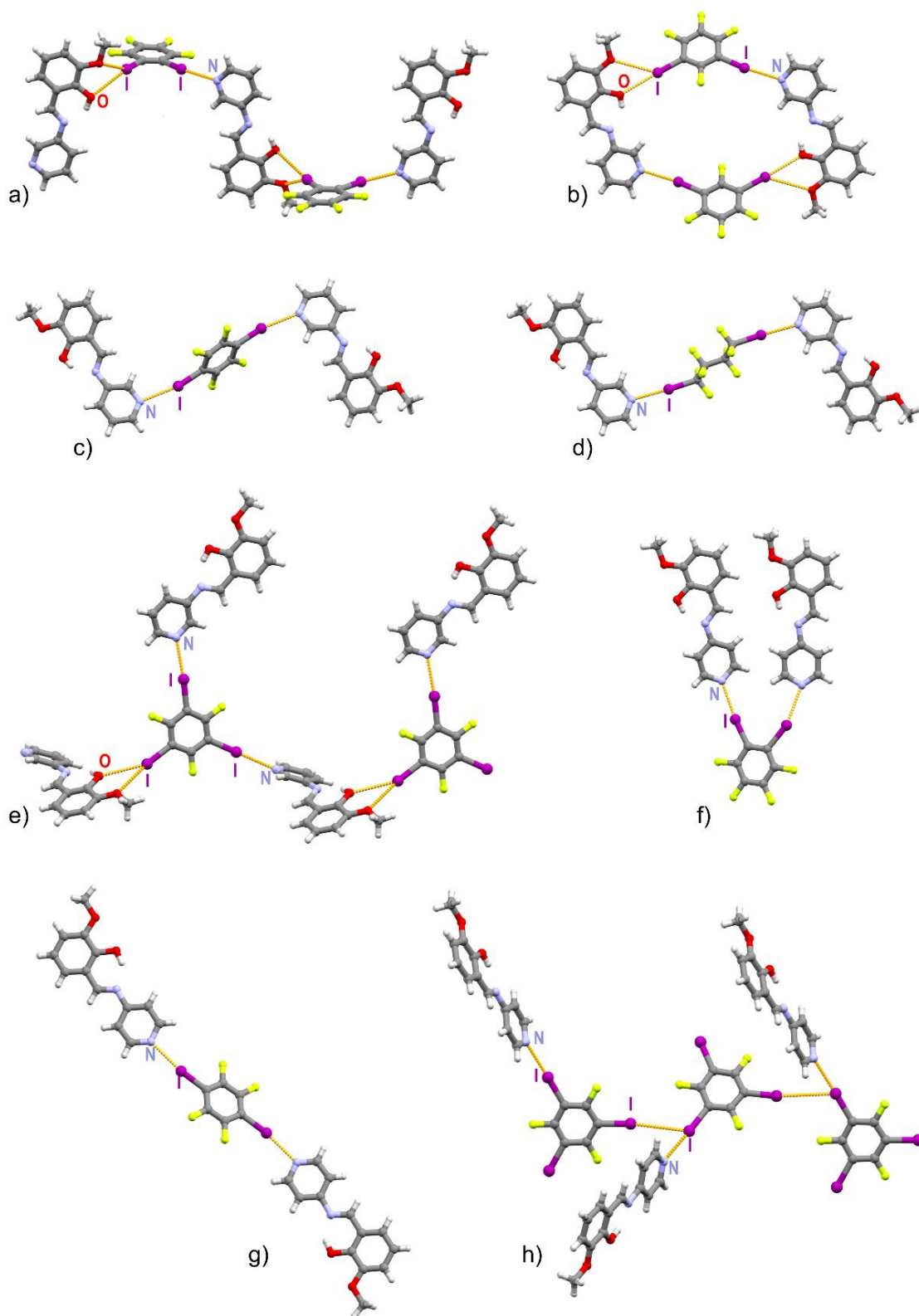


Figure 4. Ball-and-sticks representation of the structural halogen-bonded motifs in cocrystals of **ovan3amp** with **12tfib** (a), **13tfib** (b), **14tfib** (c), **ofib** (d) or **135tfib** (e) and of **ovan4amp** with **12tfib** (f) **14tfib** (g) **135tfib** (h).

5.3.2. Solid-state photochromism

The photochromic behavior was investigated by irradiating the microcrystalline powders at 365 nm. An *N*-salicylideneaniline derivative is photochromic if irradiation is followed by a change in its visible absorption spectrum. An increase of the 450-600 nm spectral region ascribed to the formation of the photoproduct, the *trans*-keto form, is usually observed. This change is consistent with a yellow-to-red or orange-to-red color transition. However, cases of negative photochromism (characterized by a decrease of the 450-600 absorption band) have been reported for some *N*-salicylideneaniline derivatives.^{70,71}

Compound **ovan3amp** is non-photochromic as early reported.¹⁶ Compound **ovan4amp** is a viscous oil at room temperature, therefore characterization of photochromism of this chromophore is out of the scope of this work. Solid **(ovan3amp)₂·14tfib** is reported to be non-photochromic.¹⁵ Among the cocrystals presented in this study, 3 out of 8 are photochromic and present the characteristic increase in the 450-600 spectral region (**Figure 5** and **Figure S3-S4**). For the remaining 5 cocrystals, irradiation at 365 nm did not induce any change in the coloration (and absorption spectra) of the solid compounds. Cocrystals which showed photochromism at solid-state are: **ovan3amp·12tfib**, **(ovan3amp)₂·135tfib** and **(ovan3amp)₂·ofib** (**Figure 5** and **Figure S3-S4**). After irradiation, the initial coloration of the solid can be thermally recovered by leaving the powder in the dark. This thermal decay (or fading) of the coloration was fitted by a biexponential equation.^{72,73} This is rather frequently encountered for *N*-salicylideneanilines and it is attributed to the two two-stage decay of the *trans*-keto form. However, single exponential decay has been reported for some derivatives of the series.^{17,52}

Compound **ovan3amp·12tfib** is characterized by a slow thermal fading of the coloration fitting a biexponential curve with $\tau_1 = 124 \pm 11$ min and $\tau_2 = 3211 \pm 364$ min at 298 K (**Figure S4**, **Table 2**). The compound showed to be stable during 5 photoinduced (15 min irradiation at $\lambda = 550$ nm) switching cycles.

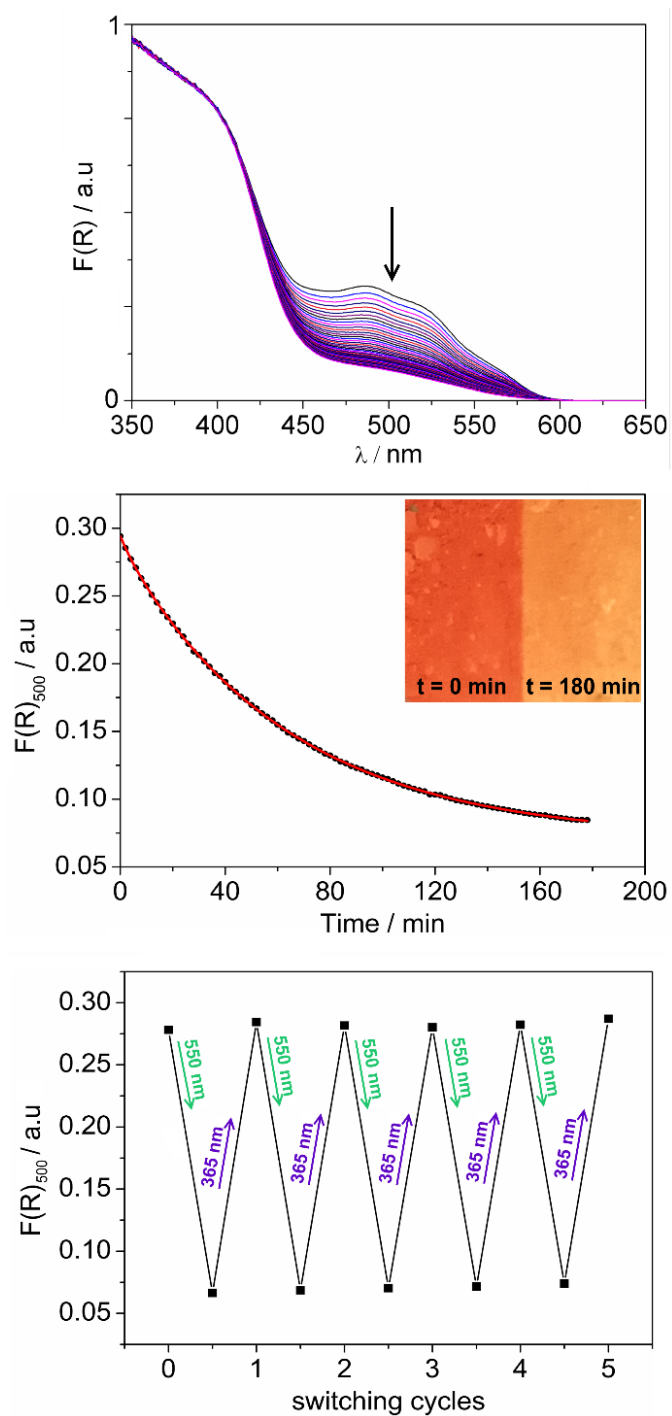


Figure 5. Diffuse reflectance spectra of $(\text{ovan3amp})_2 \cdot 135\text{tfib}$ (top) showing thermal fading of the orange-red coloration. Points at 500 nm were plotted over the time and fitted by a bi-exponential curve (middle). Repeating photochemical recovery over 5 switching cycles (bottom).

Table 2. Time constants for the three photochromic solids at 298 K. A_1 and A_2 (in parentheses) are the relative weight of the preexponential factor.

	ovan3amp·12tfib	(ovan3amp)₂·ofib	(ovan3amp)₂·135tfib
τ_1 / min (A_1)	124 ± 11 (0.19)	126 ± 12 (0.26)	4 ± 0.1 (0.03)
τ_2 / min (A_2)	3211 ± 364 (0.81)	448 ± 25 (0.74)	63 ± 4 (0.97)

Compound **(ovan3amp)₂·ofib** thermal fading fits a biexponential curve with $\tau_1 = 126 \pm 12$ min and $\tau_2 = 448 \pm 25$ min at 298 K (**Figure S3, Table 2**). However, tests of photochemical recovery of the coloration over 5 switching cycles revealed that the photoswitching ability of **(ovan3amp)₂·ofib** is already affected during the 3rd cycle. Thermal fading of **(ovan3amp)₂·135tfib** fits a biexponential curve with $\tau_1 = 4 \pm 0.1$ min and $\tau_2 = 63 \pm 4$ min at 298 K. Its initial coloration could also be recovered photochemically (upon excitation at $\lambda = 550$ nm) during repetitive photoinduced switching cycles (**Figure 5, Table 2**). This aspect evidences a good fatigue resistance and photostability of **(ovan3amp)₂·135tfib**.

5.3.3. In-depth structural comparison: Predictability of photochromism based on Φ and V_{free} .

Here follows a more detailed structure comparison in which the commonly used descriptors of the likelihood of solid-state photochromism will be provided. Those descriptors are the dihedral angle Φ and the average available free space (V_{free}). It has been proposed that when the conformation is “non-planar” – when $\Phi > 30^\circ$ – the *N*-salicylideneaniline will likely be photochromic. Instead, when the dihedral angle (Φ) is less than 20° , the solid will likely be non-photochromic.^{17,45,50,55,74} For the V_{free} , no general threshold value beyond which the solid is photochromic has so far been proposed. However, it has been suggested that the bigger V_{free} , the more likely the solid will be photochromic.^{51,55} One of the advantages of working with structural isomers is that they can have (almost) identical molecular volumes. The three

isomeric co-formers used in this work (**12tfib**, **13tfib** and **14tfib**) are all planar molecules in which the only variation is the disposition of the halo-atoms. Calculated molecular volumes for the three isomeric co-formers is about 152 Å³. Calculated molecular volume for the two chromophores **ovan3amp** and **ovan4amp** is of 208 Å³. This aspect means that the free available space will strictly be a function of the molecular packing and not of the differences in the molecular volumes of the constituents of the cocrystal. For this purpose, we also decided to give particular attention to the comparison of cocrystals having the same molecular formula (therefore same stoichiometry). The examination of these cocrystals of isomers as groups gives helpful information about the features of molecular geometry, free volume and intermolecular interactions, that differentiate these structures from each other. This information will be used to derive a relation between structure and solid-state photochromism. When comparing compounds having the same molecular formula, the experimental crystal density (ρ) calculated from the X-ray diffraction experiments is an evaluation of the compactness of the crystal packing.

1:1 cocrystals with ditopic isomeric co-formers: **ovan3amp·12tfib** and **ovan3amp·13tfib**.

Molecules of **ovan3amp** display a planar conformation in both crystal structures. The dihedral angle, Φ , is of 13.0(6)° in **ovan3amp·12tfib** and of 5.1(4)° in **ovan3amp·13tfib**. Only **ovan3amp·12tfib** is photochromic. Solid **ovan3amp·12tfib** is an exception to the Φ rule: despite its planar conformation, the compound is photochromic. Another aspect to take into account is V_{free} : **ovan3amp·12tfib** is the solid with the higher density (and lower V_{free} , **Table 3**) of the two compounds. These results are both in contradiction with the current model proposed for the prediction of photochromism of *N*-salicylideneanilines based on the sole evaluation of the free available space parameter (V_{free}) and of the dihedral angle Φ . In both crystal structures, **ovan3amp** is bound through halogen bonds to its two sides: vanillidene and aminopyridine (I··O and I··N type, respectively). In the case

of **ovan3amp·12tfib**, molecules are arranged following infinite chains in which the two constituents alternate. In the case of **ovan3amp·13tfib**, we observe a finite 4-membered ring arrangement (**Figure 4**). Closer analysis of the XB distances (**Table 1**) and angles reveals the “poor” directionality of XBs in **ovan3amp·12tfib** when compared to those of **ovan3amp·13tfib**. Specifically, in the first solid, the I··N distance is of 3.014(5) Å with an angle C-I··N of 163.2(2)° whereas, in the second one, the same interaction is characterized by a distance of 2.861(4) Å and by an angle of 173.2(1)°. Distances for the I··O interactions follow the same trend (**Table 1**). We speculate that this aspect could account, in part, for the difference in the photochromic behavior of the two solids. As a matter of fact, these results suggest that when the *N*-salicylideneaminopyridine molecule is bound to both its moieties (pyridine and vanillidene), photochromism is unlikely to occur even for high values of V_{free} . This aspect is corroborated by the fact that, although **ovan3amp·12tfib** is photochromic, the thermal fading of its coloration is much slower in comparison to the other two photochromic cocrystals (**(ovan3amp)₂·ofib** and **(ovan3amp)₂·135tfib**) reported in this study.

1:2 cocrystals with ditopic isomeric co-formers: **(ovan3amp)₂·14tfib**, **(ovan4amp)₂·12tfib** and **(ovan4amp)₂·14tfib**.

None of the cocrystals belonging to this group showed photochromic properties. Intermolecular halogen interactions involve the pyridine moiety of the *N*-salicylideneaminopyridine derivative. V_{free} values range from about 87 Å³ for **(ovan4amp)₂·14tfib**, to about 101 Å³ for **(ovan3amp)₂·14tfib**. Two over three solids are non-photochromic and follow the Φ angle rule (near-flat *N*-salicylideneaminopyridines, see **Table 4**). Instead, solid **(ovan3amp)₂·14tfib** is non-photochromic even if $\Phi > 30^\circ$.¹⁵ Interesting outcomes arise from the structural comparison of this latter with **(ovan3amp)₂·ofib** (see next section).

Table 3. Molecular, packing parameters and experimentally determined photochromism for **ovan3amp·12tfib** and **ovan3amp·13tfib**

	$\Phi / ^\circ$	$V_{\text{free}} / \text{\AA}^3$	$\rho / (\text{g cm}^{-3})$	photochromism
ovan3amp·12tfib	13.0(6) $^\circ$	136	2.110	Yes
ovan3amp·13tfib	5.1(4) $^\circ$	161	2.010	No

Table 4. Molecular packing parameters and experimentally determined photochromism for **(ovan3amp)₂·14tfib**, **(ovan4amp)₂·12tfib** and **(ovan4amp)₂·14tfib**.

	$\Phi / ^\circ$	$V_{\text{free}} / \text{\AA}^3$	$\rho / (\text{g cm}^{-3})$	photochromism
(ovan3amp)₂·14tfib	34.3(4) $^\circ$	101	1.850	No
(ovan4amp)₂·12tfib	10.9(5) $^\circ$ 2.0(4) $^\circ$	106	1.828	No
(ovan4amp)₂·14tfib	6.3(5) $^\circ$	88	1.918	No

Isomorphous cocrystals: **(ovan3amp)₂·14tfib** and **(ovan3amp)₂·ofib**

Our recent work has been based on the rationalization of the effect of intermolecular interactions on photochromism.⁵⁵ For this purpose, we preferred to work on isomorphous solids⁷⁵ (and their solid solutions, when possible) in which we studied the effects of small “point” modifications on the solid-state photochromism.¹⁵ Rather surprisingly, we found that despite the isomorphism,¹⁵ *N*-salicylideneaniline solids can behave differently with respect to photochromism. For example, replacement of bromine with iodine led to loss of photochromism in isomorphous single-component solids. Replacement of bromine by iodine in cocrystals with *p*-diiodotetrafluorobenzene led, instead, to a slowdown of the thermal fading rate of the photoinduced coloration of about three times.¹⁵ This same approach has been used by other groups to study the thermal expansion⁷⁶ of cocrystals, the rotational dynamics of molecular rotors⁷⁷ and the thermomechanical effect in molecular crystals.⁷⁸

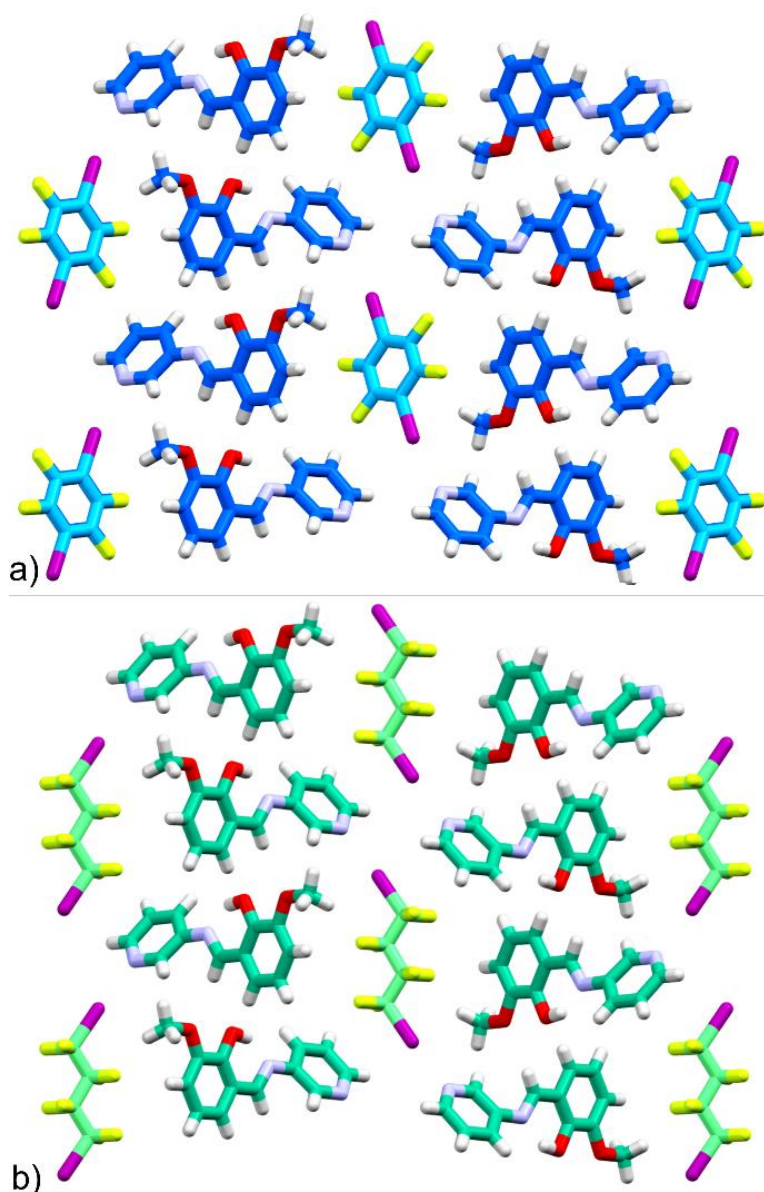


Figure 6. Packing view along the *a*-axis of (a) $(\text{ovan3amp})_2 \cdot 14\text{tfib}$ (blue sticks) and $(\text{ovan3amp})_2 \cdot 12\text{F8C4}$ (green sticks). The two solids are isomorphous.

Herein, we report an additional case of isomorphism which involves cocrystals $(\text{ovan3amp})_2 \cdot 14\text{tfib}$ and $(\text{ovan3amp})_2 \cdot \text{ofib}$ (Figure 6). Despite their isomorphism, only compound $(\text{ovan3amp})_2 \cdot \text{ofib}$ is photochromic. Molecules of **ovan3amp** are stacked along the *a*-axis. These stacks of chromophores are then interconnected by bridging co-formers through halogen bonds directed toward the pyridine moieties. Stacking parameters of **ovan3amp** are similar in the two structures. Centroid distances (centroids calculated on the vanillidene ring) are of about 4.6 Å, for

(ovan3amp)₂·14tfib, and of about 4.8 Å, for **(ovan3amp)₂·ofib**, with interplanar separation between molecules of about 3.4 Å and 3.5 Å, respectively. Both solids are characterized by a $\Phi > 30^\circ$ ($34.3(4)^\circ$ and $37.3(3)^\circ$ respectively) as well as by close values of V_{free} (101 \AA^3 and 110 \AA^3) indicating that photochromism is hardly predictable on the basis of those parameters, given that small structural modifications can have a strong impact on the expression of the photochromic properties in the solid state. (**Table 5**).

Cocrystals with the tritopic co-former: **(ovan3amp)₂·135tfib** and **ovan4amp·135tfib**

Cocrystallization of **ovan3amp** and **ova4amp** with **I35tfib** interestingly generated cocrystals with different stoichiometry. A 2:1 stoichiometry was found for the first cocrystal while a 1:1 was found for the second one.

Solid **(ovan3amp)₂·135tfib** is photochromic and the two crystallographically independent chromophores in its structure show Φ of $8.6(7)^\circ$ and $38.2(6)^\circ$. This system fulfills the selection criterion of the Φ rule. Comparison of this solid with the 2:1 cocrystals discussed previously (**(ovan3amp)₂·14tfib**, **(ovan4amp)₂·12tfib** and **(ovan4amp)₂·14tfib**) is of interest because the only difference in the molecular volume of the constituents is due to the substitution of a fluorine with an iodine atom. The V_{free} value of **(ovan3amp)₂·135tfib** is higher than the ones found for the other three 2:1 cocrystals (see **Table 4** and **Table 6**), therefore its photochromic behavior is also in accordance with the V_{free} model.

Solid **ovan4amp·135tfib** is non-photochromic. The *N*-salicylideneaminopyridine molecules are planar with $\Phi = 7.2(4)^\circ$. For this reason, the cocrystal fulfills the Φ rule. When, instead, we compare this cocrystal to the two 1:1 cocrystals discussed previously (**ovan3amp·12tfib** and **ovan3amp·13tfib**), we notice that despite the fact that its V_{free} has the largest value, the compound does not show photochromic properties.

Table 5. Molecular packing parameters and experimentally determined photochromism for **(ovan3amp)₂·14tfib** and **(ovan3amp)₂·ofib**.

	$\Phi / ^\circ$	$V_{\text{free}} / \text{Å}^3$	photochromism
(ovan3amp)₂·14tfib	34.3(4) $^\circ$	101	No
(ovan3amp)₂·ofib	37.3(3) $^\circ$	110	Yes

Table 6. Molecular packing parameters and experimentally determined photochromism for **(ovan3amp)₂·135tfib** and **ovan4amp·135tfib**.

	$\Phi / ^\circ$	$V_{\text{free}} / \text{Å}^3$	photochromism
(ovan3amp)₂·135tfib	8.6(7) $^\circ$	123	Yes
	38.2(6) $^\circ$		
ovan4amp·135tfib	7.2(4) $^\circ$	163	No

A closer look to the **ovan4amp·135tfib** structure reveals that molecules form dimers stacked in a head-to-tail fashion with short interplanar distances (of about 3.4 Å). This structural feature has been linked with the absence of the solid-state photochromism in a class of *N*-salicylideneaminopyridinium derivatives.⁶⁹

5.4. Conclusions

A series of halogen bonded cocrystals were synthesized by a one-pot one-step mechanochemical procedure. Molecules were assembled following a 1:1 or a 2:1 stoichiometry and formed various types of supramolecular assemblies, namely infinite chains, rings (tetramer), and discrete three-membered assemblies. Of the eight cocrystals, three exhibited photochromic properties with retention of the photocolouration ranging from three hours (**ovan3amp·135tfib**) to several days (**ovan3amp·12tfib**). All the photochromic cocrystals remained photoactive during several photoinduced switching cycles.

The 1:1 cocrystals with ditopic isomeric co-formers (**ovan3amp·12tfib** and **ovan3amp·13tfib**) formed structures in which the *N*-salicylideneaminopyridine is bound to both its sides (pyridine and vanillidene) through halogen bonds. This assembly generated a non-photochromic cocrystal (**ovan3amp·13tfib**) and a photochromic one, this latter (**ovan3amp·12tfib**) characterized by an extremely slow thermal fading of the coloration. Its photochromic behavior could not be described by the sole evaluation of Φ rule ($\Phi = 13.0(6)^\circ$) nor by the evaluation of V_{free} . Remarkably, **ovan3amp·12tfib** exhibited photochromism although it is denser ($\rho = 2.110 \text{ g cm}^{-3}$, $V_{\text{free}} = 135.9 \text{ \AA}^3$) than **ovan3amp·13tfib** ($\rho = 2.010 \text{ g cm}^{-3}$, $V_{\text{free}} = 160.8 \text{ \AA}^3$). This comparison suggests that when the *N*-salicylideneaminopyridine molecule is strongly bound through both halogen acceptor sites (pyridine and vanillidene), photochromism is unlikely to occur, even for high values of V_{free} . Alternatively, this assembly can give rise to photochromic systems with extremely slow rates of thermal fading of the photoinduced coloration.

The 2:1 cocrystals with ditopic isomeric co-formers (**(ovan3amp)₂·14tfib**, **ovan4amp)₂·12tfib** and **(ovan4amp)₂·14tfib**) formed structures in which the *N*-salicylideneaminopyridine derivative is involved in discrete 3-membered assembly through I \cdots N interactions on the N-atom of the pyridine moiety. All cocrystals were found to be non-photochromic, possibly because this stoichiometry led to compact packing with V_{free} values ranging from about 87 \AA^3 to 101 \AA^3 (much below V_{free} values found for the 1:1 cocrystals discussed above). Moreover, compound **(ovan3amp)₂·14tfib** represented another exception to the Φ rule being non-photochromic despite $\Phi = 34.3(4)^\circ$. However, when **14tfib** is replaced by **ofib** in the structure of **(ovan3amp)₂·ofib** (isomorphous to **(ovan3amp)₂·14tfib**), the resulting cocrystal is photochromic.

Although, generally, photoisomerization of *N*-salicylideneaniline derivatives is a phenomenon depending on the compactness of the crystal packing – therefore explainable in some cases through Φ and V_{free} – we have shown how subtle structural changes can dramatically affect photochromism in the solid-state. Some

incongruences can also be attributed to the fact that V_{free} does not provide any description of the localization of the voids into the unit cell. This last factor is of tremendous importance when working with multicomponent crystal forms because not all the free available space areas in a multicomponent crystal are actually/equally employed by the chromophore for the *cis-trans* isomerization. We do believe that the combined Φ/V_{free} model, grossly oversimplifies the complexity of the dynamic phenomenon behind the photoisomerization of *N*-salicylideneanilines. For the above-mentioned reasons, careful examination of intermolecular interactions and crystals packing (localization of voids, evaluation of intermolecular interactions and stacking modes) should be taken into account and used to supplement the current proposed model based on Φ and V_{free} .

5.5. References

- 1) Schmidt, G. M. J. *Pure Appl. Chem.* **1971**, 27, 647–678.
- 2) Braga, D. *Chem. Commun.* **2003**, 108, 2751–2754.
- 3) Braga, D.; Brammer, L.; Champness, N. R. *CrystEngComm* **2005**, 7, 1–19.
- 4) Desiraju, G. R. *J. Am. Chem. Soc.* **2013**, 135, 9952–9967.
- 5) Desiraju, G. R. *Angew. Chemie Int. Ed.* **2007**, 46, 8342–8356.
- 6) Duggirala, N. K.; Perry, M. L.; Almarsson, Ö.; Zaworotko, M. J. *Chem. Commun.* **2016**, 52, 640–655.
- 7) Schultheiss, N.; Newman, A. *Cryst. Growth Des.* **2009**, 9, 2950–2967.
- 8) Tilborg, A.; Norberg, B.; Wouters, J. *Eur. J. Med. Chem.* **2014**, 74, 411–426.
- 9) Yan, D.; Delori, A.; Lloyd, G. O.; Friščić, T.; Day, G. M.; Jones, W.; Lu, J.; Wei, M.; Evans, D. G.; Duan, X. *Angew. Chemie Int. Ed.* **2011**, 50, 12483–12486.
- 10) d’Agostino, S.; Grepioni, F.; Braga, D.; Ventura, B. *Cryst. Growth Des.* **2015**, 15, 2039–2045.
- 11) Grepioni, F.; d’Agostino, S.; Braga, D.; Bertocco, A.; Catalano, L.; Ventura, B. *J. Mater. Chem. C* **2015**, 3, 9425–9434.

- 12) MacGillivray, L. R.; Papaefstathiou, G. S.; Friščić, T.; Hamilton, T. D.; Bučar, D.-K.; Chu, Q.; Varshney, D. B.; Georgiev, I. G. *Acc. Chem. Res.* **2008**, 41, 280–291.
- 13) MacGillivray, L. R. *CrystEngComm* **2002**, 4, 37.
- 14) Morimoto, M.; Irie, M. *J. Am. Chem. Soc.* **2010**, 132, 14172–14178.
- 15) Carletta, A.; Spinelli, F.; d'Agostino, S.; Ventura, B.; Chierotti, M. R.; Gobetto, R.; Wouters, J.; Grepioni, F. *Chem. - A Eur. J.* **2017**, 23, 5317–5329.
- 16) Carletta, A.; Buol, X.; Leysens, T.; Champagne, B.; Wouters, J. *J. Phys. Chem. C* **2016**, 120, 10001–10008.
- 17) Johmoto, K.; Sekine, A.; Uekusa, H. *Cryst. Growth Des.* **2012**, 12, 4779–4786.
- 18) Aakeröy, C. B.; Wijethunga, T. K.; Haj, M. A.; Desper, J.; Moore, C. *CrystEngComm* **2014**, 16, 7218.
- 19) Adak, A.; Panda, T.; Raveendran, A.; Bejoymohandas, K. S.; Asha, K. S.; Prakasham, A. P.; Mukhopadhyay, B.; Panda, M. K. *ACS Omega* **2018**, 3, 5291–5300.
- 20) Liu, G.; Liu, J.; Ye, X.; Nie, L.; Gu, P.; Tao, X.; Zhang, Q. *Angew. Chemie* **2017**, 129, 204–208.
- 21) Zbačnik, M.; Kaitner, B. *Croat. Chem. Acta* **2016**, 89, 125–132.
- 22) Zbačnik, M.; Pičuljan, K.; Parlov-Vuković, J.; Novak, P.; Roodt, A. *Crystals* **2017**, 7, 25.
- 23) Sagara, Y.; Yamane, S.; Mitani, M.; Weder, C.; Kato, T. *Adv. Mater.* **2016**, 28, 1073–1095.
- 24) Sun, Y.; Lei, Y.; Dong, H.; Zhen, Y.; Hu, W. *J. Am. Chem. Soc.* **2018**, 140, 6186–6189.
- 25) McNeil, S. K.; Kelley, S. P.; Beg, C.; Cook, H.; Rogers, R. D.; Nikles, D. E. *ACS Appl. Mater. Interfaces* **2013**, 5, 7647–7653.
- 26) Christopherson, J.-C.; Topić, F.; Barrett, C. J.; Friščić, T. *Cryst. Growth Des.* **2018**, acs.cgd.7b01445.

- 27) Christopherson, J.-C.; Potts, K. P.; Bushuyev, O. S.; Topić, F.; Huskić, I.; Rissanen, K.; Barrett, C. J.; Friščić, T. *Faraday Discuss.* **2017**, 203, 441–457.
- 28) Bushuyev, O. S.; Friščić, T.; Barrett, C. J. *Cryst. Growth Des.* **2016**, 16, 541–545.
- 29) Shen, J. P.; Duan, X. H.; Luo, Q. P.; Zhou, Y.; Bao, Q.; Ma, Y. J.; Pei, C. H. *Cryst. Growth Des.* **2011**, 11, 1759–1765.
- 30) Kent, R. V.; Wiscons, R. A.; Sharon, P.; Grinstein, D.; Frimer, A. A.; Matzger, A. J. *Cryst. Growth Des.* **2018**, 18, 219–224.
- 31) Yang, Z.; Li, H.; Zhou, X.; Zhang, C.; Huang, H.; Li, J.; Nie, F. *Cryst. Growth Des.* **2012**, 12, 5155–5158.
- 32) Cavallo, G.; Metrangolo, P.; Milani, R.; Pilati, T.; Priimägi, A.; Resnati, G.; Terraneo, G. *Chem. Rev.* **2016**, 116, 2478–2601.
- 33) Desiraju, G. R.; Ho, P. S.; Kloo, L.; Legon, A. C.; Marquardt, R.; Metrangolo, P.; Politzer, P.; Resnati, G.; Rissanen, K. *Pure Appl. Chem.* **2013**, 85, 1711–1713.
- 34) Nemec, V.; Cinčić, D. *CrystEngComm* **2016**, 18, 7425–7429.
- 35) Bedeković, N.; Stilinović, V.; Friščić, T.; Cinčić, D. *New J. Chem.* **2018**, 42, 10584–10591.
- 36) Stilinović, V.; Horvat, G.; Hrenar, T.; Nemec, V.; Cinčić, D. *Chem. - A Eur. J.* **2017**, 23, 5244–5257.
- 37) Murray, J. S.; Lane, P.; Clark, T.; Politzer, P. *J. Mol. Model.* **2007**, 13, 1033–1038.
- 38) Politzer, P.; Murray, J. S.; Clark, T. *Phys. Chem. Chem. Phys.* **2010**, 12, 7748.
- 39) Troff, R. W.; Mäkelä, T.; Topić, F.; Valkonen, A.; Raatikainen, K.; Rissanen, K. *European J. Org. Chem.* **2013**, 2013, 1617–1637.
- 40) Cinčić, D.; Friščić, T.; Jones, W. *Chem. Mater.* **2008**, 20, 6623–6626.
- 41) Nemec, V.; Fotović, L.; Friščić, T.; Cinčić, D. *Cryst. Growth Des.* **2017**, 17, 6169–6173.
- 42) Christopherson, J.-C.; Potts, K. P.; Bushuyev, O. S.; Topić, F.; Huskić, I.; Rissanen, K.; Barrett, C. J.; Friščić, T. *Faraday Discuss.* **2017**, 203, 441–457.

- 43) Bushuyev, O. S.; Tan, D.; Barrett, C. J.; Frišćić, T. *CrystEngComm* **2015**, 17, 73–80.
- 44) Yan, D.; Bučar, D.-K.; Delori, A.; Patel, B.; Lloyd, G. O.; Jones, W.; Duan, X. *Chem. - A Eur. J.* **2013**, 19, 8213–8219.
- 45) Amimoto, K.; Kawato, T. *J. Photochem. Photobiol. C Photochem. Rev.* **2005**, 6, 207–226.
- 46) Cohen, M. D.; Schmidt, G. M. J.; Flavian, S. 388. *J. Chem. Soc.* **1964**, 0, 2041.
- 47) Cohen, M. D.; Hirshberg, Y.; Schmidt, G. M. J. 389. *J. Chem. Soc.* **1964**, 0, 2051.
- 48) Harada, J.; Uekusa, H.; Ohashi, Y. X-Ray *J. Am. Chem. Soc.* **1999**, 121, 5809–5810.
- 49) Harada, J.; Ogawa, K. *Chem. Soc. Rev.* **2009**, 38, 2244.
- 50) Hadjoudis, E.; Mavridis, I. M. *Chem. Soc. Rev.* **2004**, 33, 579–588.
- 51) Jacquemin, P.-L.; Robeyns, K.; Devillers, M.; Garcia, Y. *Chem. - A Eur. J.* **2015**, 21, 6832–6845.
- 52) Robert, F.; Naik, A. D.; Tinant, B.; Robiette, R.; Garcia, Y. *Chem. - A Eur. J.* **2009**, 15, 4327–4342.
- 53) Hutchins, K. M.; Dutta, S.; Loren, B. P.; MacGillivray, L. R. *Chem. Mater.* **2014**, 26, 3042–3044.
- 54) Jacquemin, P.-L.; Robeyns, K.; Devillers, M.; Garcia, Y. *Chem. Commun.* **2014**, 50, 649–651.
- 55) Sugiyama, H.; Uekusa, H. *CrystEngComm* **2018**, 20, 2144–2151.
- 56) Cinčić, D.; Brekalo, I.; Kaitner, B. *Chem. Commun.* **2012**, 48, 11683.
- 57) a) Zbačnik, M.; Kaitner, B. *CrystEngComm* **2014**, 16, 4162. b) Stilinović, V.; Cinčić, D.; Zbačnik, M.; Kaitner, B. *Croat. Chem. Acta*, **2012**, 85, 485–493.
- 58) Carletta, A.; Dubois, J.; Tilborg, A.; Wouters, J. *CrystEngComm* **2015**, 17, 3509–3518.
- 59) Zbačnik, M.; Vitković, M.; Vulić, V.; Nogalo, I.; Cinčić, D. *Cryst. Growth Des.* **2016**, 16, 6381–6389.

- 60) Zbačnik, M.; Pajski, M.; Stilinović, V.; Vitković, M.; Cinčić, D. *CrystEngComm* **2017**, 19, 5576–5582.
- 61) James, S. L.; Adams, C. J.; Bolm, C.; Braga, D.; Collier, P.; Friščić, T.; Grepioni, F.; Harris, K. D. M.; Hyett, G.; Jones, W.; Krebs, A.; Mack, J.; Maini, L.; Orpen, A. J.; Parkin, I. P.; Shearouse, W. C.; Steed, J. W.; Waddell, D.C. *Chem. Soc. Rev.* **2012**, 41, 413–447.
- 62) Friščić, T. *Chem. Soc. Rev.* **2012**, 41, 3493.
- 63) Sheldrick, G. M. *Acta Crystallogr. Sect. A Found. Adv.* **2015**, 71, 3–8.
- 64) Sheldrick, G. M. *Acta Crystallogr. Sect. C, Struct. Chem.* **2015**, 71, 3.
- 65) Macrae, C. F.; Edgington, P. R.; McCabe, P.; Pidcock, E.; Shields, G. P.; Taylor, R.; Towler, M.; van de Streek, J. Mercury : *J. Appl. Crystallogr.* **2006**, 39, 453–457.
- 66) Wood, P. A.; Olsson, T. S. G.; Cole, J. C.; Cottrell, S. J.; Feeder, N.; Galek, P. T. A.; Groom, C. R.; Pidcock, E. *CrystEngComm* **2013**, 15, 65–72.
- 67) Molinspiration Property Calculation Service,
<http://www.molinspiration.com/services/volume.html>.
- 68) Gates, B. C.; Knözinger, H.; Jentoft, F. C. *Advances in Catalysis Vol. 52*; Academic Press, 2009.
- 69) Carletta, A.; Colaço, M.; Mouchet, S. R.; Plas, A.; Tumanov, N.; Fusaro, L.; Champagne, B.; Lanners, S.; Wouters, J. *J. Phys. Chem. C* **2018**, 122, 10999–11007.
- 70) Mercier, G. M.; Robeyns, K.; Leyssens, T. *Cryst. Growth Des.* **2016**, 16, 3198–3205.
- 71) Safin, D. A.; Bolte, M.; Garcia, Y. *CrystEngComm* **2014**, 16, 5524.
- 72) Sliwa, M.; Létard, S.; Malfant, I.; Nierlich, M.; Lacroix, P. G.; Asahi, T.; Masuhara, H.; Yu, P.; Nakatani, K. *Chem. Mater.* **2005**, 17, 4727–4735.
- 73) Kawato, T.; Koyama, H.; Kanatomi, H.; Isshiki, M. *J. Photochem.* **1985**, 28, 103–110.

- 74) Johmoto, K.; Ishida, T.; Sekine, A.; Uekusa, H.; Ohashi, Y. *Acta Crystallogr. Sect. B Struct. Sci.* **2012**, 68, 297–304.
- 75) Cinčić, D.; Friščić, T.; Jones, W. *A New J. Chem.* **2008**, 32, 1776–1781.
- 76) Hutchins, K. M.; Kummer, K. A.; Groeneman, R. H.; Reinheimer, E. W.; Sinnwell, M. A.; Swenson, D. C.; MacGillivray, L. R. *CrystEngComm* **2016**, 18, 8354–8357.
- 77) Catalano, L.; Perez-Estrada, S.; Wang, H.-H.; Ayitou, A. J.-L.; Khan, S. I.; Terraneo, G.; Metrangolo, P.; Brown, S.; Garcia-Garibay, M. A. *J. Am. Chem. Soc.* **2017**, 139, 843–848.
- 78) Mittapalli, S.; Perumalla, D. S.; Nanubolu, J. B.; Nangia, A. *IUCrJ* **2017**, 4, 812–823.

Conclusions

Conclusion

We have shown herein a crystal engineering approach applied to photochromic materials. Cocrystallization is presented as an approach to modify or unlock photochromic properties in crystalline *N*-salicylideneaniline materials which can be used complementary/alternatively to the chemical modification of the chromophores.¹

We have reported an adapted single-step mechanochemical synthesis of cocrystals allowing for the concomitant formation of covalent (imine) and non-covalent (halogen/hydrogen) bonds. The short reaction times along with the low cost of the reactants and limited use of solvents represent an added value to this approach.

Isostructural solids and their solid solutions have been synthesized with the intention of discovering more about factors controlling photochromism in the solid state. A wide variety of methods for the synthesis of isostructural solids is presented throughout the thesis: Br/I replacement (*chapter 4*), use of bulky templating anions (*chapter 3*) and replacement of the ditopic 180° tectons (*chapters 2 and 5*). Thanks to these strategies, we have elucidated some of the aspects relating photochromism to the crystal structure. In *chapter 4*, we have shown, for example, as the replacement of bromine by iodine determines a loss of the photochromic properties in isostructural single-component solids (having tight packing) while an increase of the color retention in multicomponent solids (having an open structure, **Figure 1**). This same approach has been used by other groups to study the rotational dynamics of molecular rotors² and the thermomechanical effect in molecular crystals; their results showed a similar deactivation trend by going from chlorine to iodine.³ One aspect which remained somehow unclear is the behavior of the solid solution obtained from the combination of the photochromic bromo- (**2**) and the non-photochromic iodo-derivative (**3B**) in the ratio of **2**_{0.7}**3**_{0.3} (**Figure 1**). Contrary to expectations, **2**_{0.7}**3**_{0.3} is non-photochromic like compound **3** although this latter is the minority component of the solid solution. Interestingly, a similar trend was found for the isostructural salts of tetraphenylborate (**3** and **4**) and their solid solution (**3**_{0.62}**4**_{0.38}) reported in *chapter 3* (**Figure 2**). All three of them are photochromic but the thermal decay, and so the photochromic behavior, of the solid solution **3**_{0.62}**4**_{0.38} is closer to the one of **4**

although this latter is the minority component of the solid solution. Calculation of RMSD (obtained from the comparison of the structure of the solid solution with those of **3** and **4**) has highlighted that the solid solution is structurally closer to solid **4** than to solid **3**. This result suggests that it is not the major component that determines the thermal fading behavior but the combined effect that both components together have on the crystal structure.

24 structures have been characterized in this work (11 are photochromic). The prediction rule based on the dihedral angle Φ is satisfied for 20 over 24 structures. This means that for six solids to which the rule is applied, one of them does not follow the rule. The 4 solids which do not follow the Φ rule are joint to several other exceptions reported in the literature,⁴ and the number is expected to rise.⁵ The remarkable aspect of the exceptions we found is that two of them (solid **2**, reported in *chapter 2*, and cocrystal **(ovan3amp)₂·ofib** reported in *chapter 5*) do not behave like their isostructural counterparts (**3B** and **(ovan3amp)₂·14tfib**, respectively). This aspect represents an unicum in the ambit of photochromic *N*-salicylideneaniline solids and highlights that although, generally, photoisomerization of *N*-salicylideneanilines is a phenomenon depending on the compactness of the crystal packing (therefore explainable in some cases through Φ and V_{free}) small structural changes can dramatically affect photochromism. For these reasons, careful examination of intermolecular interactions and crystal packing should be taken into account and used to supplement the current proposed model based on Φ and V_{free} . Indeed, the case scenario suggested here is still complex and will require extensive yet focused experiments on isostructural cocrystals and solid solutions to be refined and extended (hopefully) to the whole family of *N*-salicylideneaniline solids. This aspect represents the main future perspective of this work.

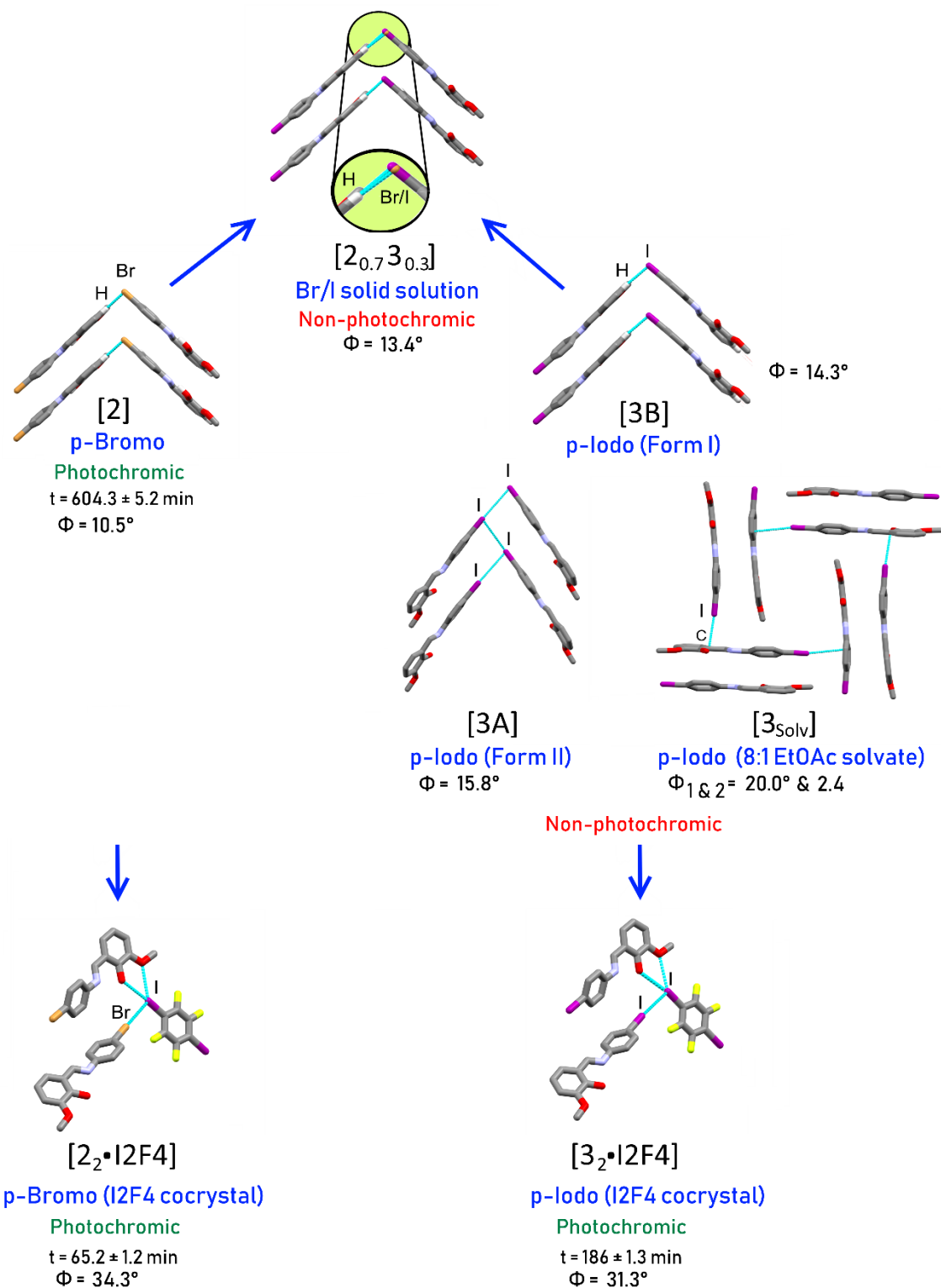


Figure 1 Some of the crystal structures reported in *chapter 4*.

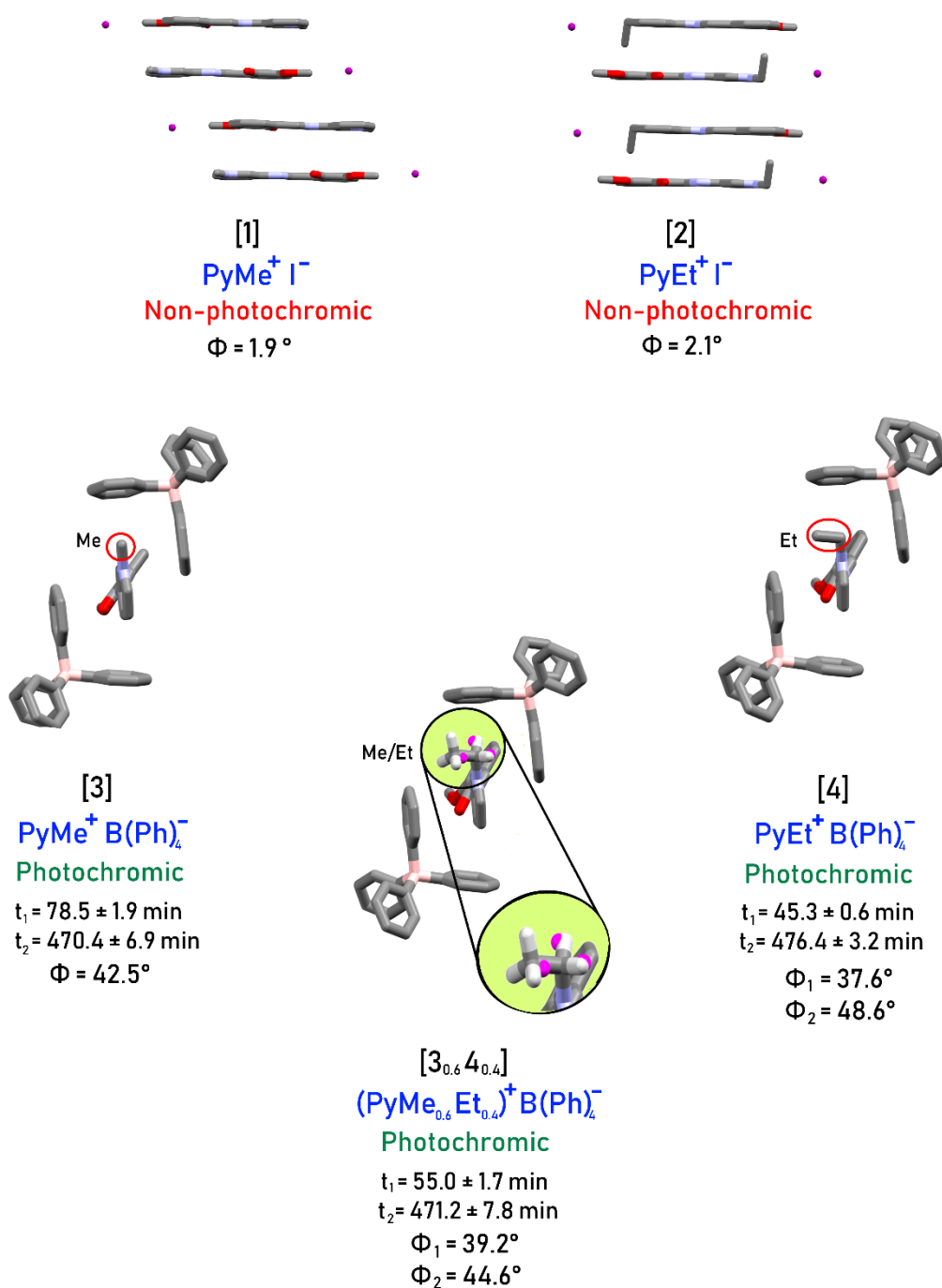


Figure 2. Crystal structures and their photochemical characterization reported in *chapter 3*.

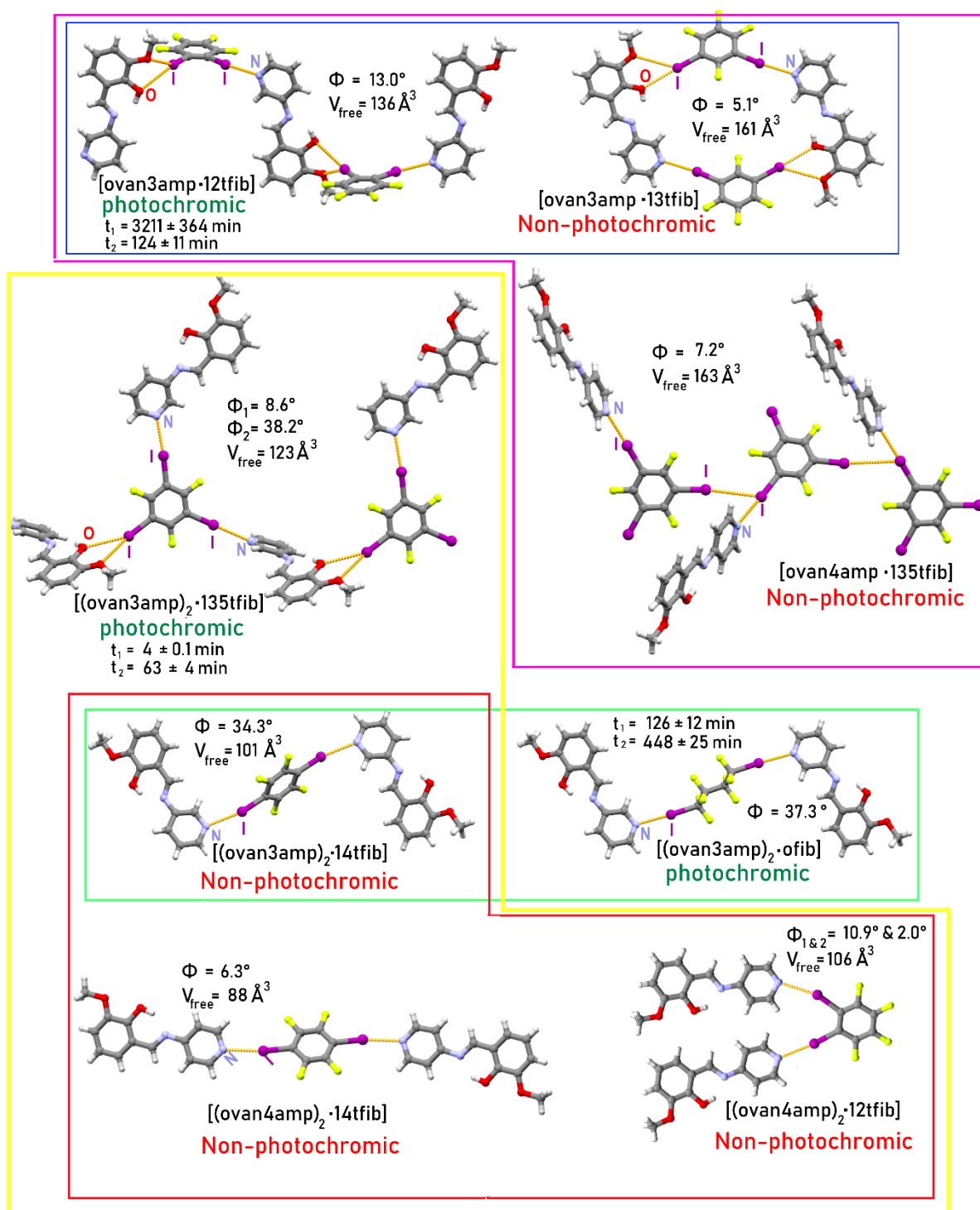


Figure 3. Crystal structures and their photochemical characterization reported in *chapter 5*. Colored boxes indicate the structural comparisons made in the chapter.

References

- 1) a) Carletta, A., Buol, X., Leyssens, T., Champagne, B., and Wouters, J. (2016). *The Journal of Physical Chemistry C*, 120(18), 10001-10008. b) Carletta, A., Spinelli, F., d'Agostino, S., Ventura, B., Chierotti, M. R., Gobetto, R., Wouters J., and Grepioni, F. (2017). *Chemistry–A European Journal*, 23(22), 5317-5329. c) Carletta, A., Colaço, M., Mouchet, S. R., Plas, A., Tumanov, N., Fusaro, L., Champagne B., Lanners S., and Wouters, J. (2018). *The Journal of Physical Chemistry C*, 122(20), 10999-11007. d) Carletta, A., Zbačnik, M., Van Gysel, M., Vitković, M., Tumanov, N., Stilinović, V., Wouters J., and Cinčić, D. (2018). *Crystal Growth & Design*, 18(11), 6833-6842.
- 2) Catalano, L., Perez-Estrada, S., Wang, H. H., Ayitou, A. J. L., Khan, S. I., Terraneo, G., Metrangolo, P., Braun, S., and Garcia-Garibay, M. A. (2017). *Journal of the American Chemical Society*, 139(2), 843-848.
- 3) Mittapalli, S., Sravanakumar Perumalla, D., and Nangia, A. (2017). *IUCrJ*, 4(3), 243-250.
- 4) a) Robert, F., Naik, A. D., Tinant, B., Robiette, R., and Garcia, Y. (2009). *Chemistry–A European Journal*, 15(17), 4327-4342. b) Avadanei, M., Cozan, V., Shova, S., and Paixão, J. A. (2014). *Chemical Physics*, 444, 43-51. c) Hutchins, K. M., Dutta, S., Loren, B. P., and MacGillivray, L. R. (2014). *Chemistry of Materials*, 26(10), 3042-3044. d) Sugiyama, H., and Uekusa, H. (2018). *CrystEngComm*, 20(15), 2144-2151.
- 5) Houjou, H., Kato, T., Huang, H., Suzuki, Y., Yoshikawa, I., & Mutai, T. (2019). *Crystal Growth & Design* 19(2), 1384-1390.

Annex A

To: Cocrystallization of N-salicylidene-3-aminopyridines with dicarboxylic acids: isostructurality, polymorphism and effects on photochromism.[†]

[†]Carletta, Andrea, et al. "Polymorphic and isomorphous cocrystals of a *N*-salicylidene-3-aminopyridine with dicarboxylic acids: tuning of solid-state photo- and thermochromism." *The Journal of Physical Chemistry C* 120 (2016): 10001-10008.

Supporting information to Chapter 2

List of Figures and Tables

Figure S1. PXRD of **1**

Figure S2. PXRD of **2** and **3**

Figure S3. PXRD of **4** and **5**

Figure S4. Isostructurality between **2** and **4**: PXRD and structure matching

Figure S5. ORTEP diagrams

Figure S6. Crystal packing of **1**, **4**, **5**

Figure S7. Histograms of the bond length in anils exhibiting their enol form

Figure S8. Histograms of the bond length in anils exhibiting their *cis*-keto form

Figure S9. Thermochromic behavior of crystals

Figure S10. UV-Vis solid-state spectra, before and after irradiation, of **1** and **5**

Figure S11. FTIR spectra

Figures S12. and **S13.** DSC: melting point determination

Table S1. Elemental Analysis of **1**

Table S2. Room Temperature SCXRD measurements: crystallographic parameters

Table S3. Selected Geometries for H-bonds.

Table S4. Selected geometries for carboxyl group in **FA** and **SA**.

Table S5. Bond lengths of the six-membered pseudocycle in anils under the enol form

Table S6. Bond lengths of the six-membered pseudocycle in anils under the *cis*-keto form

Table S7. Selected structures of SCC and MCC used for construction of model based on Hirshfeld surfaces C...C% contacts calculation.

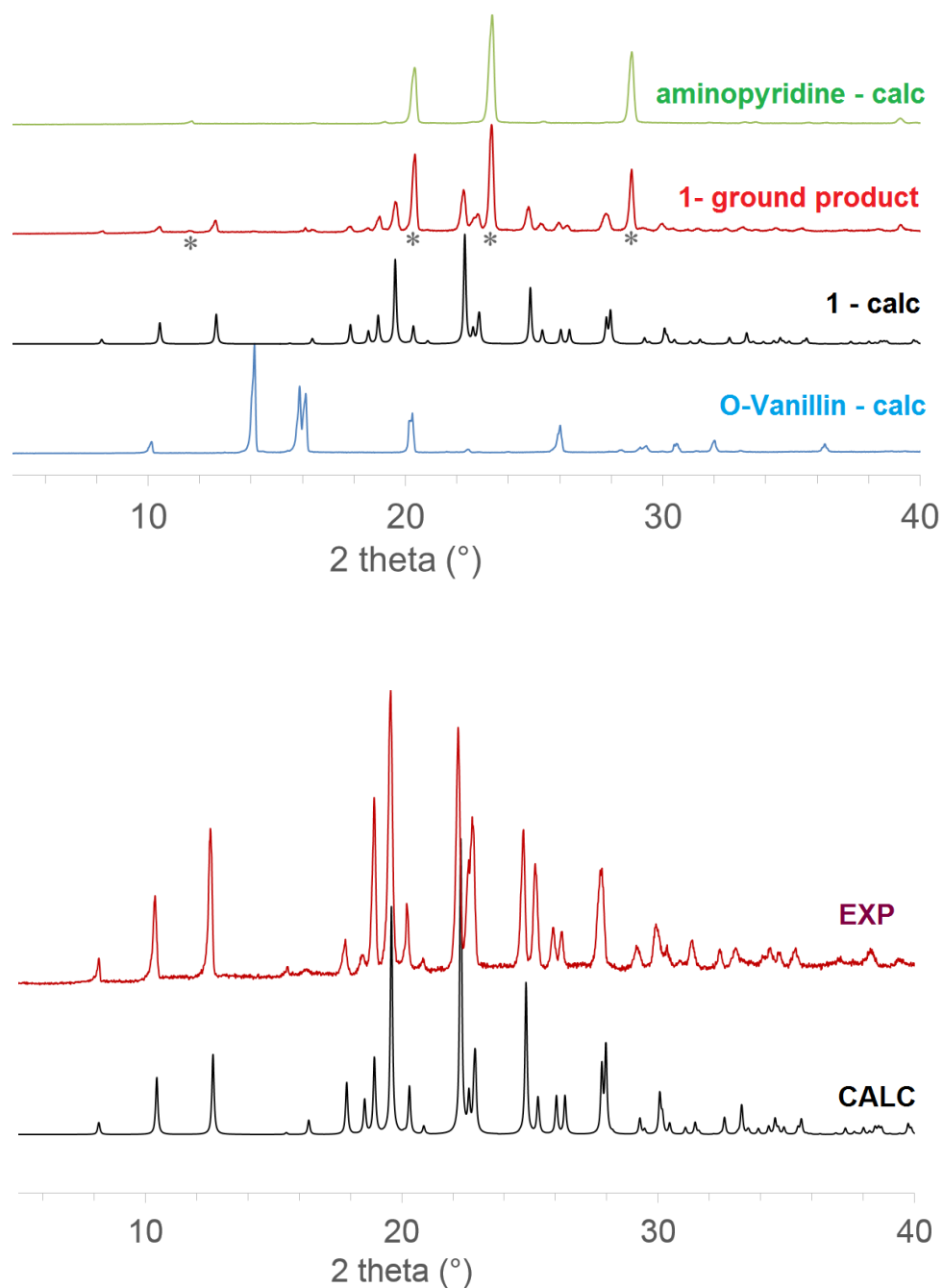


Figure S1. Powder X-ray diffraction measurement of the ground product of **1** before (top) and after (bottom) purification by recrystallization in EtOAc. Peaks indicated with black-stars are due to residual 3-aminopyridine in the ground product taken directly ball milling.

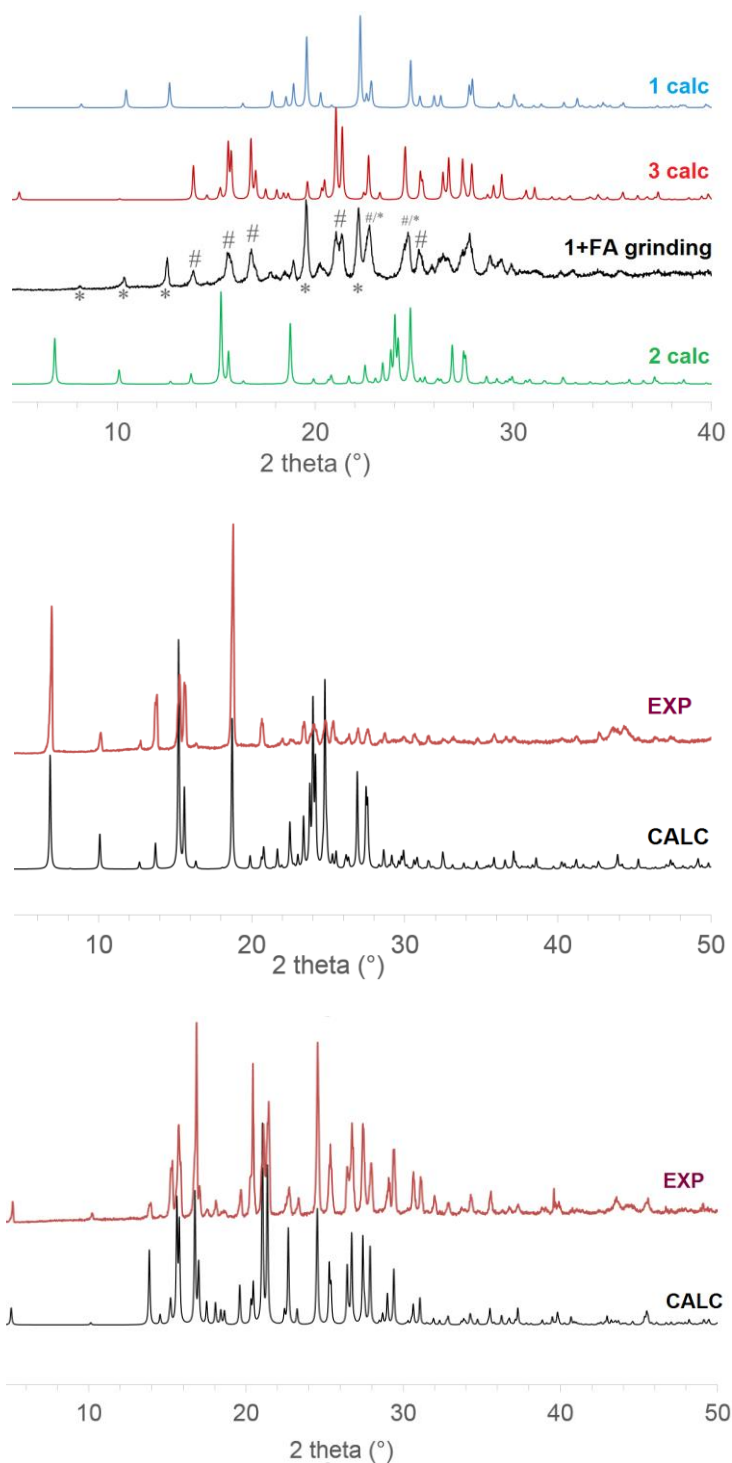


Figure S2. Powder X-ray diffraction measurement of the mechanochemical synthesis of $(\mathbf{1})_2 \cdot \text{FA}$ type cocrystals (a). PXRD of purified $\mathbf{2}$ (b) and $\mathbf{3}$ (c). Peaks indicated with black-stars are due to residual $\mathbf{1}$ in the ground product taken directly after ball milling. Peaks indicated with # are attributed to formation of $\mathbf{3}$.

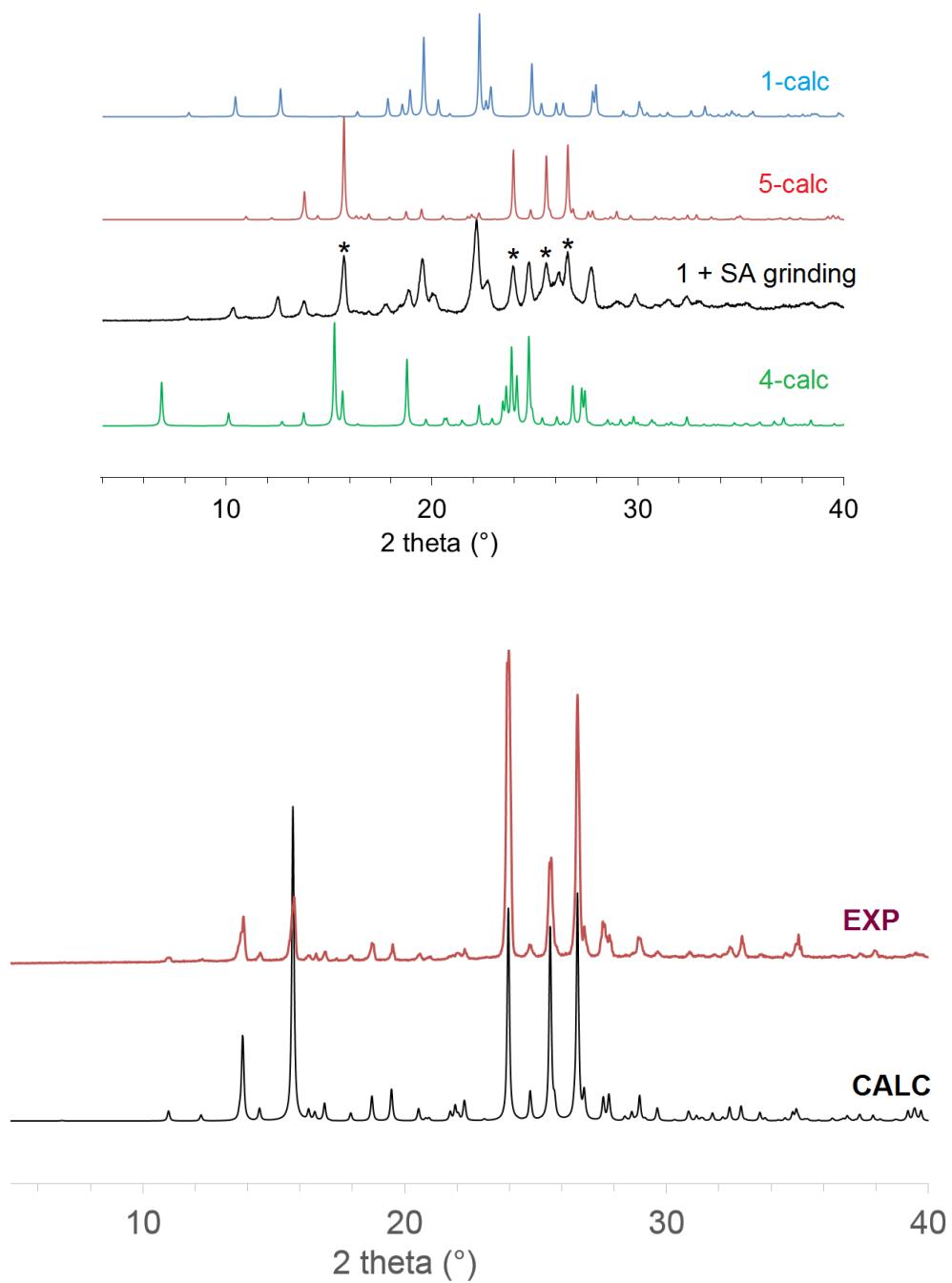


Figure S3. Powder X-ray diffraction measurement of the mechanochemical synthesis of $(\mathbf{1})_2 \cdot \mathbf{SA}$ cocrystals (a). PXRD of purified $\mathbf{5}$ (b). Peaks indicated with black-stars are due to $\mathbf{5}$.

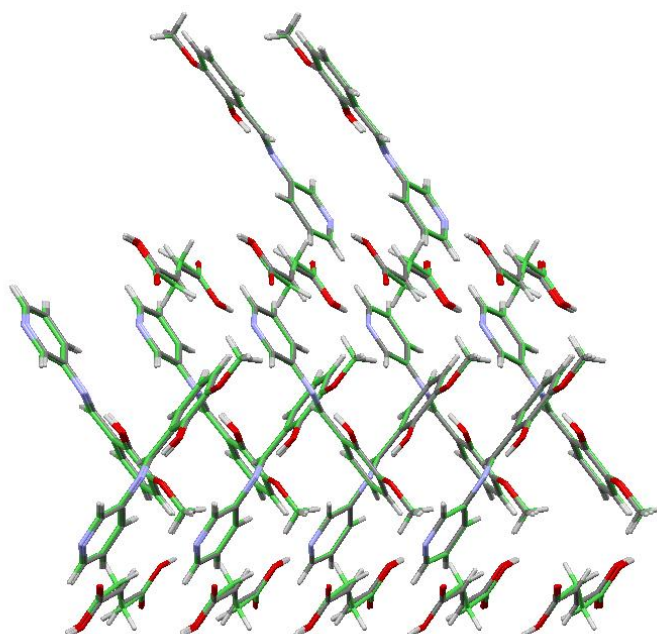
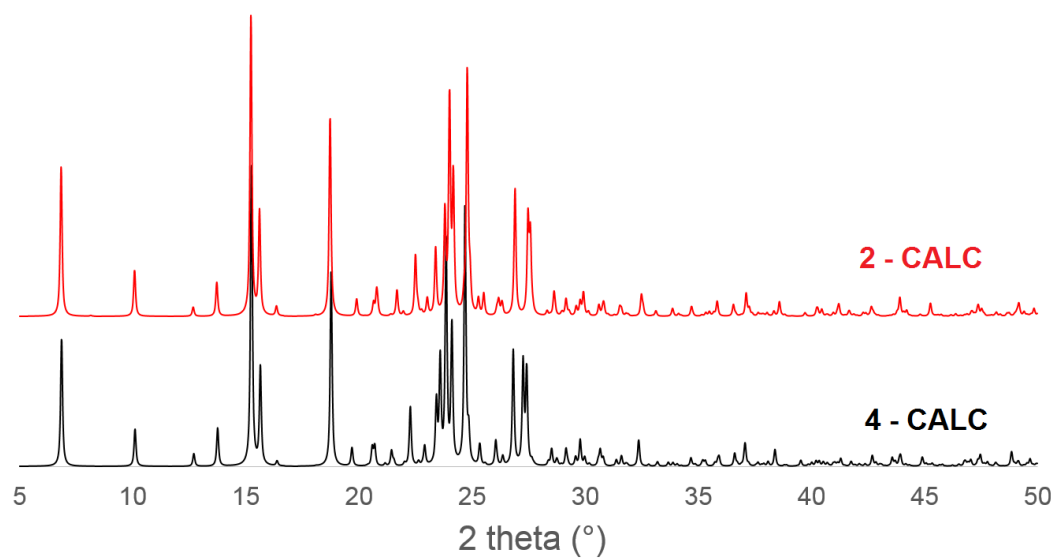


Figure S4. Calculated Powder X-ray diffractograms showing isostructurality between cocrystal **2** and cocrystal **4** (top) and perfect matching (bottom) between the two crystallographic structures (**2** is represented in grey sticks while **4** is represented in green sticks, RMS = 0.098 Å).

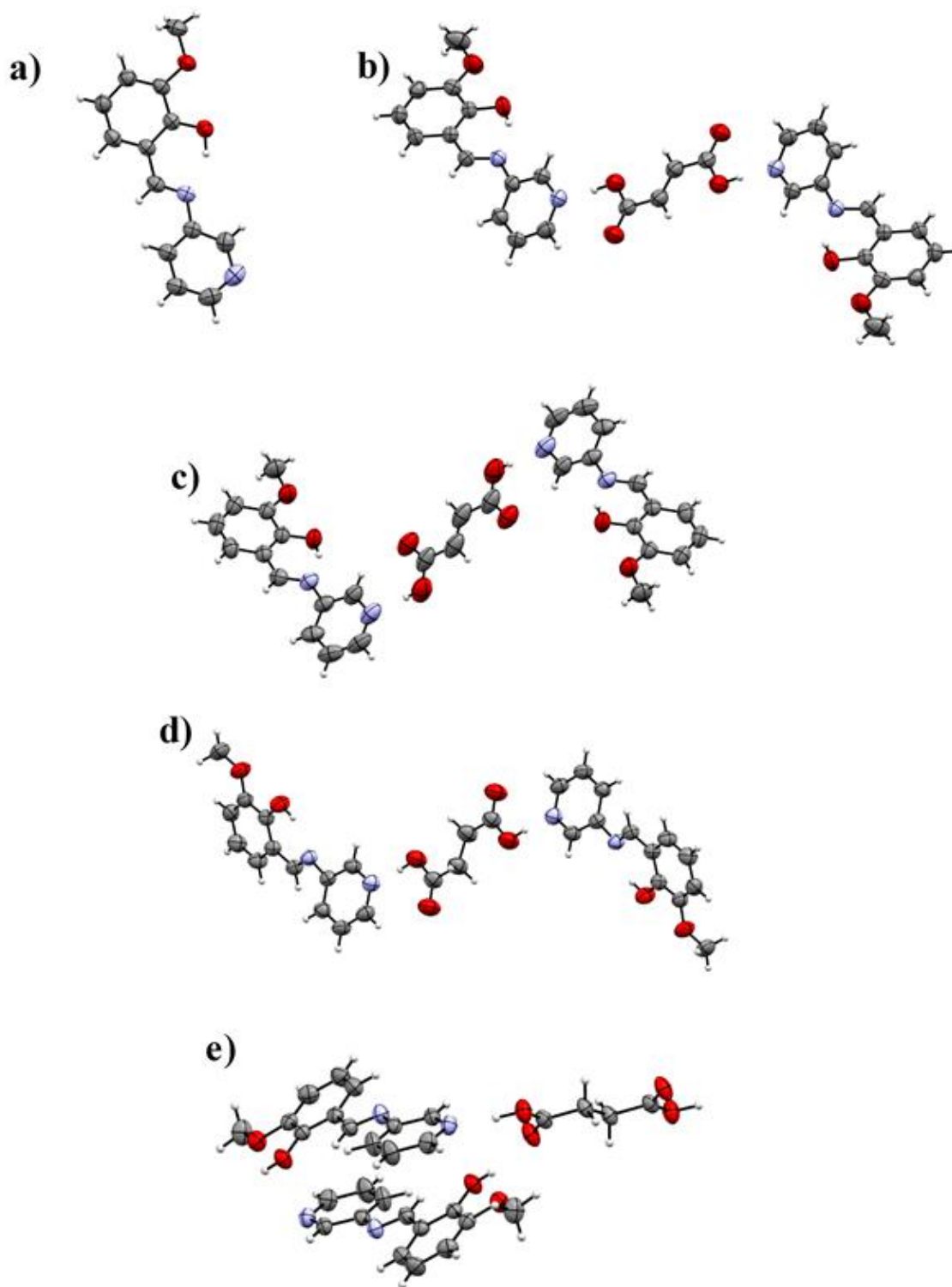


Figure S5. ORTEP diagrams (50% probability ellipsoids) for **1** (a, 105K structure), **2** (b), **3** (c), **4** (d) and **5** (e)

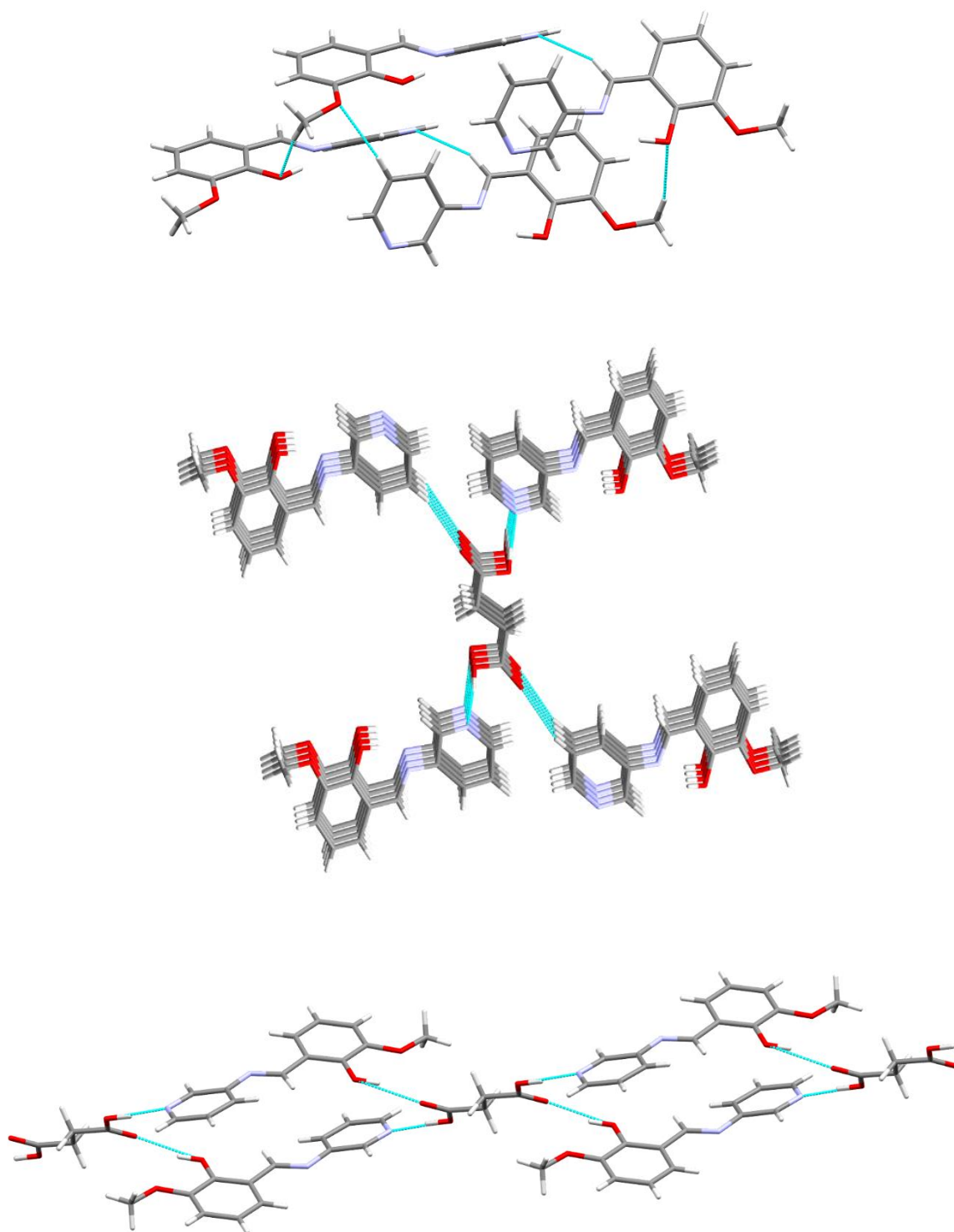


Figure S6. Crystal packing for **1** (top), **4** (middle) and **5** (bottom)

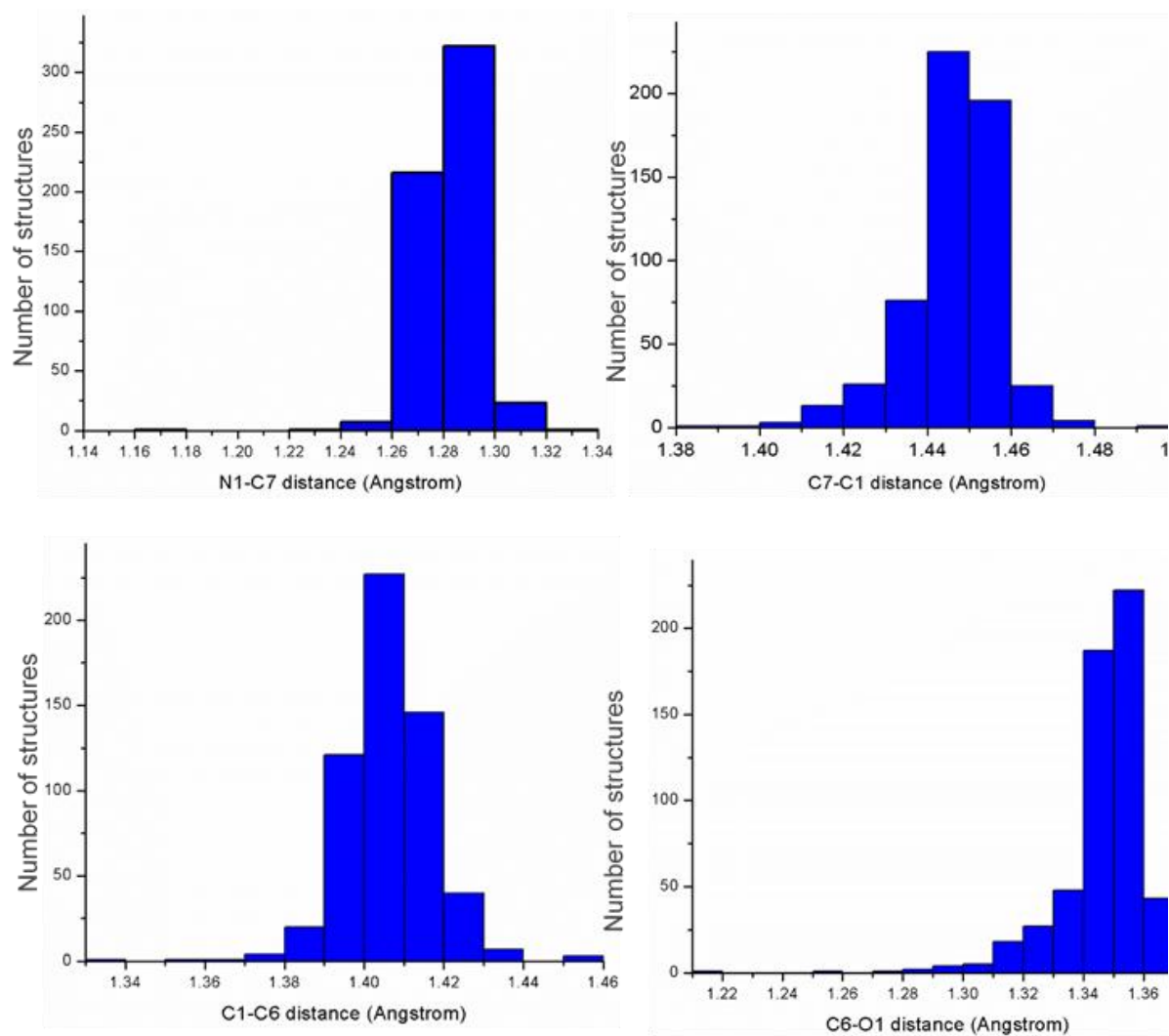


Figure S7. Histograms presenting the bond length in anils exhibiting their cis-enol form.

Molecules have been retrieved from the CSD database (update January 2016). Only structures with $R\% < 5$ and with no disorder have been selected.

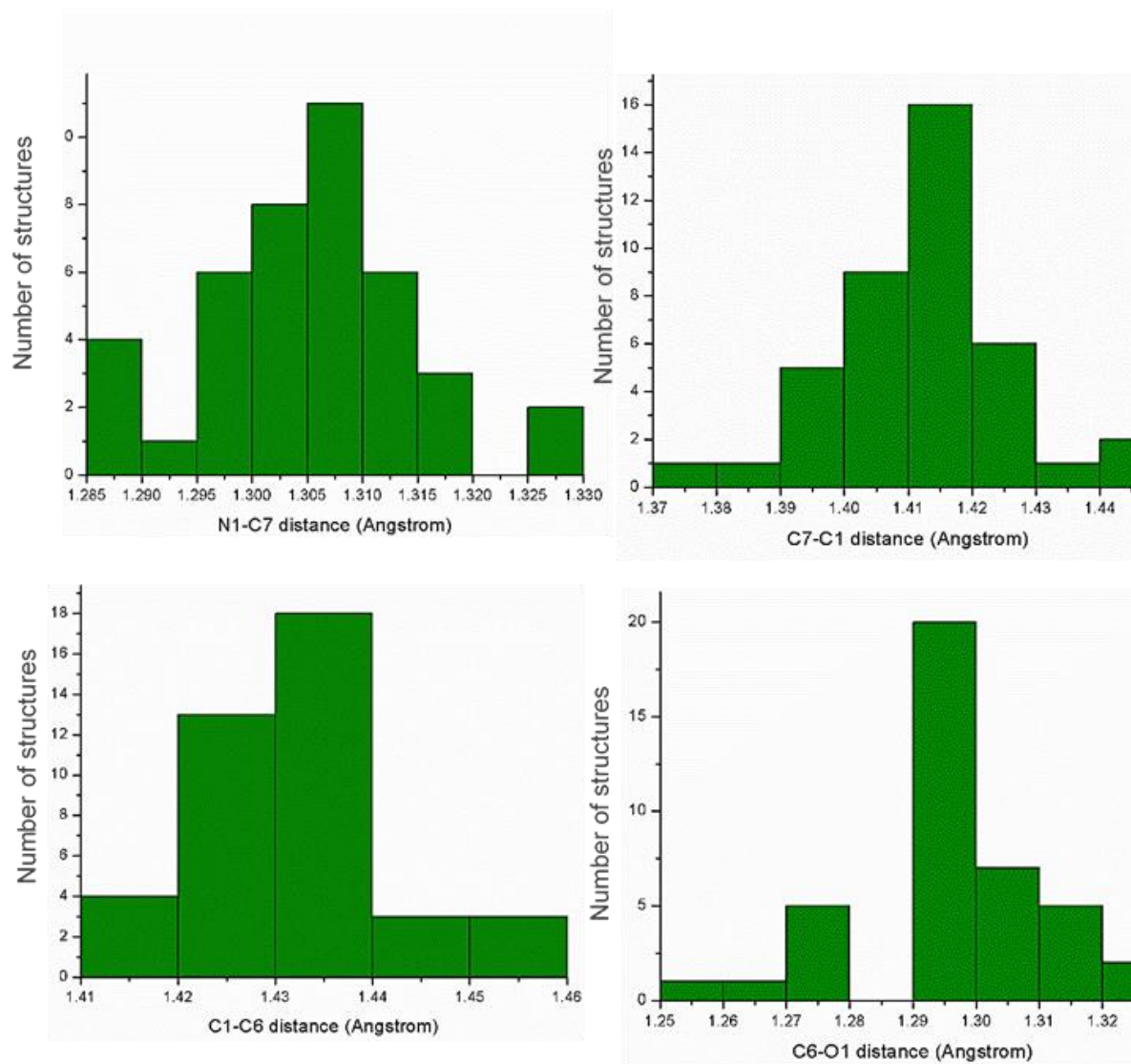


Figure S8. Histograms presenting the bond length in anils exhibiting their cis-keto form. Molecules have been retrieved from the CSD database (update January 2016). Only structures with $R\% < 5$ and with no disorder have been selected.

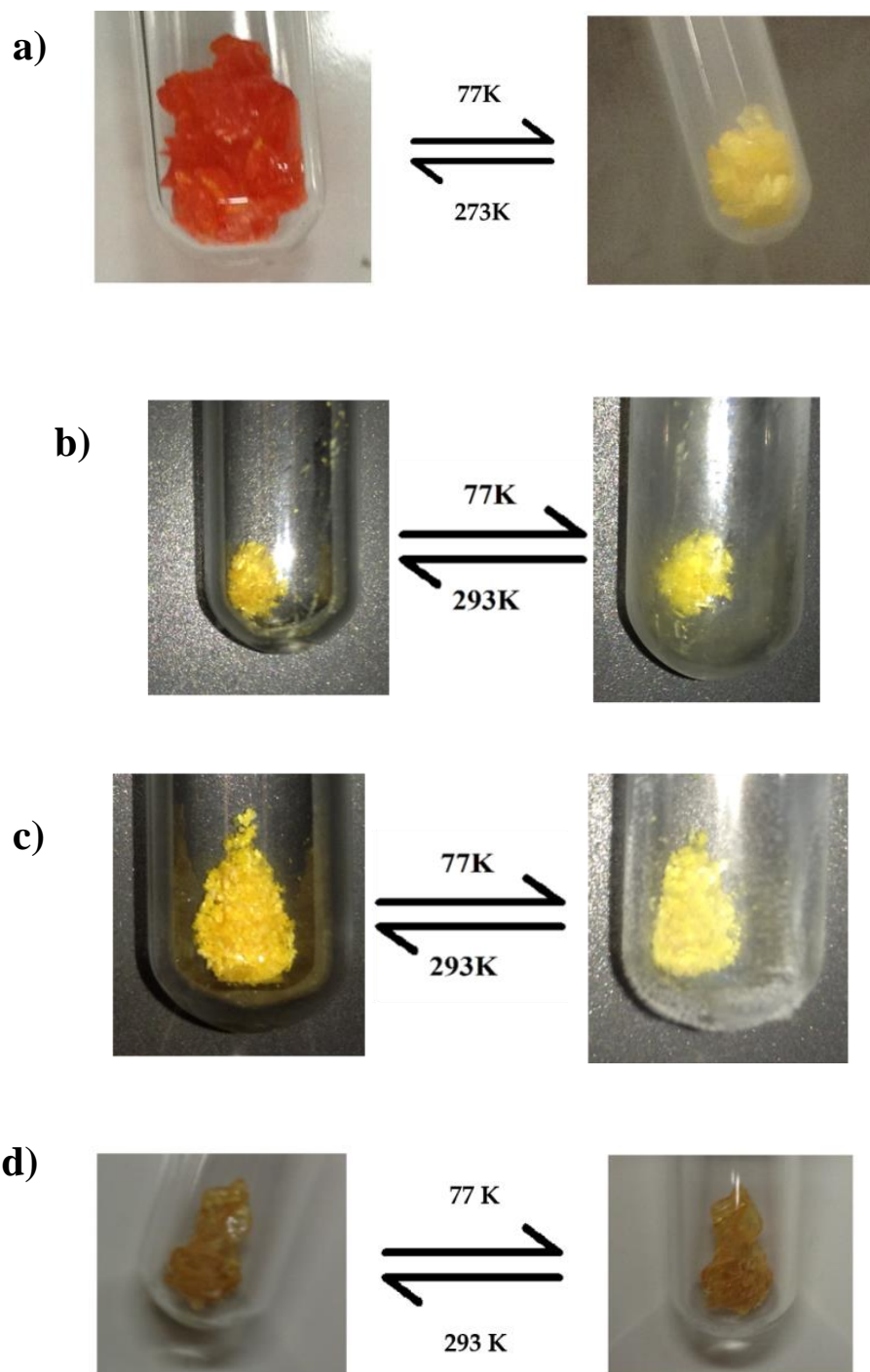


Figure S9. Liquid nitrogen exposure for 1-3 and 5. Crystals of one are strongly thermochromic, cocrystals 2-3 are slightly thermochromic. No color change observed for 5.

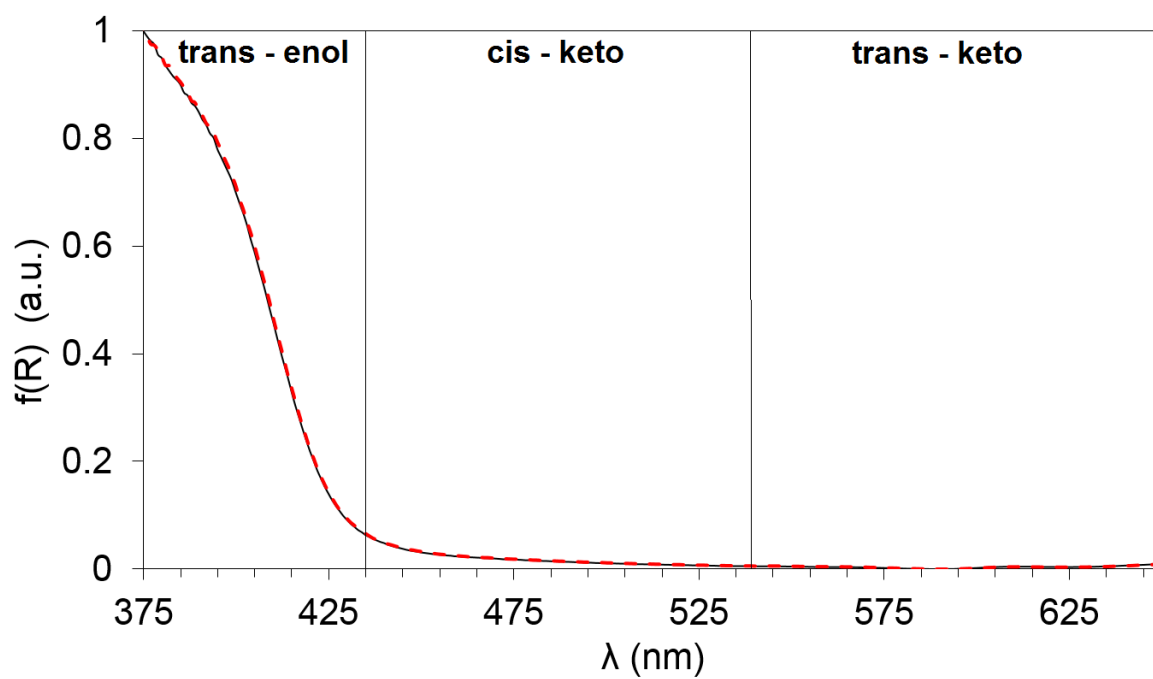
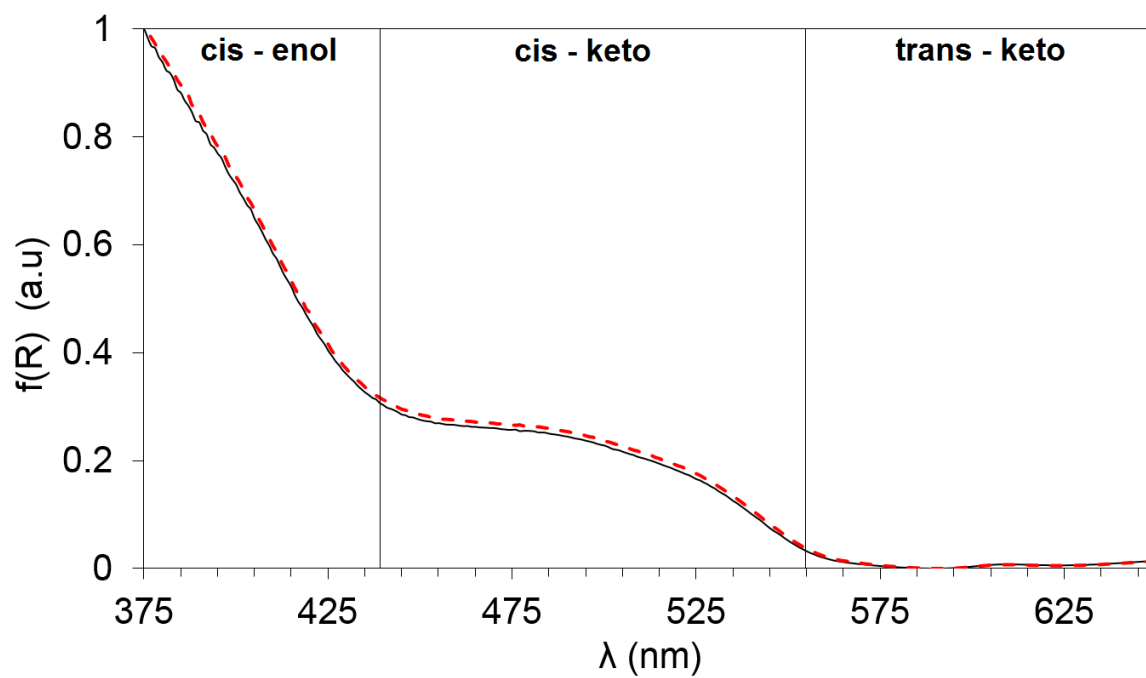


Figure S10. Kubelka-Munk spectra before (black solid line) and after (red dotted line) irradiation for **1** (top) and **5** (bottom)

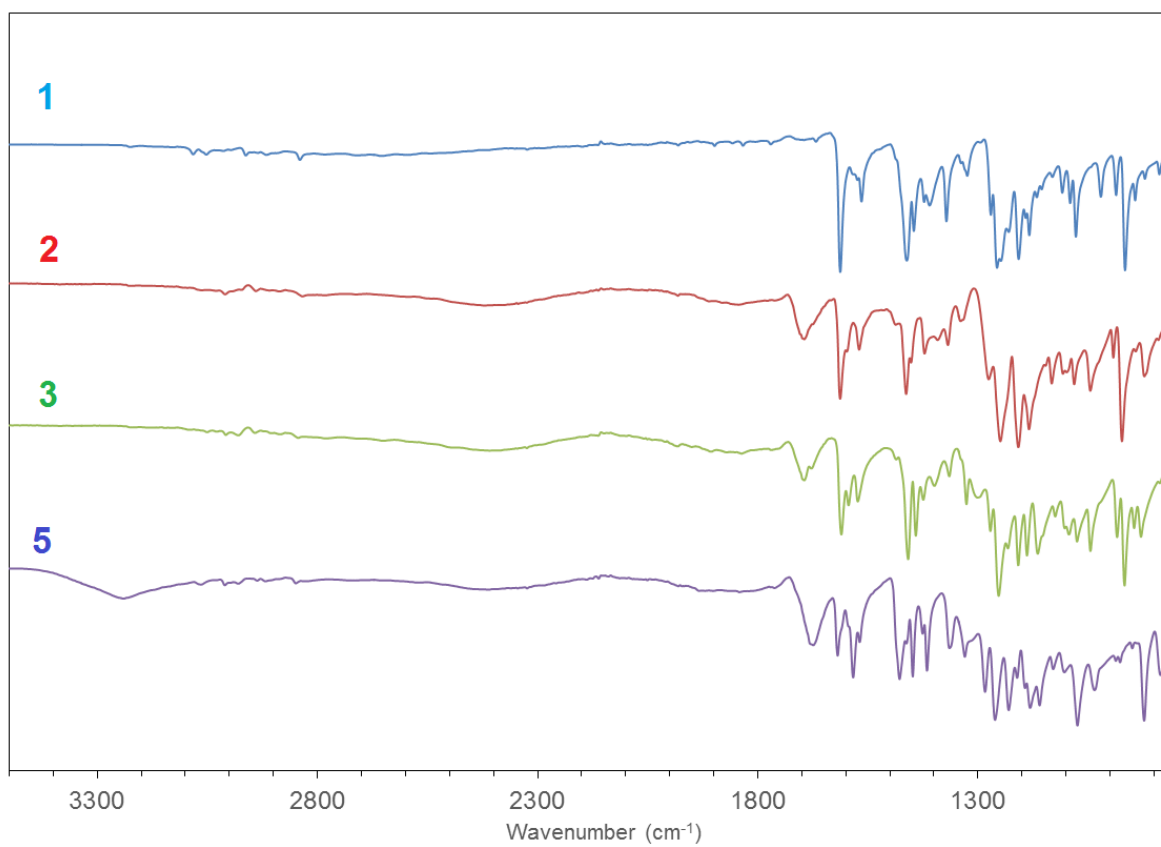


Figure S11. FTIR spectra of **1**, **2**, **3** and **5**.

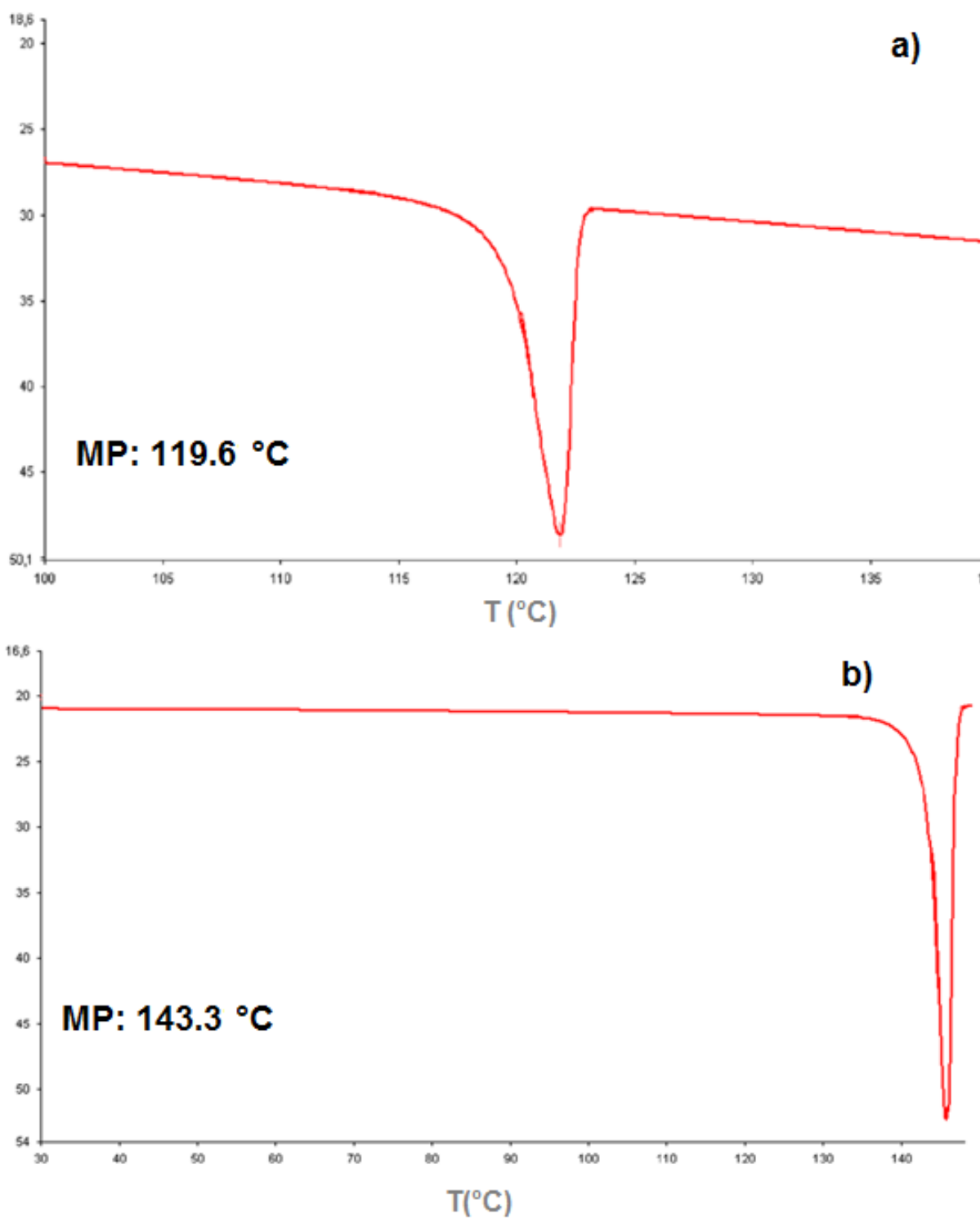


Figure S12. Melting point (onset), of crystals **1** and **2** measured by means of a Perkin Elmer DSC 7.0 calorimeter equipped with the PYRIS 1997-1998 program.

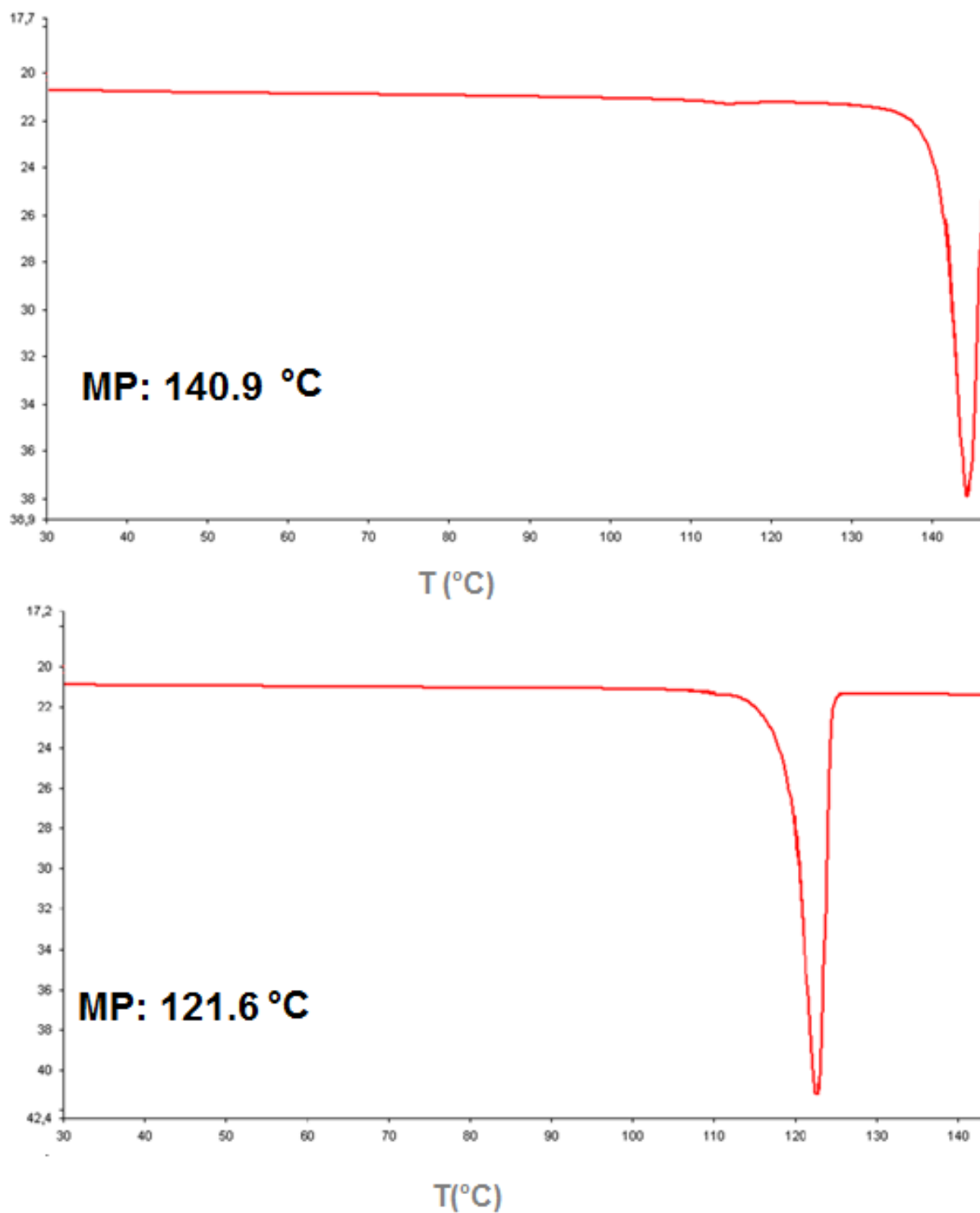


Figure S13. Melting point (onset) of cocrystals **3** (top) and **5** (bottom) measured by means of a Perkin Elmer DSC 7.0 calorimeter equipped with the PYRIS 1997-1998 program. Measurements have been performed in the range 30 to 150°C at a speed of 5°C/min

Table S1. Elemental analysis on crystals of **1**.

Element	Calculated	Experimental
N	12.27%	12.29%
C	68.41%	68.76%
H	5.30%	5.25%
O	14.02%	13.7%
Empirical formula C₁₃H₁₂N₂O₂		

Table S2. Room Temperature SCXRD measurements: crystallographic parameters

	1	2	3	4	5
Empirical formula	C ₁₃ H ₁₂ N ₂ O ₂	C ₁₃ H ₁₂ N ₂ O ₂ , 0.5(C ₄ H ₄ O ₄)	C ₁₃ H ₁₂ N ₂ O ₂ , 0.5(C ₄ H ₄ O ₄)	C ₁₃ H ₁₂ N ₂ O ₂ , 0.5(C ₄ H ₆ O ₄)	C ₁₃ H ₁₂ N ₂ O ₂ , 0.5(C ₄ H ₆ O ₄)
Fw (g/mol)	228.25	286.28	286.28	287,29	287,29
Crystal system	Orthorhombic	Monoclinic	Monoclinic	Monoclinic	Monoclinic
Space group	<i>P</i> 2 ₁ 2 ₁ 2 ₁	<i>P</i> 2 ₁ / <i>n</i>	<i>P</i> 2 ₁ / <i>n</i>	<i>P</i> 2 ₁ / <i>n</i>	<i>I</i> 2/ <i>a</i>
<i>a</i> (Å)	5.6190(4)	4.5344(1)	6.2578(2)	4.5815(2)	16.2457(15)
<i>b</i> (Å)	9.2825(7)	25.7895(7)	34.9486(11)	25.7191(6)	6.6244(4)
<i>c</i> (Å)	21.7490(14)	11.9533(3)	6.8516(3)	11.9326(6)	25.818(2)
<i>α</i> (°)	90	90	90	90	90
<i>β</i> (°)	90	93.524(2)	108.390(4)	93.106(4)	97.188(7)
<i>γ</i> (°)	90	90	90	90	90
<i>V</i> (Å³)	1134.39(14)	1395.18(6)	1421.93(10)	1403.98(10)	2756.7(4)
<i>Z</i>	4	4	4	4	8
Crystal size (mm)	0.20 x 0.40 x 0.54	0.12 x 0.20 x 0.27	0.10 x 0.1 x 0.30	0.06 x 0.26 x 0.5	0.20 x 0.30 x 0.50
T (K)	293	293	293	293	293
Radiation (Å)	MoK α : 0.71073	CuK α : 1.54184	CuK α :1.54184	CuK α :1.54184	MoK α : 0.71073
Nref, Npar	1983, 160	2462, 203	2508, 203	2474, 207	2432, 207
R[<i>I</i>>2σ(<i>I</i>)], GoF, wR²	0.0370, 1.10, 0.0809	0.0458, 1.30, 0.1289	0.0417, 1.27, 0.1351	0.0411, 1.04, 0.1175	0.0375, 1.00, 0.0987

Table S3. Selected geometries for H-bonds

Crystal structure	D—H···A	H···A (Å)	D···A (Å)	Angle (°)
1	O1—H1O···N1	1.74(3)	2.611(2)	151(3)
2	O1—H1O···N1	1.82(4)	2.648(3)	152(3)
	O3—H2O···N2	1.67(4)	2.641(3)	175(3)
3	O1—H1O···N1	1.69(3)	2.582(3)	153(3)
	O3—H2O···N2	1.81(3)	2.622(3)	176(3)
4	O1—H1O···N1	1.87(2)	2.647(2)	150(2)
	O3—H2O···N2	1.68(2)	2.656(2)	173(2)
5	O1—H1O···O4	1.95(2)	2.780(2)	155.9(2)
	O3—H2O···N2	1.67(2)	2.652(2)	174(2)

Table S4. Selected geometries for carboxyl group in FA and SA.

Crystal structure	C14-O3 (Å)	C14-O4 (Å)	Salt/Cocrystal
2	1.308(3)	1.206(3)	Cocrystal
3	1.302(4)	1.220(3)	Cocrystal
4	1.316(2)	1.201(2)	Cocrystal
5	1.312(2)	1.218(2)	Cocrystal

Table S5. Selected structures of SCC and MCC used for construction of model based on Hirshfeld surfaces C...C% contacts calculation.

Structure number	Photo- (P)/ Thermochromic (T)	MCC/SCC	CSD refcode	C...C%	T1 (°)
1	T	SCC	1, in this study	2.7	32.2
2	P	MCC	2, in this study	5.2	31.4
3	P	MCC	3, in this study	2.3	40.6
4	P	MCC	4, in this study	5.2	31.6
5	T	SCC	BADDAL12	6.1	5.9
6	T	SCC	CAVQAR	5.5	6.06
7	T	SCC	CAVQOF	6.3	7
8	T	SCC	CULPOO	7.1	8.48
9	P	SCC	DAWFEN	2.2	41.58
10	T	SCC	EKUGEW	6.8	13.54
11	T	SCC	ETAYUX	7	9.92
12	T	SCC	ETAYUX01	5.4	13.46
13	P	SCC	FAXWIM	0.3	45.42
14	P	SCC	FAXWOS	1	46.1
15	P	SCC	FAXWUY	1.1	46.54
16	T	SCC	GAWKEV	6.5	15

17	T	SCC	GOFLAP	4.2	3.3
18	T	SCC	GOKPAZ	8.5	3.2
19	T	SCC	HACZAN	7.1	9.82
20	P	SCC	IVOHIL	0.8	25.96
21	T	SCC	KEZFUQ	7	4.67
22	P	SCC	KIPMEB	1.9	45.68
23	P	MCC	KIPTOU	0	17.81
24	P	MCC	KIPTOU01	0	21.5
25	T	SCC	KOGVEH01	9.1	36.54
26	T	SCC	KUFLUU	6.1	1.37
27	T	SCC	KUFLUU01	4	26.94
28	T	SCC	NADZUO	8.6	7.25
29	T	MCC	NEZXAT	7.9	11.08
30	P	MCC	NEZXEX	1.2	41.58
31	T	SCC	NEZXIB	7.4	6.68
32	T	MCC	NEZXOH	7.4	16.36
33	P	MCC	NEZXUN	1.8	45.01
34	T	SCC	NEZYAU	9.5	27.56
35	T	SCC	NUQXAA01	4	2.48
36	T	SCC	NUQXAA02	6.3	4.71
37	T	SCC	NUQXAA03	7	2.12
38	T	SCC	POFSEJ	8.1	3.93
39	T	SCC	QOXVIJ01	3.2	39.82
40	T	SCC	QOXVOP	8	2.46
41	P	MCC	ROTHERP	0.7	3
42	P	MCC	ROTHIT	0.8	1.15
43	P	MCC	ROTREZ	0.7	0.67
44	T	MCC	RUDLIN	4.2	10.68
45	P	MCC	RUDLOT	2.4	30.27
46	P	MCC	RUDMAG	0	23.74
47	P	MCC	RUDMEK	0	6.27
48	P	MCC	RUDMIO	0	14.73
49	P	SCC	SALCAN01	1.4	47.72
50	P	SCC	SLCPYA	7.6	14.12
51	P	MCC	WIGFOJ	2.5	35.57
52	P	MCC	WIGFUP	5.2	35.12
53	T	MCC	WIGGAW	3.5	9.09
54	T	MCC	WIGGEA	4.2	15.09
55	T	MCC	WIGGIE	4.2	8.53
56	T	SCC	YOCRAK01	6.2	6.42

Annex B

To: N-salicylideneaminopyridinium salts and the strategy of the bulky anions: anion induced isostructurality, solid solubility and photochromism induced through tetra-aryl boxes[†]

[†]Carletta, Andrea, et al. "Tetraphenylborate Anion Induces Photochromism in *N*-Salicylideneamino-1-alkylpyridinium Derivatives Through Formation of Tetra-Aryl Boxes." *The Journal of Physical Chemistry C* 122, (2018): 10999-11007.

Supporting Information to chapter 3

List of Figures and Tables

Figure S1. PXRD diffractograms of **1-4**

Table S1. SCXRD parameters of **1-4**

Table S2. SCXRD parameters of **30.6240.38**.

Table S3. Selected torsion angles and dihedral angle in **1-4**.

Table S4. Selected bond lengths.

Figure S2. Disorder of the pyrimidine moiety in structure **3**.

Figure S3. Structure of **30.6240.32**.

Figure S4. Comparison of Kubelka-Munk spectra taken before and after 365 nm irradiation of **1**

Figure S5. Comparison of Kubelka-Munk spectra taken before and after 365 nm irradiation of **2**.

Figure S6. Thermal fading process in **3** evaluated at 500 nm.

Figure S7. Two-step thermal fading of **4** evaluated at 500 nm.

Figure S8. Two-step thermal fading of **30.6240.38** evaluated at 500 nm.

Figure S9. structure overlap (6 molecules, number of points = 150) and calculation of root mean square deviation (RMSD) for the pairs **30.6240.38** vs **3** and **30.6240.38** vs **4**.

Figure S10. Thermochromism in **1-4**

Figure S11. Indexing of crystal faces in **1**.

Figure S12. Dichroism observed in the (0-11) crystal face of **1**.

Figure S13. Dichroism observed in the (-100) crystal face of **1**.

Figure S14. CIE chromaticity diagrams for dichroic color change in the (0-11) face and in the (-100) crystal face of crystal **1**.

Figure S15. Color change observed in the (-100) crystal face of **1** associated to variation of the plane-polarized light angle.

Figure S16. Color change observed in the (001) crystal face (top) and in the (0-11) crystal face (bottom) of **2** associated to variation of the plane-polarized light angle.

Figure S17. ^1H NMR spectra of **3**_{0.68}**4**_{0.32}. Zoom of the 0-5 ppm region of the spectrum taken from polycrystalline powder and from single crystal.

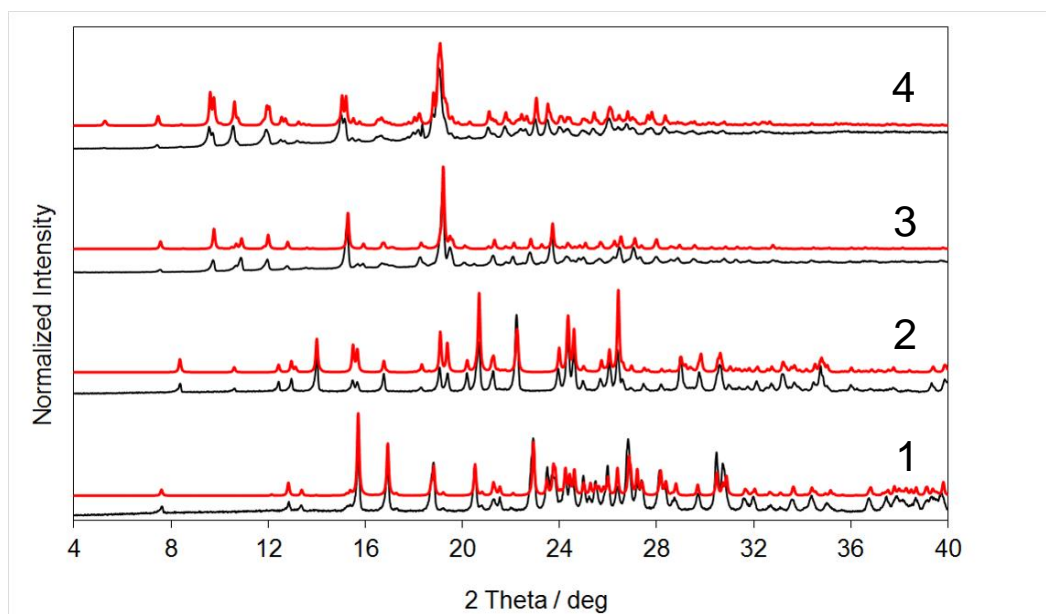


Figure S1. PXRD diffractograms of **1-4** (Experimental diffractograms are in black; those calculated on the basis of the single-crystal structure are in red)

Table S1. SCXRD parameters of **1-4**

	1	2	3	4
Empirical formula	$C_{14}H_{15}IN_2O_2$	$C_{15}H_{17}IN_2O_2$	$C_{38}H_{35}BN_2O_2$	$C_{39}H_{37}BN_2O_2$
Formula weight	370.18	384.20	562.49	576.51
Crystal system	Monoclinic	Monoclinic	Monoclinic	Triclinic
Space group	$P2_1/c$	$P2_1/c$	$P2_1/n$	$P-1$
<i>a</i> (Å)	11.9341(4)	6.74888(18)	11.2697(2)	11.3269(3)
<i>b</i> (Å)	8.0517(3)	16.7024(3)	16.2411(2)	16.7355(5)
<i>c</i> (Å)	14.9549(4)	13.6796(3)	17.4036(3)	17.4740(5)
α (°)	90	90	90	89.396(2)
β (°)	102.757(3)	90.922(2)	104.2390(18)	74.793(3)
γ (°)	90	90	90	88.828(2)
<i>V</i> (Å³)	1401.55(8)	1541.80(6)	3087.56(9)	3195.71(17)
<i>Z</i>	4	4	4	4
Crystal size (mm)	0.148 x 0.076 x 0.028	0.519 x 0.394 x 0.300	0.416 x 0.301 x 0.190	0.433 x 0.110 x 0.030
Temperature (K)	293(2)	295(2)	293(2)	295(2)
Wavelength (Å)	0.71073	0.71073	0.71073	1.54184
Nref (unique)	3768	8207	6077	11379
Npar	178	187	467	799
R	0.0314	0.0357	0.0497	0.0468
GoF	1.020	1.022	1.036	1.026
wR₂	0.0601	0.0955	0.1305	0.1289
CSD refcodes	1827939	1827940	1827941	1827942

Table S2. SCXRD parameters of **30.6240.38**.

30.6240.38	
Empirical formula (Assessed by ¹ HNMR)	C _{38.38} H _{35.76} BN ₂ O ₂
Crystal system	Triclinic
Space group	<i>P</i> - 1
<i>a</i> (Å)	11.2975(2)
<i>b</i> (Å)	16.5277(2)
<i>c</i> (Å)	17.3521(3)
α (°)	89.2858(12)
β (°)	75.1350(15)
γ (°)	88.9588(13)
<i>V</i> (Å ³)	3130.96(9)
Z	4
Crystal size (mm)	0.430 x 0.110 x 0.030
Temperature (K)	295(2)
Wavelength (Å)	1.54184
Nref (unique)	11016
Npar	804
R, GoF, wR₂	0.0512, 1.075, 0.1484
CSD refcode	1827943

Table S3. Selected torsion angles and dihedral angle in in **1-4**.

	1	2	3	4	30.6240.38
T1 (°)	1.3(4)	0.0(2)	37.6(2)/ -144.5(3)	36.3(3)/ -138.6(3)/	37.3(2)/ -141.4(3)
T2 (°)	1.7(4)	0.2(3)	7.7(3)	-1.3(2) /5.4(2)	-1.8(2)/ 5.1(3)
ϕ (°)	1.9	2.1	42.5/ 44.3	37.6/ 48.6	39.2/ 44.6

Table S4. Selected bond lengths.

bond	1 (Å)	2 (Å)	3 (Å)	4 (Å)	30.6240.38 (Å)
N1-C7	1.288(3)	1.283(3)	1.288(3)	1.279(3)/ 1.283(3)	1.281(2)/ 1.282(2)
C7-C1	1.440(4)	1.441(4)	1.443(2)	1.442(2)/ 1.432(3)	1.445(2)/ 1.435(2)
C1-C6	1.401(3)	1.400(4)	1.393(3)	1.401(3)/ 1.404(3)	1.400(2)/ 1.403(3)
C6-O1	1.348(3)	1.348(3)	1.359(3)	1.350(2)/ 1.357(3)	1.352(2)/ 1.355(3)

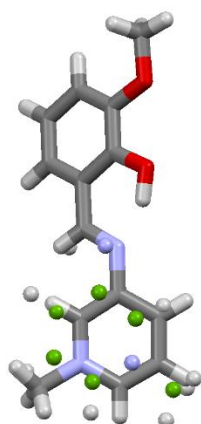


Figure S2. Disorder of the pyrimidine moiety in structure **3**.

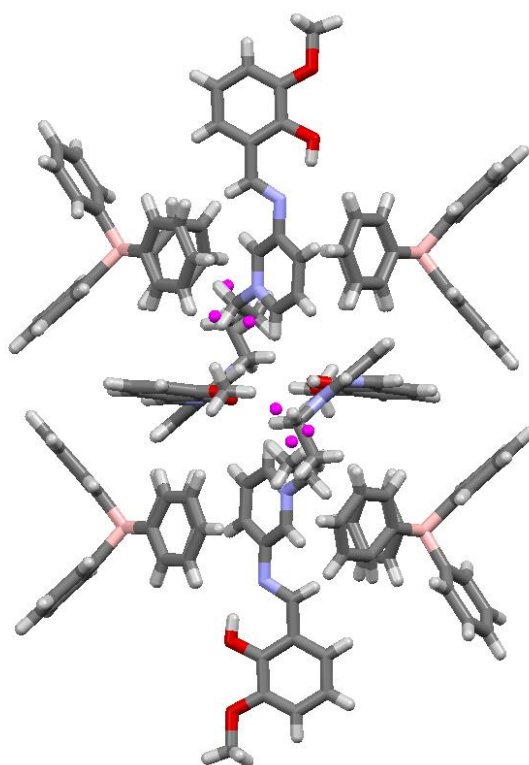


Figure S3. Structure of **30.6240.32**. (Disorder of the alkyl group highlighted in magenta).

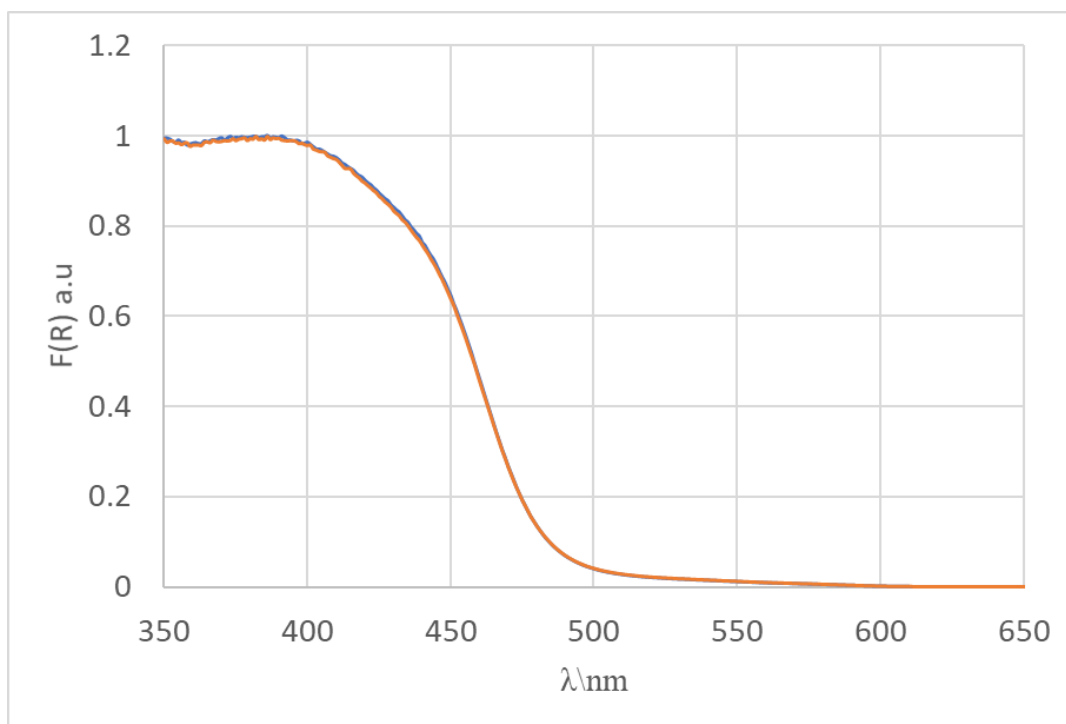


Figure S4. Comparison of Kubelka-Munk spectra taken before (blue) and after (orange) 365 nm irradiation of **1**. No spectral change observed.

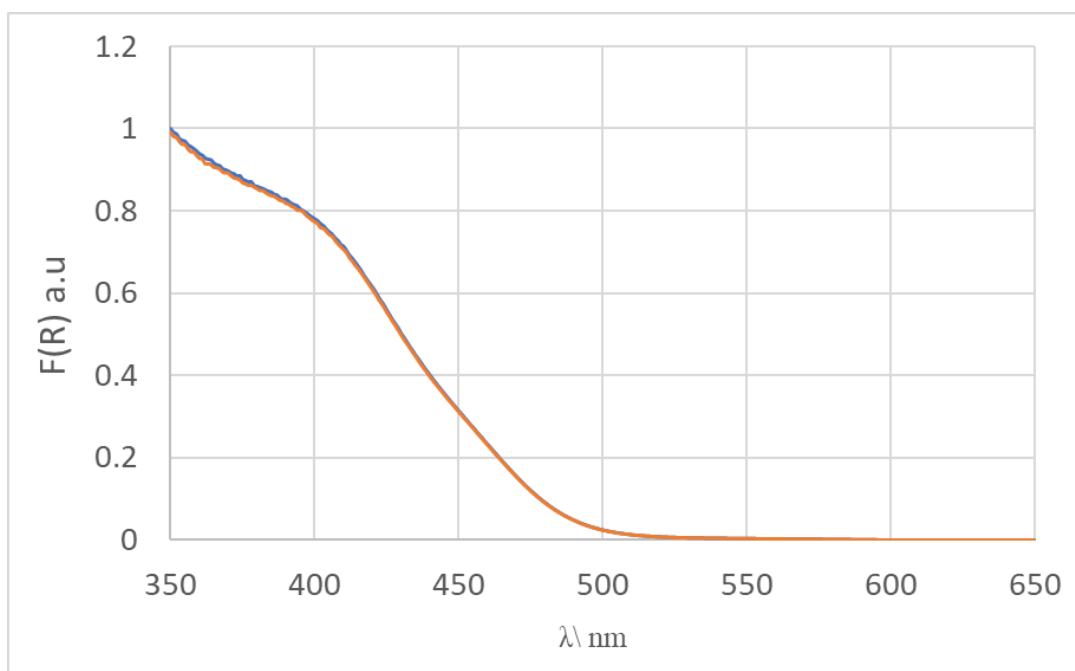


Figure S5. Comparison of Kubelka-Munk spectra taken before (blue) and after (orange) 365 nm irradiation of **2**. No spectral change observed.

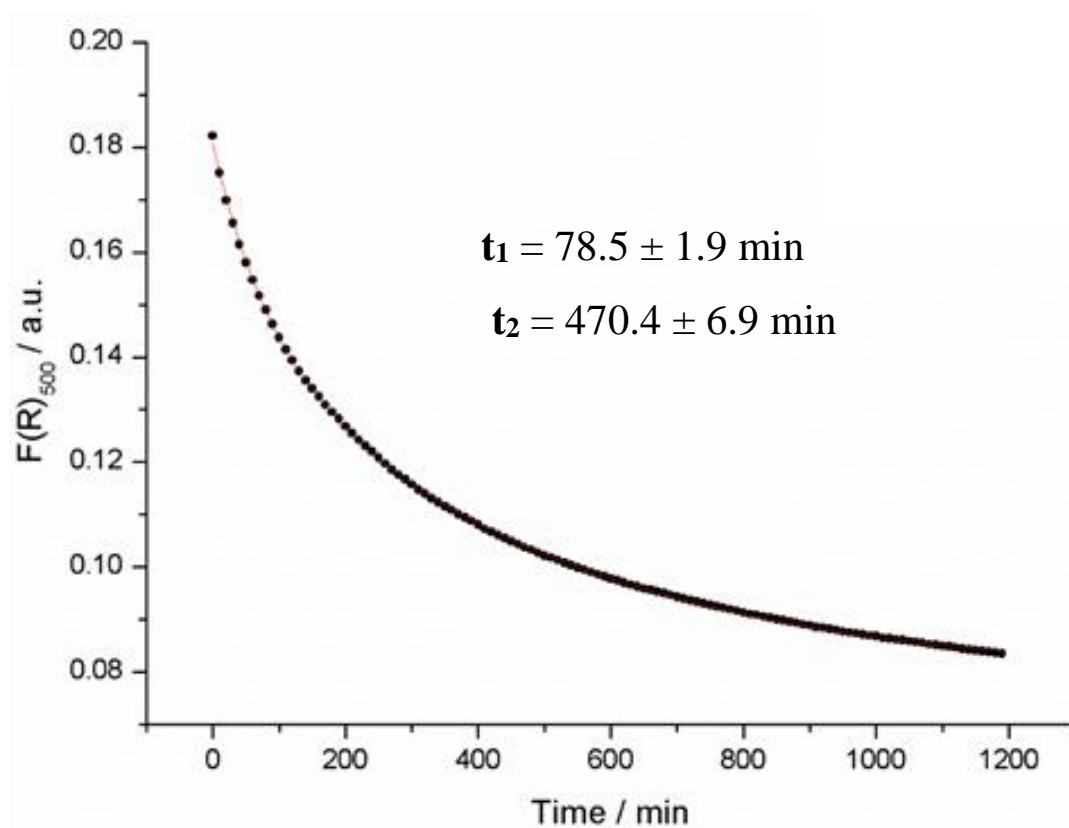
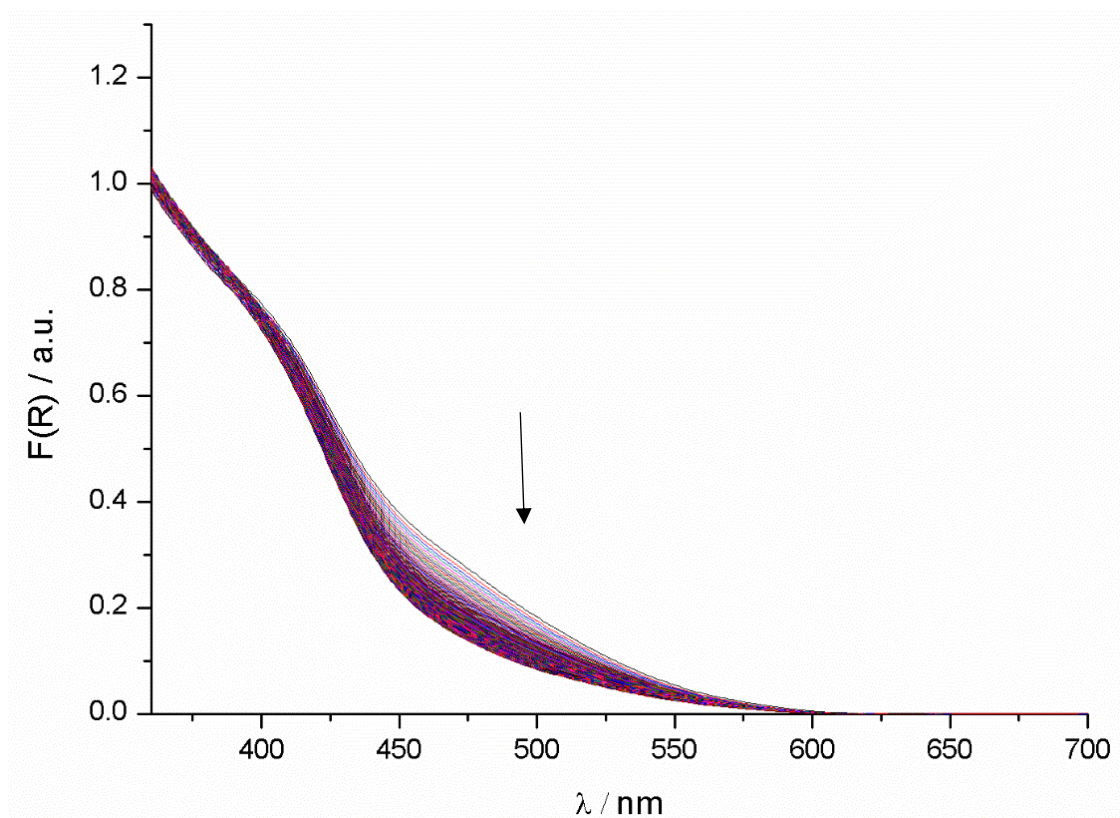


Figure S6. Thermal fading process in **3** evaluated at 500 nm.

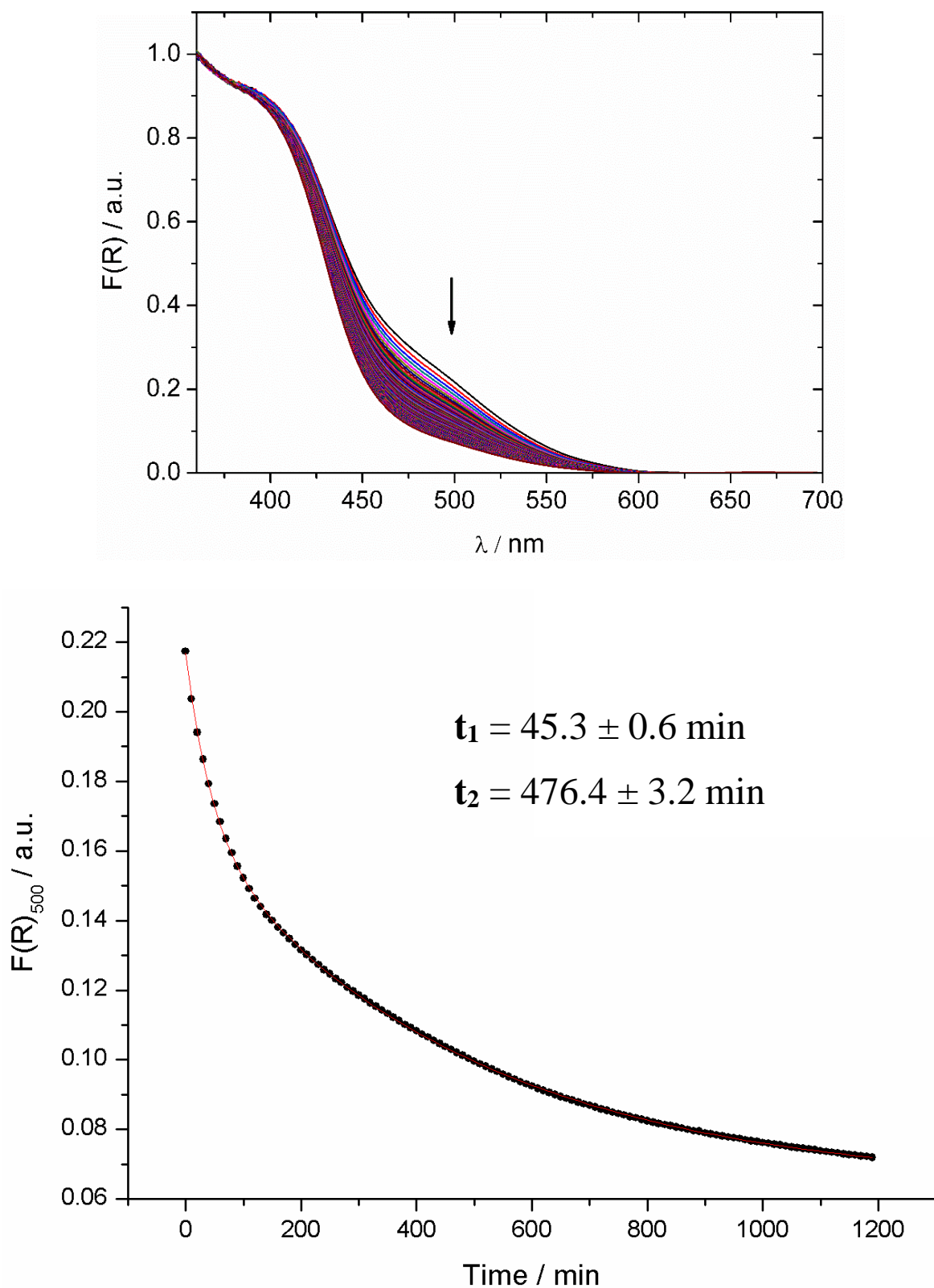


Figure S7. Two-step thermal fading of **4** evaluated at 500 nm. (the figure on the top is also provided as **Figure 8** in the manuscript)

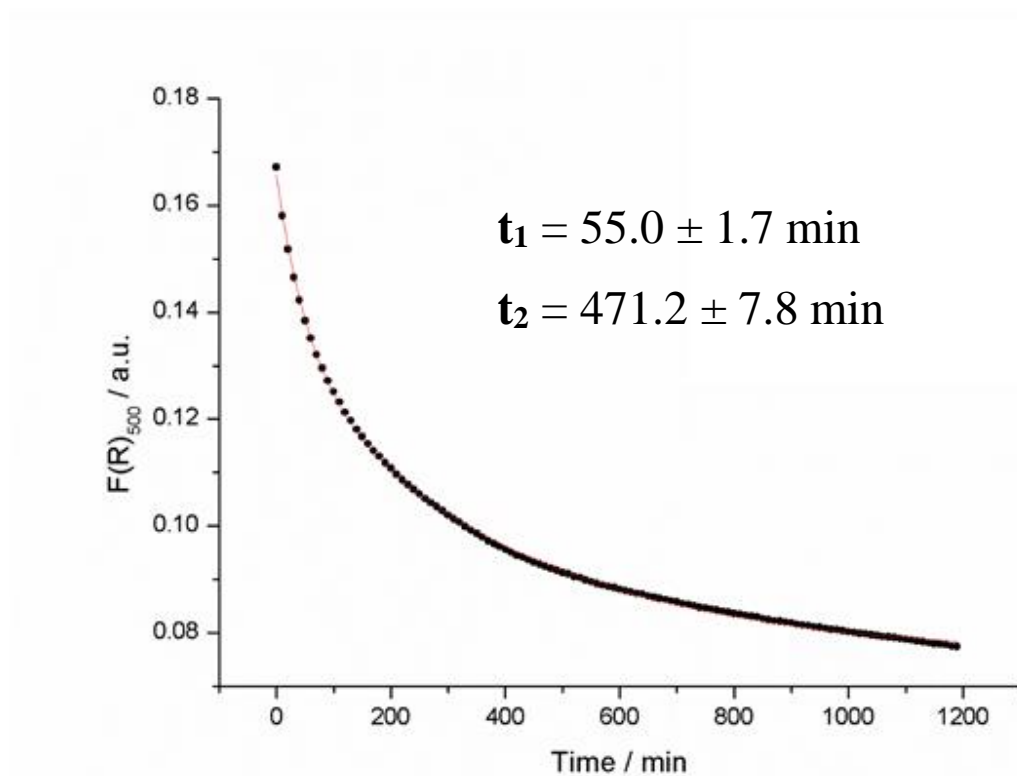
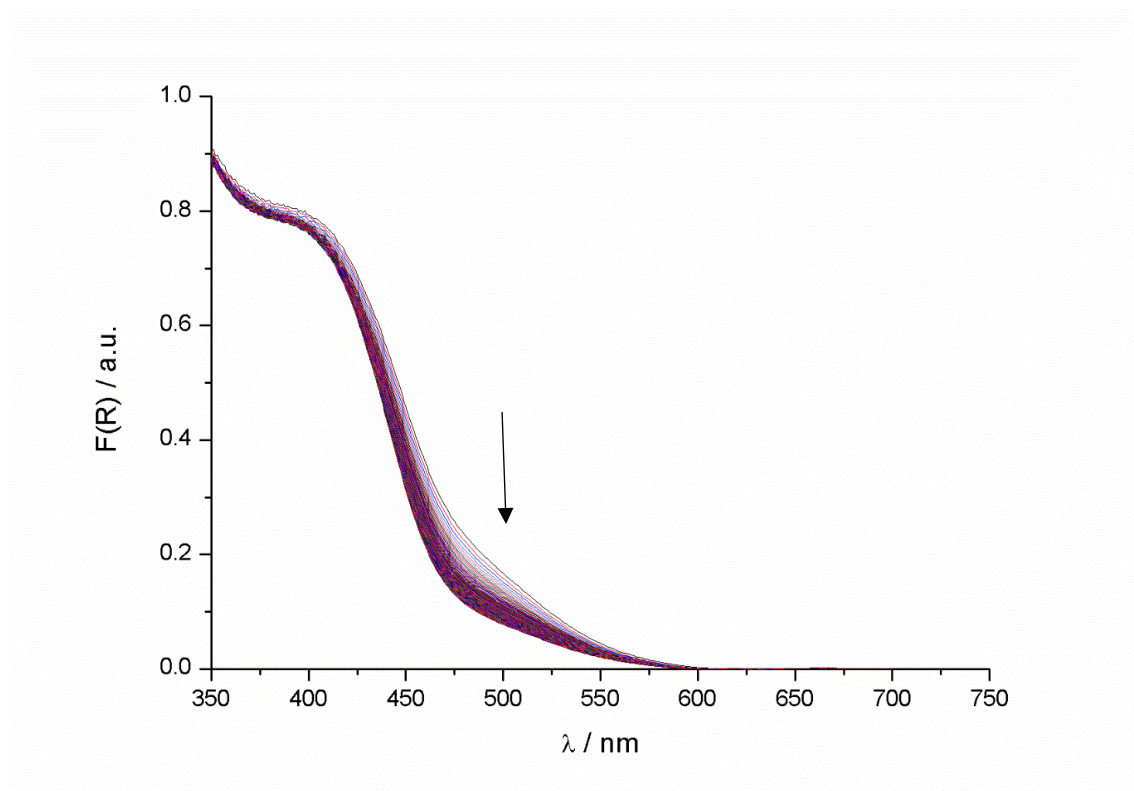


Figure S8. Two-step thermal fading of $30.6240.38$ evaluated at 500 nm.

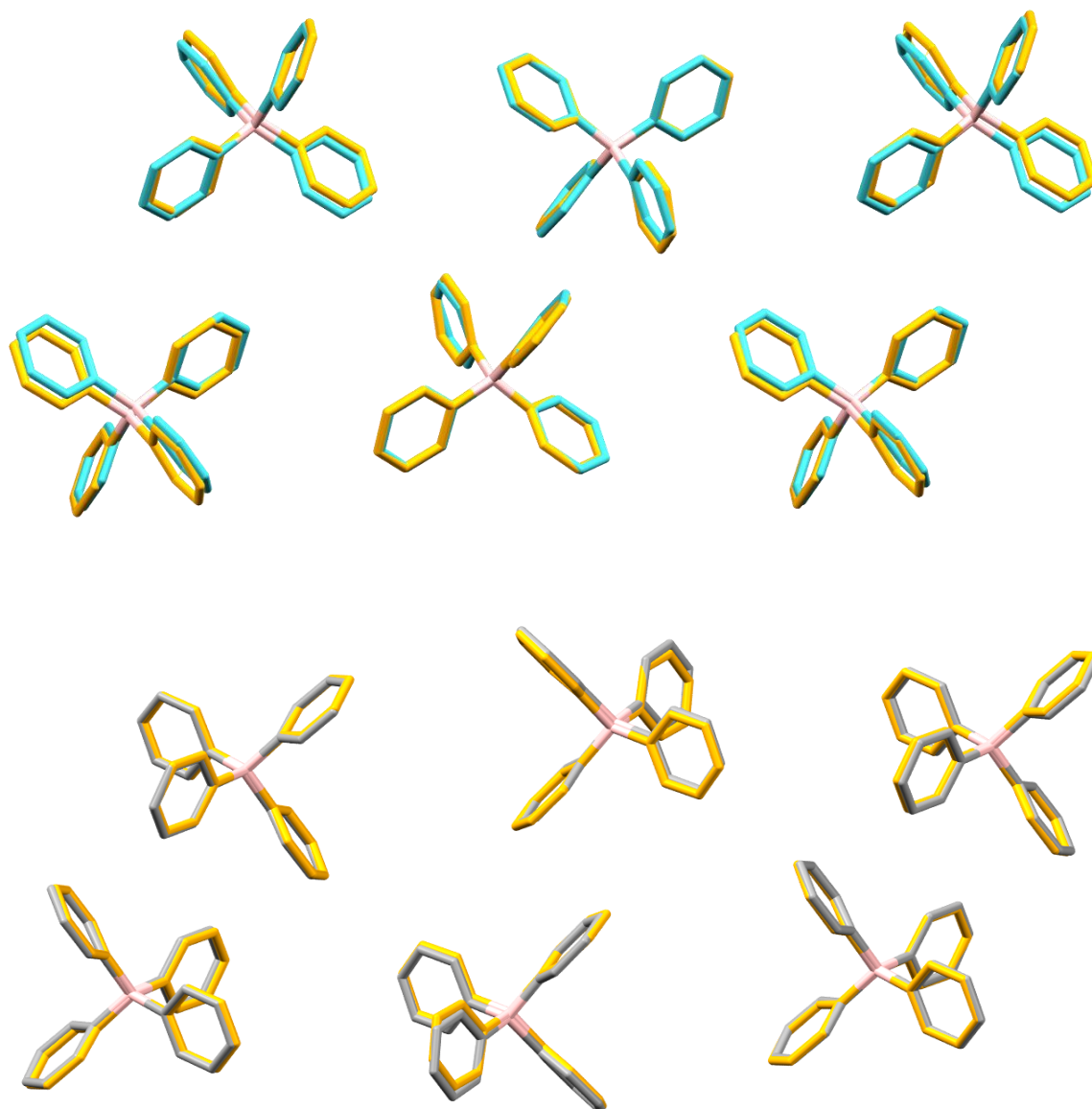


Figure S9. Structure overlap (6 molecules, number of points = 150) and calculation of root mean square deviation (RMSD) for the pairs **3**_{0.62-40.38} vs **3** (top, RMSD = 0.294 Å) and **3**_{0.62-40.38} vs **4** (bottom, RMSD = 0.166 Å). Color code: **3** = blue, **4** = grey, **3**_{0.62-40.38} = orange.

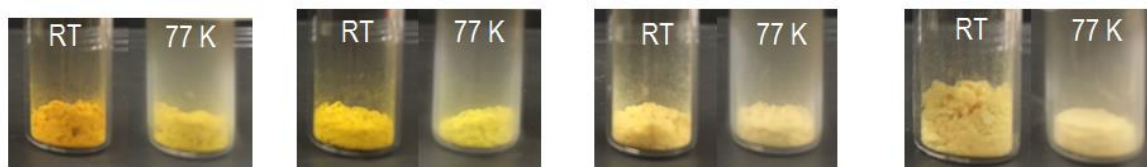


Figure S10. Thermochromism in **1-4** (left to right)

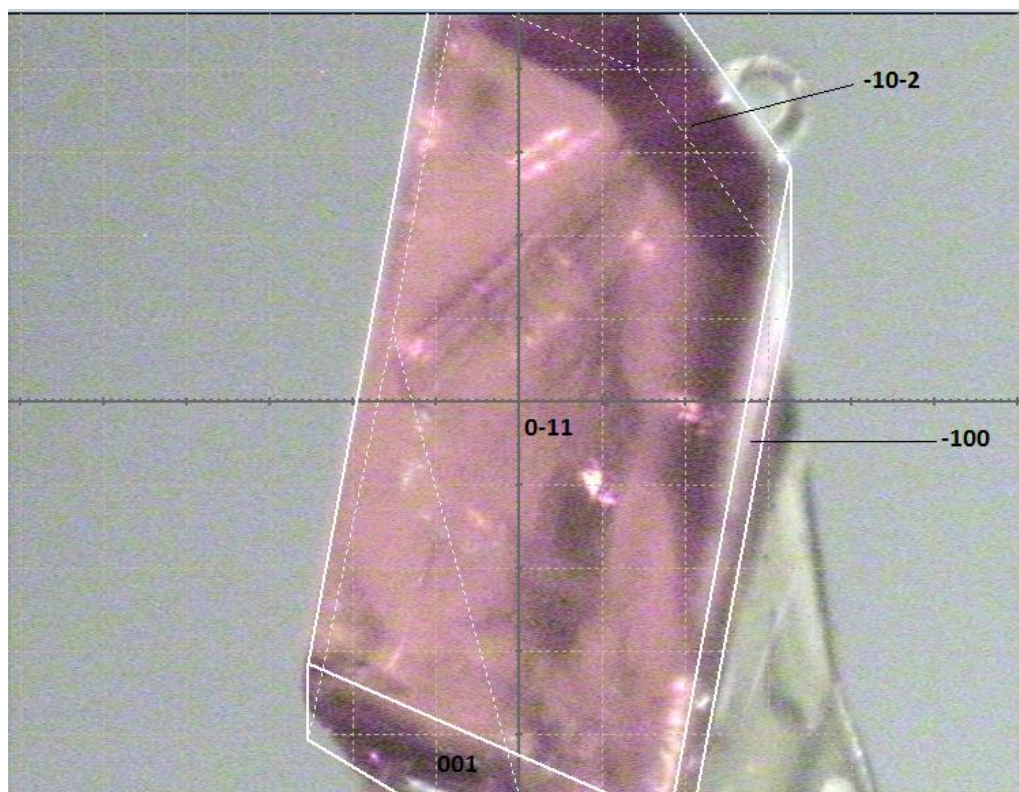


Figure S11. Indexing of crystal faces in **1**.

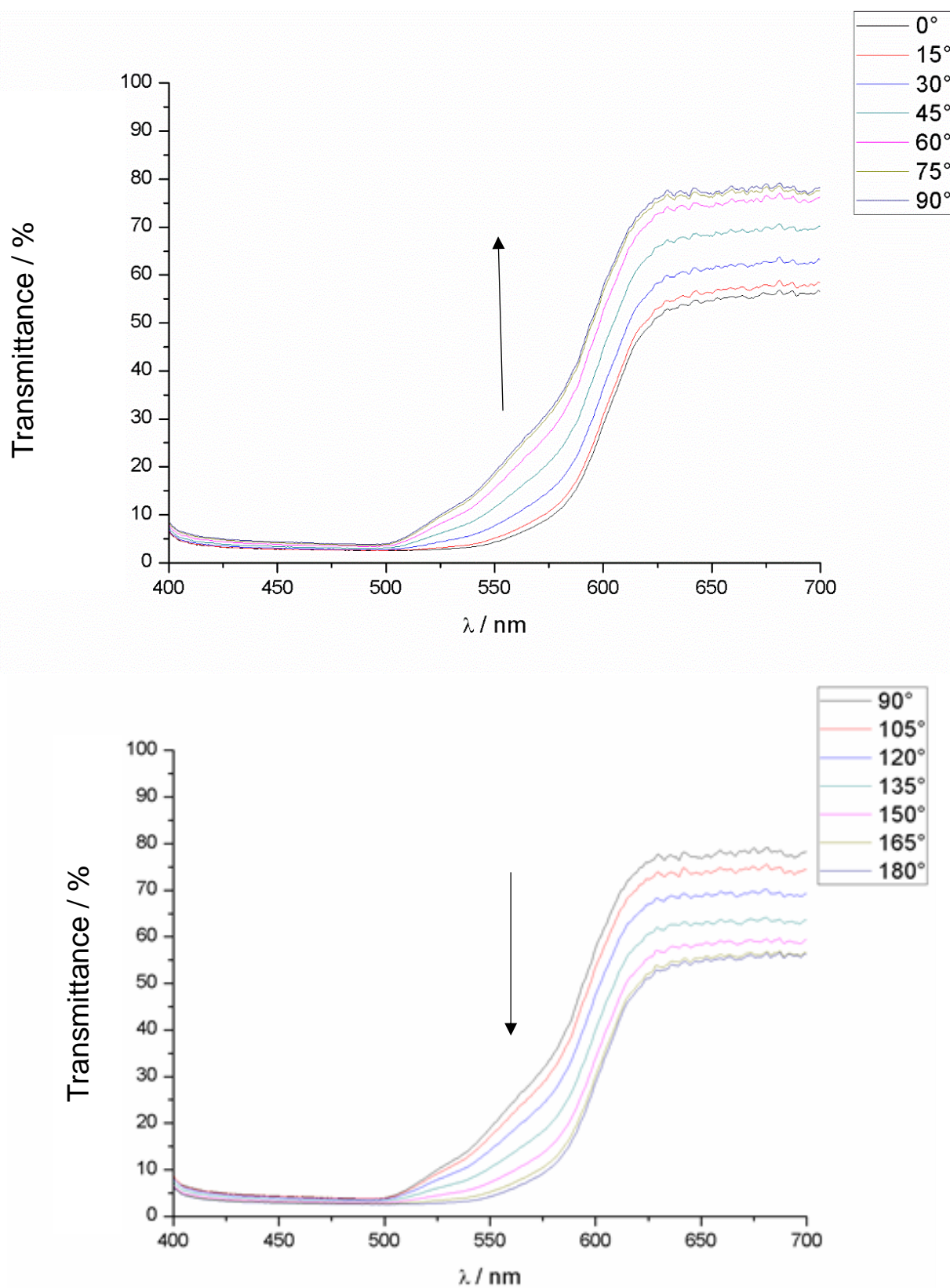


Figure S12. Dichroism observed in the (0-11) crystal face of **1**. Transmittance variation from 0 to 90° is also provided in the main text as **Figure 9**

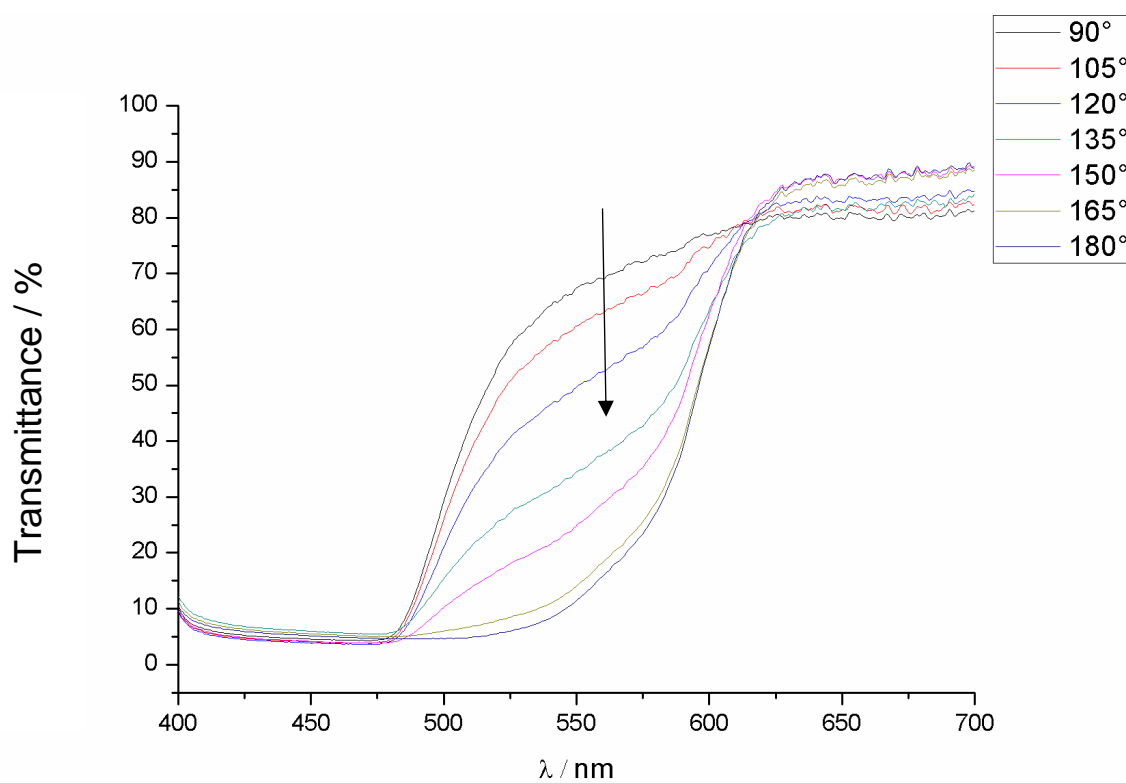
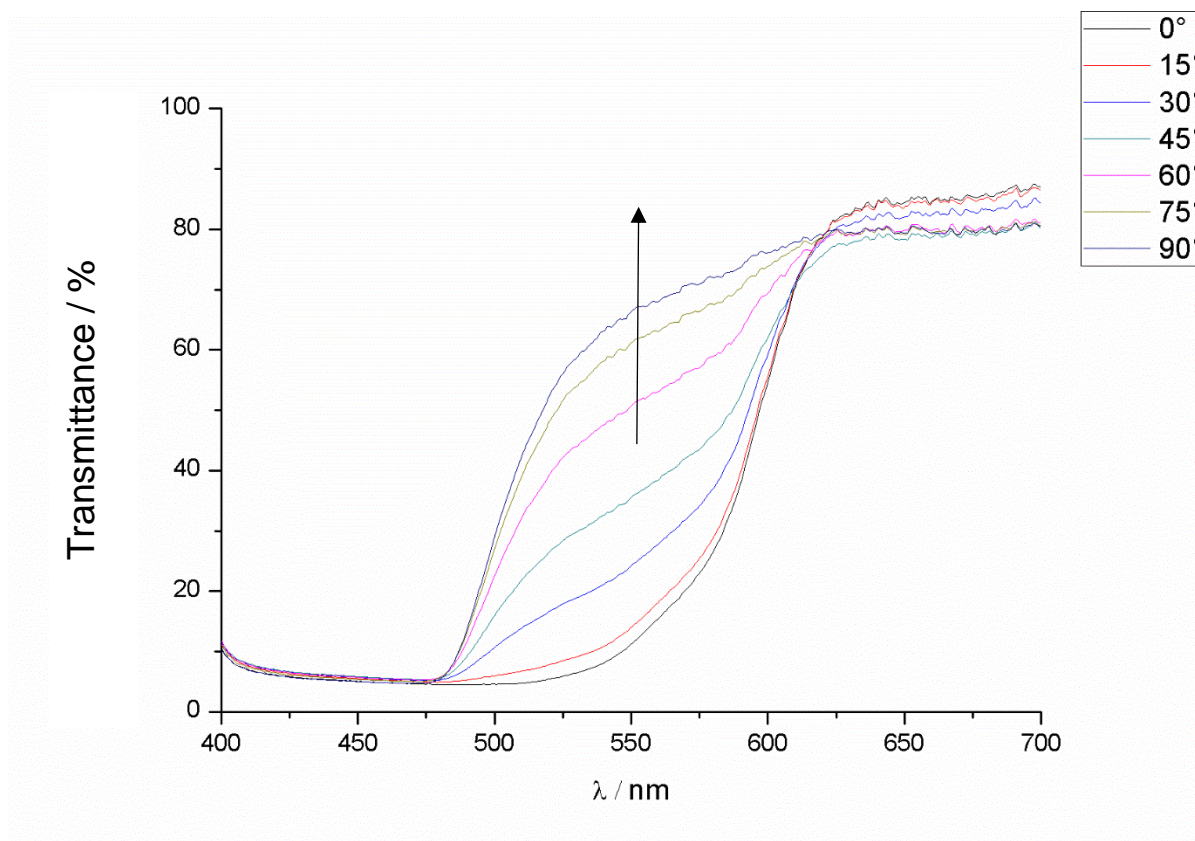
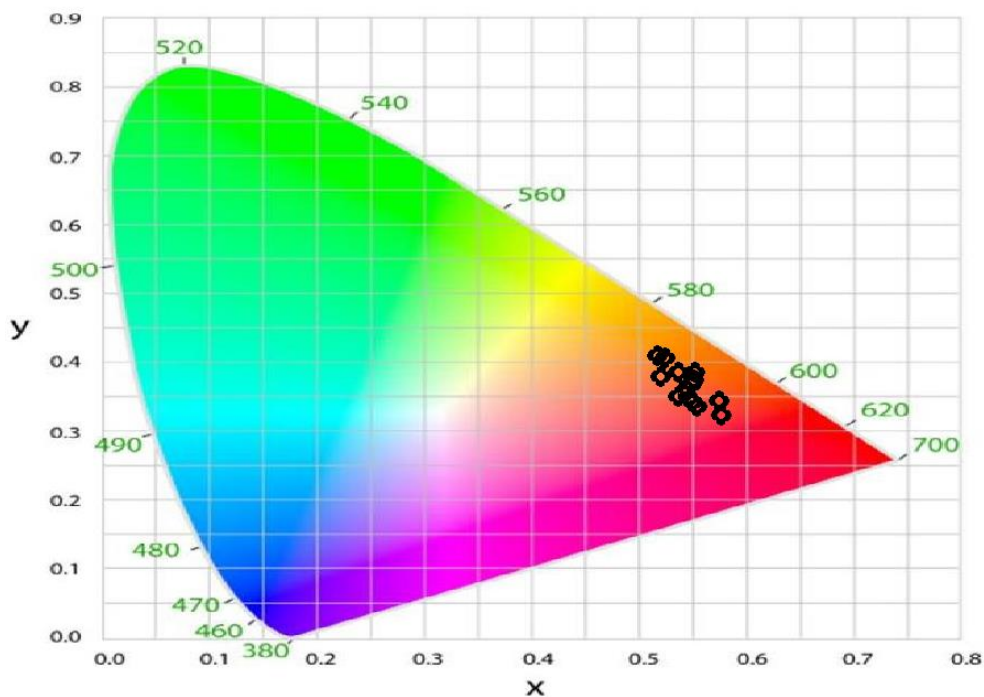


Figure S13. Dichroism observed in the (-100) crystal face of **1**. Transmittance variation from 0 to 90° is also provided in the main text as **Figure 9**.

CIE Chromaticity Diagram



CIE Chromaticity Diagram

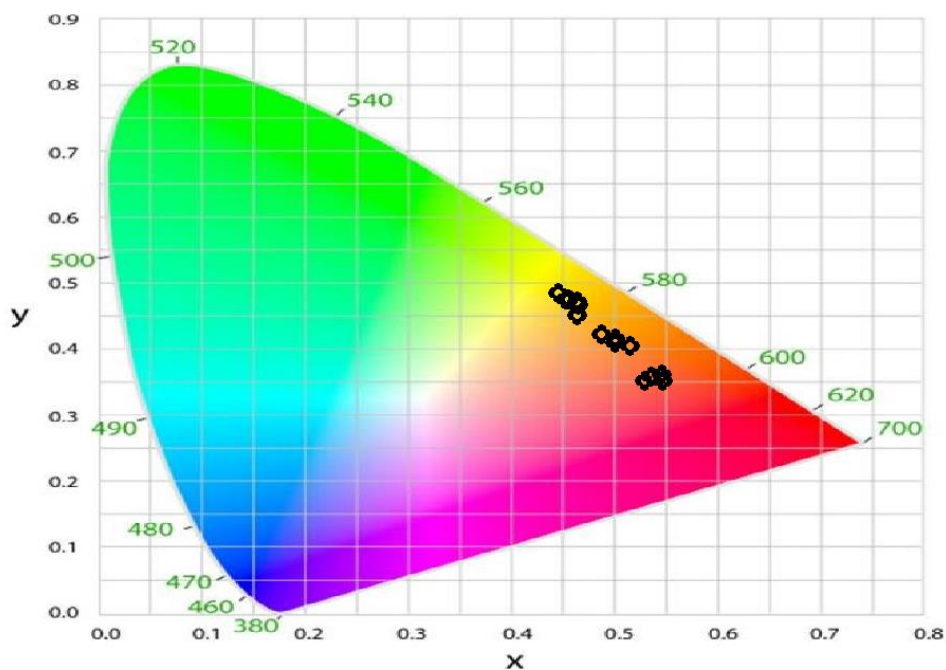


Figure S14. CIE chromaticity diagrams for dichroic color change in the (0-11) face (top) and in the (-100) crystal face (bottom) of crystal 1.

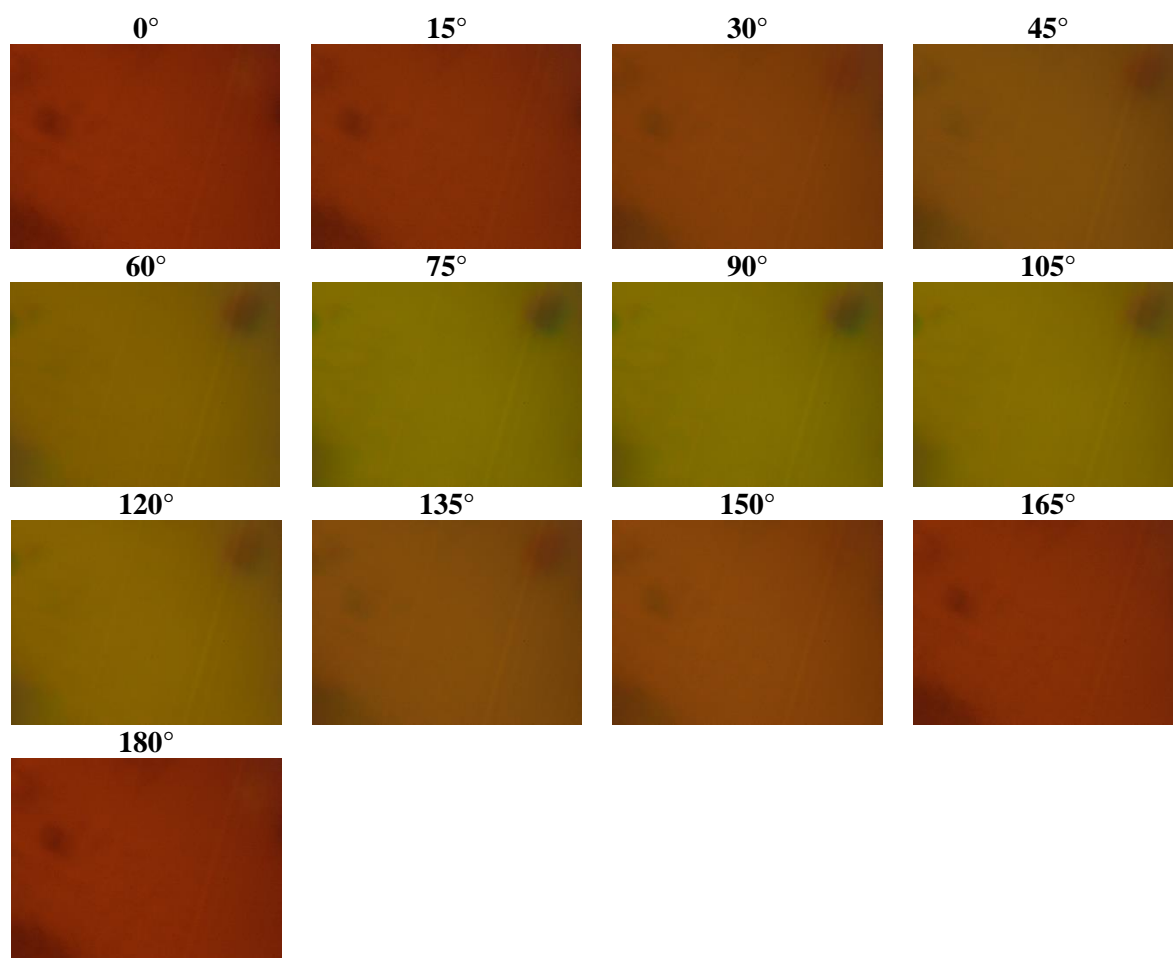


Figure S15. Color change observed in the (-100) crystal face of **1** associated to variation of the plane-polarized light angle.

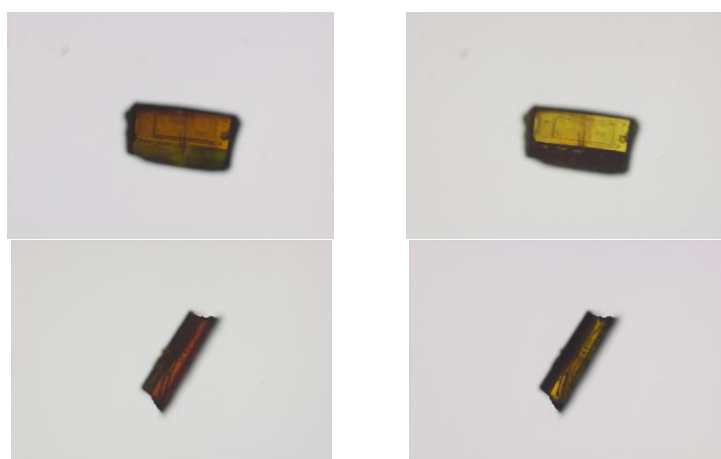


Figure S16. Color change observed in the (001) crystal face (top) and in the (0-11) crystal face (bottom) of **2** associated to variation of the plane-polarized light angle

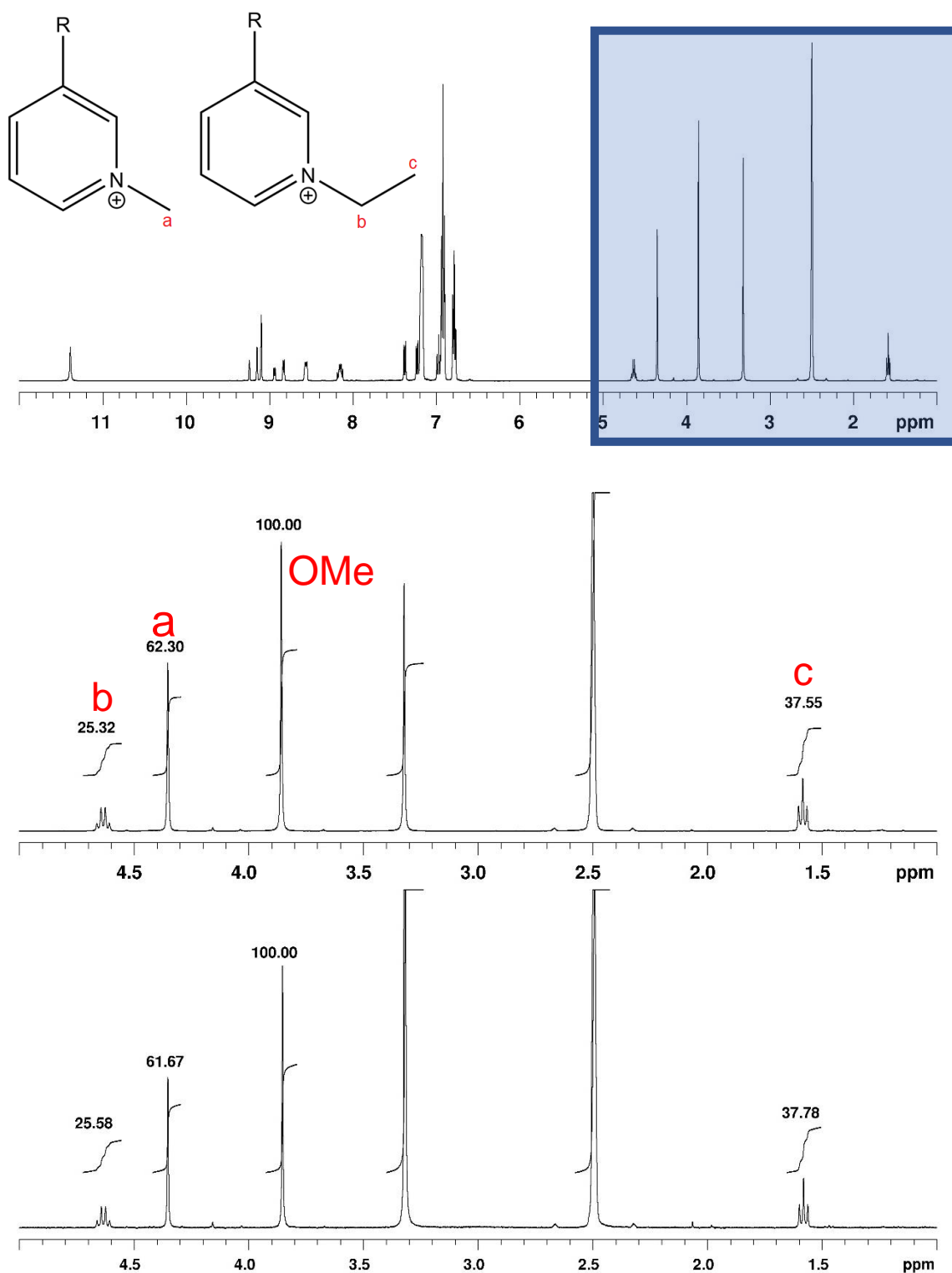


Figure S17. ^1H NMR spectra of **30.6840.32** (top). Zoom of the 0-5 ppm region of the spectrum taken from polycrystalline powder (middle) and from single crystal (bottom).

Annex C

*To: Designing photochromic materials through halogen bond: Bromo-
vs Iodo-substitution.[†]*

[†]Carletta, Andrea, et al. "Halogen-Bond Effects on the Thermo-and Photochromic Behaviour of Anil-Based Molecular Co-crystals." *Chemistry—A European Journal* 23, (2017): 5317-5329.

Supporting information to Chapter 4

List of Figures and Tables

Figure S1. ORTEP diagrams for single component crystal structures

Figure S2. ORTEP diagrams for multicomponent crystal structures

Figure S3. Disorder in **3A**

Table S1. Crystal data and details of measurements for **1**, **2** and **3_{solv}**

Table S2. Crystal data and details of measurements for **3A**, **3B** and **2_{0.73}0.3**

Table S3. Crystal data and details of measurements for **1₂·I2F4**, **2₂·I2F4** and **3₂·I2F4**

Table S4. Selected parameters for halogen bonds

Figure S4. Normalized absorption spectra of single crystal samples

Figure S5. Normalized room temperature emission spectra of single crystal samples

Figure S6. Normalized room temperature excitation spectra of powder samples

Figure S7. Normalized room temperature excitation spectra of single crystal samples

Figure S8. Normalized emission spectra at 77 K of single crystal samples

Figure S9. Normalized excitation spectra at 77 K of powder samples

Figure S10. Normalized excitation spectra at 77 K of single crystal samples

Figure S11. Superposition of normalized excitation spectra of compound **1** (powder sample) at room temperature and at 77 K

Figure S12. Thermochromism in **1**, **2**, **3_{solv}** and respective cocrystals

Figure S13. Absorption spectra of powder samples of **1**, **1₂·I2F4**, and **3_{solv}** before and after irradiation at 365 nm

Figure S14. Absorption and emission spectra of **2** before and after irradiation at 365 nm

Figure S15. Absorption and emission spectra of **2₂·I2F4** before and after irradiation at 365 nm

Figure S16. Normalized excitation spectra of powder samples of **2** (a), **2₂·I2F4** (b) and **3₂·I2F4** (c) collected at 575 nm and 650 nm in the photostationary state.

Figure S17. Absorption spectral changes of **2**: photochemical back reaction and thermal back reaction.

Figure S18. Absorption spectral changes of **2₂·I2F4**: photochemical back reaction and thermal back reaction

Figure S19. Absorption spectral changes of **3₂·I2F4**: photochemical back reaction and thermal back reaction

Figure S20. Powder X-ray diffraction patterns recorded on crushed KBr pellets containing samples of **1** and **2**.

Figure S21. Powder X-ray diffraction patterns recorded on crushed KBr pellets containing samples of **3A**, **3B** and **1₂·I2F4**.

Figure S22. Powder X-ray diffraction patterns recorded on crushed KBr pellets containing samples of **2₂·I2F4** and **3₂·I2F4**.

Figure S23. FTIR spectra and pictures for compounds **1**, **2** and **3A** dispersed in KBr pellets.

Figure S24. FTIR spectra and pictures for compounds **3B**, and co-crystals **1₂·I2F4** and **3₂·I2F4** dispersed in KBr pellets.

Figure 25. PXRD of the as mechanosynthesized powder products.

Table S5. Solid-state NMR acquisition parameters for samples **1**, **2** and **3_{solv}** and their co-crystals

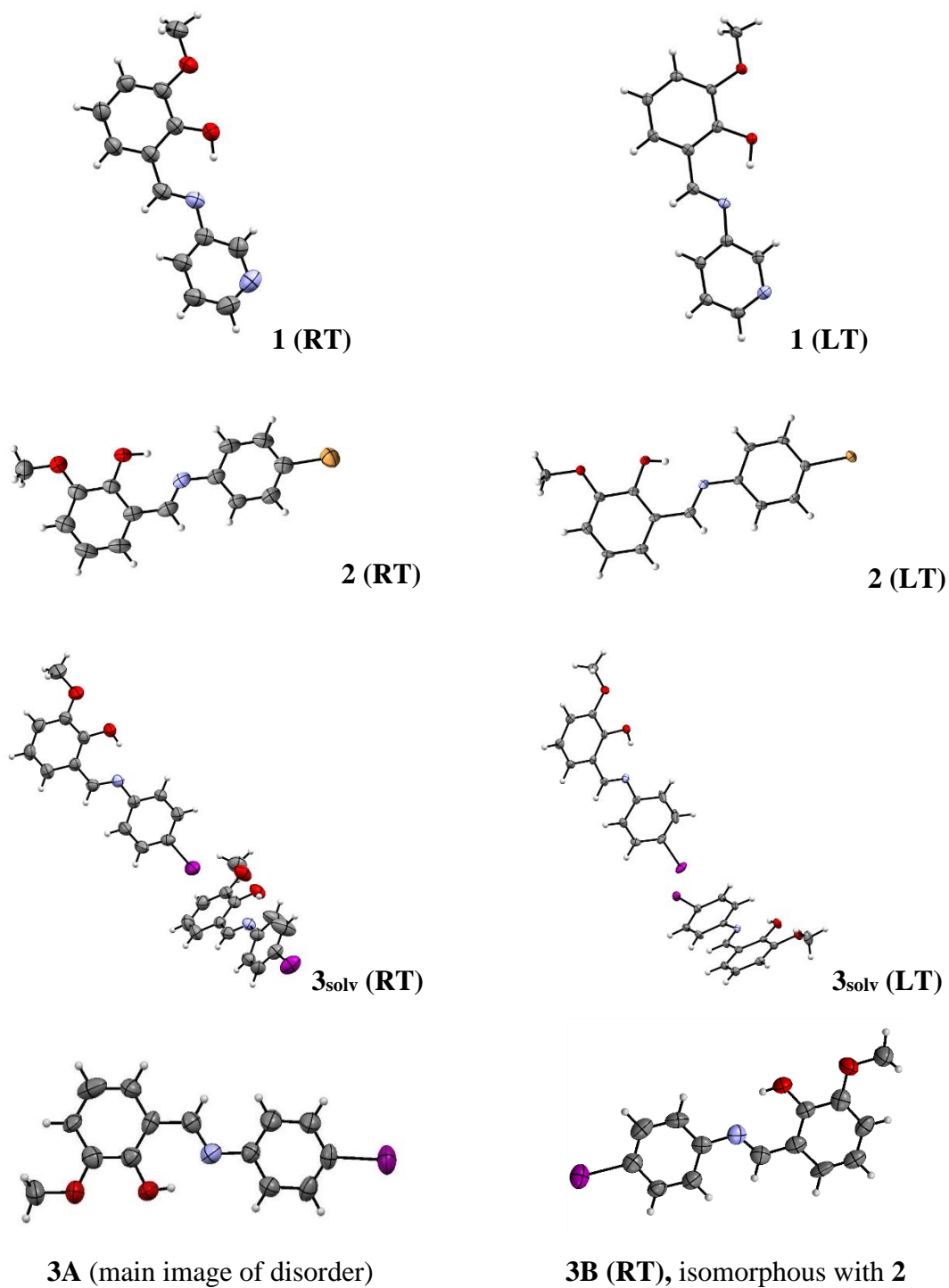


Figure S1. ORTEP diagrams for single component crystal structures.

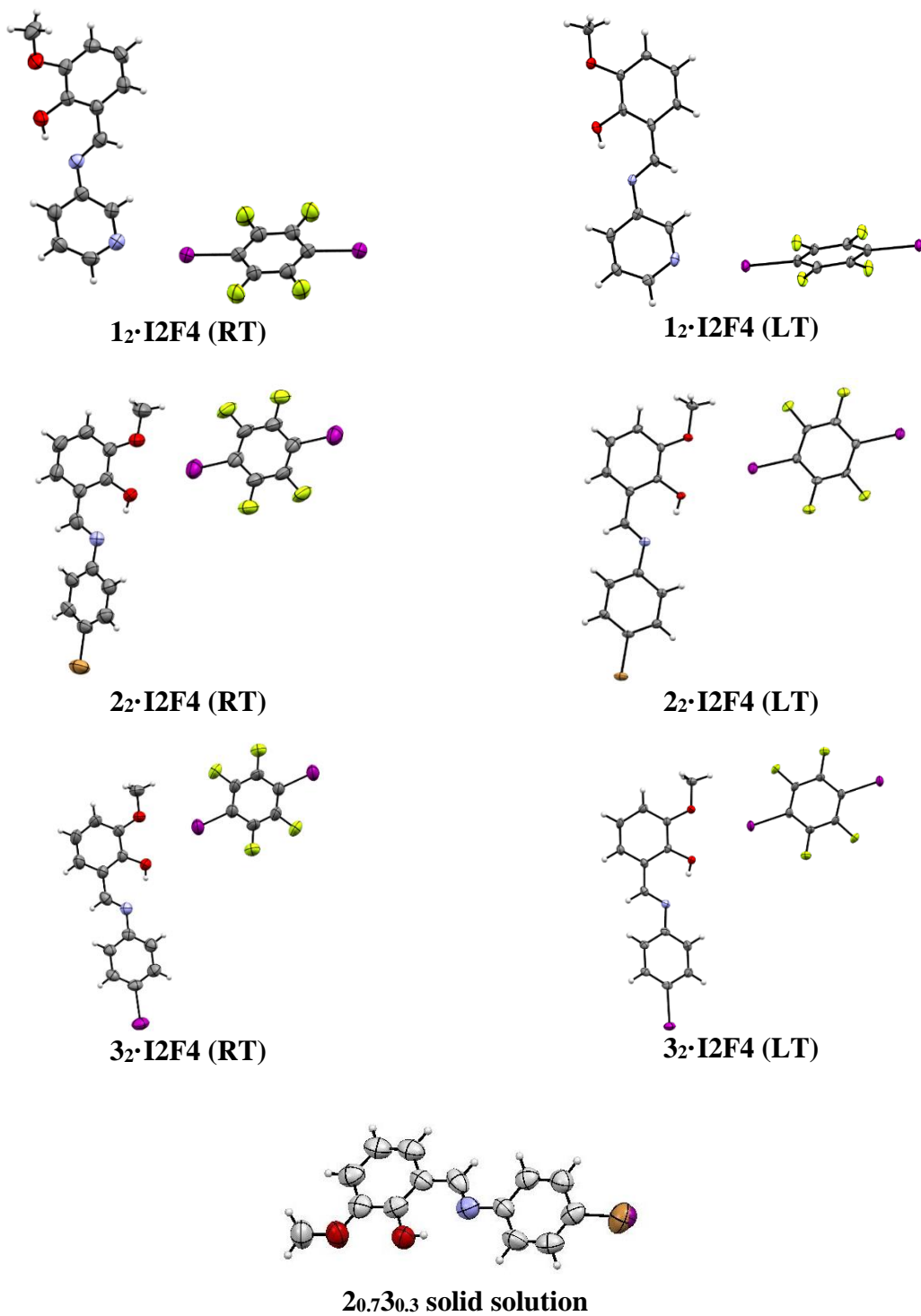


Figure S2. ORTEP diagrams for multicomponent crystal structures.

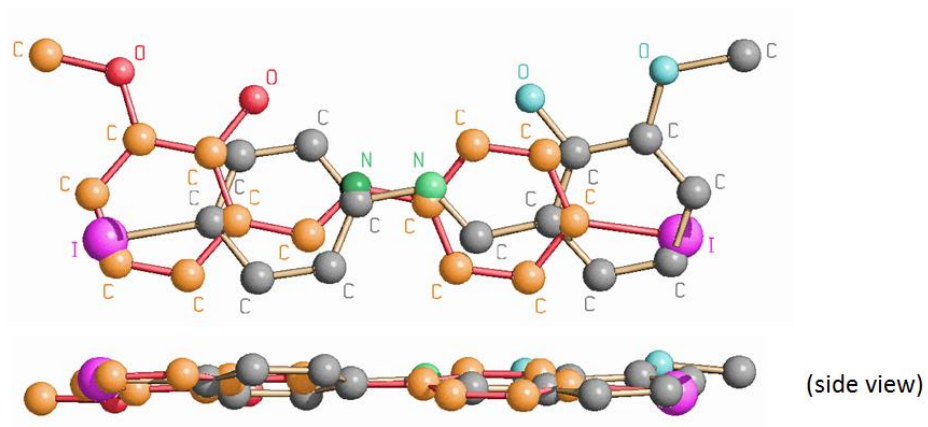


Figure S3. Disorder in **3A**. The occupancy ratio is 70:30 (bonds in red define the main image)

Table S1. Crystallographic data and details of measurements for **1**, **2** and **3_{solv}** at room and low temperature.

	1 (RT)	2 (RT)	3_{solv} (RT)	1 (LT)	2 (LT)	3_{solv} (LT)
Empirical formula	C ₁₃ H ₁₂ N ₂ O ₂	C ₁₄ H ₁₂ Br NO ₂	C ₁₄ H ₁₂ IN O ₂	C ₁₃ H ₁₂ N ₂ O ₂	C ₁₄ H ₁₂ BrN O ₂	C ₁₄ H ₁₂ INO 2
Fw (g/mol)	228.25	306.16	353.15	228.25	306.16	353.15
Crystal system	Orthorhombic	Orthorhombic	Triclinic	Orthorhombic	Orthorhombic	Triclinic
Space group	P2 ₁ 2 ₁ 2 ₁	P2 ₁ 2 ₁ 2 ₁	P $\bar{1}$	P2 ₁ 2 ₁ 2 ₁	P2 ₁ 2 ₁ 2 ₁	P $\bar{1}$
<i>a</i> (Å)	5.6190(4)	4.9234(2)	11.2134 (6)	5.5415(4)	4.8229(3)	11.0853 (4)
<i>b</i> (Å)	9.2825(7)	12.5234 (8)	12.4384 (7)	9.197(3)	12.5498 (11)	12.2243 (6)
<i>c</i> (Å)	21.7490 (14)	20.5990 (11)	12.7482 (8)	21.5766 (15)	20.3554 (10)	12.4559 (5)
<i>α</i> (°)	90	90	109.977 (4)	90	90	110.222 (3)
<i>β</i> (°)	90	90	108.168 (5)	90	90	106.487 (4)
<i>γ</i> (°)	90	90	103.656 (6)	90	90	102.947 (5)
<i>V</i> (Å³)	1134.39 (14)	1270.09 (12)	1466.26 (19)	1099.7 (4)	1232.04 (15)	1418.06 (13)
<i>Z</i>	4	4	4	4	4	4
Crystal size (mm)	0.20 x 0.40 x 0.54	0.35 x 0.38 x 0.58	0.17 x 0.28 x 0.50	0.20 x 0.45 x 0.55	0.55, 0.30, 0.18	0.25 x 0.45 x 0.53
<i>T</i>(K)	293	293	293	108	147	108
N_{ref}	1983	2222	5164	1783	2091	4984
N_{par}	160	168	329	159	168	335
<i>R</i>	0.0321	0.0408	0.0432	0.0347	0.0244	0.0269
GoF	1.03	1.07	1.03	1.08	1.070	1.04
wR²	0.0791	0.0855	0.1038	0.0796	0.0479	0.0695

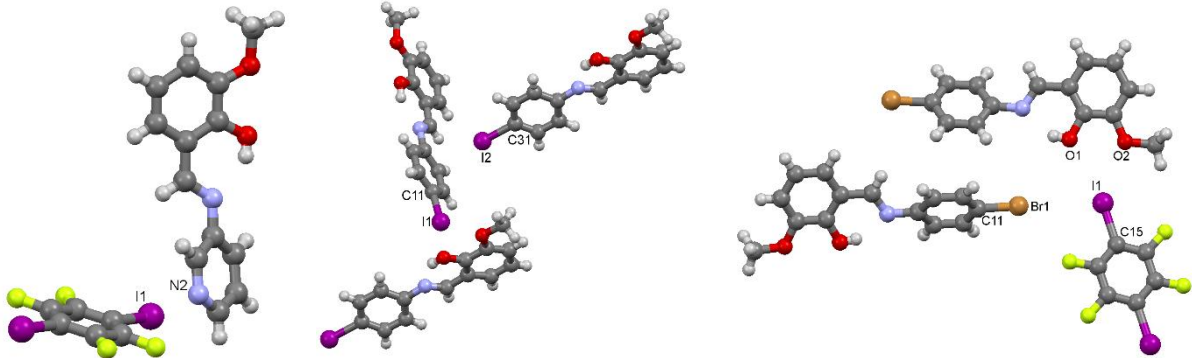
Table S2. Crystallographic data and details of measurements for **3A**, **3B** and **2_{0.7}3_{0.3}**.

	3A	3B	2_{0.7}3_{0.3}
Empirical formula	C ₁₄ H ₁₂ INO ₂	C ₁₄ H ₁₂ INO ₂	C ₁₄ H ₁₂ Br _{0.70} I _{0.30} NO ₂
Fw (g/mol)	353.16	353.15	320.25
Crystal system	Monoclinic	Orthorhombic	Orthorhombic
Space group	P21/c	P212121	P212121
<i>a</i> (Å)	12.3849(11)	4.958(5)	4.9488(5)
<i>b</i> (Å)	16.7076(10)	12.518(5)	12.5366(13)
<i>c</i> (Å)	6.6782(5)	21.479(5)	20.993(2)
<i>α</i> (°)	90	90	90
<i>β</i> (°)	104.83	90	90
<i>γ</i> (°)	90	90	90
<i>V</i> (Å³)	1335.78(17)	1333.1(15)	1302.5(2)
<i>Z</i>	4	4	4
Crystal size (mm)	0.05 x 0.04 x 0.03	0.1 x 0.05 x 0.04	0.05 x 0.04 x 0.03
<i>T</i> (K)	293	293	293
Nref	2783	2647	2968
Npar	194	166	175
<i>R</i>	0.0559	0.0605	0.0725
GoF	0.979	1.130	1.016
wR²	0.1784	0.1702	0.2225

Table S3. Crystallographic data and details of measurements for 1₂·I₂F₄, 2₂·I₂F₄ and 3₂·I₂F₄ at room and low temperature.

	1₂·I₂F₄ (RT)	2₂·I₂F₄ (RT)	3₂·I₂F₄ (RT)	1₂·I₂F₄ (LT)	2₂·I₂F₄ (LT)	3₂·I₂F₄ (LT)
Empirical formula	C ₁₃ H ₁₂ N ₂ O ₂ , 0.5 (C ₆ F ₄ I ₂)	C ₁₄ H ₁₂ Br NO ₂ , 0.5 (C ₆ F ₄ I ₂)	C ₁₄ H ₁₂ IN O ₂ , 0.5 (C ₆ F ₄ I ₂)	C ₁₃ H ₁₂ N ₂ O ₂ , 0.5 (C ₆ F ₄ I ₂)	C ₁₄ H ₁₂ Br NO ₂ , 0.5 (C ₆ F ₄ I ₂)	C ₁₄ H ₁₂ INO ₂ , 0.5 (C ₆ F ₄ I ₂)
Fw (g/mol)	429.18	507.09	554.08	429.18	507.09	554.08
Crystal system	Monoclinic	Monoclinic	Monoclinic	Monoclinic	Monoclinic	Monoclinic
Space group	P2 ₁ /n	P2 ₁ /n	P2 ₁ /n	P2 ₁ /n	P2 ₁ /n	P2 ₁ /n
a (Å)	4.6502(3)	7.1058(5)	7.5577 (4)	4.6036 (3)	7.0795 (3)	7.6958 (3)
b (Å)	28.0826(19)	9.4229(7)	9.2626 (4)	27.982(2)	9.3289(4)	9.0189(3)
c (Å)	12.1429(8)	26.348(2)	25.9451 (17)	12.0308 (6)	25.9574 (12)	25.5175 (11)
α (°)	90	90	90	90	90	90
β (°)	94.695(6)	93.649(8)	96.577 (5)	96.165(5)	93.004(4)	98.428(4)
γ (°)	90	90	90	90	90	90
V (Å³)	1580.42(18)	1760.6(2)	1804.31 (17)	1540.82 (17)	1711.97 (13)	1751.98 (12)
Z	4	4	4	4	4	4
Crystal size (mm)	0.10 x 0.20 x 0.35	0.15 x 0.29 x 0.56	0.17 x 0.50 x 0.60	0.05 x 0.25 x 0.60	0.20 x 0.34 x 0.60	0.28 x 0.37 x 0.60
T(K)	293	293	293	115	105	150
Nref	2795	3102	3159	2724	3014	3001
Npar	210	223	222	213	222	222
R	0.0409	0.0411	0.0374	0.0574	0.0281	0.0211
GoF	1.11	1.08	1.09	1.12	1.00	1.30
wR²	0.0805	0.0978	0.0869	0.1451	0.0616	0.0527

Table S4. Selected parameters for halogen bonds.

							
1₂·I₂F₄		3_{solv}			2₂·I₂F₄		
halogen...halogen interaction (type II)					Halogen bond		
Contact type	X...X distance (Å)	θ1 (deg) (C11-X...I)	θ2 (deg) (X...I-C15)	Contact type	A...I distance (Å) (A = O, N)	A...I-C angle (deg) (A = O, N)	
1₂·I₂F₄	/	/	/	/	I1...N2	2.878(4)	168.9
1₂·I₂F₄ (LT)	/	/	/	/	I1...N2	2.855(6)	168.5
2₂·I₂F₄	I1...Br1	3.9239 (9)	173.4	106.5	I1...O1	3.447(4)	169.1
2₂·I₂F₄ (LT)	I1...Br1	3.8775 (6)	173.8	107.5	I1...O2	3.263(4)	141.3
3₂·I₂F₄	I2...I1	3.9568 (7)	173.5	108.4	I2...O1	3.442(2)	169.0
3₂·I₂F₄ (LT)	I2...I1	3.8810 (5)	172.3	107.8	I2...O2	3.208(2)	141.6
					I2...O1	3.501(3)	169.3
					I2...O2	3.243(3)	145.1
					I2...O1	3.488(2)	168.8
					I2...O2	3.198(2)	145.5
C-I...π halogen bond							
	Contact type	I...Cg distance (Å)	C...Cg distance (Å)	C-I...Cg angle (deg)			
3_{solv}	C31-I2...Cg1	3.56	5.66	178.7			
	C11-I1...Cg2	3.57	5.63	166.5			
3_{solv} (LT)	C31-I2...Cg1	3.46	5.56	177.7			
	C11-I1...Cg2	3.46	5.52	160.3			
Cg1 = calculated at C8-C13 six-membered ring (molecule A)							
Cg2 = calculated at C21-C27 bond (molecule A)							

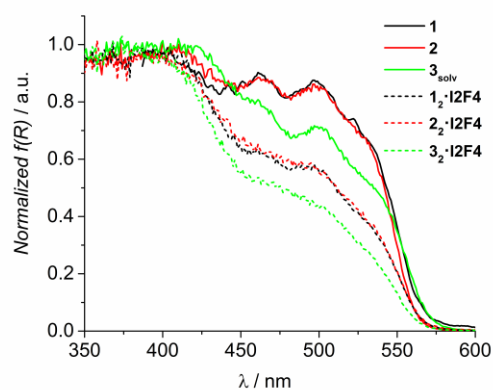


Figure S4. Normalized absorption spectra of single crystal samples of compounds **1**, **2**, **3_{solv}** and respective co-crystals.

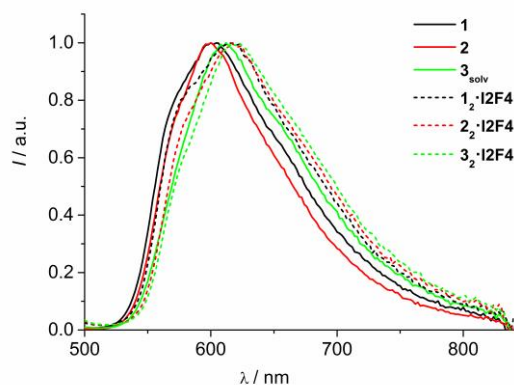


Figure S5. Normalized room temperature emission spectra of single crystal samples of compounds **1**, **2**, **3_{solv}** and respective co-crystals. $\lambda_{exc} = 480$ nm.

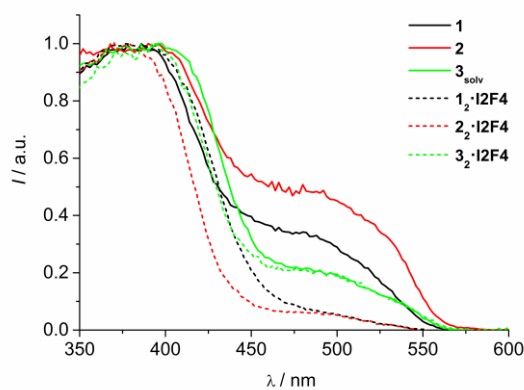


Figure S6. Normalized room temperature excitation spectra of powder samples of compounds **1**, **2**, **3_{solv}** and respective co-crystals. $\lambda_{em} = 650$ nm.

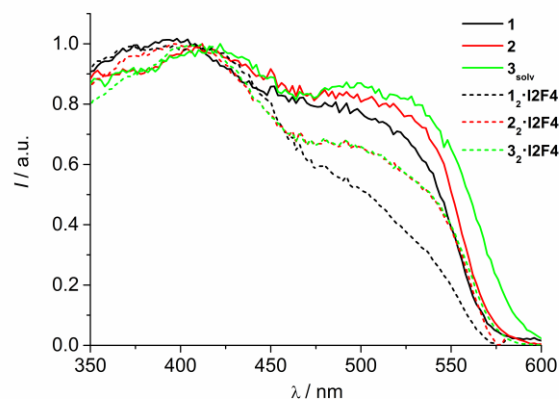


Figure S7. Normalized room temperature excitation spectra of single crystal samples of compounds **1**, **2**, **3_{solv}** and respective co-crystals. $\lambda_{em} = 660$ nm.

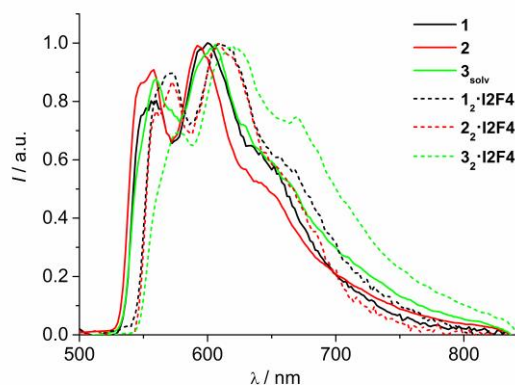


Figure S8. Normalized emission spectra at 77 K of single crystal samples of compounds **1**, **2**, **3_{solv}** and respective co-crystals. $\lambda_{exc} = 450$ nm.

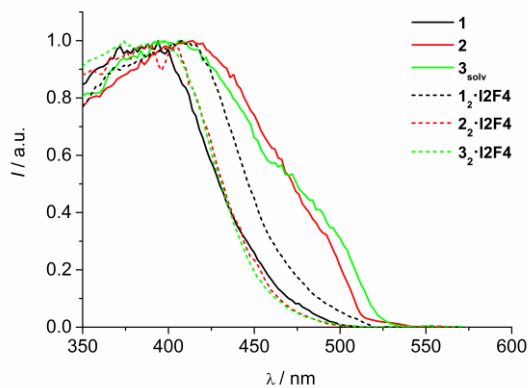


Figure S9. Normalized excitation spectra at 77 K of powder samples of compounds **1**, **2**, **3_{solv}** and respective co-crystals. $\lambda_{em} = 600/620$ nm.

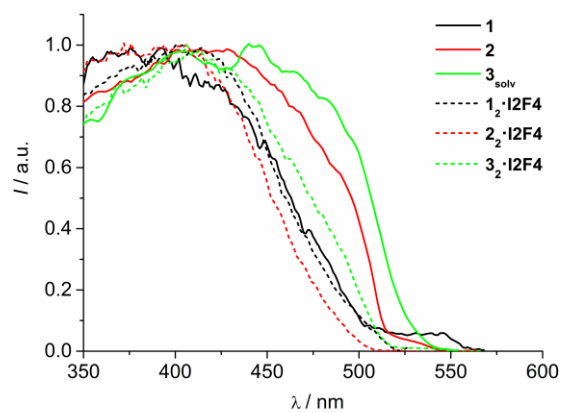


Figure S10. Normalized excitation spectra at 77 K of single crystal samples of compounds **1**, **2**, **3_{solv}** and respective co-crystals. $\lambda_{em} = 600$ nm.

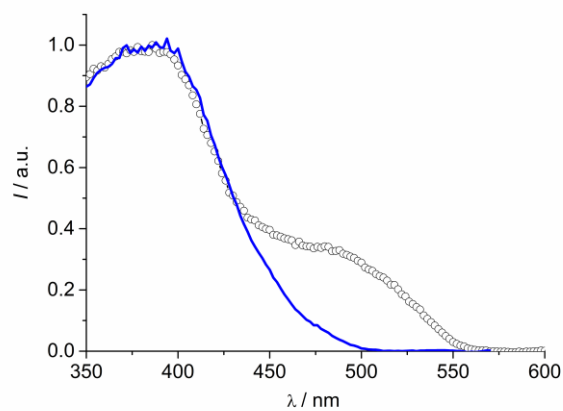


Figure S11. Normalized excitation spectra of compound **1** (powder sample) at room temperature (open dots, $\lambda_{em} = 650$ nm) and at 77 K (blue line, $\lambda_{em} = 600$ nm).

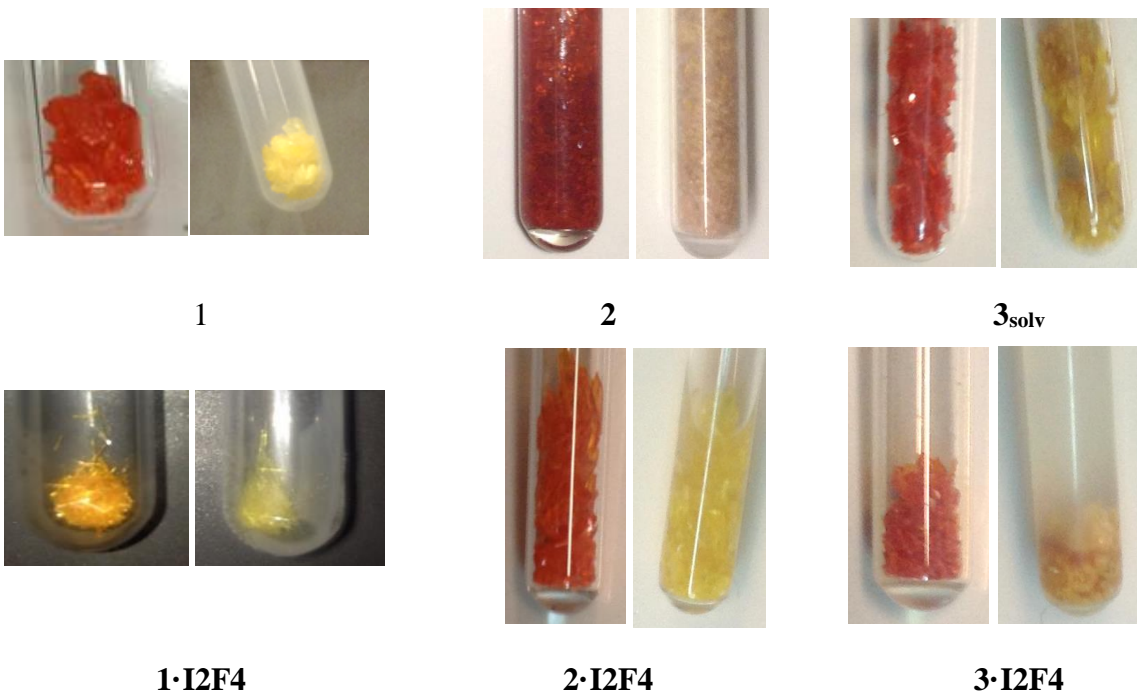


Figure S12. Thermochromism in **1**, **2**, **3_{solv}** and respective co-crystals before (left) and after (right) immersion in liquid nitrogen (77 K).

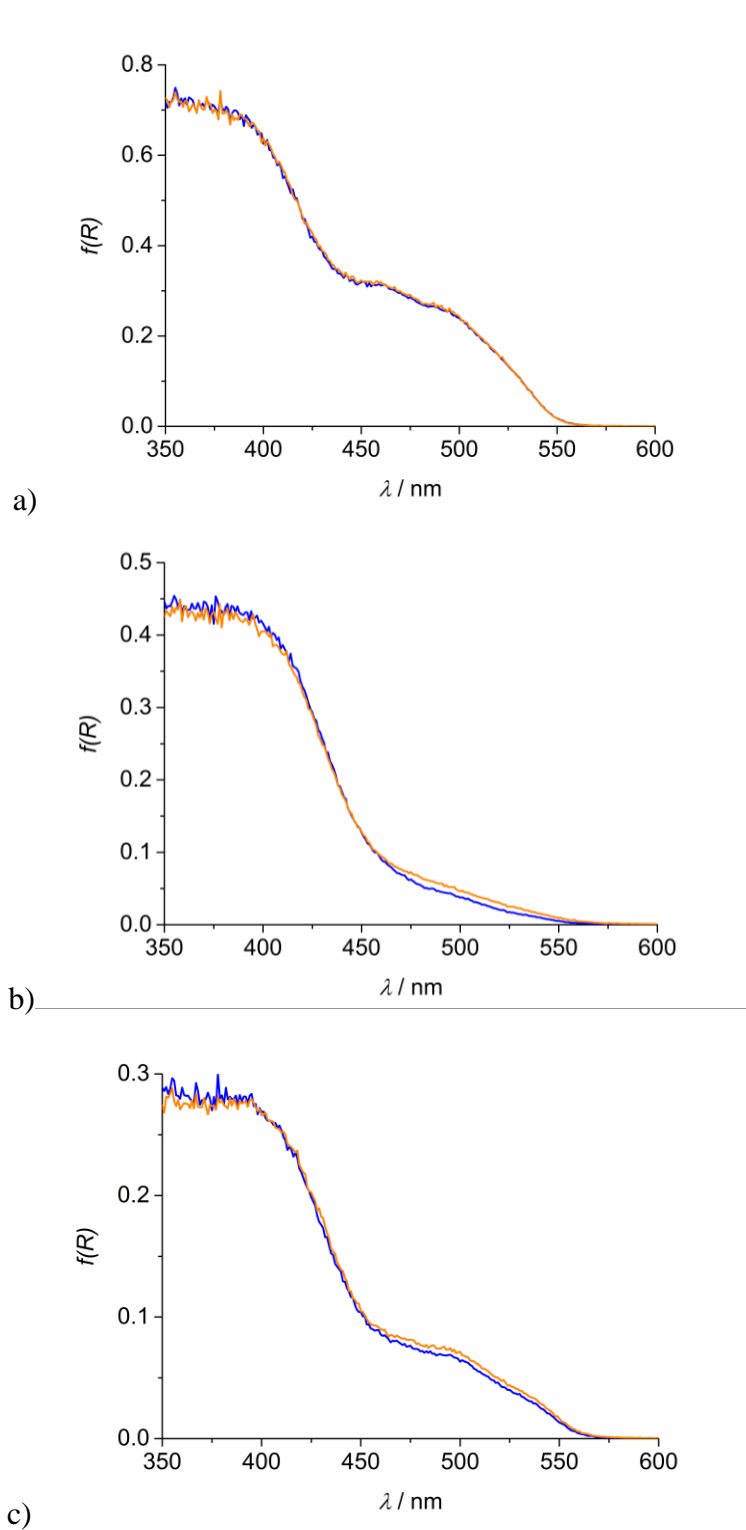


Figure S13. Absorption spectra of powder samples of compounds **1** (a), **12-I2F4** (b), and **3_{solv}** (c) before (blue) and after (orange) HP irradiation (see Experimental Section for details) at 365 nm for 20 min.

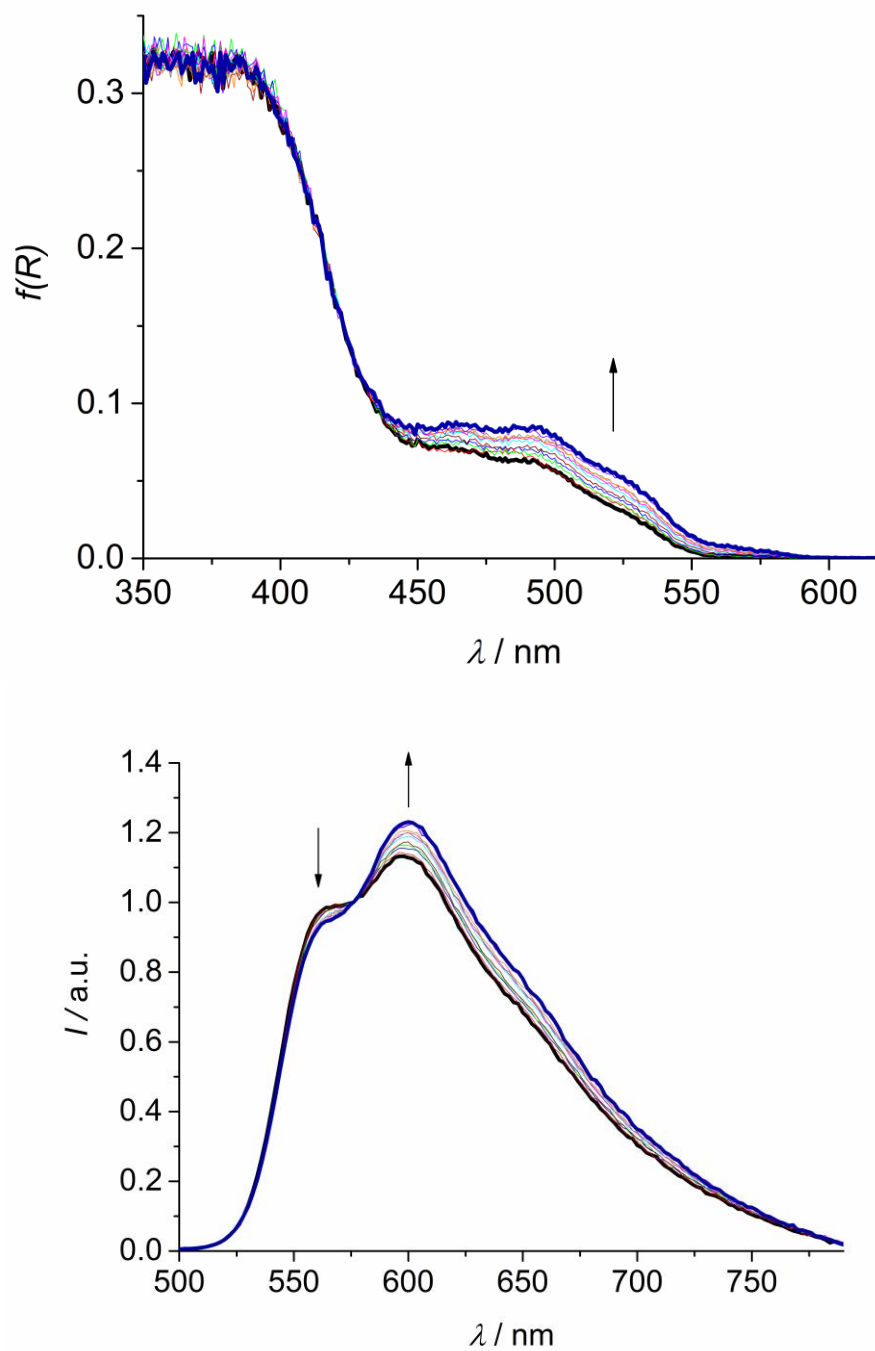


Figure S14. Absorption (a) and emission (b) spectra of **2** before (black thick) and after (blue thick) irradiation at 365 nm for 40 min (20 min LP and 20 min HP, see Experimental Section for details). Thin lines represent spectra at intermediate times. In (b) the spectra are arbitrarily normalized at 576 nm; $\lambda_{\text{exc}} = 400$ nm.

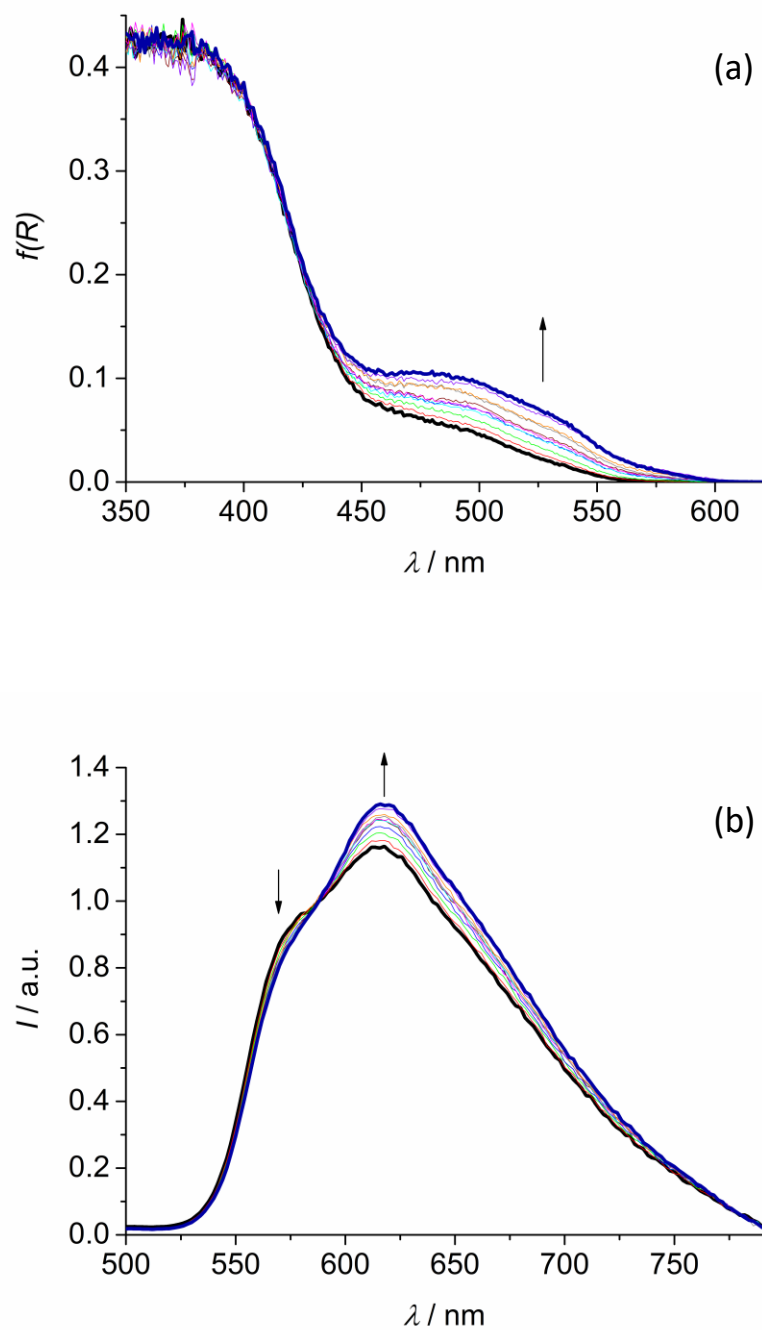


Figure S15. Absorption (a) and emission (b) spectra of **22·I2F4** before (black thick) and after (blue thick) irradiation at 365 nm for 40 min (20 min LP and 20 min HP, see Experimental Section for details). Thin lines represent spectra at intermediate times. In (b) the spectra are arbitrarily normalized at 588 nm; $\lambda_{\text{exc}} = 400$ nm.

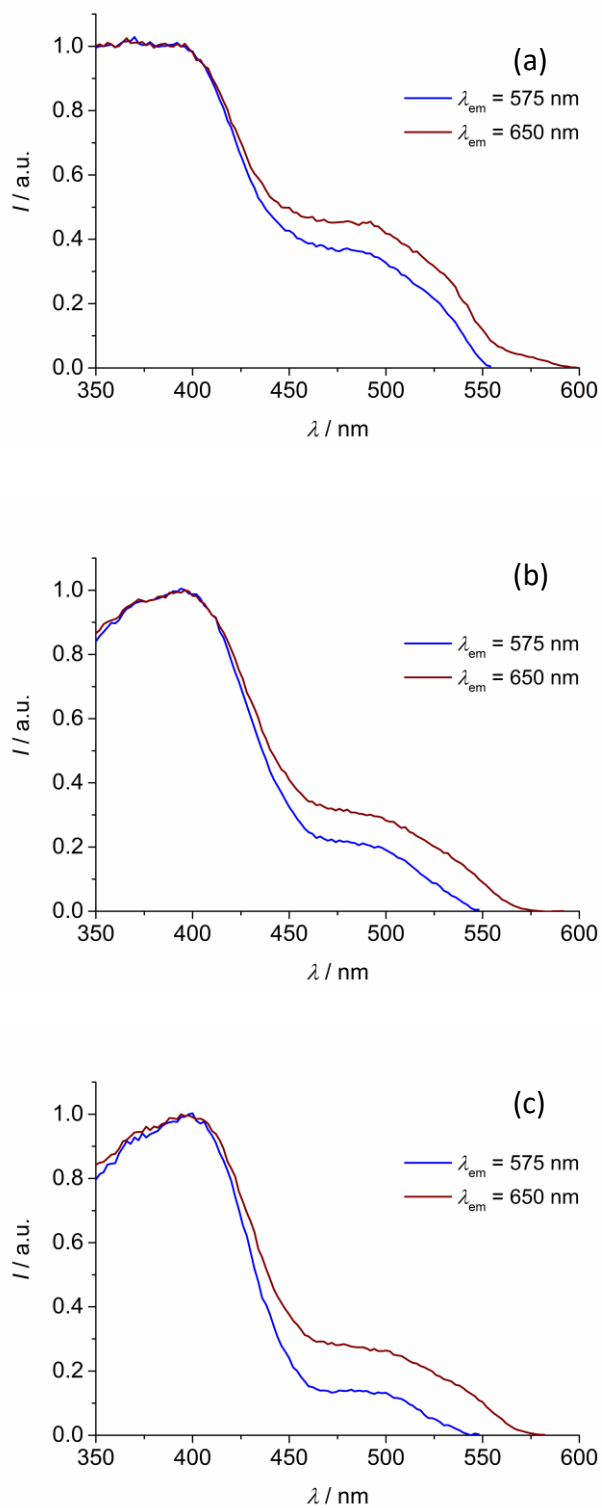


Figure S16. Normalized excitation spectra of powder samples of **2** (a), **2·I2F4** (b) and **3·I2F4** (c) collected at 575 nm and 650 nm in the photostationary state.

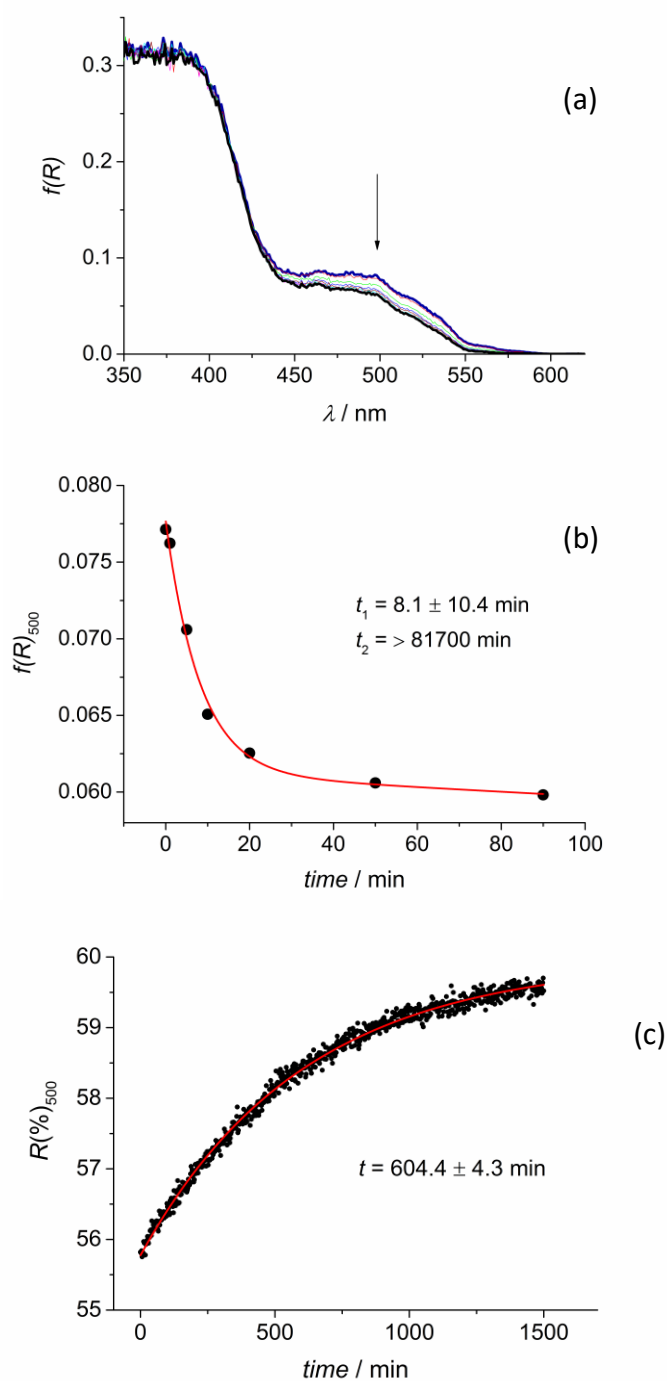


Figure S17. (a) Absorption spectral changes of **2** starting from the photostationary state and following irradiation at 465 nm for 90 min. (b) Data points at 500 nm from graph (a) and bi-exponential fitting (red). (c) Variation of the reflectance of **2** at 500 nm as a function of time, starting from the photostationary state and following the thermal back reaction; in red the mono-exponential fitting.

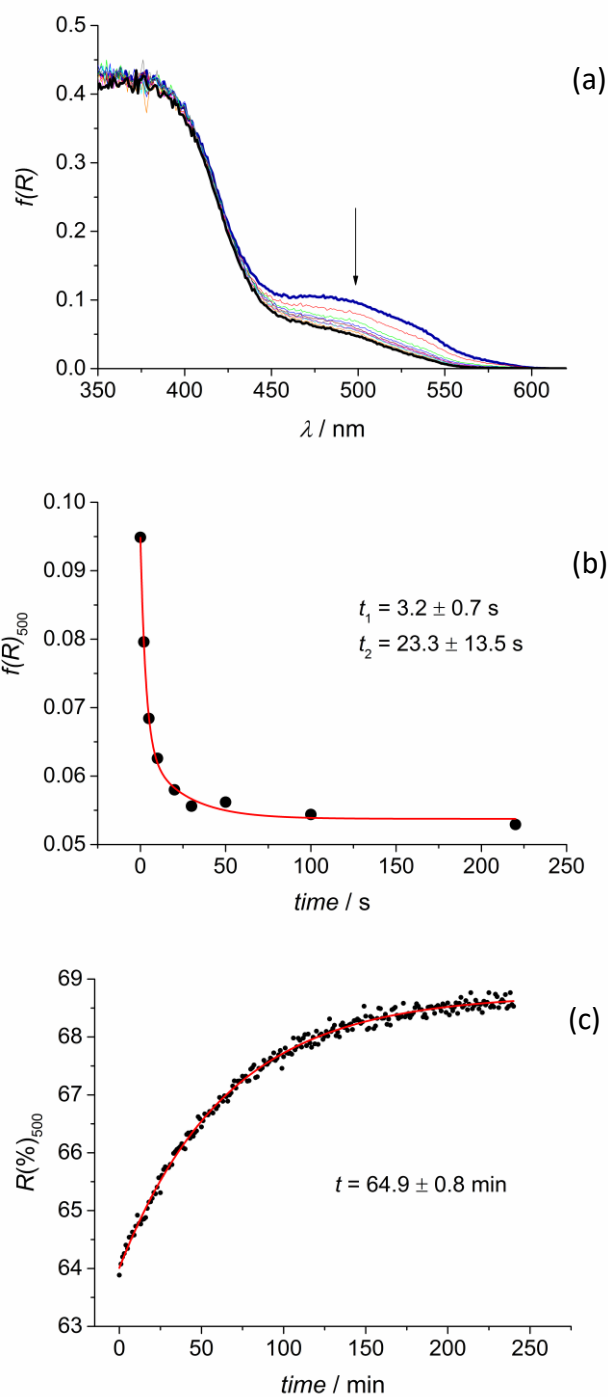


Figure S18. (a) Absorption spectral changes of 2_2 -I2F4 starting from the photostationary state and following irradiation at 465 nm for 220 s. (b) Data points at 500 nm from graph (a) and bi-exponential fitting (red). (c) Variation of the reflectance of 2_2 -I2F4 at 500 nm as a function of time, starting from the photostationary state and following the thermal back reaction; in red the mono-exponential fitting.

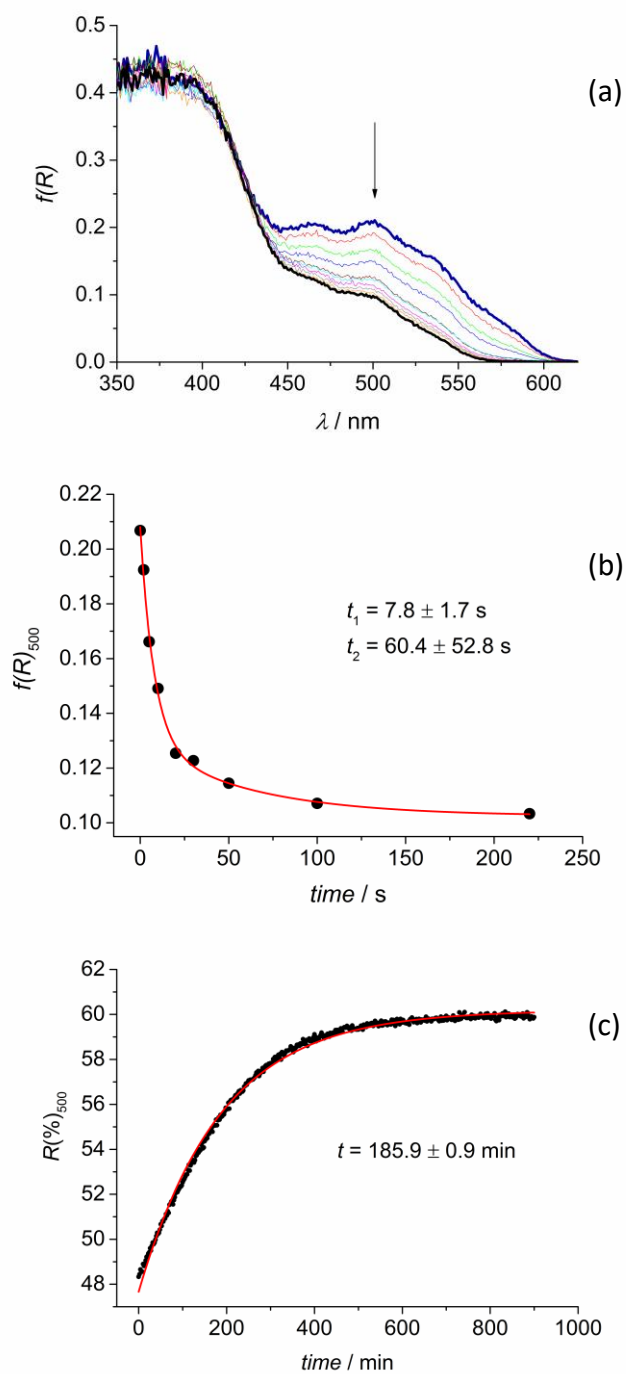


Figure S19. (a) Absorption spectral changes of **3₂·I₂F₄** starting from the photostationary state and following irradiation at 465 nm for 220 s. (b) Data points at 500 nm from graph (a) and bi-exponential fitting (red). (c) Variation of the reflectance of **3₂·I₂F₄** at 500 nm as a function of time, starting from the photostationary state and following the thermal back reaction; in red the mono-exponential fitting.

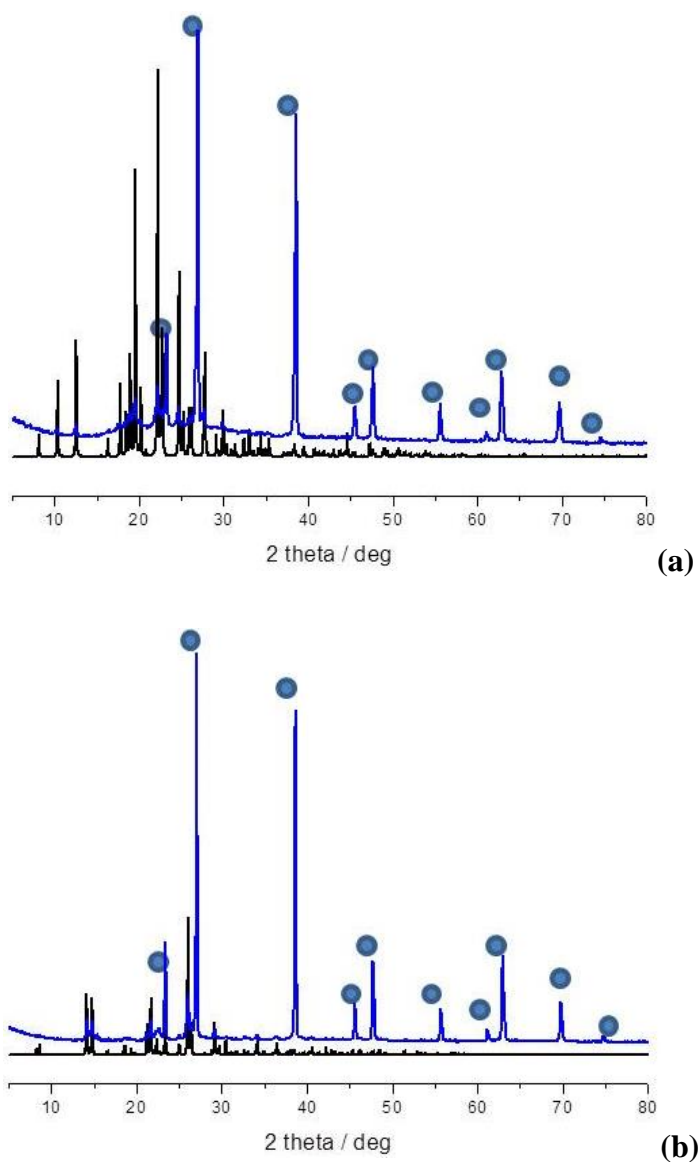


Figure S20. Powder X-ray diffraction patterns recorded on crushed KBr pellets containing samples of **1** (a) and **2** (b). Experimental (blue line) and simulated (black line) X-ray powder diffraction patterns. Blue circles indicate the KBr phase.

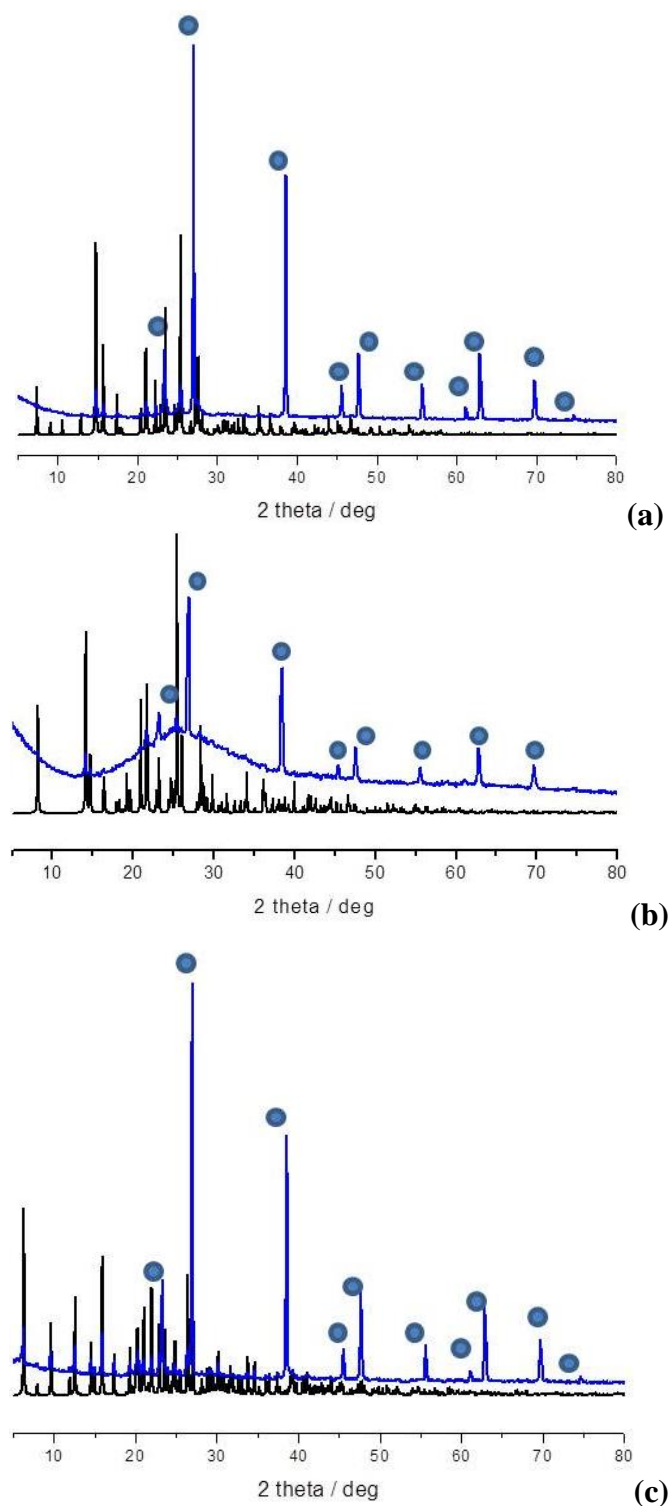


Figure S21. Powder X-ray diffraction patterns recorded on crushed KBr pellets containing samples of **3a** (a), **3** (b) and **1₂·I2F4** (c). Experimental (blue line) and simulated (black line) X-ray powder diffraction patterns. Blue circles indicate the KBr phase.

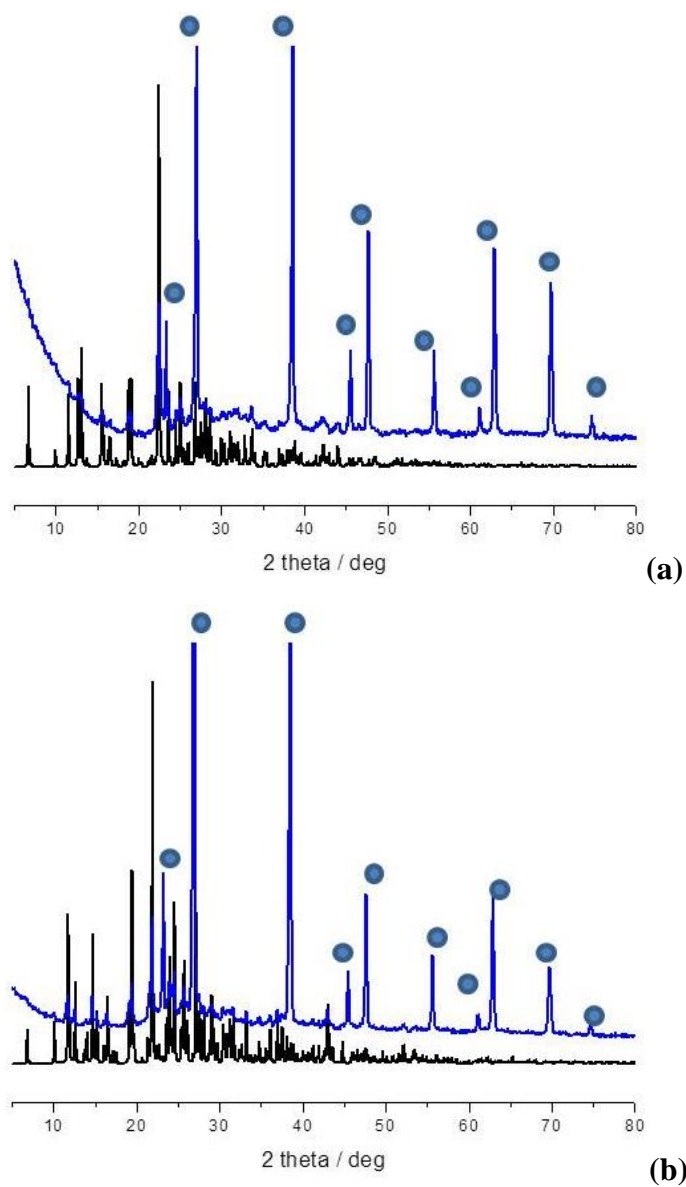


Figure S22. Powder X-ray diffraction patterns recorded on crushed KBr pellets containing samples of $2z \cdot \text{I}_2\text{F}_4$ (a) and $3z \cdot \text{I}_2\text{F}_4$ (b). Experimental (blue line) and simulated (black line) X-ray powder diffraction patterns. Blue circles indicate the KBr phase.

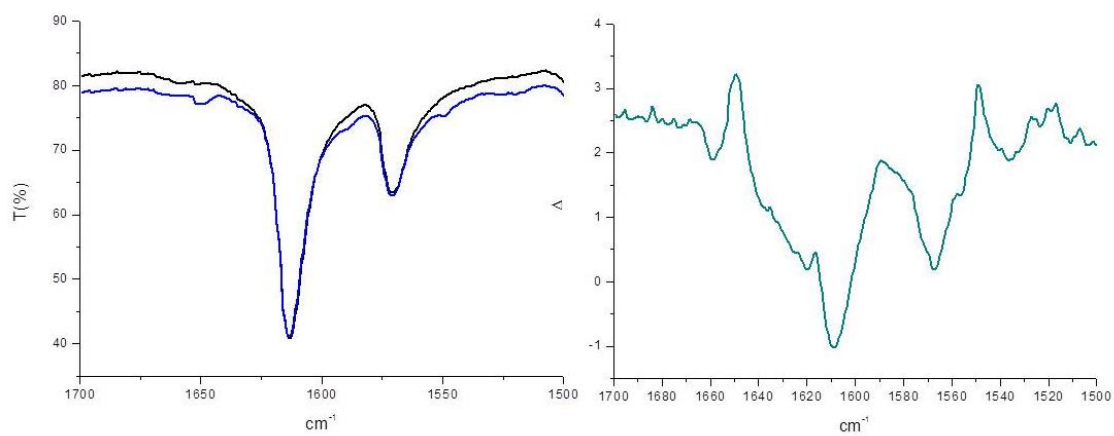
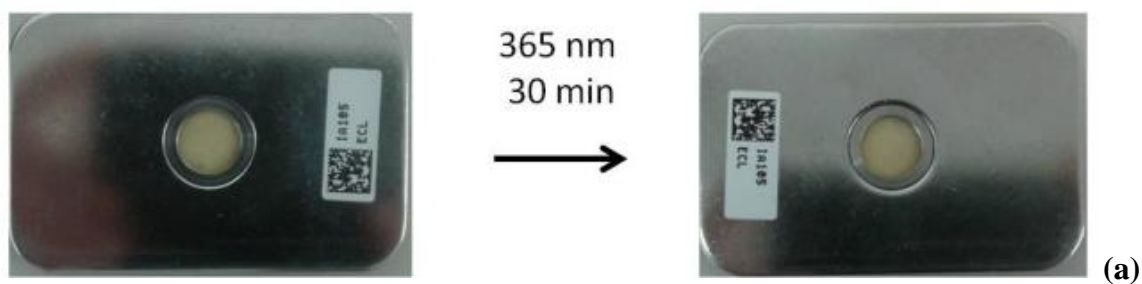
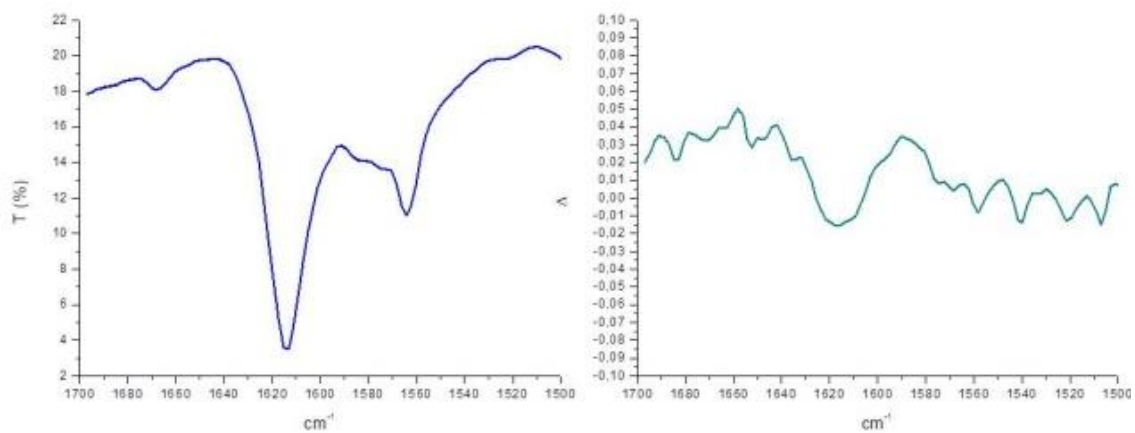


Figure S23(a/b). FTIR spectra and pictures for compounds **1** (a) and **2** (b)

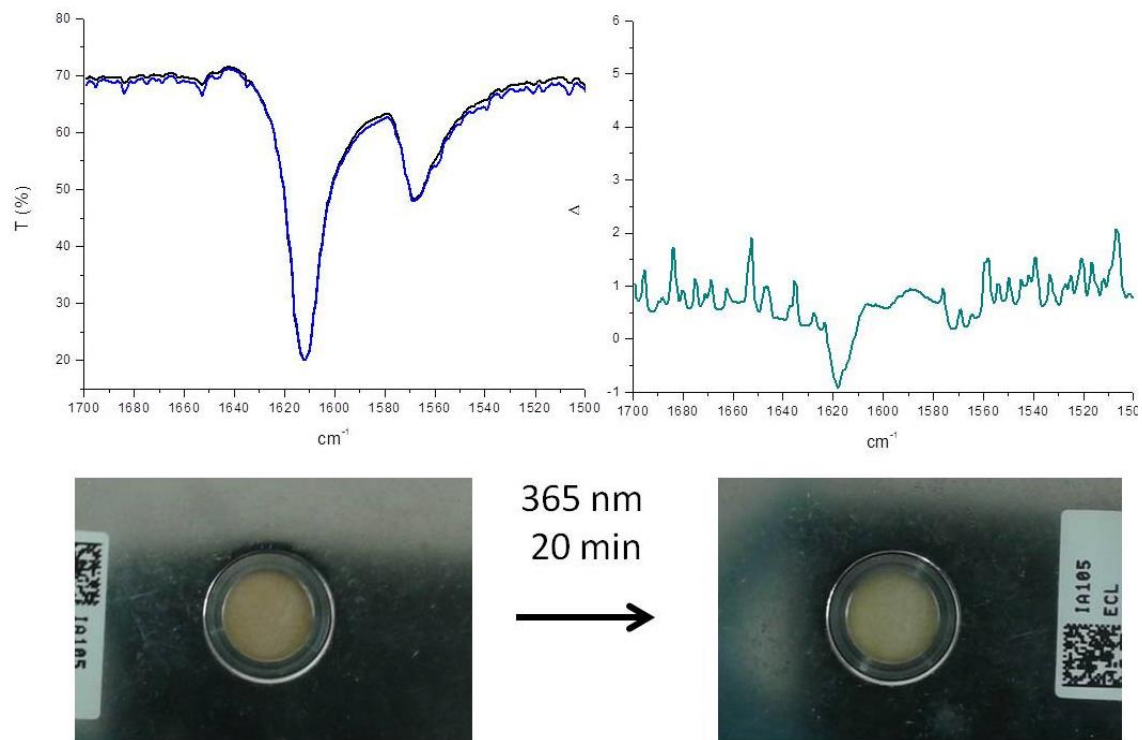


Figure S24c. FTIR spectra and pictures for **3A** dispersed in KBr pellets.

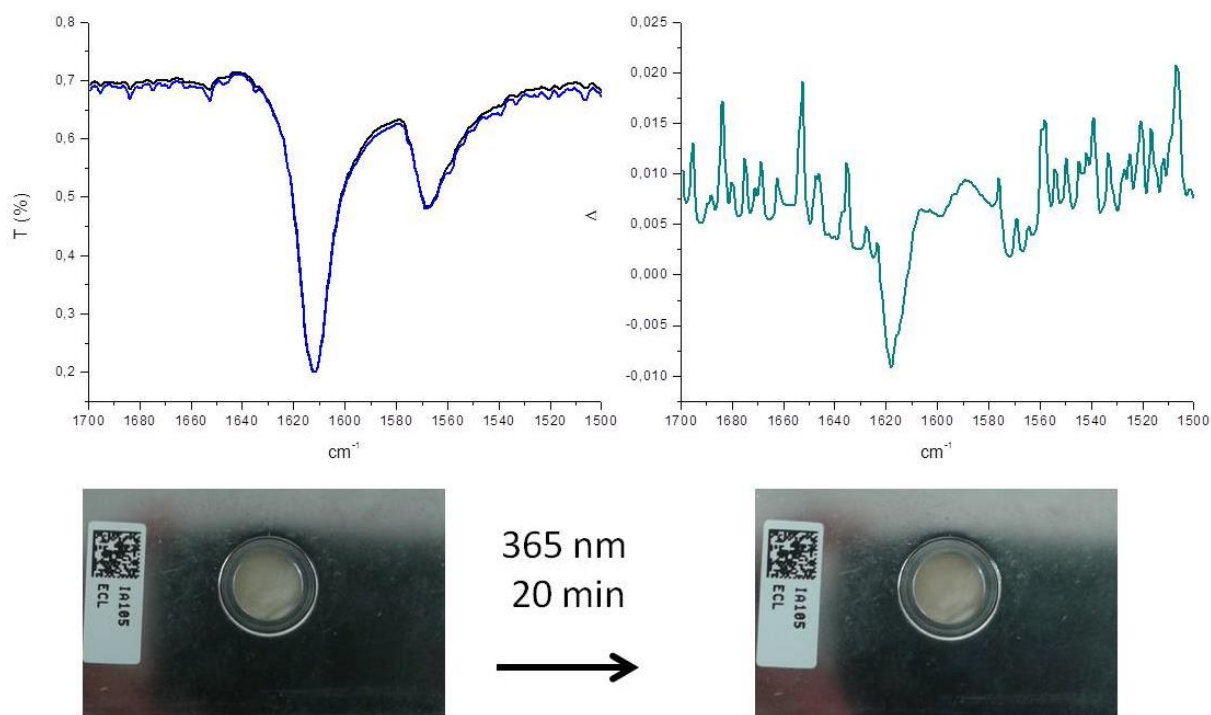


Figure S25a. FTIR spectra and pictures for compound **3B**

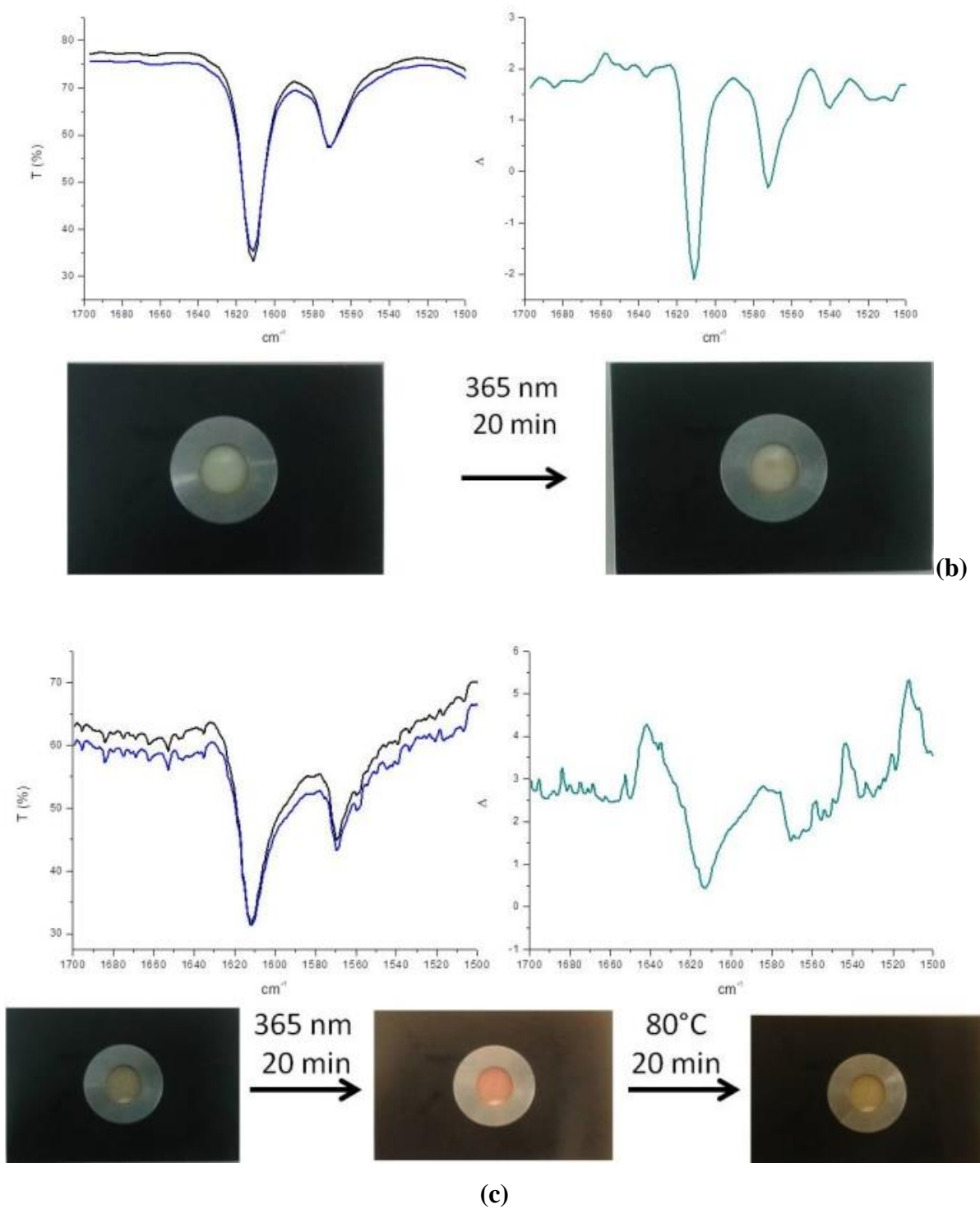
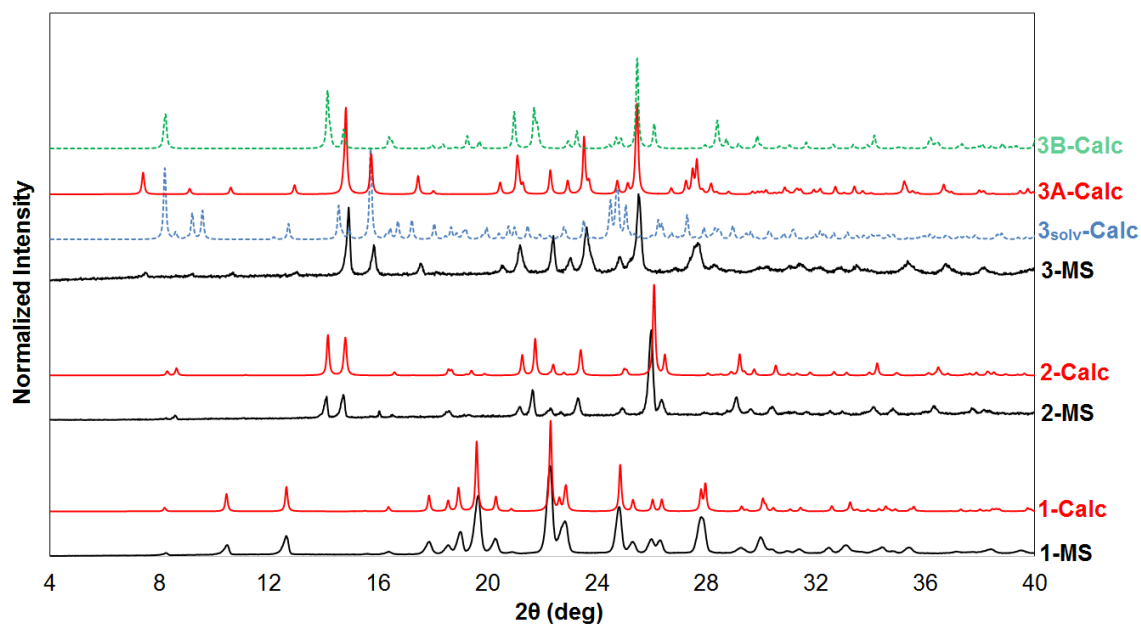


Figure S26(b/c). FTIR spectra and pictures for compounds **1₂-I₂F₄** (b) and **3₂-I₂F₄** (c) dispersed in KBr pellets.



MS = mechanosynthesis Calc = calculated

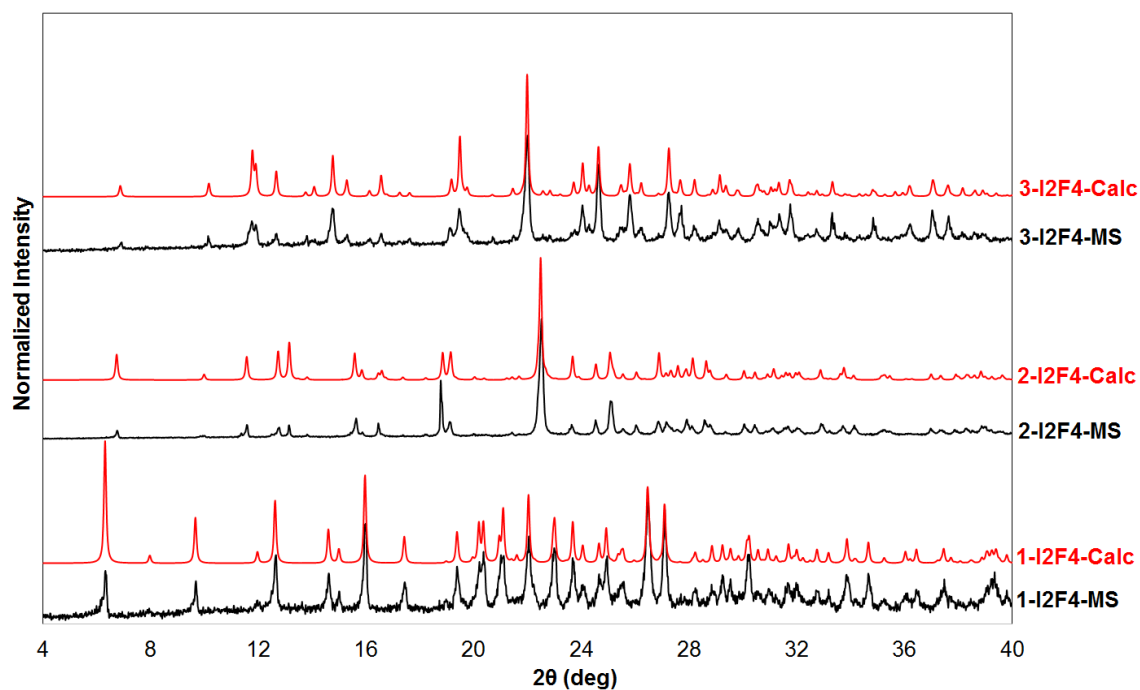


Figure S27. PXRD of the as mechanosynthesized powder products. Syntheses of the starting compounds (top) and of their cocrystals (bottom).

Table S5. Solid-state NMR acquisition parameters for samples **1**, **2** and **3_{solv}** and their co-crystals.

sample	¹³ C		¹⁵ N		Relaxation delay (s)
	Resolution (Hz)	scans	Resolution (Hz)	scans	
1	30	274	30	8000	11.4
1 ₂ -I2F4	30	1700	30	11000	14.8
2	30	2500	26	10500	6.0
2 ₂ -I2F4	30	1000	26	34000	7.3
3	30	1600	31	27500	9.1
3 ₂ -I2F4	30	8000	26	14000	5.8

Annex D

To: Playing with structural isomers and stoichiometry.[†]

[†]Carletta, Andrea, et al. "Playing with Isomerism: Cocrystallization of Isomeric *N*-Salicylideneaminopyridines with Perfluorinated Compounds as Halogen Bond Donors and Its Impact on Photochromism." *Crystal Growth & Design* 18 (2018): 6833-6842

Supporting information to Chapter 5

List of Figures and Tables

Figure S1. PXRD patterns of **ovan4amp** cocrystals mechanosyntheses

Figure S2. PXRD patterns of **ovan3amp** cocrystals mechanosyntheses.

Table S1. Crystallographic parameters of **ovan3amp** and **ovan4amp** co-crystals.

Figure S3. Diffuse reflectance spectra of **(ovan3amp)₂·ofib**.

Figure S4. Diffuse reflectance spectra of **ovan3amp·12tfib**

Figure S5. Superimposition of **(ovan3amp)₂·14tfib** and **(ovan3amp)₂·ofib**

Table S2. Results of TG analysis.

Table S3. Results of TG analysis.

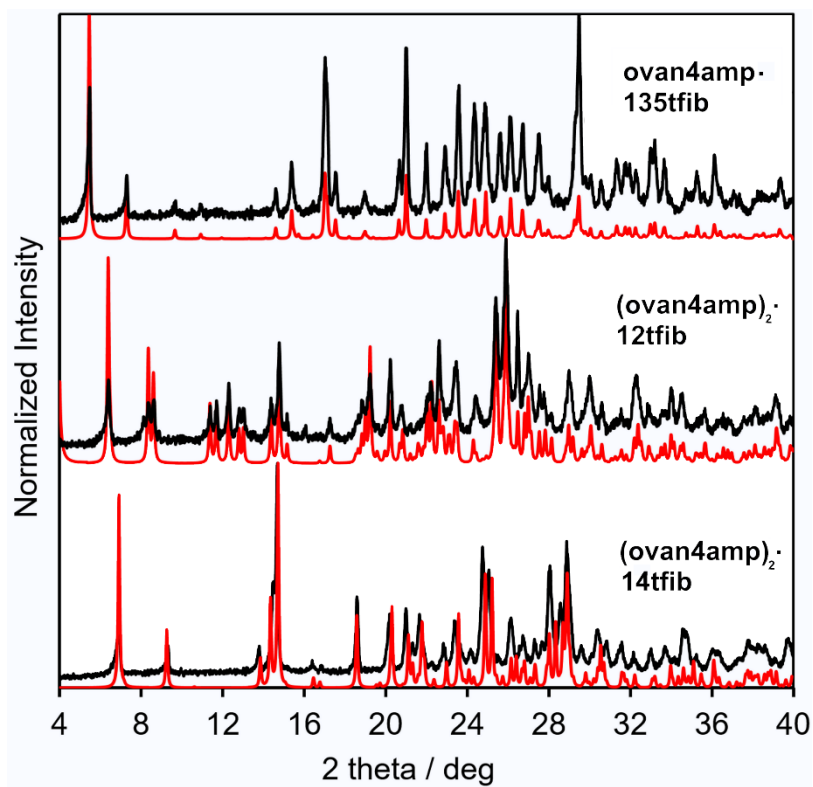


Figure S1. PXRD patterns of **ovan4amp** cocrystals mechanosyntheses (red = simulated pattern; black = experimental pattern)

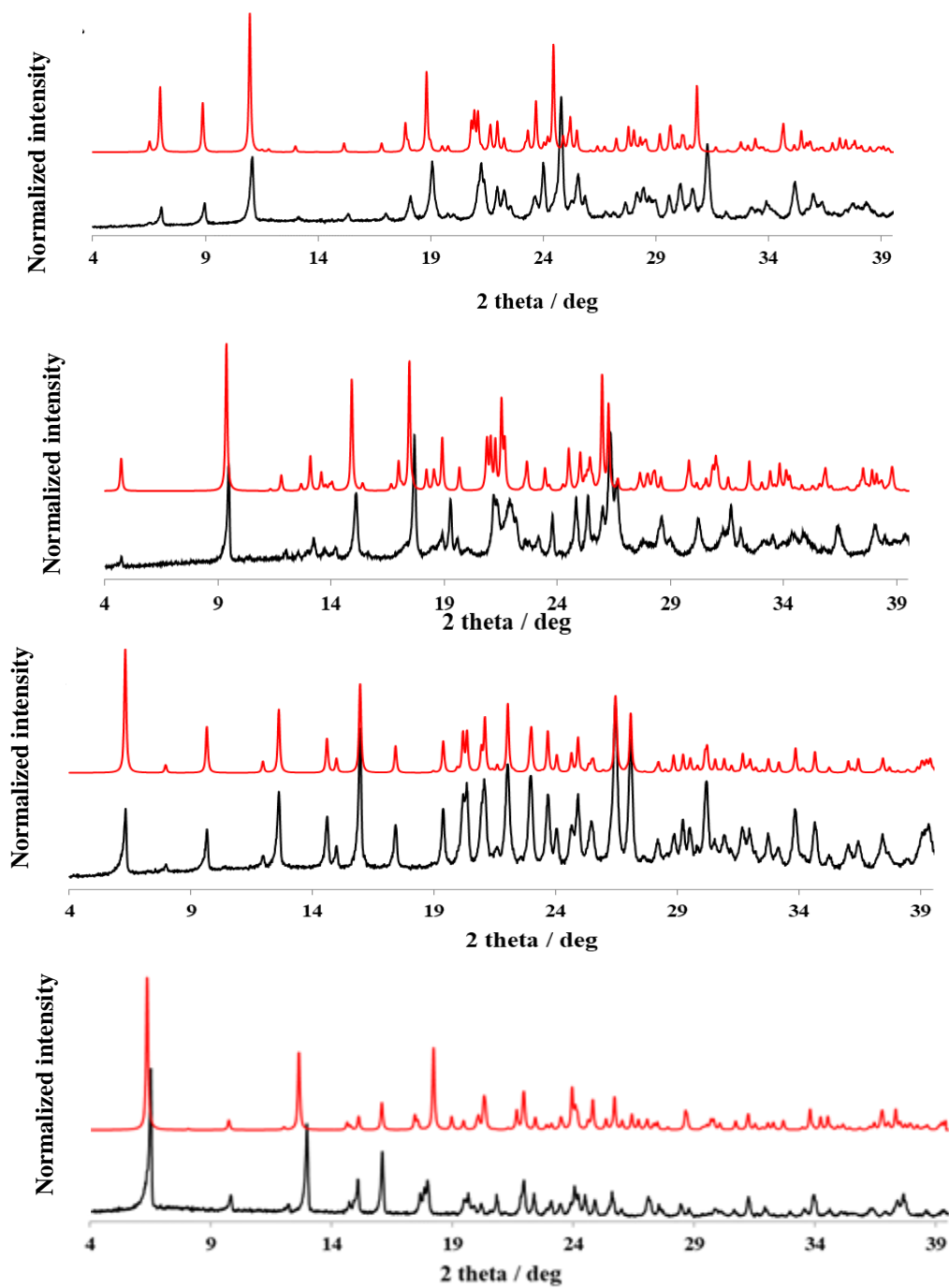


Figure S2. PXRD patterns of **ovan3amp** cocrystals (from top to bottom: **ovan3amp**·12tfib, **ovan3amp**·13tfib, (**ovan3amp**)₂·14tfib, (**ovan3amp**)₂·ofib) mechanosyntheses.

Table S1. Crystallographic parameters of **ovan3amp** and **ovan4amp** cocrystals.

	ovan3amp· 12tfib	ovan3amp· 13tfib	(ovan3amp)₂· 14tfib	(ovan3amp)₂· 135tfib
Chemical formula	C ₁₃ H ₁₂ N ₂ O ₂ · C ₆ F ₄ I ₂	C ₁₃ H ₁₂ N ₂ O ₂ · C ₆ F ₄ I ₂	C ₁₃ H ₁₂ N ₂ O ₂ · 0.5(C ₆ F ₄ I ₂)	2(C ₁₃ H ₁₂ N ₂ O ₂)· C ₆ F ₃ I ₃
M_r	630.11	630.11	429.18	966.25
Crystal system	Orthorhombic	Monoclinic	Monoclinic	Triclinic
Space group	<i>P</i> 2 ₁ 2 ₁ 2 ₁	<i>P</i> 2 ₁ / <i>c</i>	<i>P</i> 2 ₁ / <i>n</i>	<i>P</i> $\bar{1}$
T (K)	295	298	115	293
a, b, c (Å)	4.9559 (1), 15.9467 (5), 25.0955 (7)	19.597 (2), 7.1629 (7), 15.5499 (18)	4.6036 (3), 27.982 (2), 12.0308 (6)	4.9424 (4), 14.3285 (10), 23.8841 (18)
α, β, γ (°)	90, 90, 90	90, 107.431 (12), 90	90, 96.165 (5), 90	82.468 (6), 89.490 (7), 84.574 (6)
V (Å³)	1983.30 (9)	2082.5 (4)	1540.81 (18)	1669.3 (2)
Z	4	4	4	2
CSD REFCODE	1850125	1547940	SEDFIT01	1850126
	(ovan3amp)₂· ofib	(ovan4amp)₂· 12tfib	(ovan4amp)₂· 14tfib	ovan4amp· 135tfib
Chemical formula	C ₁₃ H ₁₂ N ₂ O ₂ · 0.5 (C ₄ F ₈ I ₂)	(C ₁₃ H ₁₂ N ₂ O ₂) ₂ · C ₆ F ₄ I ₂	C ₁₃ H ₁₂ N ₂ O ₂ · 0.5(C ₆ F ₄ I ₂)	C ₁₃ H ₁₂ N ₂ O ₂ · C ₆ F ₃ I ₃
M_r	455.17	858.35	429.18	738.01
Crystal system	Monoclinic	Triclinic	Monoclinic	Orthorhombic
Space group	<i>P</i> 2 ₁ / <i>n</i>	<i>P</i> $\bar{1}$	<i>P</i> 2 ₁ / <i>n</i>	<i>Pbca</i>
T (K)	100(2)	293	150	298
a, b, c (Å)	4.89023(7), 27.7231(5), 11.86723(20)	4.7846 (3), 14.4237 (8), 23.5788 (12)	16.6673 (6), 4.6723 (2), 19.0963 (9)	18.2946 (6), 7.3264 (3), 32.3563 (14)
α, β, γ (°)	90, 92.9167(13) 90	90, 89.176 (4), 85.918 (4)	90, 92.004 (4), 90	90, 90, 90
V (Å³)	1606.78(5)	1559.57 (16)	1486.21 (12)	4336.8 (3)
Z	4	2	4	8
CSD REFCODE	1582770	1552262	1548172	1548140

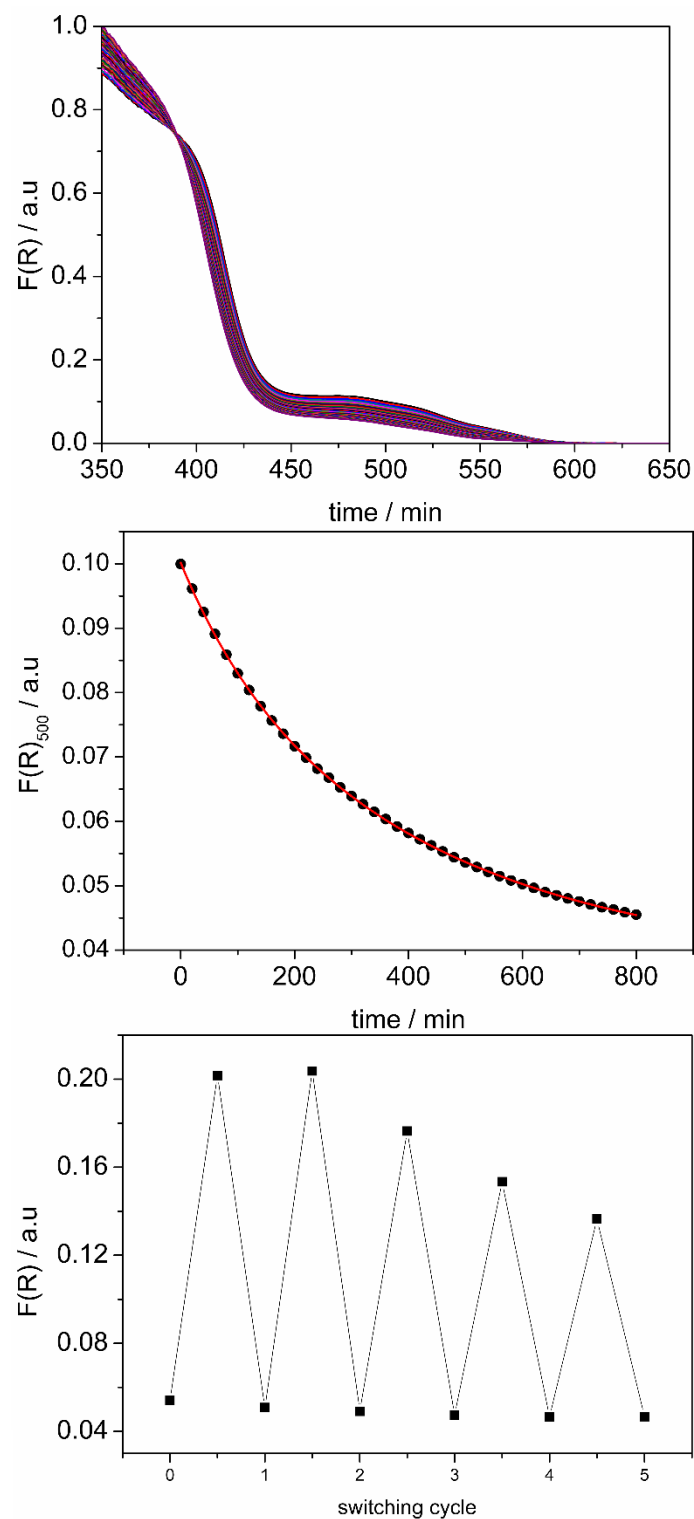


Figure S3. Diffuse reflectance spectra of **(ovan3amp)₂·ofib** (top) showing thermal fading of the orange-red coloration. Points at 500 nm were plotted over the time and fitted by a bi-exponential curve (middle). Repeating photochemical recovery over 5 switching cycles (bottom).

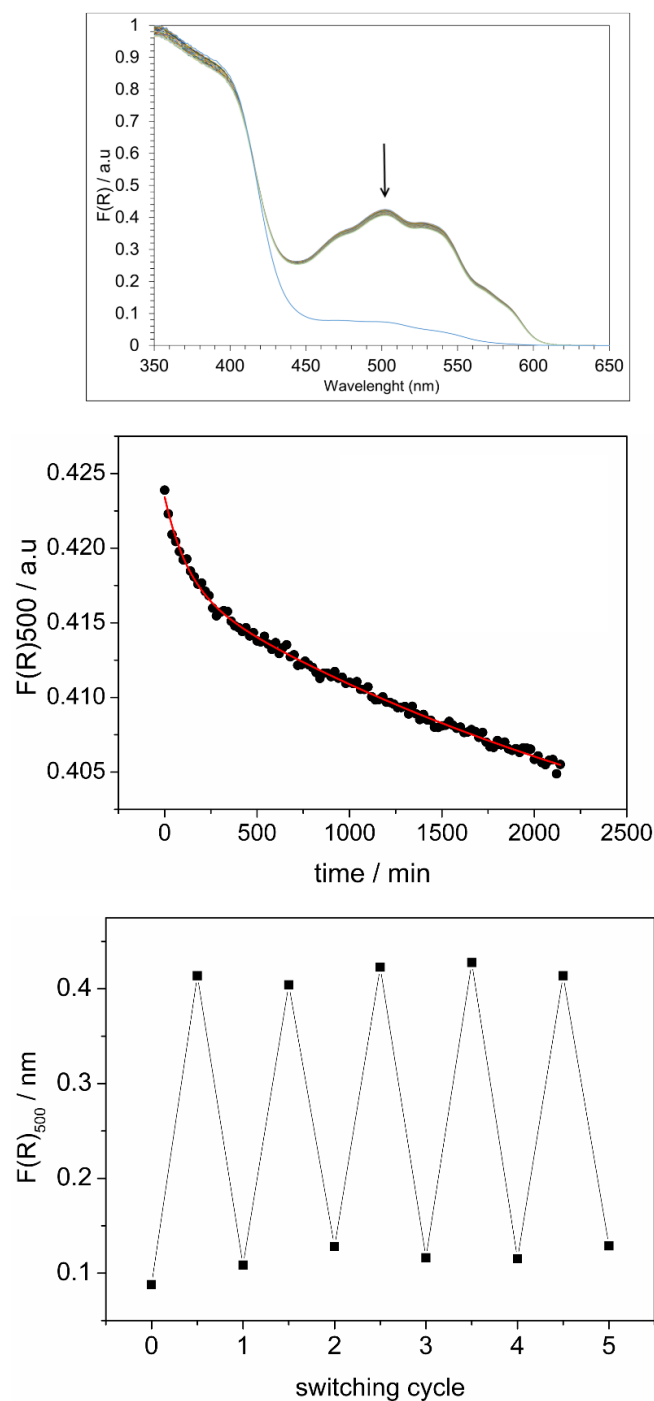


Figure S4. Diffuse reflectance spectra of **ovan3amp·12tfib** (top) showing thermal fading of the orange-red coloration. Points at 500 nm were plotted over the time and fitted by a bi-exponential curve (middle). Repeating photochemical recovery over 5 switching cycles (bottom).

Table S2. The results of TG analysis.

Cocrystal	$t_1 / ^\circ\text{C}$	$t_2 / ^\circ\text{C}$	%
ovan3amp·12tfib	119	367	62.3
ovan3amp·13tfib	113	365	61.6
(ovan3amp)₂·14tfib	117	381	59.8
(ovan3amp)₂·135tfib	150	358	55.1
(ovan4amp)₂·12tfib	107	239	12.8
	239	390	10.2
(ovan4amp)₂·14tfib	118	255	20.5
	255	469	20.8
ovan4amp·135tfib	161	404	50.8

Table S3. The results of DSC analysis.

Cocrystal	$t_e / ^\circ\text{C}$	$\Delta H / \text{kJmol}^{-1}$
ovan3amp·12tfib	92	34.09
ovan3amp·13tfib	99	0.46
	104	20.92
(ovan3amp)₂·14tfib	110	65.69
(ovan3amp)₂·135tfib	112	46.52
(ovan4amp)₂·12tfib	96	45.14
(ovan4amp)₂·14tfib	150	58.74
ovan4amp·135tfib	136	33.37

List of articles:

Playing with Isomerism: Cocrystallization of Isomeric N-Salicylideneaminopyridines with Perfluorinated Compounds as Halogen Bond Donors and Its Impact on Photochromism

Carletta, A., Zbačnik, M., Van Gysel, M., Vitković, M., Tumanov, N., Stilinović, V., Wouters, J. & Cinčić, D. *Crystal Growth and Design*. **2018**, 18, 11, 6833–6842.

Direct Access by Mechanochemistry or Sonochemistry to Protonated Merocyanines: Components of a Four-State Molecular Switch

Colaço, M., Carletta, A., Van Gysel, M., Robeyns, K., Tumanov, N. & Wouters, J., *ChemistryOPEN*. **2018**, 7, 7, 520-526.

Tetraphenylborate Anion Induces Photochromism in N-Salicylideneamino-1-alkylpyridinium Derivatives Through Formation of Tetra-Aryl Boxes

Carletta, A., Colaço, M., Mouchet, S., Plas, A., Tumanov, N., Fusaro, L., Champagne, B., Lanners, S. & Wouters, J. *Journal of Physical Chemistry C*. **2018**, 122, 20, 10999–11007.

Halogen-bonded cocrystals of N-salicylidene Schiff bases and iodoperfluorinated benzenes: Hydroxyl oxygen as a halogen bond acceptor

Carletta, A., Zbačnik, M., Vitković, M., Tumanov, N., Stilinović, V., Wouters, J. & Cinčić, D., *CrystEngComm*. **2018**, 20, 36, 5332-5339.

Assessing density functional theory approaches for predicting the structure and relative energy of salicylideneaniline molecular switches in the solid state

Quertinmont, J., Carletta, A., Tumanov, N. A., Leysens, T., Wouters, J. & Champagne, B. *The Journal of Physical Chemistry C*. **2017**, 121, 12, 6898-6908.

Halogen-Bond Effects on the Thermo- and Photochromic Behaviour of Anil-Based Molecular Co-crystals

Carletta, A., Spinelli, F., d'Agostino, S., Ventura, B., Chierotti, M. R., Gobetto, R., Wouters, J. & Grepioni, F., *Chemistry - A European Journal*. **2017**, 23, 22, 5317-5329.

Polymorphic and Isomorphic Cocrystals of a N-Salicylidene-3-aminopyridine with Dicarboxylic Acids: Tuning of Solid-State Photo- and Thermochromism

Carletta, A., Buol, X., Leyssens, T., Champagne, B. & Wouters, J., *Journal of Physical Chemistry C*. **2016**, 120, 10001-10008.

How does binding of imidazole-based inhibitors to heme oxygenase-1 influence their conformation? Insights combining crystal structures and molecular modelling

Carletta, A., Tilborg, A., Moineaux, L., De Ruyck, J., Basile, L., Salerno, L., Romeo, G., Wouters, J. & Guccione, S. *Acta Crystallographica Section B: Structural Science, Crystal Engineering and Materials*. **2015**, 71, 447-454.

Structural and energy insights on solid-state complexes with trimethoprim: A combined theoretical and experimental investigation

Tilborg, A., Carletta, A. & Wouters, J. *Acta Crystallographica Section B: Structural Science, Crystal Engineering and Materials*. **2015**, 71, 406-415

Solid-state investigation on a new dimorphic substituted N-salicylidene compound: Insights into its thermochromic behaviour

Carletta, A., Dubois, J., Tilborg, A. & Wouters, J., *CrystEngComm*. **2015**, 17, 18, 3509-3518.

Solid-state investigation of polymorphism and tautomerism of phenylthiazole-thione: A combined crystallographic, calorimetric, and theoretical survey

Carletta, A., Meinguet, C., Wouters, J. & Tilborg, A., *Crystal Growth and Design*. **2015**, 15, 5, 2461-2473.